



**HAL**  
open science

# Metabolic labelling of bacterial isoprenoids produced by the methylerythritol phosphate pathway: a starting point towards a new inhibitor

Zoljargal Baatarkhuu

► **To cite this version:**

Zoljargal Baatarkhuu. Metabolic labelling of bacterial isoprenoids produced by the methylerythritol phosphate pathway: a starting point towards a new inhibitor. Other. Université de Strasbourg, 2017. English. NNT: 2017STRAF029 . tel-02003538

**HAL Id: tel-02003538**

**<https://theses.hal.science/tel-02003538>**

Submitted on 1 Feb 2019

**HAL** is a multi-disciplinary open access archive for the deposit and dissemination of scientific research documents, whether they are published or not. The documents may come from teaching and research institutions in France or abroad, or from public or private research centers.

L'archive ouverte pluridisciplinaire **HAL**, est destinée au dépôt et à la diffusion de documents scientifiques de niveau recherche, publiés ou non, émanant des établissements d'enseignement et de recherche français ou étrangers, des laboratoires publics ou privés.

**ÉCOLE DOCTORALE DES SCIENCES CHIMIQUES**  
**UMR 7177 & 7199**

**THÈSE** présentée par :  
**Zoljargal BAATARKHUU**

soutenue le : **05 Septembre 2017**

pour obtenir le grade de : **Docteur de l'université de Strasbourg**

Discipline/ Spécialité : Chimie Bio-Organique

**Metabolic labelling of bacterial isoprenoids  
produced by the Methylerythritol phosphate  
pathway : A starting point towards a new inhibitor**

**THÈSE dirigée par :**

**Dr Alain WAGNER**

Directeur de recherche, CNRS

**Dr Myriam SEEMANN**

Directeur de recherche, CNRS

**RAPPORTEURS :**

**Dr Joelle DUBOIS**

Directeur de recherche,  
Institut de Chimie des Substances Naturelles, Paris

**Dr Alain BURGER**

Professeur, Université de Nice, Nice

ᠨᠢᠰᠢᠯᠠᠭᠤ ᠨᠢᠰᠢᠯᠠᠭᠤ ᠨᠢᠰᠢᠯᠠᠭᠤ ᠨᠢᠰᠢᠯᠠᠭᠤ  
ᠨᠢᠰᠢᠯᠠᠭᠤ ᠨᠢᠰᠢᠯᠠᠭᠤ ᠨᠢᠰᠢᠯᠠᠭᠤ ᠨᠢᠰᠢᠯᠠᠭᠤ

*(In memory of my beloved father Baatarkhuu Dugajii)*

# Résumé de thèse en français

## 1) Introduction

Les isoprénoïdes forment une famille de produits naturels parmi les plus diverses avec plus de 50000 composés connus.<sup>1</sup> Ils sont présents dans tous les organismes vivants. Ils ont de nombreux rôles biologiques, allant du transport d'électrons, à la biosynthèse des membranes cellulaires. Malgré la diversité des isoprénoïdes, ils sont synthétisés à partir de deux précurseurs : le diphosphate d'isopentényle (IPP) et le diphosphate de diméthylallyle (DMAPP). Deux voies de biosynthèse existent pour la formation de ces molécules : la voie du mévalonate et la voie du méthylérythritol phosphate (MEP), découverte plus récemment.<sup>2, 3</sup> Cette dernière voie de synthèse est utilisée par les micro-organismes dont des pathogènes comme *Mycobacterium tuberculosis* (bactérie responsable de la tuberculose), *Vibrio cholerae* (bactérie responsable du choléra) et *Plasmodium falciparum* (parasite responsable de la malaria). Elle est cependant absente chez l'humain et, par conséquent, est une cible de choix pour le développement d'un nouveau médicament antibactérien ou antiparasitaire.

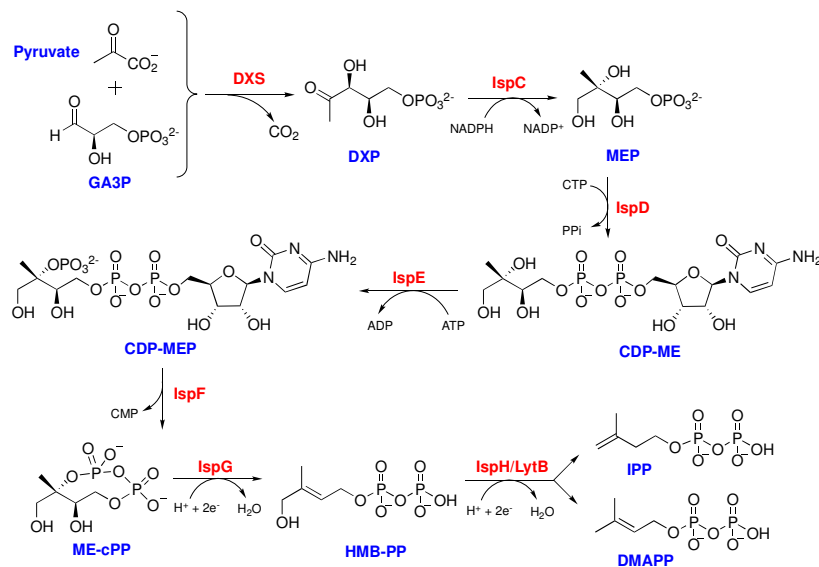


Figure 1. Voie MEP et ses enzymes et substrats

Le marquage métabolique est un outil puissant pour l'élucidation d'un métabolisme. Cette technique repose sur l'assimilation de molécules marquées *via* la machinerie d'organismes vivants, puis, sur la détection ou la capture des biomolécules marquées transformées en utilisant différentes méthodes. Les réactions bioorthogonales font partie des méthodes couramment

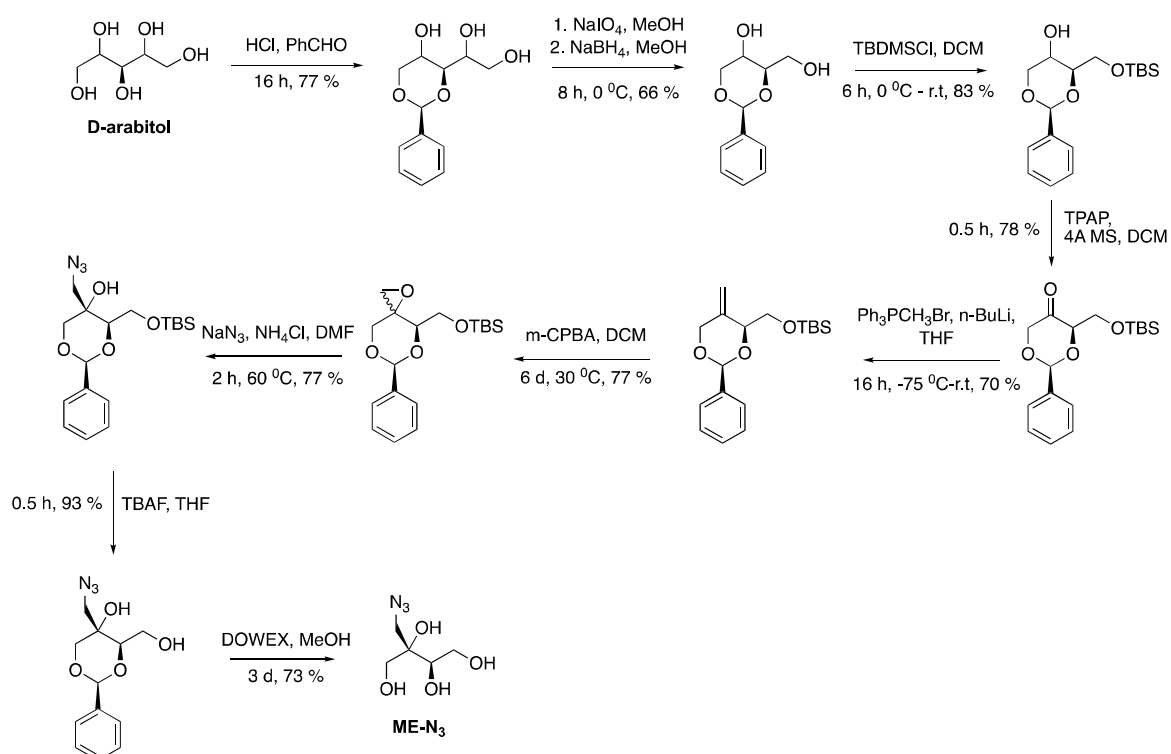
mises en œuvre pour le marquage métabolique. La réaction de cycloaddition azoture-alcyne (Huisgen) est majoritairement utilisée. Le principal avantage de cette réaction est que les deux fonctions réactives, l'azoture et l'alcyne, sont presque absentes des systèmes biologiques, orthogonales entre elles et très peu réactives vis-à-vis des autres fonctions bioorthogonales.<sup>4, 5</sup> Pour la détection d'une molécule marquée, l'azoture et l'alcyne peuvent être liés à différentes sondes qui sont détectables par fluorescence ou par spectrométrie de masse. Le tris(2,4,6-trimethoxyphenyl)phosphine (TMPP) est une sonde qui augmente le signal lors d'une analyse en spectrométrie de masse et est largement utilisée pour la détection de biomolécules marquées.<sup>6, 7</sup> Utiliser une chimie bioorthogonale pour le marquage métabolique de la voie du MEP serait une stratégie viable pour enregistrer l'activité de cette voie et des enzymes impliqués dans la formation des isoprénoïdes finaux, mais également pour étudier l'effet de petites molécules, comme par exemple des inhibiteurs potentiels de la voie du MEP.

Un deuxième sujet de la thèse, concerne le développement de linkers pour la formation de conjugués anticorps-médicaments. Les conjugués anticorps-médicaments (aussi appelés ADC) se sont imposés comme une méthode prometteuse pour le traitement du cancer. Cet outil est supérieur à la chimiothérapie classique en terme d'efficacité et dispose d'effets secondaires plus faibles. Les ADC reposent sur trois parties, une charge cytotoxique, un lien (appelé linker) et un anticorps. Pour maximiser l'efficacité des ADC, le linker doit se coupler de manière sélective avec un anticorps, être stable lors de sa circulation dans le plasma et être clivable ou non après l'endocytose.<sup>8</sup> Le 3-ArylPropioNitrile (APN, Figure 3) a été décrit comme possédant une meilleure sélectivité vis-à-vis des thiols par rapport à des réactifs conventionnels. L'utilisation de dérivés APN pourrait mener à des agents de bioconjugaison ayant un potentiel supérieur aux linkers accessibles actuellement.

## 2) Résultats et discussions

### 2a) Marquage métabolique de la voie du MEP

Afin d'étudier la voie du méthylérythritol phosphate (MEP) par le marquage métabolique et en utilisant la chimie orthogonale, nous avons décidé d'introduire un marqueur azoture (étiquette) sur l'intermédiaire clé de cette voie : le MEP. Il a été précédemment décrit que le méthylérythritol (ME) exogène pouvait être transporté dans la bactérie *E. coli* et être ensuite phosphorylé pour conduire au MEP. Ainsi, notre objectif initial était de synthétiser le méthylérythritol marqué par un azoture. Celui-ci devrait être transporté, phosphorylé lors de son transport dans la bactérie et converti par les enzymes de la voie du MEP. La synthèse du méthylérythritol portant l'azoture a été effectuée *via* une synthèse en neuf étapes (rendement global de 12%), à partir du D-arabitol et en se basant sur une approche décrite dans la littérature.<sup>9</sup> (Schème 1)



Schème 1. La synthèse du ME-N<sub>3</sub>

Le BCN-TMPP a été synthétisé en liant le bicyclo[6.1.0]nonyne (BCN) à la sonde TMPP afin de l'utiliser pour les analyses en spectrométrie de masse. Cette molécule bioorthogonale permet la détection des métabolites marqués. Lors de la détermination des constantes cinétiques de la réaction entre le ME-N<sub>3</sub> et le BCN-TMPP, la limite de détection du produit 'cliqué' a été mesurée par spectrométrie de masse. Le produit 'cliqué' est observable jusqu'à une concentration de 10 nM, limite de détection que nous avons jugée suffisante pour le marquage métabolique.

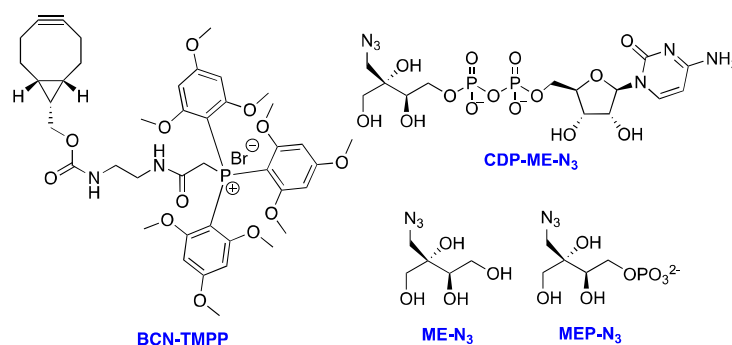


Figure 2. Structures des analogues marqués et BCN-TMPP

La procédure générale pour le marquage métabolique consiste, d'abord, à incuber la bactérie *E.coli* avec le ME-N<sub>3</sub>, à effectuer une lyse bactérienne, puis à incuber le BCN-TMPP dans le lysat bactérien pour finalement analyser les résultats en spectrométrie de masse. Ces analyses n'ont pas révélé de métabolites marqués lors des premiers essais. Si la molécule marquée est transformée par la voie du MEP, celle-ci pourrait être incorporée dans plusieurs isoprénoïdes, ce qui serait très difficile à élucider par spectrométrie de masse. Par conséquent, nous avons incubé le ME-N<sub>3</sub> en présence d'un mutant d'*E.coli* qui n'exprime pas l'enzyme IspG (voir Figure 1). Ainsi, si ME-N<sub>3</sub> s'engage dans la voie du MEP, celui-ci s'arrêtera avant l'étape enzymatique de IspG. Ainsi, nous serions capables de détecter l'accumulation du ME-cPP azoture. Les analyses spectrométriques du lysat du mutant *E.coli* n'ont pas produit de résultats pertinents, probablement liés à l'incapacité du ME-N<sub>3</sub> à pénétrer la membrane de la bactérie, ainsi qu'à des limitations en terme de sensibilité.

Afin de vérifier si l'enzyme IspD (2-C-méthyl-D-érythritol-4-phosphate cytidylyltransférase) aussi appelée YgbP, responsable de la conversion du méthylérythritol phosphate en CDP-ME (Figure 1), prend en charge l'analogue azoturé, nous avons synthétisé l'azoture méthylérythritol

phosphate (MEP-N<sub>3</sub>). IspD convertit le MEP en 4-diphosphocytidyl-2-C-méthyl-D-erythritol (CDP-ME) en présence de CTP.<sup>10, 11</sup> Les paramètres cinétiques, tels que la constante de Michaelis (K<sub>m</sub>) ou la vélocité maximale (V<sub>max</sub>) de l'enzyme IspD de *E. coli* purifiée ont été mesurées et sont en accord avec la littérature. Les résultats ont montrés qu'IspD de *E. coli* était capable de convertir le MEP-N<sub>3</sub> en son produit correspondant (CDP-ME-N<sub>3</sub>, Figure 2).

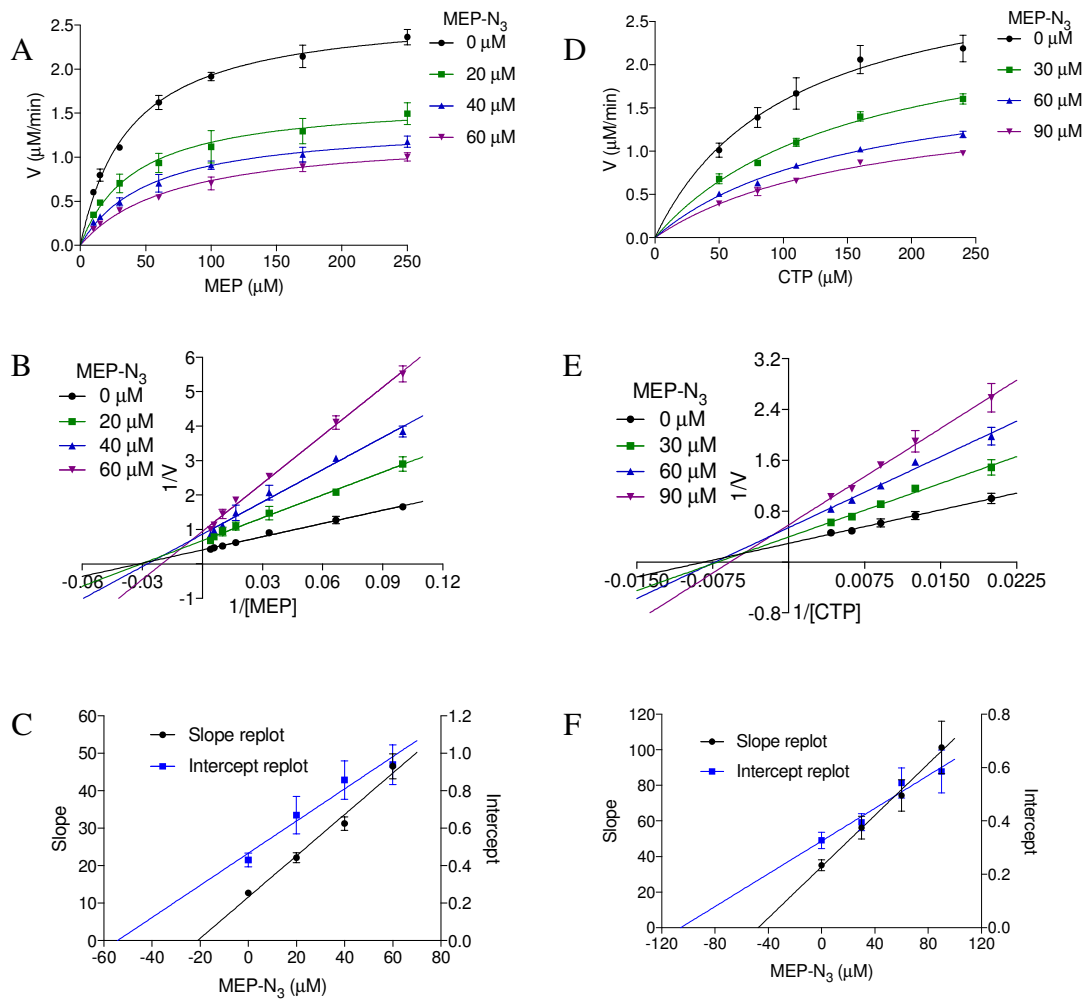


Figure 3. Inhibition de IspD par MEPN<sub>3</sub> : **A.** Vitesse initiale en fonction de la concentration de MEP en utilisant 200μM CTP et en fixant la concentration de MEPN<sub>3</sub> à 0 μM (noir), 20 μM (vert), 40 μM (bleu), 60 μM (violet). **B.** Représentation de Lineweaver-Burk de A; **C.** Tracé de la pente et de l'ordonné à l'origine des différentes droites obtenues sur le graphe B. **D.** Vitesse initiale en fonction de la concentration de CTP en utilisant 250μM MEP et en fixant la concentration MEPN<sub>3</sub> à 0 μM (noir), 30 μM (vert), 60 μM (bleu), 90 μM (violet). **E.** Représentation de Lineweaver-Burk de D. **F.** Tracé de la pente et de l'ordonné à l'origine des différentes droites obtenues sur le graphe C.

Ce résultat a été validé par réaction « click » en utilisant le BCN-TMPP et des analyses de spectrométrie de masse. Il est à noter que, bien qu'IspD convertisse le MEP-N<sub>3</sub>, la vitesse de réaction est environ 100 fois plus lente que celle avec le substrat naturel. Nous avons observé une inhibition de IspD par le substrat à des concentrations en MEP-N<sub>3</sub> supérieures à 500 µM. Par conséquent, les paramètres cinétiques de IspD ( $K_m$ ,  $V_{max}$ ), pour ce produit, n'ont pas pu être déterminés par une analyse cinétique à l'état stationnaire. Alors que nous cherchions à mesurer les paramètres cinétiques, MEP-N<sub>3</sub> a montré une activité inhibitrice sur la réaction catalysée par IspD.

Afin de déterminer l'efficacité inhibitrice du MEP-N<sub>3</sub>, des études cinétiques d'inhibition de IspD ont été entreprises. Comme IspD a deux substrats (MEP et CTP), ces études ont été réalisées pour différentes concentrations en inhibiteur en maintenant la concentration d'un des deux substrats constante et en faisant varier la concentration de l'autre substrat. Nous avons obtenu une constante d'inhibition ( $K_i$ ) de 21 µM lorsque la concentration de MEP était la variable, et de 47 µM lorsque la concentration de CTP variait (Figure 3). Bien que plusieurs inhibiteurs de l'enzyme IspD issue de *Plasmodium falciparum*, *Mycobacterium tuberculosis* ou *Arabidopsis thaliana* soient décrits, seuls quelques inhibiteurs ont été décrits pour IspD de *E.Coli*. Nous avons découvert que MEP-N<sub>3</sub> possède l'activité inhibitrice la plus élevée parmi les inhibiteurs connus d'IspD de *E.Coli*. De plus, MEP-N<sub>3</sub> inhibe l'activité de IspD suivant un modèle mixte, indiquant qu'il peut se lier à l'enzyme libre, mais aussi au complexe enzyme-substrat.

Plusieurs inhibiteurs de l'IspD de la plante *A. Thaliana* et du parasite *P. falciparum* sont décrits dans la littérature dont quelques-uns montrent des IC<sub>50</sub> de l'ordre du nanomolaire. Cependant, l'homologie de ces enzymes avec celle d'*E. coli* n'est pas très élevée (24.4% identité par rapport à *A.thaliana* et 7.8% identité par rapport à *P.falciparum*). Trois inhibiteurs de IspD de *E. coli* sont décrits dans la littérature : le D-erythritol-4 -phosphate (IC<sub>50</sub>=1.38 mM), le L-erythritol-4-phosphate ( $K_i$ = 240 mM)<sup>12</sup> et la fosmidomycine (IC<sub>50</sub>= 20.4 mM)<sup>13</sup>. (Figure 4) Bien que le MEP-N<sub>3</sub> ne soit pas un inhibiteur optimal, il représente le meilleur inhibiteur de IspD de *E. coli*.

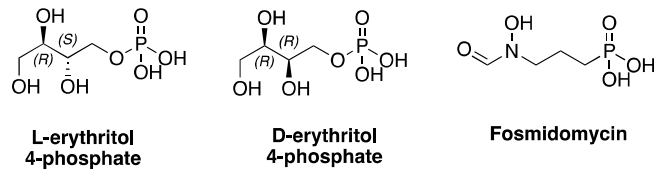


Figure 4. Les structures des inhibiteurs de l'IspD

A partir d'une expérience de 'pulse-chase', il a été proposé que le mécanisme réactionnel d'IspD était séquentiel: le CTP se fixe d'abord à l'enzyme suivi du MEP qui se lie au complexe Enzyme-CTP pour former un complexe tertiaire<sup>14</sup> (Figure 5). Cependant, ce mécanisme n'a jamais été confirmé en utilisant une analyse cinétique à l'état stationnaire. Ainsi, en utilisant une étude cinétique à l'état stationnaire, nous avons confirmé que la réaction suit bien un mécanisme séquentiel. Nous avons également pu déterminer les paramètres cinétiques de la réaction d'IspD à partir de ces expériences. Les paramètres cinétiques, tels que  $K_m$  ou  $V_{max}$ , obtenus sont en accord avec les valeurs obtenues en utilisant la méthode classique de Michaelis-Menten.

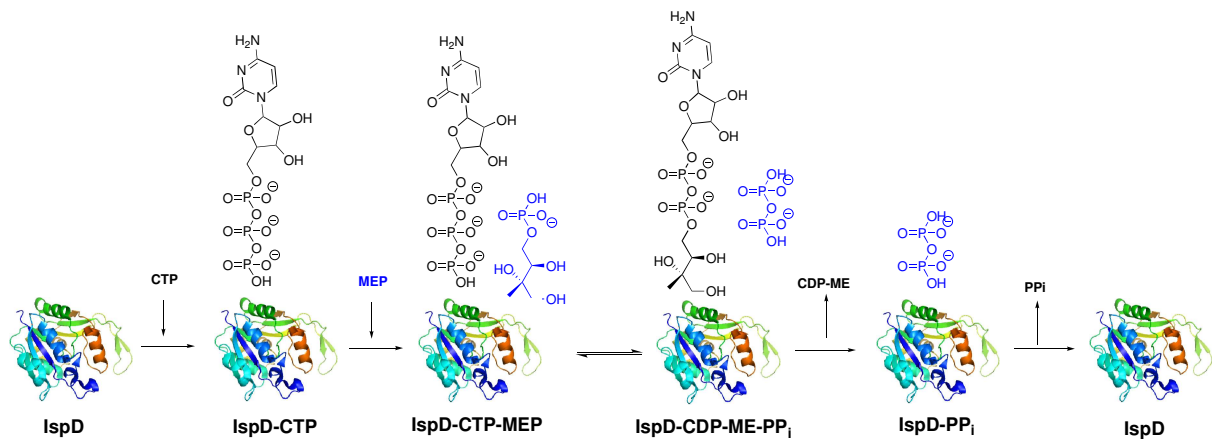


Figure 5. Mécanisme ordonné de l'IspD

## 2b) Nouveaux linkers pour ADC

Concernant le développement du nouveau linker pour ADC, *p*-(maleimide)phenylpropionitrile (MAPN), un analogue d'APN, a été synthétisé en 4 étapes. Lors du test de compatibilité pour l'hétéroconjugaison « thiol-to-thiol », nous avons observé une efficacité supérieure à celle du *p*-phénylène-maléimide (la structure n'est pas affichée), un réactif commercial.

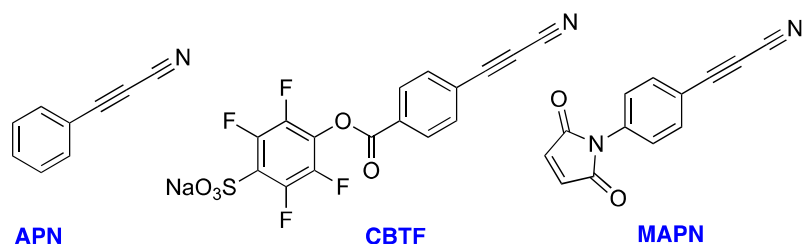


Figure 3. Structures de l'APN et de ses dérivés

Les analyses HPLC ont révélées que l'addition séquentielle du thiol aboutit à une conversion complète et propre du MAPN, convertit en hétéroconjugué correspondant, tandis que le réactif commercial a montré une conversion incomplète, comprenant un mélange de homo et hétéroconjugués. De plus, la compatibilité du MAPN pour l'hétéroconjugaison a été validé en couplant le Trastuzumab et un fluorophore. La réaction a été suivie par analyse SDS-PAGE. Le 4-((4-(cyanoéthynyl)benzoyloxy)-2,3,5,6-tétrafluorobenzènesulfonate (CBTF), un autre dérivé d'APN, a été préparé en 5 étapes à partir de l'acide 4-iodobenzoïque. Sa compatibilité pour l'hétéroconjugaison « amine-to-thiol » a été confirmée par SDS-PAGE après avoir réagi avec un fluorophore aminé et le Trastuzumab réduit. Concernant le ratio drogue-anticorps, un facteur important pour les ADC, il est comparable avec ceux des réactifs commerciaux. Nous avons découvert que CBTF était extrêmement stable par rapport au réactif commercial, contenant une fonction maléimide. Après 120h d'incubation, 8% du conjugué CBTF était dégradé, tandis que l'analogue maléimide était dégradé à hauteur de 70%.

### 3) Conclusion

La synthèse de ME-N<sub>3</sub> comme sonde chimique a été réalisée avec succès *via* une synthèse multi-étapes. Lorsque ME-N<sub>3</sub> a été utilisé comme marqueur bactérien de la voie du MEP, aucun produit marqué n'a été observé en utilisant la spectrométrie de masse. Ce résultat négatif est probablement lié à l'incapacité de la bactérie à transporter le ME-N<sub>3</sub> à travers sa membrane.

Comme ME-N<sub>3</sub> ne pouvait pas être utilisé comme sonde chimique, le MEP-N<sub>3</sub> a été synthétisé afin de déterminer si l'enzyme IspD (aussi appelée YgbP) pouvait convertir cet analogue en un intermédiaire de la voie du MEP contenant une fonction azoture. MEP-N<sub>3</sub> est un substrat de IspD, mais montre également une activité inhibitrice de IspD. Les tests d'inhibition de l'enzyme IspD d'*E.Coli*, par le MEP-N<sub>3</sub> ont montré que cette molécule est le meilleur inhibiteur connu à ce jour pour IspD de *E.Coli*. Le modèle d'inhibition de MEP-N<sub>3</sub> est mixte, signifiant qu'il peut être en compétition avec les substrats pour l'enzyme libre, à la manière d'un inhibiteur compétitif mais également pour le complexe EI. Nous pouvons en déduire que, bien que MEP-N<sub>3</sub> soit converti par l'enzyme IspD, ce n'est pas un bon candidat pour le marquage métabolique, sachant qu'il inhibe l'enzyme. Pour la première fois, nous avons déterminé le mécanisme de l'enzyme IspD par une analyse cinétique à l'état stationnaire. Le mécanisme d'IspD est un mécanisme séquentiel dans lequel les substrats sont ajoutés à l'enzyme dans un certain ordre et les résultats obtenus confirment les données de la littérature.

Pour le développement d'un nouveau linker pour ADC, CBTF, un analogue d'APN a été synthétisé avec un bon rendement. Par rapport aux réactifs disponibles dans le commerce, il est supérieur en terme de stabilité dans le plasma, ce qui fait du CBTF un nouvel agent de conjugaison approprié, la stabilité étant un élément clé. MAPN, un autre analogue d'APN, possédant une hétérobiofonctionnalité, a été synthétisé et appliqué à l'hétéroconjugaison « thiol-to-thiol ». La conversion est propre et complète, menant à un unique produit, avec une efficacité supérieure aux réactifs commerciaux.

#### 4) Références

1. D. H. R. Barton, K. Nakanishi and O. Meth-Cohn, in *Comprehensive Natural Products Chemistry*, ed. D. E. Cane, Elsevier, Oxford, 1999, vol. 2.
2. M. Rohmer, *Nat. Prod. Rep.*, 1999, **16**, 565-574.
3. M. Rohmer, M. Knani, P. Simonin, B. Sutter and H. Sahm, *Biochem. J.*, 1993, **295**, 517-524.
4. R. J. Griffin, *Prog Med Chem*, 1994, **31**, 121-232.
5. N. J. Agard, J. A. Prescher and C. R. Bertozzi, *J. Am. Chem. Soc.*, 2004, **126**, 15046-15047.
6. A. J. Cartwright, P. Jones, J.-C. Wolff and E. H. Evans, *J. Anal. At. Spectrom.*, 2005, **20**, 75-80.
7. H.-K. Woo, E. P. Go, L. Hoang, S. A. Trauger, B. Bowen, G. Siuzdak and T. R. Northen, *Rapid Commun. Mass Spectrom.*, 2009, **23**, 1849-1855.
8. R. V. J. Chari, M. L. Miller and W. C. Widdison, *Angew Chem Int Edit*, 2014, **53**, 3796-3827.
9. C. Lagisetti, M. Urbansky and R. M. Coates, *J. Org. Chem.*, 2007, **72**, 9886-9895.
10. S. B. Richard, M. E. Bowman, W. Kwiatkowski, I. Kang, C. Chow, A. M. Lillo, D. E. Cane and J. P. Noel, *Nat. Struct. Biol.*, 2001, **8**, 641-648.
11. S. Herz, J. Wungsintaweeikul, C. A. Schuhr, S. Hecht, H. Luttgen, S. Sagner, M. Fellermeier, W. Eisenreich, M. H. Zenk, A. Bacher and F. Rohdich, *Proc Natl Acad Sci U S A*, 2000, **97**, 2486-2490.
12. A. M. Lillo, C. N. Tetzlaff, F. J. Sangari and D. E. Cane, *Bioorg. Med. Chem. Lett.*, 2003, **13**, 737-739.
13. B. Zhang, K. M. Watts, D. Hodge, L. M. Kemp, D. A. Hunstad, L. M. Hicks and A. R. Odom, *Biochemistry*, 2011, **50**, 3570-3577.
14. S. B. Richard, A. M. Lillo, C. N. Tetzlaff, M. E. Bowman, J. P. Noel and D. E. Cane, *Biochemistry*, 2004, **43**, 12189-12197.

## LISTE DES PRESENTATIONS

### *Présentation orale :*

1. **Zoljargal BAATARKHUU**, Alain WAGNER, Myriam SEEMANN. « Development of a *novel inhibitor targeting YgbP, an enzyme of the MEP pathway in isoprenoid biosynthesis* » Journée de l'UMR 7199. Université de Strasbourg. Illkirch. 15 décembre 2016.

### *Communication par affiche*

1. **Zoljargal BAATARKHUU**, Alain WAGNER, Myriam SEEMANN. « Discovery of MEP-N<sub>3</sub> a novel inhibitor of YgbP/IspD enzyme in the MEP pathway of isoprenoid biosynthesis » 7<sup>th</sup> HIPS Symposium. Helmholtz-Zentrum für Infektionsforschung, Saarbrücken, Germany. 29 juin 2017

## LISTE DES PUBLICATIONS

1. Kolodych, S.; Koniev, O.; Baatarkhuu, Z.; Bonnefoy, J. Y.; Debaene, F.; Cianferani, S.; Van Dorsselaer, A.; Wagner, A. CBTF: New Amine-to-Thiol Coupling Reagent for Preparation of Antibody Conjugates with Increased Plasma Stability. *Bioconjugate Chem* **2015**, 26 (2), 197-200.
2. Koniev, O.; Kolodych, S.; Baatarkhuu, Z.; Stojko, J.; Eberova, J.; Bonnefoy, J. Y.; Cianferani, S.; Van Dorsselaer, A.; Wagner, A. MAPN: First-in-Class Reagent for Kinetically Resolved Thiol-to-Thiol Conjugation. *Bioconjugate Chem* **2015**, 26 (9), 1863-1867.

### *En préparation*

3. **Z. Baatarkhuu**, P. Chaignon, A. Wagner, M. Seemann, "Synthesis and kinetic studies of a novel inhibitor for YgbP, an enzyme in the Methylerythritol phosphate pathway",

## Table of Contents

List of schemes.....	iv
List of figures .....	vii
List of equations .....	x
List of abbreviations.....	xi
Abstract .....	xiv
Acknowledgement.....	xv
<b>1 Introduction .....</b>	<b>1</b>
1.1 Isoprenoid Biosynthesis .....	1
1.2 Mevalonate Pathway .....	7
1.3 Methylerythritol Phosphate (MEP) Pathway .....	10
1.4 MEP pathway enzymes .....	12
1.4.1 1-Deoxy-D-xylulose 5-phosphate synthase (DXS).....	12
1.4.2 1-deoxy-D-xylulose-5 phosphate reductase (IspC).....	14
1.4.3 2-C-Methyl-D-erythritol cytidylyltransferase (IspD).....	15
1.4.4 4-diphosphocytidyl-2-C-Methyl-D-erythritol kinase (IspE).....	17
1.4.5 2-C-Methyl-D-erythritol 2,4-cyclodiphosphate synthase (IspF).....	19
1.4.6 Bifunctional IspDF .....	21
1.4.7 (E)-4-Hydroxy-3-methyl-but-2-enyl diphosphate synthase (IspG).....	22
1.4.8 (E)-4-Hydroxy-3-methyl-but-2-enyl diphosphate reductase (IspH) .....	24
1.5 Metabolic labelling.....	29
1.5.1 Radioisotope labelling.....	29
1.5.2 Stable isotope labelling .....	29
1.5.3 Bioorthogonal labelling.....	30
1.5.4 Click Chemistry (bioorthogonal ligation) in metabolic labelling .....	37

<b>2</b>	<b>Metabolic labelling of the MEP pathway</b> .....	47
2.1	Introduction .....	47
2.2	Synthesis of ME-N <sub>3</sub> .....	49
2.3	Synthesis of BCN-TMPP .....	58
2.4	Kinetic study of click reaction between ME-N <sub>3</sub> and BCN-TMPP.....	60
2.5	Limit of detection of ME-N <sub>3</sub> -BCN-TMPP by LC-MS.....	61
2.6	LC-MS analysis of ME-N <sub>3</sub> incorporation in <i>E.coli</i> .....	63
2.7	Synthesis and LC-MS analysis of N <sub>3</sub> -DMAPP .....	66
2.8	ME-N <sub>3</sub> incorporation study using mutant <i>E.coli</i> EcAB4-5.....	70
<b>3</b>	<b>Kinetic Studies of IspD enzyme</b> .....	74
3.1	Introduction to enzyme kinetics .....	74
3.1.1	Enzyme inhibition kinetics.....	77
3.2	Synthesis of MEP-N <sub>3</sub> .....	80
3.3	Investigation of the kinetics of IspD. ....	83
3.3.1	MEP-N <sub>3</sub> : a substrate of IspD? .....	83
3.3.2	MEP-N <sub>3</sub> : an inhibitor of IspD?.....	89
3.3.3	Investigation of the mechanism catalysed by IspD .....	96
<b>4</b>	<b>Development of Novel ADC linkers</b> .....	105
4.1	Introduction .....	105
	MAPN: First-in-Class Reagent for Kinetically Resolved Thiol-to-Thiol Conjugation .....	
	Supporting Information .....	
	CBTF: New Amine-to-Thiol Coupling Reagent for Preparation of Antibody Conjugates with Increased Plasma Stability .....	
	Supporting information .....	
	<b>General conclusion</b> .....	110
	<b>Perspectives</b> .....	112

<b>Experimental section</b> .....	114
<b>References</b> .....	144
<b>Appendix</b> .....	176

## List of schemes

Scheme 1. A. Mechanism of first step of chain elongation.....	2
Scheme 2. A. Ionisation-Condensation-Elimination mechanism.....	2
Scheme 3. Stereochemistry of chain elongation by prenyltransferases .....	4
Scheme 4. Monoterpene synthesis .....	5
Scheme 5. Sesquiterpene biosynthesis .....	6
Scheme 6. First committed steps of Paclitaxel biosynthesis .....	6
Scheme 7. Mevalonate pathway .....	8
Scheme 8. Alternate mevalonate pathways.....	9
Scheme 9. MEP pathway. ....	11
Scheme 10. Catalytic mechanism of DXS in the presence of Thiamine pyrophosphate .....	13
Scheme 11. Catalytic mechanism of IspC.....	15
Scheme 12. IspD catalytic mechanism.....	17
Scheme 13. Catalytic mechanism of IspE.....	18
Scheme 14. ygbB product from CDM-ME or CDP-MEP. ....	19
Scheme 15. Catalytic mechanism of IspF. ....	21
Scheme 16. Proposed mechanism of IspG.....	24
Scheme 17. Proposed mechanism of IspH. ....	26
Scheme 18. MEP and mevalonate pathways.....	28
Scheme 19. Carbonyl ligation methodologies.....	31
Scheme 20. Native chemical ligation methods .....	32
Scheme 21. Staudinger ligation mechanism .....	34
Scheme 22. 1,3-dipolar azide alkyne cycloaddition reaction.....	35
Scheme 23. Labelling of protein using unnatural amino acids and genetically engineered tRNA synthase.....	38
Scheme 24. Labelling of carbohydrates using click chemistry .....	40

Scheme 25. Labelling of lipid with the tagged phosphatidic acid reported by Schultz .....	42
Scheme 26. Strategy of identification of novel lipid binding proteins using click chemistry. 43	
Scheme 27. Labelling of DNA synthesis using click chemistry. ....	44
Scheme 28. <sup>13</sup> C labelling experiments to identify the first intermediates of the MEP pathway .....	47
Scheme 29. Synthetic approach for deuterium labelled D and L isomers of ME .....	49
Scheme 30. ME synthesis through 1,2-dioxin.....	50
Scheme 31. Synthesis of ME starting from 1,2-O-isopropylidene- $\alpha$ -D-xylofuranose.....	50
Scheme 32. Synthesis of MEP starting from 1,2-O-isopropylidene- $\alpha$ -D-xylofuranose .....	51
Scheme 33. Synthesis of MEP starting from a propanediol.....	52
Scheme 34. ME synthesis via dioxanone .....	53
Scheme 35. Initial synthetic approach for ME-N <sub>3</sub> .....	53
Scheme 36. Synthesis of intermediate ketone .....	55
Scheme 37. Synthesis of ME-N <sub>3</sub> via epoxide intermediate .....	57
Scheme 38. Synthetic pathway to BCN-TMPP .....	59
Scheme 39. Possible synthesis of N <sub>3</sub> -DMAPP starting from isoprene. ....	66
Scheme 40. Synthesis of azido alcohol .....	66
Scheme 41. Rearrangement observed by Pulley and co-workers. ....	67
Scheme 42. Synthesis of N <sub>3</sub> -DMAPP .....	68
Scheme 43. Ordered sequential mechanism.....	75
Scheme 44. Random sequential mechanism .....	76
Scheme 45. Ping pong mechanism.....	76
Scheme 46. Competitive inhibition.....	77
Scheme 47. Uncompetitive inhibition.....	78
Scheme 48. Non-competitive inhibition.....	79
Scheme 49. Planned synthetic route to MEP-N <sub>3</sub> .....	81

Scheme 50. Synthesis of MEP-N <sub>3</sub> .....	82
Scheme 51. Principle of the colorimetric assay. ....	83
Scheme 52. Substrate binding to the enzyme for sequential mechanism.....	97
Scheme 53. Determination of V <sub>max</sub> and K <sub>m</sub> values of MEP and CTP for IspD. ....	103

## List of Figures

Figure 1. Some example of isoprenoids. ....	1
Figure 2. Chain elongation of isoprene units .....	3
Figure 3. IPP carbon atom origin from <sup>13</sup> C labelled glucose .....	10
Figure 4. Crystal structure of <i>E.coli</i> DXS enzyme.....	12
Figure 5. Crystal structure of <i>E.coli</i> IspC.....	14
Figure 6. Crystal structure of substrate and product of <i>E.coli</i> IspD inside the catalytic pocket .....	16
Figure 7. Crystal structure of <i>E.coli</i> IspE enzyme .....	18
Figure 8. Crystal structure of <i>E.coli</i> IspF enzyme.....	20
Figure 9. Crystal structure of IspDF of <i>Campylobacter jejuni</i> overexpressed in <i>E.coli</i> . ....	22
Figure 10. 3D illustration of IspG ( <i>Thermus thermophilus</i> ) homodimer form, substrate, intermediate and the product in the active site .....	23
Figure 11. Crystal structure of <i>E.coli</i> IspH with an intact [4Fe-4S] cluster in the presence of either its substrate or its product .....	25
Figure 12. Metabolic labelling with bioorthogonal ligation .....	31
Figure 13. Mechanism of metal catalysed azide alkyne cycloaddition.....	36
Figure 14. Structures of erythritol derivatives. ....	48
Figure 15. <sup>1</sup> H NMR spectra of crude mixture of epoxidation reaction .....	56
Figure 16. Structure of BCN, TMPP and BCN-TMPP molecules.....	58
Figure 17. Click reaction kinetics. ....	60
Figure 18. MS spectra of clicked product. ....	62
Figure 19. Limit of detection of clicked product using ME-N <sub>3</sub> (1 eq) : BCN-TMPP (20 eq) .	62
Figure 20. Structure and molecular weight of MEP pathway products clicked with BCN-TMPP .....	64
Figure 21. Fragmentation of DMAPP during MS analysis and structure of possible fragmented clicked product. ....	65

Figure 22. Chromatogram of MS analysis of the bacterial extract after incubation of ME or ME-N <sub>3</sub> in <i>E.coli</i> using SIR mode. ....	65
Figure 23. <sup>1</sup> H NMR spectra and structure of <i>E/Z</i> and azide shifted N <sub>3</sub> -DMAPP. ....	69
Figure 24. A) Structure of N <sub>3</sub> -DMAPP and BCN-TMPP clicked product, B) Mass spectra of molecule <b>75</b> .....	69
Figure 25. MS scan (SIR mode – 1078 Da) of molecule <b>75</b> . ....	70
Figure 26. Structure of azide tagged MEP pathway metabolites that could be produced from ME-N <sub>3</sub> in <i>E.coli</i> EcAB4-5 mutant.....	71
Figure 27. Growth curves of <i>E.coli</i> . ....	72
Figure 28. Michaelis-Menten equation fitted curve .....	75
Figure 29. Double-reciprocal analysis of competitive inhibition.....	78
Figure 30. Double-reciprocal analysis of uncompetitive inhibition.....	79
Figure 31. Double-reciprocal analysis for pure non-competitive inhibition.....	80
Figure 32. Illustration of ME conversion into MEP and CDP-ME by IspD.....	81
Figure 33. Time course measurement of diphosphate production by IspD. ....	84
Figure 34. IspD kinetics using varied MEP concentrations. ....	85
Figure 35. IspD kinetics using varied CTP concentrations.....	86
Figure 36. LC-MS analysis of MEP-N <sub>3</sub> conversion by IspD.....	87
Figure 37. IspD kinetics using varied MEP-N <sub>3</sub> concentrations. ....	88
Figure 38. Comparison of IspD reaction in the presence or in the absence of MEP-N <sub>3</sub> .....	89
Figure 39. IspD inhibition by MEP-N <sub>3</sub> (MEP as a varied substrate). ....	90
Figure 40. IspD inhibition by MEP-N <sub>3</sub> in double reciprocal form (MEP was varied) .....	90
Figure 41. Slope replot of double reciprocal analysis (MEP as a varied substrate).....	91
Figure 42. Intercept replot of double reciprocal analysis (MEP as a varied substrate).....	92
Figure 43. IspD inhibition by MEP-N <sub>3</sub> (CTP as a varied substrate). ....	92
Figure 44. IspD inhibition by MEP-N <sub>3</sub> in double reciprocal form (CTP varied).....	93

Figure 45. Slope replot of double reciprocal analysis (CTP as a varied substrate).....	94
Figure 46. Intercept replot of double reciprocal analysis (CTP as a varied substrate) .....	94
Figure 47. Structure of <i>E.coli</i> IspD enzyme inhibitors. ....	95
Figure 48. Determination of $V_{max}$ and $K_m$ values using Dalziel's method when A is varied substrate.....	99
Figure 49. Double reciprocal plot of IspD kinetics (MEP as a varied substrate).....	100
Figure 50. Slope replot of double reciprocal analysis (MEP as a varied substrate).....	100
Figure 51. Intercepts replot of primary double reciprocal plot (MEP as a varied substrate).	101
Figure 52. Double reciprocal plot of IspD kinetics (CTP as a varied substrate).....	101
Figure 53. Slope replot of double reciprocal analysis (CTP as a varied substrate).....	102
Figure 54. Intercept replot of double reciprocal analysis (CTP as a varied substrate). ....	103
Figure 55. Examples of chemotherapy agents. ....	105
Figure 56. Examples of anticancer drugs .....	106
Figure 57. Structure and mechanism of ADC .....	107
Figure 58. Examples of chemical conjugation .....	108
Figure 59. Structure of APN and its derivatives. ....	109
Figure 60. Possible azide tagged MEP analogues for further metabolic studies. ....	112
Figure 61. MEP-N <sub>3</sub> molecule docked in IspD with ME-CDP .....	113
Figure 62. Second order rate constant determination.....	132
Figure 63. MS scans (SIR mode) of clicked product <b>69</b> in bacterial lysate for determination of LOD.....	134
Figure 64. MS scans (SIR mode) of clicked product <b>69</b> in PBS for determination of LOD.	135

## List of equations

Equation 1 and 1'. Michaelis-Menten equation and its reciprocal form.....	74
Equation 2. Rate equation of competitive inhibition.....	77
Equation 3. Rate equation of competitive inhibition in double reciprocal form.....	77
Equation 4. Rate equation of uncompetitive inhibition.....	78
Equation 5. Rate equation of uncompetitive inhibition in double reciprocal form.....	78
Equation 6. Rate equation of non-competitive inhibition .....	80
Equation 7. Rate equation of non-competitive inhibition in double reciprocal form .....	80
Equation 8. Rate equation for substrate inhibition in Michaelis-Menten form.....	87
Equation 9 and 9'. Rate equation of sequential mechanism in double reciprocal form.....	97
Equation 10 and 10'. Expression of equation 9 and 9' when $1/[V]$ plotted as a function of $1/[A$ or $1/[B]$ .....	97
Equation 11 and 11'. Slope replot from equation 10 and 10' .....	98
Equation 12 and 12'. Intercept replot from equation 10 and 10' .....	98

## List of abbreviations

Ac	Acetyl
AMP	Adenosine monophosphate
ATP	Adenosine triphosphate
$\alpha$	alpha
$^{13}\text{C}$	Carbon 13 isotope
$\delta$	Chemical shift
$J$	Coupling constant
CTP	Cytidine triphosphate
Da	Dalton
DNA	Deoxyribonucleic acid
DCM	Dichloromethane
DCC	Dicyclohexylcarbodiimide
DIBALH	Diisobutylaluminium hydride
DMAP	4-dimethylaminopyridine
DMF	Dimethylformamide
DMSO	Dimethylsulfoxide
d	Doublet
dd	Doublet of doublet
ENDOR	Electron nuclear double resonance
EPR	Electron paramagnetic resonance
ESI	Electron spray ionisation
<i>E.coli</i>	Escherichia Coli
Et	Ethyl
g	Gramme

IC <sub>50</sub>	Half maximal inhibitory concentration
Hz	Herz
HPLC	High Performance Liquid Chromatography
<sup>1</sup> H	Hydrogen 1 isotope
HYSCORE	Hyperfine sub-level correlation
IR	Infrared
kDa	Kilodalton
LC	Liquid chromatography
L	Litre
LB	Lysogeny Broth
MS	Mass spectrometry
m/z	Mass to charge ratio
MHz	Mega Herz
m-CPBA	Metachloro per benzoic acid
Me	Methyl
μL	Microlitre
μM	Micromolar
mU	Milli unit
mg	Milligramme
mL	Millilitre
mM	Millimolar
mmol	Millimole
min	Minute
M	Mole
MS	Molecular sieve

m	Multiplet
NMO	N-methylmorpholine 4-Oxide
nm	Nanometre
NADP	Nicotinamide adenine dinucleotide phosphate
NMR	Nuclear magnetic resonance
OD	Optical density
Ph	Phenyl
PBS	Phosphate buffered saline
<sup>31</sup> P	Phosphorus 31 isotope
pH	Potential of hydrogen
RNA	Ribonucleic acid
r.t	Room temperature
rpm	Rounds per minute
s	Singlet
t-BuOH	Tert-butanol
TBSCl	Tert-butyl dimethyl silyl chloride
TBAF	Tetrabutyl ammonium fluoride
THF	Tetrahydrofuran
TPAP	Tetrapropyl ammonium perruthenate
TLC	Thin layer chromatography
tRNA	Translational ribonucleic acid
TMSBr	Trimethyl silyl bromine
t	Triplet
UV	Ultra violet

## Abstract

Isoprenoids are present in every organism and synthesised through the mevalonate or the Methylerythritol phosphate (MEP) pathways. The latter pathway has been discovered in the late 80s and since has been studied intensively. Most of the deadly pathogenic microorganisms including *Mycobacterium tuberculosis* (bacteria responsible for tuberculosis) and *Plasmodium falciparum* (parasite responsible for malaria) utilise solely the MEP pathway for the biosynthesis of their isoprenoids whereas humans exclusively use the mevalonate pathway. This feature makes the MEP pathway an attractive target for antibacterial or antiparasitic drug development.

In order to study the pathway further, ME-N<sub>3</sub> as a MEP pathway intermediate analogue was synthesised and its incorporation into the pathway was studied by virtue of metabolic labelling approach using bioorthogonal ligation reaction. No tagged metabolite was detected and this could be due to several reasons such as non-permeability of ME-N<sub>3</sub> through cell membrane or ME-N<sub>3</sub> is a poor substrate of the enzyme.

IspD, 3<sup>rd</sup> enzyme of the MEP pathway, catalyses the conversion of MEP into CDP-ME (Cytidine diphosphate methylerythritol). MEP-N<sub>3</sub>, as an azide tagged MEP analogue, was prepared and found to be converted by IspD. Moreover, the IspD kinetics for MEP-N<sub>3</sub> were further investigated and led to the conclusion that MEP-N<sub>3</sub> was indeed an inhibitor with highest inhibitory activity among the known inhibitors of *E.coli* IspD.

The catalytic mechanism of IspD was investigated using steady state kinetic analysis for the first time. It was found that IspD catalyses the reaction in ordered sequential mechanism confirming the previous literature result obtained by pulse-chase experiment.

In the last part of the thesis, novel antibody drug conjugate (ADC) linkers, that are based on APN (3-arylpropionitrile) which was previously discovered and exploited in our laboratory, were synthesised and examined *in vitro*. Newly prepared linkers were found to be superior to commercially available linkers in terms of stability in the plasma and efficiency.

## Acknowledgement

First of all, I would like to thank to my supervisors, Dr Alain Wagner and Dr Myriam Seemann, for their guidance, training and teaching throughout my study period. I am glad that you have been most patient with me and allowed me to go until the end of my PhD study.

I would also like to thank to the International Centre for Frontier Research in Chemistry for funding my project. I would like to thank to my defence committee members that include Dr Joelle Dubois and Professor Alain Burger for accepting to evaluate my work and their interest in my project.

A very special gratitude goes to my family. My mother Tsetsegdari Sengebat who devoted her life for her children's bright future and better life. My brother Azjargal Tsetsegdari and his family – without whom it would be impossible to obtain my educations. My fiancée Urangoo Bars who encouraged me when I fail, shared my griefs and joys in the times of sorrow and happiness. You have become an inseparable part of my life and I could not successfully conclude my study without your help and support. I would also like to thank to my family members in Mongolia, specially to my grandmother Sumya Dendev and my aunt Oyuntuya Dugajii as well as her husband Ganzorig Tsambajav.

I am grateful to our laboratory members in Illkirch campus: Michel Mosser, Eric Thomas, Dr H el ene Steffner, Dr Isabel Kuhn, Dr S ebastien Dautrey, Elisabetta Tobaldi, Igor Dovgan and Dr Sylvain Ursuegui – thank you for being nice to me. Also previous lab members (Dr Marion Recher, Dr Oleksandr Koniev, Dr Sergii Kolodych, Dr Corinne Baehr and Dr Sylvain Jacques) who helped me during my initial study period of unknown and curiosity. I am also grateful to laboratory members in Esplanade campus: Dr Philippe Chaignon who provided a lot of supports to my project and Magali Parris e who trained me in biological experiments and assisted in my research. I would also like to thank to Dr Patrick Neuberg, Manon Ripoll, C elia Jacobberger and Alexandre Hardy for their help with my research. I am also grateful to Dr Jean-Luc Ferrer and Franck Borel (IBS, Grenoble) for their contribution to my project.

Finally, I am also grateful to all the local Mongolian families in Strasbourg with special mention to families of Khasar Lkhagvasuren and Saranbat Tseedamdin. I am glad that you all have been supporting me throughout my study and together we shared plenty of memorable days.

# CHAPTER-1

## Introduction

## 1.1 Isoprenoid Biosynthesis

Isoprenoids are the most diverse family of natural compounds with more than 50000 members found in all three domains including eubacteria, archaebacteria and eukaryotes.<sup>15, 16</sup> They play important metabolic, regulatory and structural roles in biological systems. For example, ubiquinone and menaquinones are involved in electron transport while cholesterol is involved in cell wall and membrane biosynthesis as well as precursor to bile acids.<sup>17, 18</sup> Because of their unique characteristics, isoprenoids have also been used by humans as odour compounds such as menthol or pharmaceuticals as in the case of paclitaxel or materials like polyisoprenoid rubber.<sup>19</sup> (Figure 1)

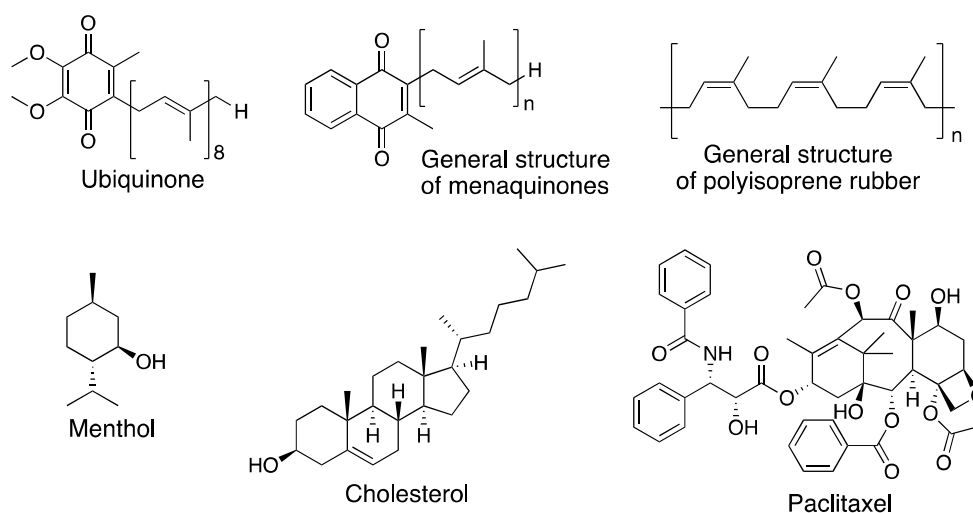
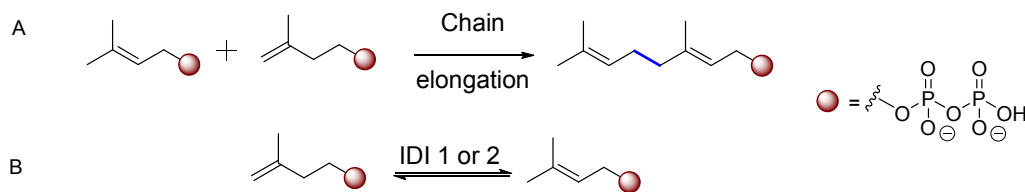


Figure 1. Some example of isoprenoids.

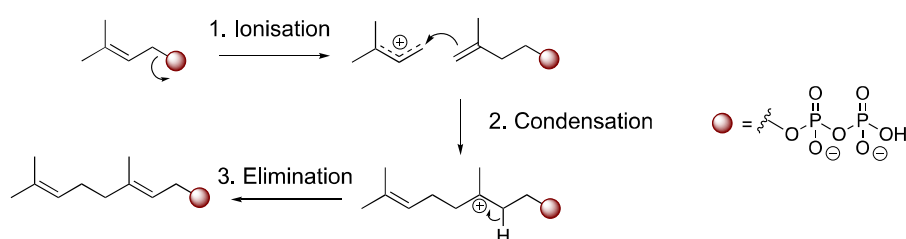
Despite their diversity, all isoprenoids derive from five carbon precursor units: isopentenyl diphosphate (IPP) and dimethylallyl diphosphate (DMAPP) (Figure 2). Both DMAPP and IPP are supplied through two distinct pathways: The mevalonate pathway and the Methylerythritol Phosphate (MEP) pathway. In contrast to the mevalonate pathway, the MEP pathway yields a mixture of IPP and DMAPP in a 5:1 ratio. This ratio can be explained by IPP being the main elongation unit which is added to DMAPP, hence more IPP is needed for chain elongation reaction. On the other hand, the mevalonate pathway produces IPP which is further converted into DMAPP by isopentenyl diphosphate isomerase (IDI) (Scheme 1, B).<sup>19</sup> Currently two types

of IDI enzymes are known: IDI type 1 and 2. IDI-1 had been discovered in the late 1950s<sup>20</sup> and IDI-2 was reported more recently in 2001.<sup>21</sup>



Scheme 1. A. Mechanism of first step of chain elongation. B. Isomerisation of IPP.

These two building blocks (IPP and DMAPP) condense with each other and the chain elongates. This chain elongation process is catalysed by chain-length selective prenyltransferases. The first step in chain elongation proceeds via head-to-tail directed 1-4 addition of IPP to DMAPP followed by elimination of diphosphate and this process is repeated further (Scheme 1, A). Poulter and co-workers have contributed substantially in terms of studying the general mechanism of prenyltransferases. Through their research, they have found that prenyltransferases catalyse the polyisoprenoid chain elongation reaction in three formal steps: 1-Ionisation of DMAPP, 2- Nucleophilic addition of IPP to ionised DMAPP and 3- Elimination of a proton to form a double bond.<sup>22-25</sup> (Scheme 2).



Scheme 2. A. Ionisation-Condensation-Elimination mechanism.

A raw illustration of polyisoprenoid chain elongation reaction is depicted in Figure 2 below.

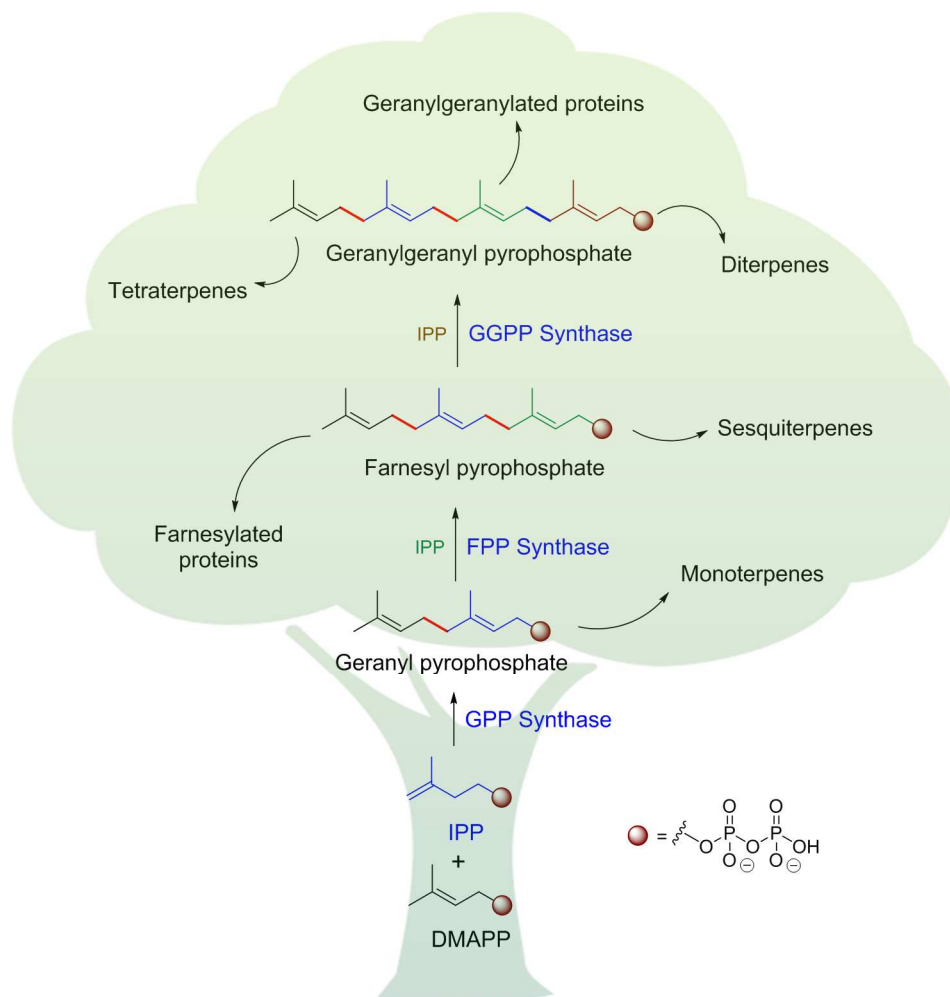


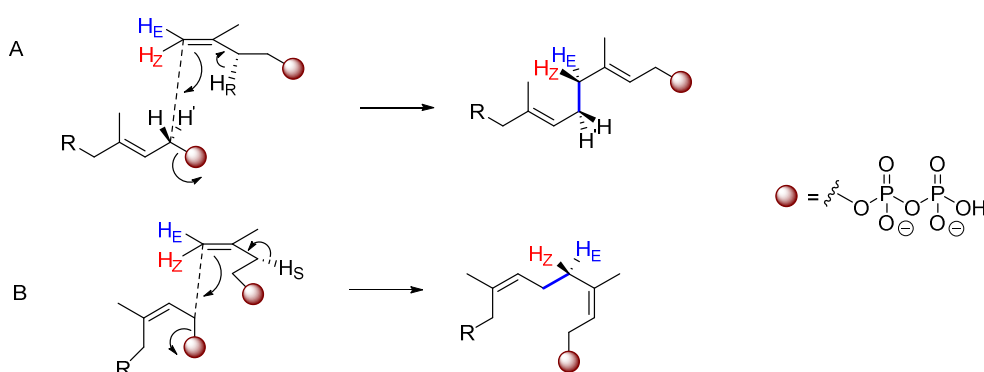
Figure 2. Chain elongation of isoprene units.<sup>26</sup>

According to Ogura and Koyama, prenyltransferases are classified into four different groups.<sup>27</sup>

- Prenyltransferase I (short chain prenyl diphosphate synthase)
- Prenyltransferase II (medium chain prenyl diphosphate synthase)
- Prenyltransferase III (long chain (*E*) - prenyl diphosphate synthase)
- Prenyltransferase IV (*Z*) - polyprenyl diphosphate synthase)

Geranylpyrophosphate synthases (GPP synthase) are included in the first class of prenyltransferases with homodimeric structure. This type of enzymes are found in plants, bacteria and mammals. Prenyltransferase II is mostly found in bacteria and elongates the chain

up to C<sub>35</sub> with (*E*)-selective character. The next class (prenyltransferase III) of enzyme elongates chain up to C<sub>50</sub> and a good example is solanesyl diphosphate synthase which elongates GPP up to C<sub>45</sub>-PP. Prenyltransferase IV synthesises (*Z*)-prenyl chains with roles to generate polyprenyl lipids which are carbohydrate transporters in the biosynthesis of bacterial cell wall and eukaryotic glycoproteins. An example of this type of enzyme is undecaprenyl diphosphate synthase which adds IPP to all (*E*) – farnesyl moiety to produce C<sub>55</sub> prenyl diphosphate with (*E*) and (*Z*) mixed stereochemistry.<sup>27</sup> The stereochemistry of (*E*) and (*Z*) selective prenyltransferase reaction is depicted in Scheme 3.



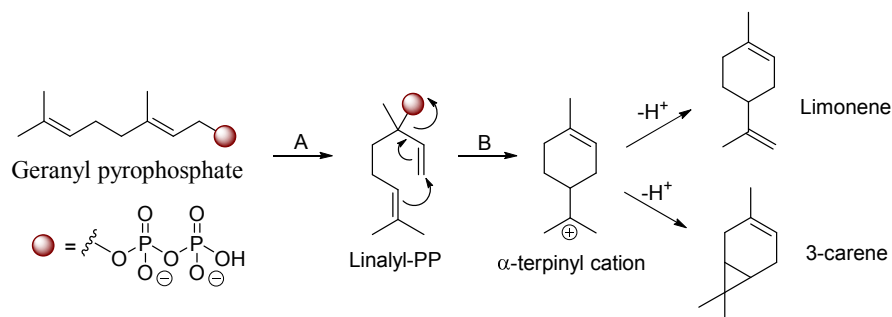
Scheme 3. Stereochemistry of chain elongation by prenyltransferases.<sup>19</sup>

(*E*)- selective reaction proceeds as follows (Scheme 3, A): An inversion of configuration occurs at C-1 atom (carbon atom bound to the diphosphate moiety) of the polyisoprenoid chain upon C-C bond formation by nucleophilic attack from IPP<sup>28,29</sup> followed by the stereospecific removal of 2-pro-R proton of IPP to form (*E*) isomer. In contrast to (*E*) selective reaction, the (*Z*) selective reaction occurs via removal of 2-pro-S proton from IPP.<sup>30</sup> (Scheme 3, B)

Another interesting point in polyisoprenoid chain elongation reactions is how the chain length is determined. Previous studies suggested that the length of the polyisoprenoid chain depends mainly on the size of the hydrophobic pocket of the enzyme.<sup>31</sup>

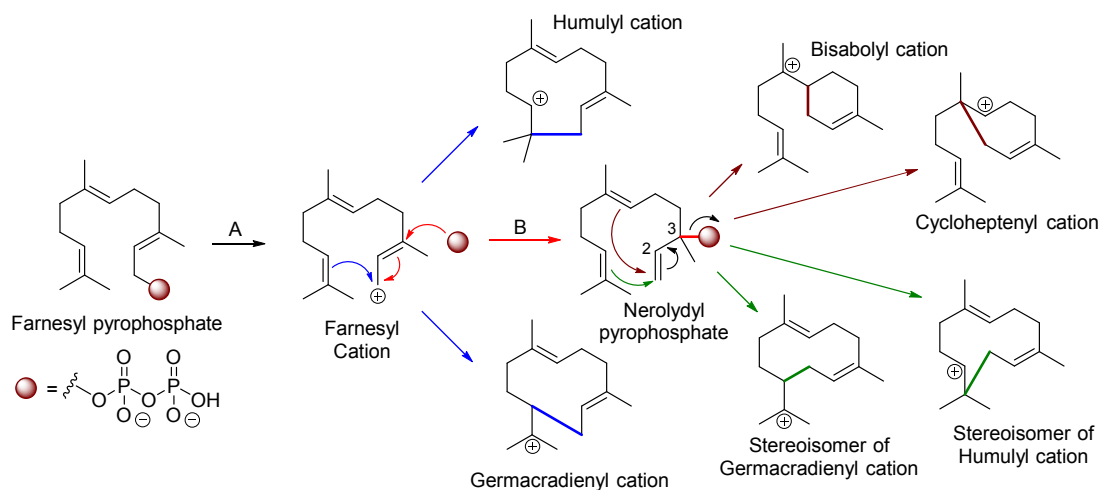
From chain elongated polyisoprenoid chains, the corresponding terpenes are synthesized through multiple stereocontrolled cyclisation reactions. Due to the large number of known isoprenoids, only the biosynthesis of a selection of isoprenoids will be described in the following contexts.

Monoterpenes are synthesized via enzymes known as monoterpene cyclases. Monoterpene synthesis from geranylpyrophosphate (GPP) starts with abstraction of the diphosphate moiety and re-attack of diphosphate on C-3 carbon to generate linalyl diphosphate which is further cyclised to form  $\alpha$ -terpinyl cation. This cation is the main intermediate for the synthesis of other monoterpenes such as 3-carene and limonene that are both formed by deprotonation of the  $\alpha$ -terpinyl cation.<sup>32</sup>



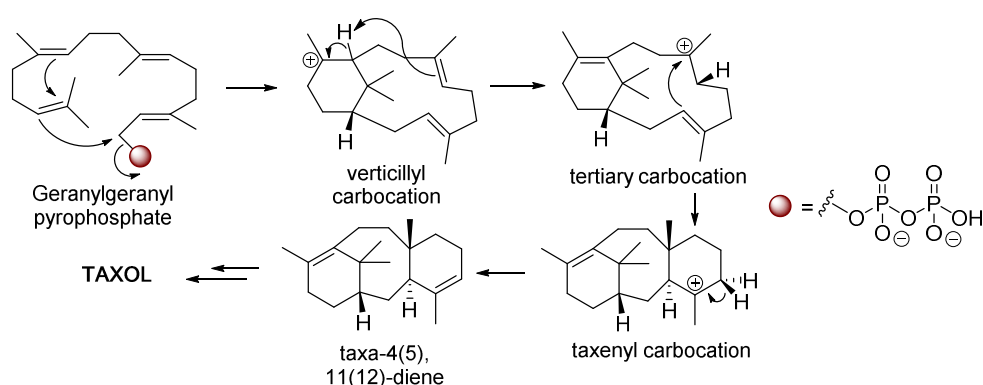
Scheme 4. Monoterpene synthesis. A) Formation of linalyl pyrophosphate. B) Formation of  $\alpha$ -terpinyl cation.

Sesquiterpene synthesis also proceeds in a similar manner as monoterpene synthesis. The cyclisation of farnesyl diphosphate can proceed via different routes as depicted in Scheme 5. The first step is the formation of the farnesyl cation by abstraction of the diphosphate moiety. There are several ways for this farnesyl cation to further cyclise to sesquiterpenes. First the farnesyl cation can be directly cyclised to humulyl cation or germacradienyl cation. Second, it can be re-attacked by a diphosphate moiety to form an intermediary molecule nerolydyl pyrophosphate which is a pre-requisite for further cyclisation products such as bisabolyl cation, cycloheptenyl cation. To produce bisabolyl and cycloheptenyl cations, initial C-2,3 bond rotation has to occur to achieve the cyclisation. The intermediary molecule nerolydyl pyrophosphate can also be cyclised to form stereoisomers of humulyl and germacradienyl cations after C-2,3 bond rotation is achieved.<sup>19,33</sup>



Scheme 5. Sesquiterpene biosynthesis. A) Formation of the allylic farnesyl cation. B) Formation of nerolydyl pyrophosphate.

One famous diterpene is Paclitaxel which is used as an anticancer agent and first isolated from *Taxus brevifolia*.<sup>34</sup> Taxadiene synthase is an enzyme responsible for the first committed steps of paclitaxel biosynthesis starting from geranylgeranyl pyrophosphate (GGPP). In the first step of paclitaxel biosynthesis, verticillyl carbocation forms from GGPP. In the next step, a rapid intramolecular proton transfer takes place to form a tertiary carbocation intermediate which further undergoes ring closure reaction to produce taxenyl carbocation. The abstraction of H-5 $\beta$  proton finishes the cascade reactions to form taxa-4(5), 11(12)-diene.<sup>35, 36</sup> (Scheme 6)

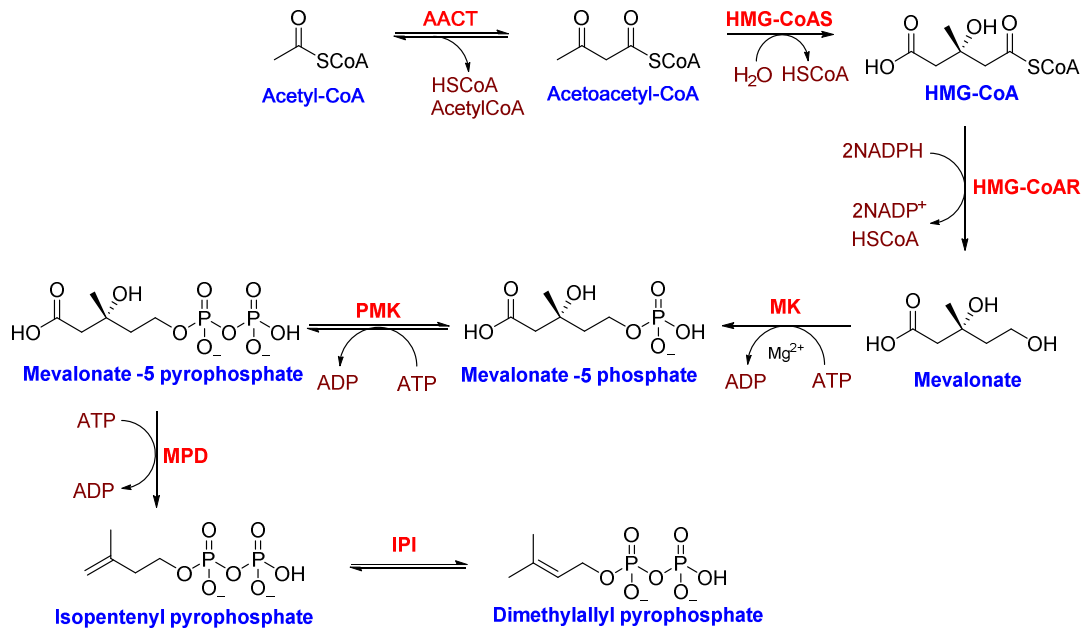


Scheme 6. First committed steps of Paclitaxel biosynthesis<sup>35</sup>

Although biosynthesis of isoprenoids has been studied extensively, it is challenging to uncover every isoprenoid biosynthetic mechanism because of their vast numbers and complexity. Their diversity is due to a cascade of cyclisations via cationic intermediates. A cationic intermediate can be attacked by one of double bonds in polyisoprenoid chain to form a cyclic product but these cyclisation reactions can proceed with different regio and stereo-selectivities which explains why a myriad of isoprenoids exist.

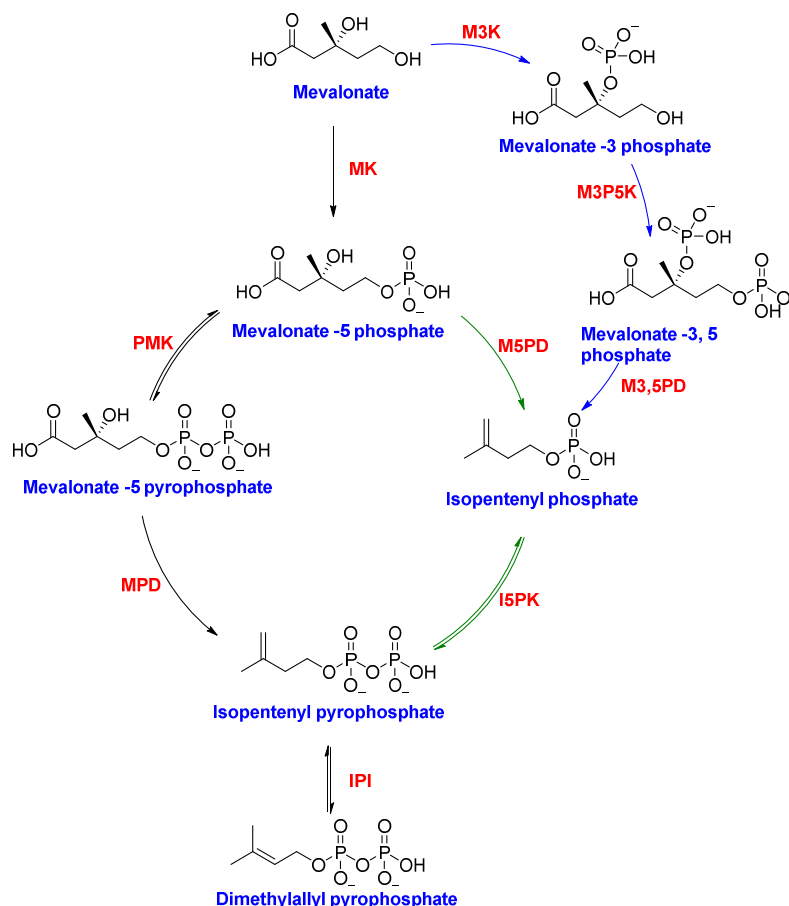
## 1.2 Mevalonate Pathway

As mentioned above, the two main building blocks for isoprenoid biosynthesis are Isopentenyl pyrophosphate (IPP) and Dimethylallyl pyrophosphate (DMAPP) which are supplied via two distinct pathways one of which, the mevalonate pathway, had been known since the late 50's. This pathway is primarily used by animals, fungi, other eukaryotes, archaea and a few bacteria. The pathway uses acetyl-CoA as a carbon source.<sup>37</sup> It starts with Claisen condensation of two molecules of acetyl-CoA by the enzyme acetoacetyl coenzyme-A thiolase (AACT) and the condensed product further converts into 3-hydroxy-3-methylglutaryl-CoA (HMG-CoA) via another condensation with acetyl-CoA catalysed by hydroxymethylglutaryl-CoA synthase (HMG-CoAS). The conversion of HMG-CoA into mevalonate proceeds via two successive reductions. The mevalonate is then phosphorylated by mevalonate kinase (MK) which transfers  $\gamma$ -phosphate group of ATP onto C5 hydroxyl group to produce mevalonate-5-phosphate. Phosphomevalonate kinase (PMK) further catalyses a reversible reaction in which mevalonate-5-phosphate is transformed into mevalonate-5-pyrophosphate. This product is later converted into isopentenyl diphosphate via an ATP dependent enzyme: mevalonate pyrophosphate decarboxylase (MPD).<sup>38</sup> Isopentenyl diphosphate can then be isomerised by isopentenyl diphosphate isomerase (IDI) to form dimethylallyl pyrophosphate (DMAPP). The mevalonate pathway is illustrated in the Scheme 7 below.



Scheme 7. Mevalonate pathway

Although this classical mevalonate pathway is well studied in most eukaryotes, recent studies revealed that the genes encoding PMK and MPD enzymes were not detectable in most archaea.<sup>39</sup> This observation raised a question whether these reactions are catalysed by non orthologous enzymes *i.e* there is an alternative pathway to produce IPP. By studying the kinase of *Methanocaldococcus jannaschii*, Grochowski *et al*<sup>40</sup> were able to identify an alternative route in the mevalonate pathway. Previous comparative genomic studies of archaea with respect to the mevalonate pathway allowed the identification of MJ0044 gene of which product is a kinase enzyme in the new route.<sup>41</sup> During their study, Grochowski *et al*, attempted to perform an enzymatic reaction with MJ0044 gene product in the presence of mevalonate and mevalonate-5 phosphate but they were unable to detect the enzymatic product. Then they speculated the gene product is perhaps a kinase (I5PK, Isopentenyl 5-phosphate kinase) which transforms isopentenyl phosphate into IPP and finally they proved it experimentally. This result confirms that there is a deviation route in the classical mevalonate pathway to produce IPP.<sup>40</sup> (Scheme 8)



Scheme 8. Alternate mevalonate pathways. Black arrows - Classical mevalonate pathway. Green and Blue arrows - Alternate mevalonate pathways.

Later, Chen *et al* were able to identify this kinase from *Methanothermobacter thermautotrophicus* and *Thermoplasma acidophilum* and characterized the enzyme kinetics. They suggested that the occurrence of I5PK homologues in a variety of archaea shows that this new route is the dominant pathway in these organisms.<sup>42</sup> The alternative route in the mevalonate pathway is illustrated in Scheme 8.

Although I5PK protein was reported by several research groups, there has been no evident research on a protein that decarboxylates mevalonate-5 phosphate to produce isopentenyl phosphate. It was speculated that it is surely a decarboxylase enzyme. VanNice *et al* were first to conduct such research on this putative decarboxylase together with the kinase enzyme of *Haloflex volcanii*. They have identified that HVO1412 gene encodes the M5PD enzyme in *H.volcanii*.<sup>43</sup>

When studying Ta1305 gene from *Thermoplasma acidophilum*, which was annotated as MPD enzyme, Vinokur *et al* discovered that this protein converts mevalonate into mevalonate-3 phosphate (Scheme 8. Route directed by blue arrows). Moreover, they have also identified the second enzyme which is responsible for the conversion of mevalonate-3 phosphate into mevalonate 3,5-diphosphate. These two new enzymes were further characterised but the conversion of mevalonate 3,5-diphosphate into isopentenyl phosphate still remains as a question.<sup>44</sup>

### 1.3 Methylerythritol Phosphate (MEP) Pathway

Compared to the mevalonate pathway, the MEP pathway was discovered more recently. Scientists had been studying the mevalonate pathway using isotopically labelled tracers but in many cases it was observed that a tracer incorporation was inconsistent with the mevalonate pathway in some organisms. Early studies in the late 1950s showed that 2-<sup>14</sup>C-mevalonate and 2-<sup>14</sup>C-acetate did not appear to be incorporated into  $\beta$ -carotene of *Chlorella pyrenoidosa* and maize seedlings respectively when fed. It was also noticed that these labelled components did not successfully incorporate into vitamin K<sub>2</sub> of *Mycobacteria* as expected.<sup>45-47</sup> In early 1980s, possibility of a potential new pathway existence in bacteria was raised based on incorporation studies and it was named acetolactate pathway but later studies contradicted this finding.<sup>48, 49</sup> Ultimately, in the late 1980s, Rohmer and Arigoni with their co-workers described the novel pathway of isoprenoid biosynthesis independently.<sup>3, 50, 51</sup> Rohmer *et al* performed <sup>13</sup>C labelled glucose feeding experiments using the bacteria *Zymomonas mobilis*. The glucose is metabolised in this bacteria according to the Entner-Doudoroff pathway.

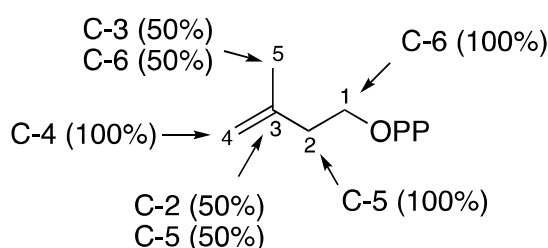
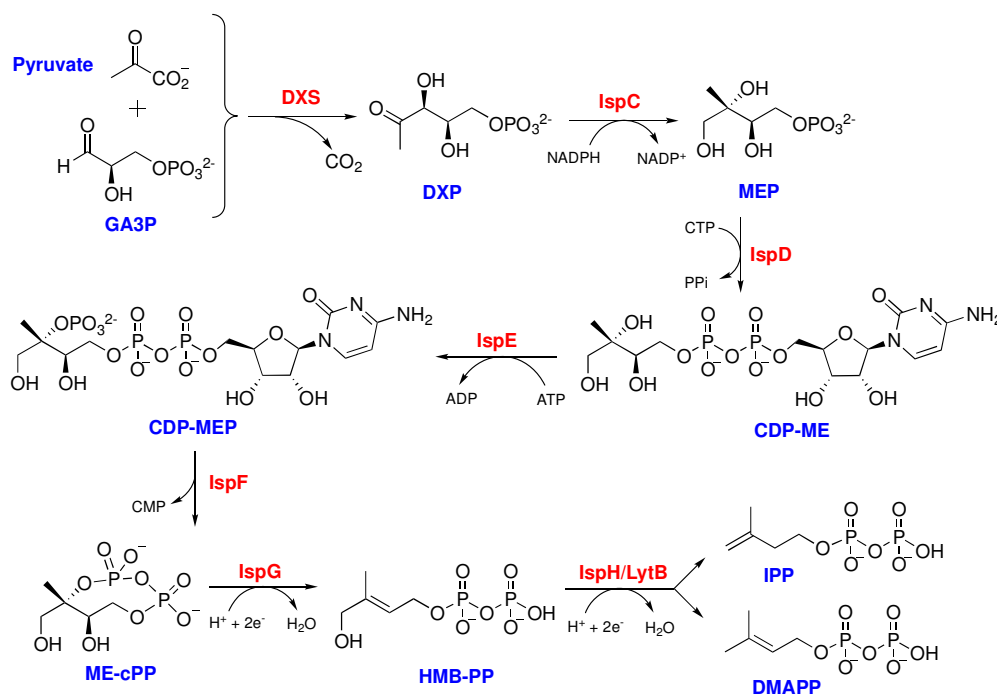


Figure 3. IPP carbon atom origin from <sup>13</sup>C labelled glucose

After feeding *Z.mobilis* with  $^{13}\text{C}$  labelled glucose at C-1, C-2, C-3, C-5 or C-6 positions and analysis of the isolated hopanoids, it could be determined that C-1, C-2 and C-4 of IPP were derived from C-6, C-5 and C-4 of glucose respectively. C-3 of IPP was found to be derived equally from C-2 or C5 of glucose while C-5 of IPP was equally derived from C-3 or C-6 of glucose. (Figure 3)

This result suggests that pyruvate is the source of  $\text{C}_2$  subunit and a triose phosphate is the source of  $\text{C}_3$  subunit of the IPP molecule.<sup>3, 52</sup> The triose phosphate was further shown to be glyceraldehyde 3-phosphate.<sup>53</sup> Since its discovery, the MEP pathway has been extensively studied and all enzymes and substrates are known to date. The MEP pathway is illustrated in Scheme 9.

The MEP pathway starts with the condensation of glyceraldehyde 3-phosphate (GA3P) with pyruvate to form 1-deoxy-D-xylulose 5-phosphate (DXP). Then DXP is converted into 2-C-methyl-D-erythritol 4-phosphate (MEP) which is further transformed into 4-diphosphocytidyl-2-C-methyl-D-erythritol (CDP-ME). CDP-ME is then phosphorylated to form 4-diphosphocytidyl-2-C-methyl-D-erythritol 2-phosphate (CDP-MEP).



Scheme 9. MEP pathway.

In the next step, cytidyl monophosphate (CMP) is released to produce 2-C-methyl-D-erythritol-2,4 cyclopyrophosphate (ME-cPP). This product is further converted by an oxygen sensitive enzyme IspG which catalyses the formation (*E*)-4-hydroxy-3-methyl-but-2-enyl diphosphate (HMB-PP). The last step of the MEP pathway entails simultaneous production of IPP and DMAPP via an another oxygen sensitive IspH enzyme. The MEP pathway enzymes and their catalytic mechanisms will be covered in the following contexts.

## 1.4 MEP pathway enzymes

### 1.4.1 1-Deoxy-D-xylulose 5-phosphate synthase (DXS)

The first identification of the DXS enzyme was reported by Sprenger *et al* in 1997.<sup>54</sup> In their study they hypothesised that formation of DXP requires decarboxylation of pyruvate. It is well known that this type of reaction is usually performed by thiamine pyrophosphate (TPP) dependent enzymes like the pyruvate dehydrogenase complex or transketolases which could catalyse transfer of acetaldehyde group from pyruvate to GA3P. Therefore, the unknown enzyme should share sequence motifs with these two types of enzymes.

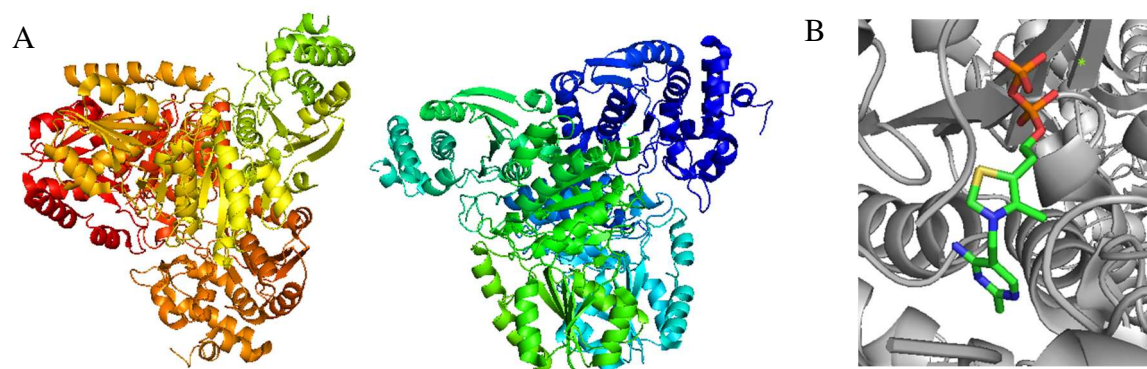
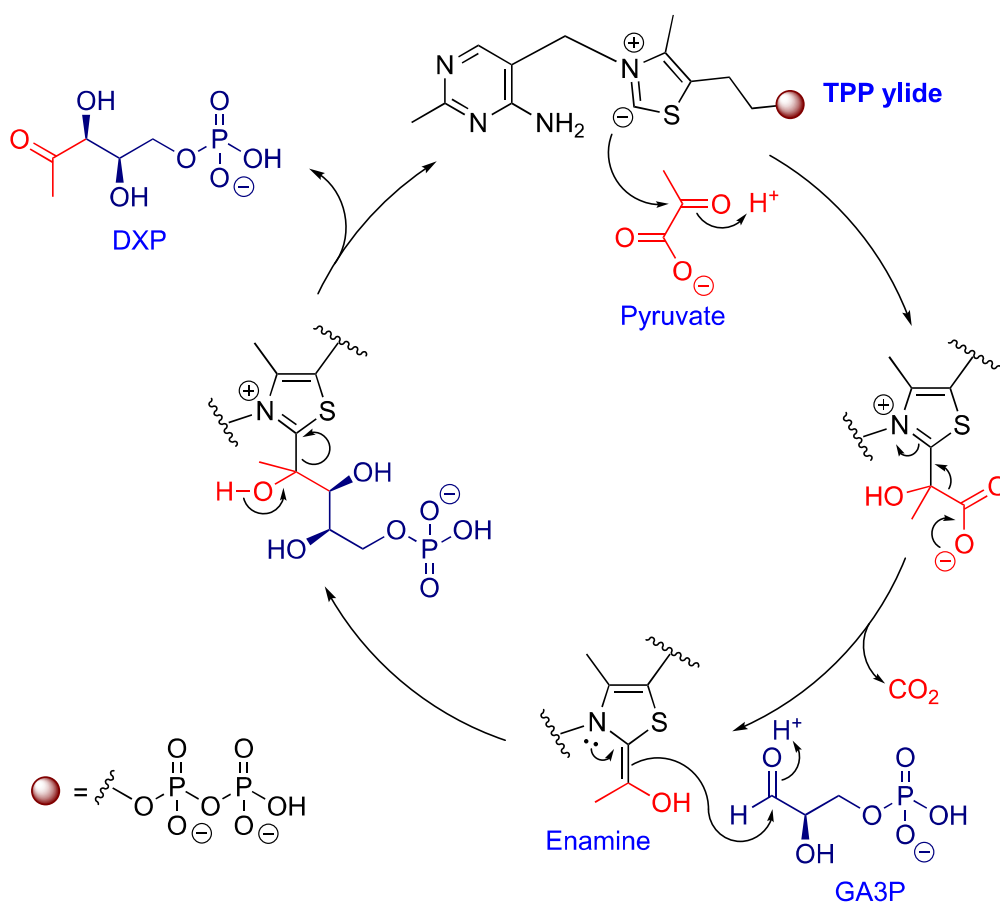


Figure 4. Crystal structure of *E.coli* DXS enzyme. A) Dimer structure of DXS. B) Cofactor TPP situated in its binding pocket. (Protein Data Bank ID 2O1S).

Using a bioinformatics approach, the authors identified, on *E.coli* chromosome, an enzyme that could catalyse DXP formation. They have cloned this gene, overexpressed and purified the corresponding protein. They proved that this enzyme yields DXP from pyruvate and GA3P

with thiamine pyrophosphate as a cofactor.<sup>54</sup> To date, crystal structures of DXS from two different bacterial species, *E.coli* and *Deinococcus radiodurans*, have been reported in the Protein Data Bank (PDB). The enzyme exists as a tightly associated dimer and the monomer entails 3 domains. The active site is situated at the intersection of domain I and II within the same monomer and has no direct contribution from the other monomer.<sup>55</sup> Structure of *E.coli* DXS enzyme is shown in Figure 4.

The mechanism of thiamine pyrophosphate (TPP) dependent acyloin condensation reaction has been well studied in numerous bacterial species. Prior to the substrate binding, an activation of cofactor TPP is required which proceeds via deprotonation of C-2 hydrogen of thiazolium ring by an adjacent N-4 of pyrimidinium ring and this deprotonation process becomes feasible when the molecule adopts so called V shaped conformation.<sup>56</sup> (Scheme 10)



Scheme 10. Catalytic mechanism of DXS in the presence of Thiamine pyrophosphate

The activated TPP is now able to make a nucleophilic attack on pyruvate yielding an enamine which further attacks on GA3P to form a TPP adduct that will release DXP upon its collapse.<sup>56</sup>  
<sup>57</sup> The mechanism of DXP production has been thought to be proceeding via ping-pong mechanism<sup>58</sup> (pyruvate binding and CO<sub>2</sub> release after which GA3P binding) but sequential mechanism (pyruvate binding and GA3P binding after which CO<sub>2</sub> and DXP are released) was more consistent with later kinetic studies hence ping-pong mechanism was disproved.<sup>59-62</sup>

#### 1.4.2 1-deoxy-D-xylulose-5 phosphate reductase (IspC)

After having identified the first enzymatic product of the MEP pathway as DXP, the search for the second enzyme and its product was under scrutiny. Duvold *et al* hypothesised that 2-C-methylerythritol 4-phosphate could be the substrate of the second enzyme. Using deuterium labelled 2-C-methyl-D-erythritol they were able to detect incorporation of this molecule into the ubiquinone side chain produced by *E.coli*.<sup>63</sup> Later, Takahashi *et al* determined the gene that encodes the protein that catalyses the formation of 2-C-methyl-D-erythritol 4-phosphate. They found that the synthesis of 2-C-methyl-D-erythritol 4-phosphate was impaired in an *E.coli* mutant harbouring a deletion in the *yeaM* gene. Overexpression of this gene product was found to catalyse MEP formation from DXP in the presence of NADPH and a divalent cation such as Mg<sup>2+</sup> and Mn<sup>2+</sup>.<sup>64</sup> The structure of *E.coli* IspC is shown in Figure 5. *yeaM* gene product was called DXR or IspC.

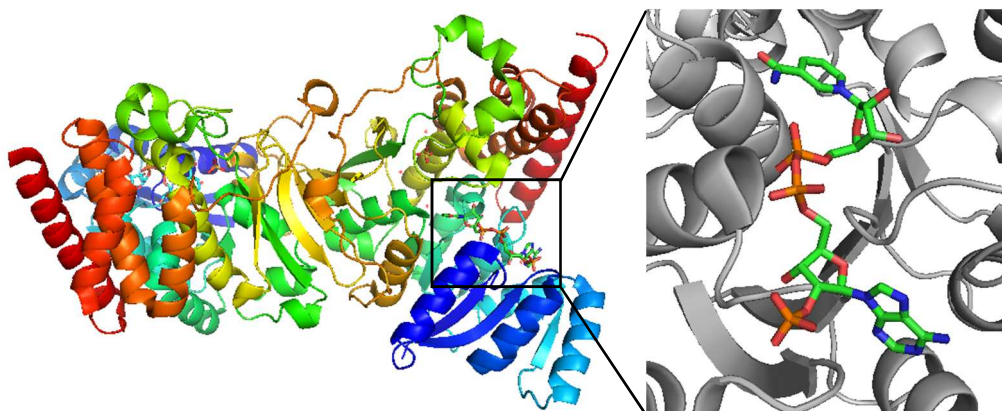
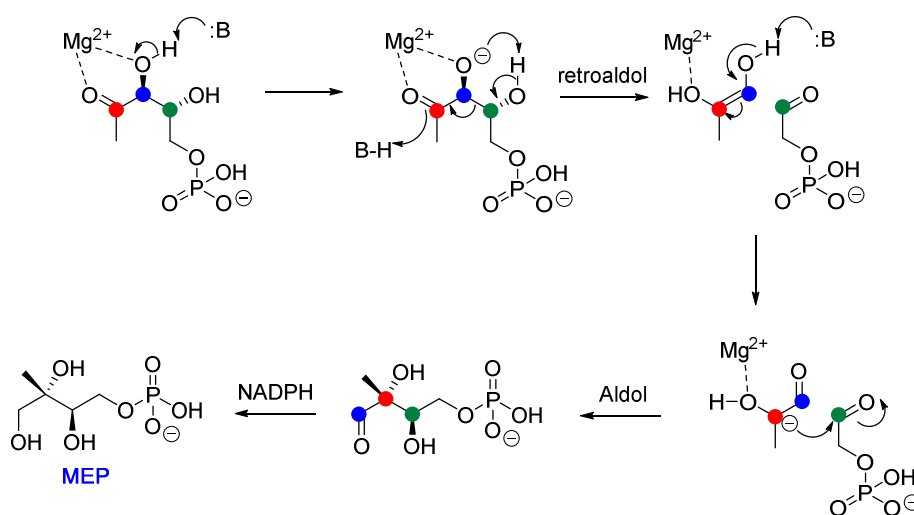


Figure 5. Crystal structure of *E.coli* IspC. Enzyme with the cofactor NADPH bound inside. (PDB ID 1JV)

Before the identification of genes encoding IspC, it was proposed that mechanistically a rearrangement should occur during catalysis. The reaction requires a cofactor NADPH and it is now shown to proceed in ordered mechanism where the cofactor and a metal ion binds first to the enzyme after which DXP binding occurs, followed by release of the product MEP and later NADP<sup>+</sup>.<sup>65</sup> The conversion of DXP into MEP could be achieved according to two ways. First proposition is  $\alpha$ -ketol rearrangement which basically suggests the cleavage of the C<sub>3</sub>-C<sub>4</sub> bond and the formation of a bond between C<sub>2</sub> and C<sub>4</sub>, with the two processes occurring simultaneously. The second proposition is a retro-aldol/aldol mechanism in which the same bond cleavage and the same bond formation take place but proceeds through the formation of two fragments (enolate form of hydroxyacetone and glycolaldehyde phosphate). Recent researches have confirmed the rearrangement does indeed proceed via retro-aldol/aldol mechanism.<sup>65-68</sup> The catalytic mechanism of IspC is illustrated in Scheme 11.



Scheme 11. Catalytic mechanism of IspC. Coloured dots represent C-2 (red), C-3 (blue), C-4 (green) atoms.

### 1.4.3 2-C-Methyl-D-erythritol cytidyltransferase (IspD)

Using radiolabelled MEP, Rohdich *et al* were able to partially purify an enzyme catalysing the transformation of MEP into an unknown metabolite, presumably a downstream enzymatic product. In their research, they have found that the reaction proceeds much better in the presence of CTP compared to ATP, which they initially added to the assay. After isolation of the unknown product that formed by a partially purified enzyme, NMR analysis revealed the structure of the product to be 4-diphosphocytidyl-2-C-methylerythritol. Using online database

search, Rohdich *et al* found that *ygbP* gene might code for the enzyme. Furthermore, this gene was also present in organisms that possess the MEP pathway but did not exist in archaea. This information leads the identification of the gene that encodes the *ygbP* protein later named IspD. *ygbP* protein from *E.coli* was overexpressed and shown to catalyse the formation of CDP-ME from MEP and CTP.<sup>69</sup> This result was simultaneously confirmed by the study of Kuzuyama *et al* using a strategy based on gene complementation for the missing parts of the pathway. The authors screened for *E.coli* mutants possessing metabolic blocks between MEP and IPP but engineered to harbour some genes of the mevalonate pathway so they were able to produce IPP from mevalonate. They found 33 mutants out of 60000 colonies that showed expected phenotypes: surviving only upon addition of mevalonate. After gene complementation, they identified the gene product that converted MEP into an unknown product in the presence of CTP and later confirmed that the unknown product was indeed CDP-ME.<sup>70</sup>

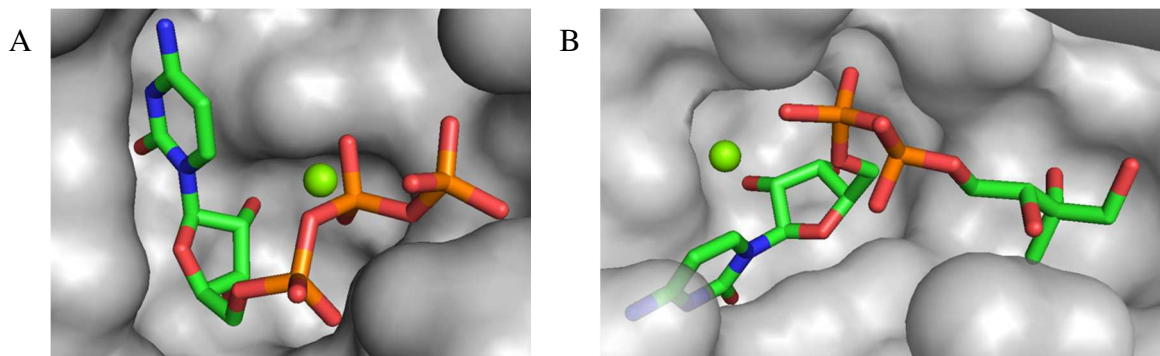
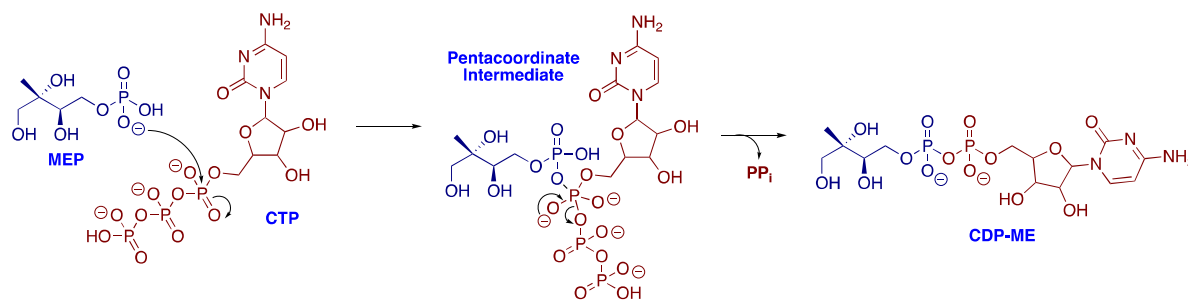


Figure 6. Crystal structure of substrate and product of *E.coli* IspD enzyme inside the catalytic pocket. A) CTP and Mg<sup>2+</sup> (green sphere), B) CDP-ME and Mg<sup>2+</sup> (green sphere). (PDB ID 1152 and 11N1)

To date numerous crystal structures of IspD from various bacterial species and plants have been determined. The mechanism of the enzyme has been studied and it was proposed to proceed via a sequential ordered mechanism. By using pulse-chase experiments, Richard *et al* provided a solid evidence that CTP binds first and this could potentially change the conformation of the active site to allow MEP entrance. They observed that upon adding solution (chase solution) of unlabelled MEP and CTP to an enzyme solution which was premixed with [2-<sup>14</sup>C] CTP (pulse solution), the radiolabelled product ([<sup>14</sup>C] CDP-ME) was efficiently detected. In the case of premixing the enzyme first with [2-<sup>14</sup>C] MEP followed by addition of the chase solution (unlabelled MEP) resulted in complete equilibration of labelled and unlabelled MEP before the conversion to the product. Crystal structure of IspD complexed with product CDP-ME supports

associative catalytic mechanism where  $\alpha$ -phosphorus atom of CTP undergoes a nucleophilic attack from phosphate moiety of MEP leading to a pentacoordinate intermediate that further collapses to CDP-ME and diphosphate. The reaction requires a divalent cation.<sup>10, 14</sup> The mechanism of IspD is illustrated in Scheme 12.



Scheme 12. IspD catalytic mechanism.

#### 1.4.4 4-diphosphocytidyl-2-C-Methyl-D-erythritol kinase (IspE)

As genes encoding enzymes of the MEP pathway only exist in organisms that produce their isoprenoids via the MEP pathway and not in organisms that use exclusively the mevalonate pathway, genes of the MEP pathway might be identified by scrutinising complete genomes in database. Luttgen *et al* precisely followed this strategy and identified unannotated *ychB* gene of *E.coli*. After overexpression of this gene, a 31 kDa (283 amino acid) protein was obtained. This protein indeed catalyses a reaction using CDP-ME and ATP to form a product that was characterised by NMR analysis and revealed to be 4-diphosphocytidyl-2-methyl-D-erythritol 2-phosphate (CDP-MEP). The authors even proved that this enzyme was actually downstream enzyme of the MEP pathway by detection of radiolabelled  $\beta$ -carotene when [2-<sup>14</sup>C]CDP-MEP was incubated in chromoplast isolated from *Capsicum annuum*.<sup>71</sup> At the same time Kuzuyama *et al* were also able to identify this gene during their study on *ygbP* gene identification experiments and performed characterisation of the product CDP-MEP.<sup>72</sup>

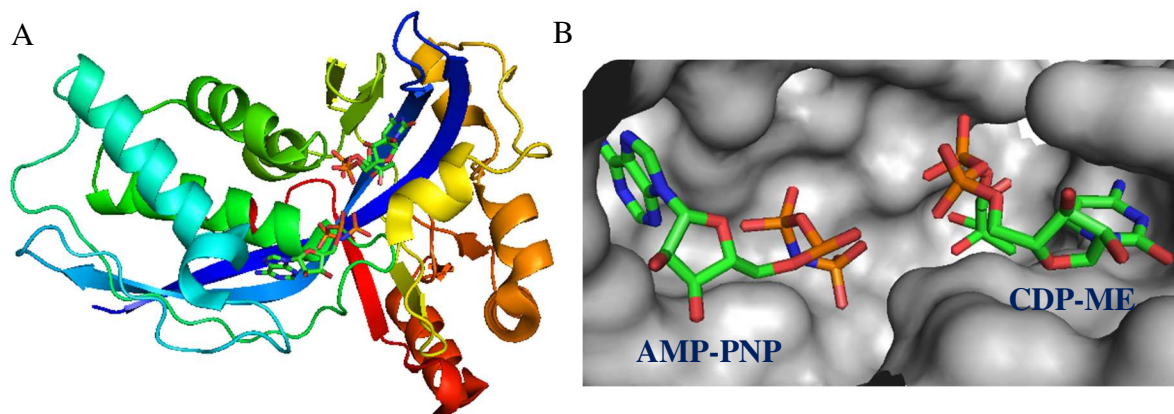
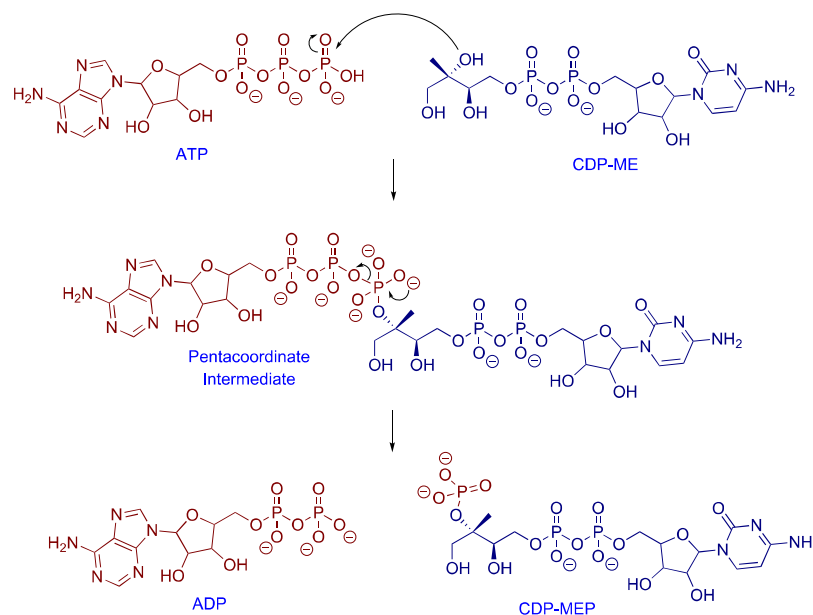


Figure 7. Crystal structure of *E. coli* IspE enzyme. A) IspE subunit with AMP-PNP and CDP-ME. B) 3D structure of AMP-PNP and CDP-ME located in the active site of IspE. (PDB ID 1OJ4)

The first crystal structure of *E. coli* IspE as a ternary complex with the substrate CDP-ME and AMP-PNP (adenylyl-imidodiphosphate, a nonhydrolysable analogue of ATP) was reported in 2003.<sup>73</sup> (Figure 7) Despite initial crystal structures that showed that IspE contains two asymmetric subunits, it was proved later that most IspE proteins exist as a monomer in solution.



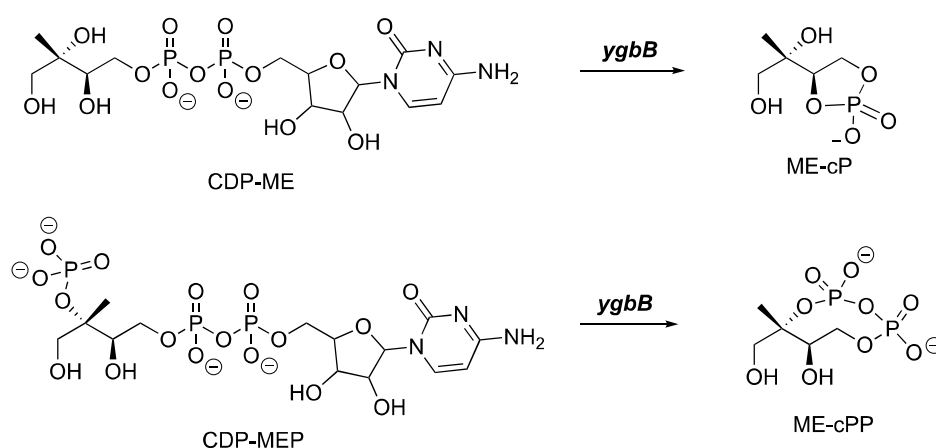
Scheme 13. Catalytic mechanism of IspE.

The homologues of this enzyme resemble GHMP (Galacto, Homoserine, Mevalonate, Phosphomevalonate kinases) superfamily kinase enzyme members. The mechanism of IspE can be explained based on crystal structures and in relation to other GHMP superfamily kinase enzymes. The mechanism of IspE is depicted in Scheme 13.

Like other GHMP family kinases, IspE catalysis was shown to proceed via associative mechanism as in IspD. Nucleophilic attack of C<sub>2</sub>-OH group of CDP-ME on  $\gamma$ -phosphate atom of ATP will form a pentacoordinate intermediate that further collapses into ADP and CDP-MEP. In terms of kinetics, the reaction proceeds through a sequential ordered mechanism where substrates bind to the enzyme orderly and where products are released from the enzyme orderly as well.<sup>73,74</sup>

#### 1.4.5 2-C-Methyl-D-erythritol 2,4-cyclodiphosphate synthase (IspF)

Previous studies have demonstrated that *ygbP* gene is tightly linked to unannotated open reading frame of *ygbB* gene in *E.coli* chromosome. *ygbP* and *ygbB* genes were found to be located adjacent to each other in 21 eubacteria suggesting the *ygbB* gene to be perhaps involved in the MEP pathway. The overexpression of this gene in *E.coli* resulted in a 17 kDa polypeptide. When this protein was added to CDP-ME or CDP-MEP in the presence of divalent cation such as Mn<sup>2+</sup> or Mg<sup>2+</sup>, it produced 2-C-methyl-D-erythritol 3,4-cyclodiphosphate (ME-cP) or 2-C-methyl-D-erythritol 2,4-cyclodiphosphate (ME-cPP), respectively (Scheme 14).



Scheme 14. *ygbB* product from CDM-ME or CDP-MEP.

The feeding experiment of radiolabeled ME-cPP in intact chromoplasts of *C. annuum* resulted in radioactive carotenoids confirming that Me-cPP is a product of the MEP pathway.<sup>75</sup> Seto and co-workers also reported similar result confirming the structure of ME-cPP produced by *ygbB* gene product (later designated IspF). For Seto and co-workers, they identified *ygbB* gene like in their previous study on *ygbP* using *E. coli* mutants impaired in the formation of IPP.<sup>76</sup>

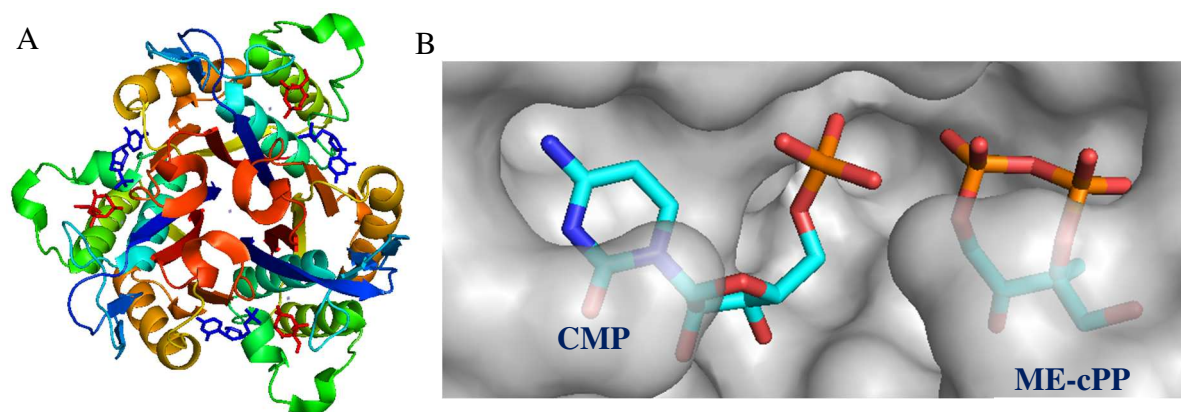
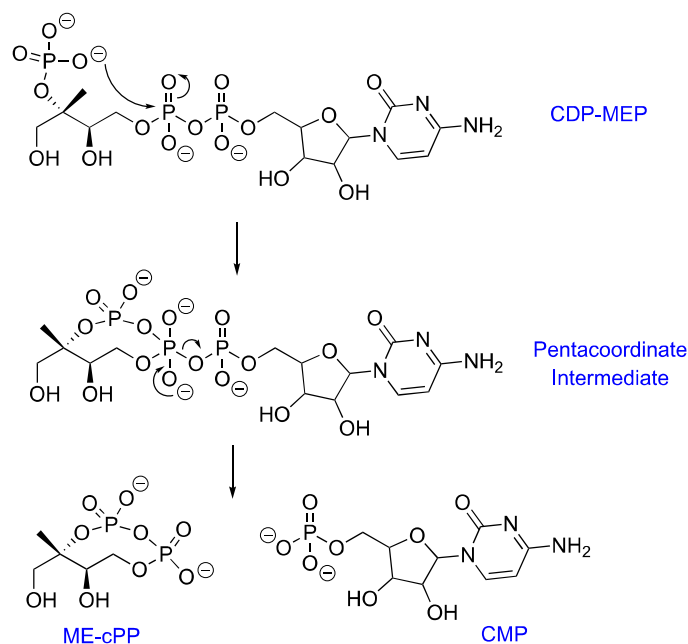


Figure 8. Crystal structure of *E. coli* IspF enzyme. A) IspF homotrimer structure with CMP and ME-cPP. B) CMP and ME-cPP in the catalytic pocket. (PDB ID 1H48)

The crystal structure of IspF shows that the enzyme folds in a homotrimeric structure and the active site is situated at the interface of two subunits (Figure 8).<sup>77</sup>

The mechanism of IspF resembles to the mechanism of IspD and IspE in terms of the formation of a pentacoordinate complex after nucleophilic attack on a phosphate moiety. The mechanism is also shown to be an associative mechanism in which the 2-phosphate moiety reacts with the phosphate group linked to the C<sub>4</sub> of ME moiety. This process results in the formation of a pentacoordinate intermediate that further collapses to ME-cPP and CMP (cytidine monophosphate).<sup>78, 79</sup> The mechanism of IspF is illustrated in Scheme 15.



Scheme 15. Catalytic mechanism of IspF.

#### 1.4.6 Bifunctional IspDF enzyme

When the first open reading frame study of *ygbP* gene was performed, it was observed that in some bacterial species *ygbB* gene was fused into a same sequence together with *ygbP* gene.<sup>69</sup> This result suggested that there could be a bifunctional enzyme that possess the catalytic activity of the enzymes encoded by those genes. The first investigation on bifunctional IspDF (Figure 9) was performed on an enzyme isolated from *Campylobacter jejuni* and the enzyme was found to transform MEP into CDP-ME. When ATP was added to this reaction mixture, no formation of CDP-MEP was observed. However, when IspE together with ATP was added to the reaction mixture, CDP-MEP formation was detected. This result shows that bifunctional enzyme does not convert CDP-ME into CDP-MEP. <sup>13</sup>C labelled CDP-MEP was used to highlight its transformation into ME-cPP by the bifunctional IspDF. In either cases, the enzyme required a divalent cation, with  $Zn^{2+}$  and  $Ca^{2+}$  ions showing highest activities.<sup>80, 81</sup> The catalytic mechanism of this enzyme is similar to IspD and IspF respectively and therefore not discussed.

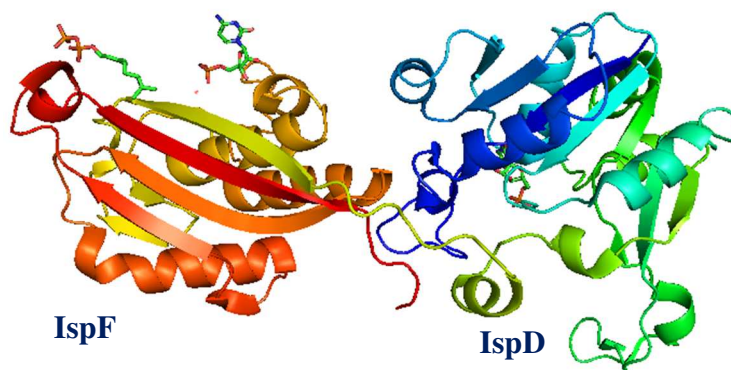


Figure 9. Crystal structure of IspDF of *Campylobacter jejuni* overexpressed in *E.coli*. (PDB ID 1W57). Catalytic domains of IspF and IspD sites are labelled.

#### 1.4.7 (*E*)-4-Hydroxy-3-methyl-but-2-enyl diphosphate synthase (IspG)

Using online database search, *gcpE* and *lytB* genes were found to exist in bacterial species and plant chloroplasts that exhibit MEP pathway. *gcpE* gene was shown to be vital for the survival of an engineered bacteria that can use exogenous mevalonate as a source of isoprenoid.<sup>82, 83</sup> When [U-<sup>13</sup>C<sub>5</sub>]-1-deoxy-D-xylulose was supplemented to *E.coli* overexpressing IspC, D, E, F and G genes, the product analysed by <sup>13</sup>C NMR revealed to be (*E*)-4-hydroxy-3-methyl-but-2-enyl diphosphate (HMB-PP).<sup>84</sup> Simultaneously, the substrate of *gcpE* gene product (later designated as GcpE or IspG) was identified as ME-cPP after incubation of [<sup>3</sup>H]-ME in an *E.coli* mutant deleted in the *gcpE* gene and capable of using mevalonate to produce IPP.<sup>85</sup> A cell free system of *E.coli* overexpressing *gcpE* revealed that IspG catalysed the conversion of ME-cPP into HMB-PP only in the absence of oxygen showing that IspG is an oxygen sensitive enzyme.<sup>86, 87</sup> The alignment of several amino acid sequences of IspG revealed some homologies with aconitase and ferredoxin that are known to contain an iron sulphur cluster,<sup>87</sup> hence it was anticipated that IspG contains an oxygen sensitive iron sulphur cluster. The first characterisation of the iron sulphur cluster of pure IspG was performed on an enzyme that was reconstituted with FeCl<sub>3</sub>, Na<sub>2</sub>S and dithiothreitol<sup>88</sup> using Mössbauer spectroscopy. The obtained spectra allowed the identification of [4Fe-4S]<sup>2+</sup> cluster in IspG.<sup>89</sup>

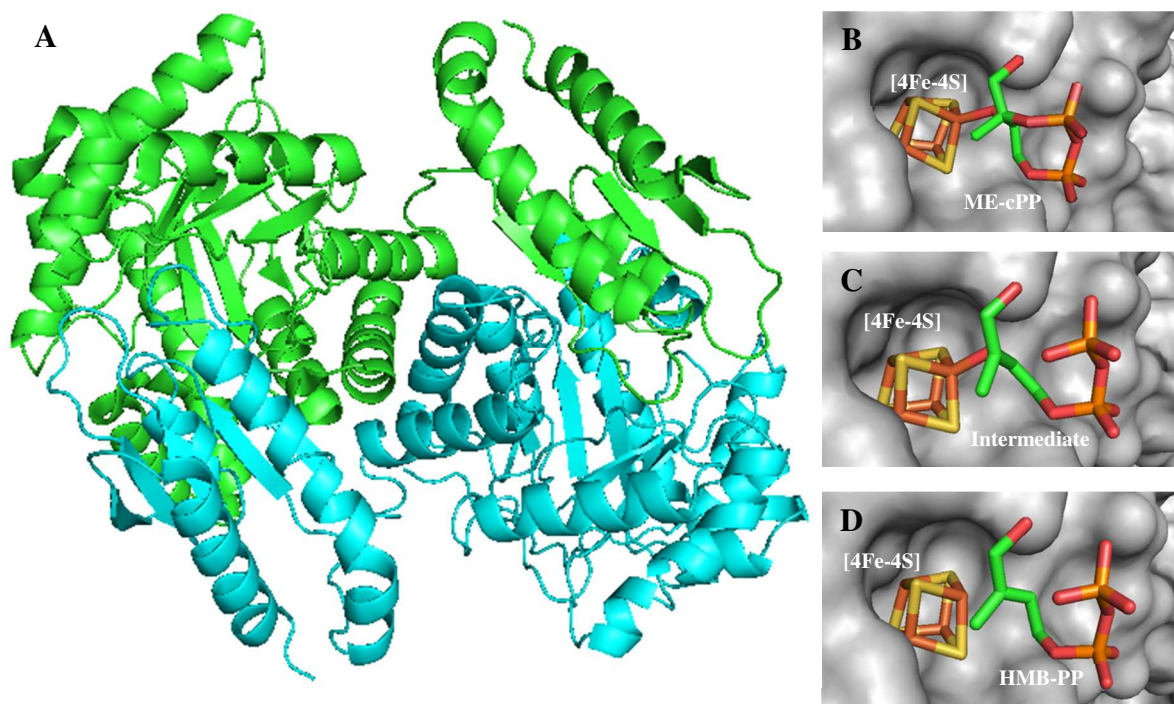
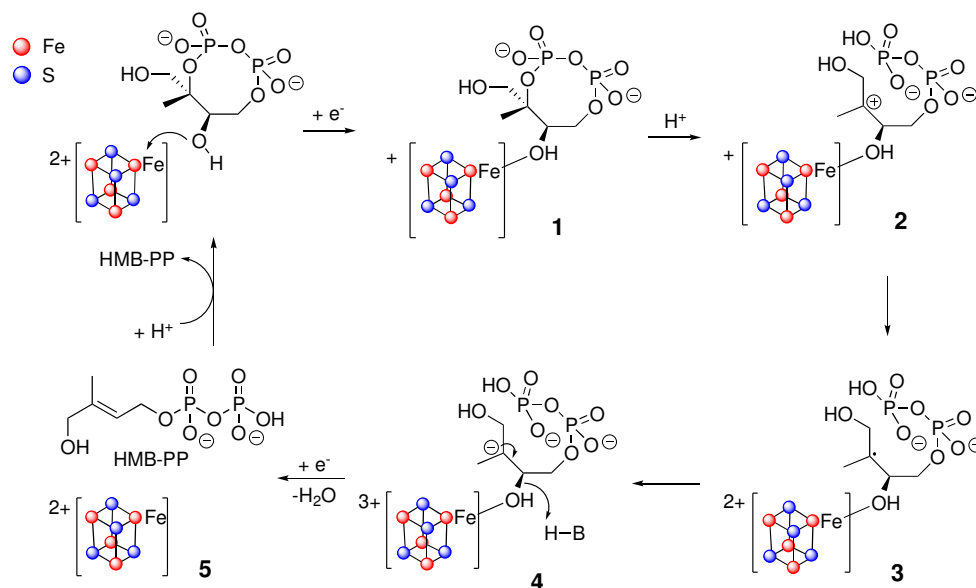


Figure 10. 3D illustration of IspG (*Thermus thermophilus*)<sup>90</sup> homodimer form, substrate, intermediate and the product in the active site. A) IspG homodimer structure showing two monomers in different colour (PDB ID 4S38) B) ME-cPP bound to the [4Fe-4S] cluster (PDB ID 4S38). C) Intermediate (PDB ID 4S3A). D) HMB-PP and [4Fe-4S] cluster (PDB ID 4S39)

The catalytic mechanism of this enzyme is extensively studied using a variety of techniques such as isotopic exchange tests, X-ray crystallography (3D illustration of IspG mechanism is shown in Figure 10) and spectroscopic methods such as EPR, ENDOR and HYSCORE and it is still under investigation. The proposed mechanism starts with formation of a coordination bond between ME-cPP and one iron atom in the iron sulphur cluster. This process is followed by a dissociation of bond between C<sub>2</sub> atom and terminal phosphate moiety to form a cationic intermediary product (2). After reduction of the [4Fe-4S]<sup>2+</sup>, a radical species (3) might be formed but it was not evidenced yet. An internal electron transfer from the cluster to this intermediate (3) results in the formation of anionic molecule (4). The second electron transfer from external source to the cluster results in double bond formation and water elimination resulting in the formation of HMB-PP.<sup>91,92</sup> (Scheme 16)



Scheme 16. Proposed mechanism of IspG.

#### 1.4.8 (*E*)-4-Hydroxy-3-methyl-but-2-enyl diphosphate reductase (IspH)

The gene encoding the last enzyme of MEP pathway was designated as *lytB* gene. The first report on this gene dates back to as early as 1990s but at that time it was only observed to be involved in antibiotic tolerance and stringent response control of *E.coli*.<sup>93</sup> The discovery of relation between *lytB* gene and the MEP pathway was reported early 2000s. This gene is present in organism that utilises the MEP pathway suggesting the involvement of this gene in the MEP pathway. An *E.coli* mutant engineered to synthesise isoprenoids using exogenous mevalonate and lacking *lytB* gene failed to survive unless supplemented with exogenous mevalonate showing that *lytB* gene encoding enzyme (later designated as IspH) is involved in the MEP pathway.<sup>94-96</sup> An *E.coli* mutant overexpressing IspC, D, E, F, G and H produced radiolabelled IPP and DMAPP from [U-<sup>13</sup>C<sub>5</sub>] 1-deoxy-D-xylulose as shown by <sup>13</sup>C NMR analysis of the crude cell lysate.<sup>97</sup> As IspH orthologous group contains three conserved cysteines and catalyses a reaction similar to IspG, it was proposed to contain an iron sulphur cluster. As IspH is oxygen sensitive, in vitro activity tests were described for *Aquifex aeolicus*<sup>98</sup> and *E.coli*<sup>99</sup> under anaerobic conditions. The enzymatic reactions were performed using either a spectrophotometric assay using dithionite<sup>98</sup> or <sup>13</sup>C NMR or HPLC using either photoreduced deazaflavin or NADPH/flavodoxine reductase as reduction system. Reconstitution of pure IspH with FeCl<sub>3</sub>, Na<sub>2</sub>S and DTT followed by EPR revealed that IspH contains a [4Fe-4S]<sup>2+</sup> cluster and that IspH converts HMB-PP into IPP and DMAPP in a ratio of 6 : 1.<sup>100</sup> Later on it was

shown using Mössbauer spectroscopy that native IspH contains a peculiar  $[4\text{Fe-4S}]^{2+}$  cluster in vivo that is conserved after purification of the enzyme in a glove box containing less than 2 ppm oxygen<sup>101</sup> and that the first step in the mechanism of IspH is the binding of the substrate to the  $[4\text{Fe-4S}]^{2+}$  via its OH group.<sup>83, 102</sup> Very recently it was shown using synchrotron based Mössbauer spectroscopy that the  $[4\text{Fe-4S}]^{2+}$  of IspH is unique as one of its iron is linked to three water molecules.<sup>103</sup>

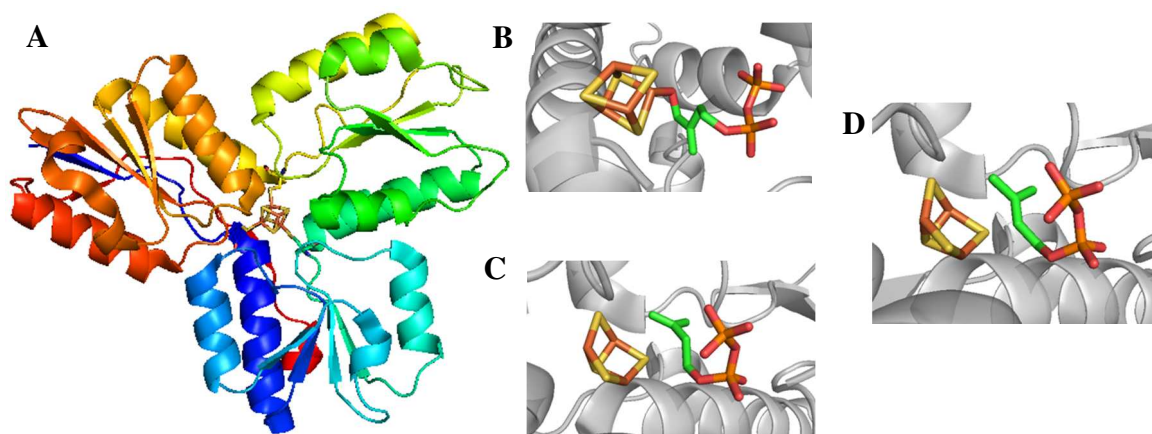
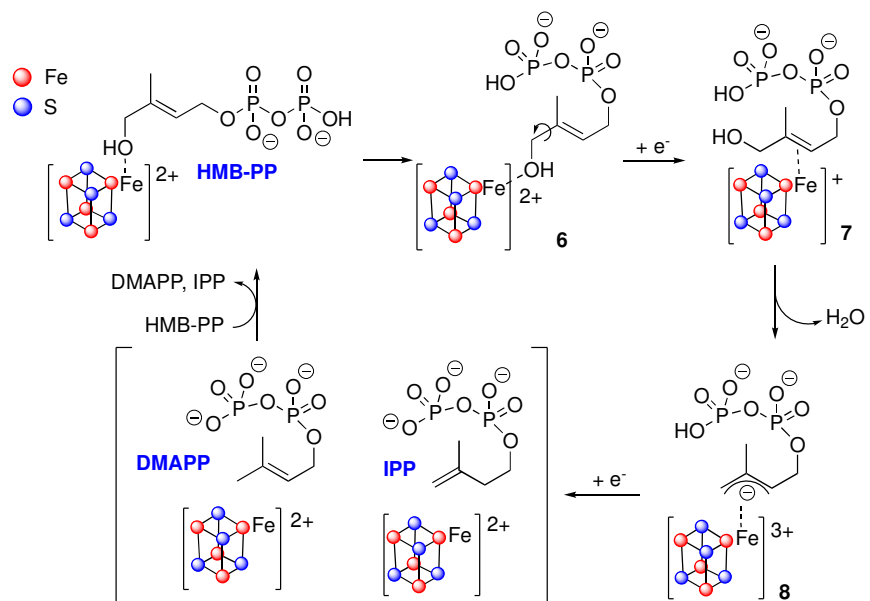


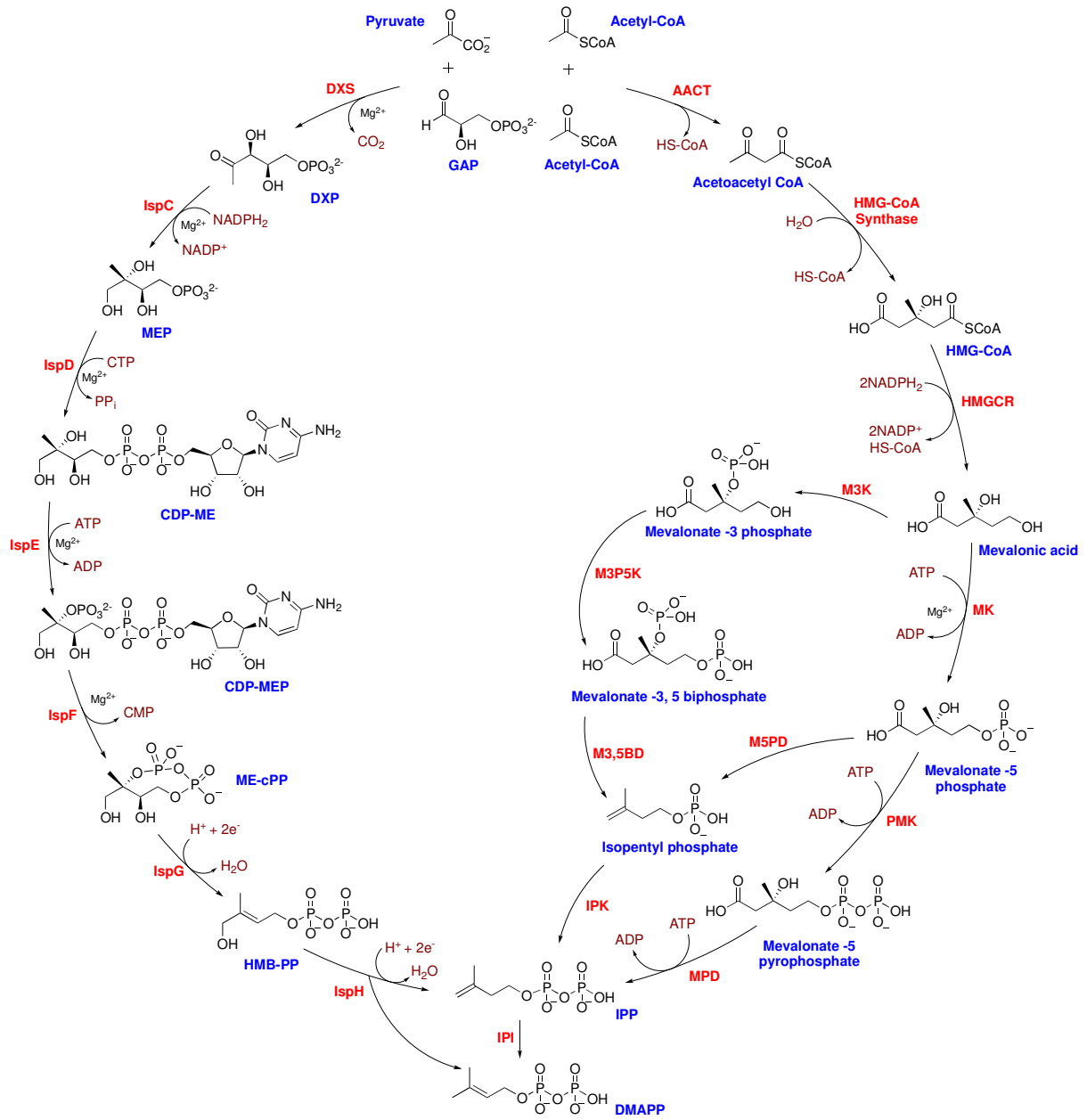
Figure 11. Crystal structure of *E.coli* IspH with an intact  $[4\text{Fe-4S}]$  cluster in the presence of either its substrate or its product. A) IspH enzyme monomer. B) HMB-PP bound with the cluster (PDB ID 4EB3) C) IPP in the active site (PDB ID 3KEM). D) DMAPP in the active site (PDB ID 3KEF)

The mechanism of this enzyme is still under investigation especially the reduction and water elimination steps. The proposed mechanism is as follows: After HMB-PP hydroxyl group binds to the iron atom of the cluster, an electron is supplied to the cluster (leading to  $[4\text{Fe-4S}]^+$ ) from an external source. This reduction of iron sulphur cluster might lead to a  $\pi$ -complex upon rotation of the C-OH bond<sup>104</sup> (Scheme 17). After reduction, two electron transfers from the iron sulphur cluster to the substrate induces O-C bond breakage that results in the formation of an allylic anion (**8**) with the cluster in a +3 charge. A second electron is then supplied to the  $[4\text{Fe-4S}]^{2+}$  cluster followed by protonation of this anion resulting in formation of IPP and DMAPP depending on which carbon atom is protonated (If C<sub>4</sub> is protonated, DMAPP forms and IPP is generated when C<sub>2</sub> is protonated).<sup>105, 106</sup>



Scheme 17. Proposed mechanism of IspH.

In conclusion, the biosynthesis of isoprenoid starts with the condensation of main building blocks, namely IPP and DMAPP. Prior to late 1980s, it was considered that these two building blocks are synthesised through the mevalonate pathway which had been known for many decades. Intensive research in isoprenoid biosynthesis throughout second half of 20<sup>th</sup> century allowed scientists finally to discover a novel pathway that is completely different from known mevalonate pathway. The new pathway was later named MEP pathway and has been extensively studied. The MEP pathway had been overlooked for years due to the fact that it entails two oxygen sensitive  $[4Fe-4S]^{2+}$  enzymes. To date, each step products and enzymes of this pathway have been determined but there are still many issues to be solved to completely elucidate this pathway. The MEP and the mevalonate pathways are shown in Scheme 18.



Scheme 18. MEP and mevalonate pathways

## 1.5 Metabolic labelling

Metabolic labelling methods have been used in elucidation of metabolism for many years. This method relies on the incorporation of labelled molecules into biomolecules via machinery of living cells. A labelled molecule can be any molecules of interest that carries a tag such as a radioactive or stable isotope, or chemical functionality (*e.g.* azide or alkyne) which can be captured or detected afterwards.

### 1.5.1 Radioisotope labelling

The utilisation of radioactive isotope in metabolic labelling studies dates back as early as 20<sup>th</sup> century. The first attempt was made in 1923 when Hevesy used radioactive isotope of lead for the investigation of this element in plants.<sup>107</sup> In 1930s, the radioactive phosphorus and other elements were used as a tracer agent for determination of mineral metabolism in animals and plants.<sup>108-111</sup>

The major advantage of a radioisotope is that it can be detected even when present in a very small quantity and the radioisotope labelled molecule has the identical chemical properties as the unlabelled natural molecule. Therefore, the labelled molecules behave same as the natural one in a biological system. On the other hand, one major drawback is the half-life of the radioisotope. Some radioisotopes have a very short lives making them impossible to be used in prolonged biological experiments.<sup>112</sup>

Today radioisotope labelling is used in many different areas such as radiometal labelled polypeptide for targeting tumour receptors or PET (Positron Emission Tomography) imaging,<sup>113</sup> analysis of pharmacokinetics and metabolism of macromolecules or drugs<sup>114</sup> and also used as a treatment agent (radiopharmaceuticals)<sup>115-117</sup>

### 1.5.2 Stable isotope labelling

Compared to the radioisotope, the stable isotopes do not decay into other elements hence they are stable and do not have radiation hazard. This feature is attractive over radioisotope that has a short life and radiation hazard. Stable isotopes have also been employed as a tracer agent in elucidation of metabolism for many decades. During 1930s, Hevesy had also experimented nitrogen stable isotope <sup>15</sup>N for its role in the metabolism of sunflower. This nitrogen stable

isotope had been extensively employed as a tracer agent for the elucidation of nitrogen metabolism in animals and bacteria.<sup>118, 119</sup>

In modern days, stable isotope labelling is used in many research areas. One example is the utilisation of stable isotope labelled amino acids (SILAC) in quantitative proteomics analysis using mass spectrometry. The core principle of SILAC technique is the incorporation of a stable isotope labelled amino acid into whole proteome of a cell. Later mass spectrometric analysis reveals the mass difference between labelled and unlabelled proteins for the quantitative analysis.<sup>120, 121</sup> Stable isotope labelling is widely used in proteomic research for identification and quantification of proteins by means of mass spectroscopy.<sup>122, 123</sup>

Another example of stable isotope labelling could be the detection of a drug like molecule's metabolite. It is important for drug developers to identify metabolites of a drug candidate for further clinical trials. For this purpose, a stable isotope labelled drug molecule is given to an experimental animal and analysis for isotope detection is latter conducted to determine how the drug molecule is metabolised and excreted from the body.<sup>124, 125</sup>

The stable isotope labelling has tremendous applications in detection and quantification of metabolites and it is one of the widely used tool for elucidation of metabolic pathways in different organisms.

### 1.5.3 Bioorthogonal labelling

The term bioorthogonal reaction (or ligation) has been coined in early 2000s and this type of reaction started to be employed in metabolic labelling studies. Bioorthogonal reaction refers to a reaction between two chemical components that are orthogonal to each other in biological systems. Despite the genetically encoded peptide tags that are used in protein study, other biomolecules such as lipids, carbohydrates and nucleic acids etc., are not susceptible to a such genetically encoded tag. These biomolecules, however, can be tagged with bioorthogonal chemical reporters. Metabolic labelling study with bioorthogonal chemical reporter consists of two steps (Figure 12). First, an organism (cell) is incubated with a metabolic precursor which carries a unique functional group – the chemical reporter. The machinery of the organism incorporates the metabolic precursor into a metabolite (or biomolecules) which can be detected, in the second step, with the treatment of a probe molecule bearing complementary bioorthogonal functionality.<sup>126</sup> There are several types of bioorthogonal ligation reactions that will be discussed below.

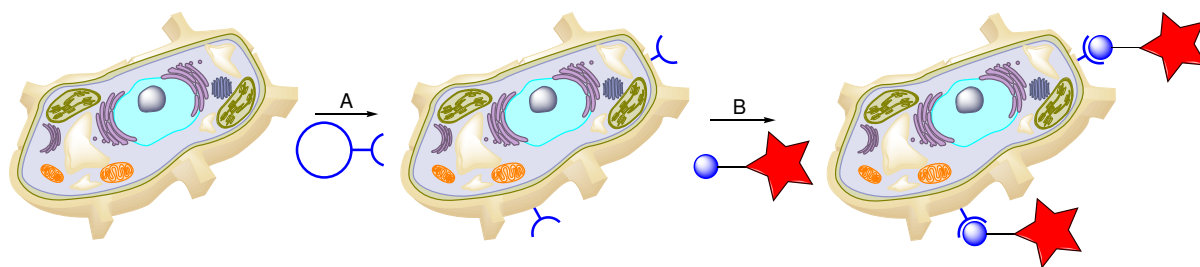
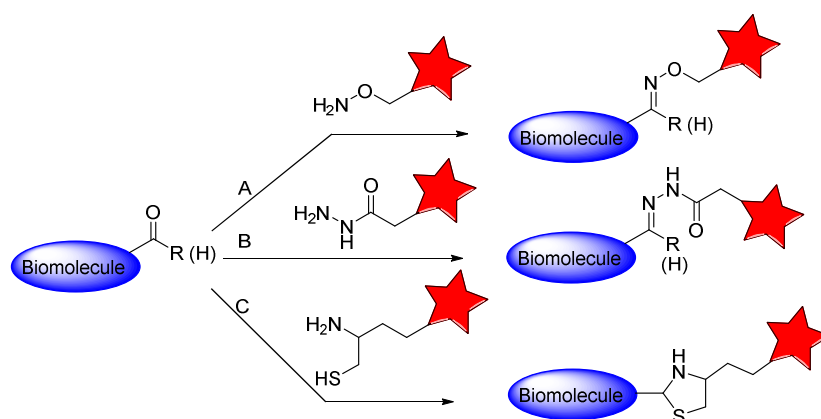


Figure 12. Metabolic labelling with bioorthogonal ligation. A. Chemical reporter is introduced to a cell (organism) using its own metabolism. B. Detection of labelled biomolecules using a probe bearing a detectable tag by virtue of bioorthogonal ligation reactions.

### 1.5.3.1 Carbonyl ligation

Aldehydes and ketones are susceptible to a nucleophilic attack and this feature makes them usable for carbonyl ligation reactions. There are several ways to perform carbonyl ligation using hydrazone, oxime and thiazolidine etc (Scheme 19). The use of carbonyl ligation in labelling biomolecules is limited due to competition with endogenous carbonyl compounds in cell. Nevertheless, they are absent on cell surface and therefore carbonyl functions in this environment can be ligated without endogenous carbonyl competition. This strategy was first employed by Mahal *et al*<sup>127</sup> and they have demonstrated that certain *N*-acetyl sugars are capable of incorporating into a cell surface oligosaccharide metabolically and presenting a ketone group. This ketone functionality can later be ligated with oxime and hydrazone probes bearing a fluorescent tag.<sup>127, 128</sup>

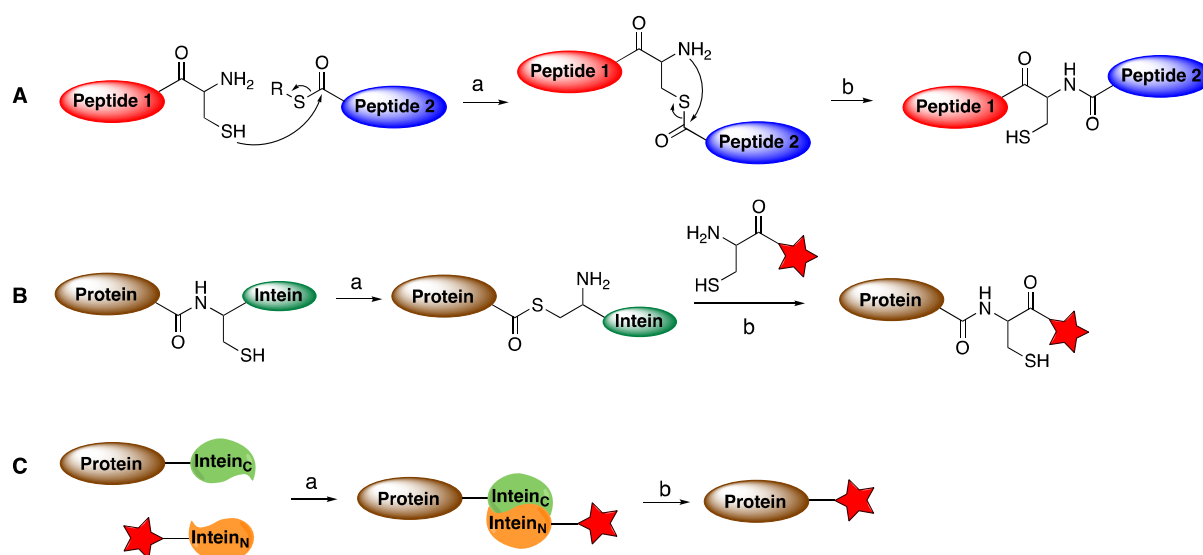


Scheme 19. Carbonyl ligation methodologies. A. Ligation with oxime. B. Ligation with hydrazone. C. Ligation with thiazolidine.

### 1.5.3.2 Native chemical ligation

By early 1990s, Kent and co-workers have reported a new type of ligation reaction which was later termed as a native chemical ligation (NCL). The principle of this reaction is that when a thioester is in close proximity of an amine group of a N-terminal cysteine residue, it forms a native amide bond with it, in a two steps transformation. First, thioesterification reaction takes place followed by intramolecular S-N acyl transfer - the second step.<sup>129</sup> The S-N acyl transfer reaction was actually discovered many years ago by Wieland *et al.* in 1953.<sup>130</sup> NCL allows scientists to ligate two highly functionalised molecules under physiological conditions in the absence of protecting group and therefore this technique was rapidly adopted as a tool for protein modification and synthesis.

After the discovery of this technique, two major methods, namely EPL (expressed protein ligation) and PTS (protein *trans* - splicing), have been developed based on NCL. These two methods both rely on the principle of self - splicing protein where a domain of a protein (called as an intein) is eliminated during a posttranslational process via NCL type of reactions. EPL is the semisynthetic version of NCL where synthetic and recombinant polypeptides are ligated chemically. In PTS, two halves of a split intein associate to form a functional intein which can undergo intramolecular protein splicing reaction to ligate polypeptides while intein excises itself (Scheme 20).<sup>131</sup>

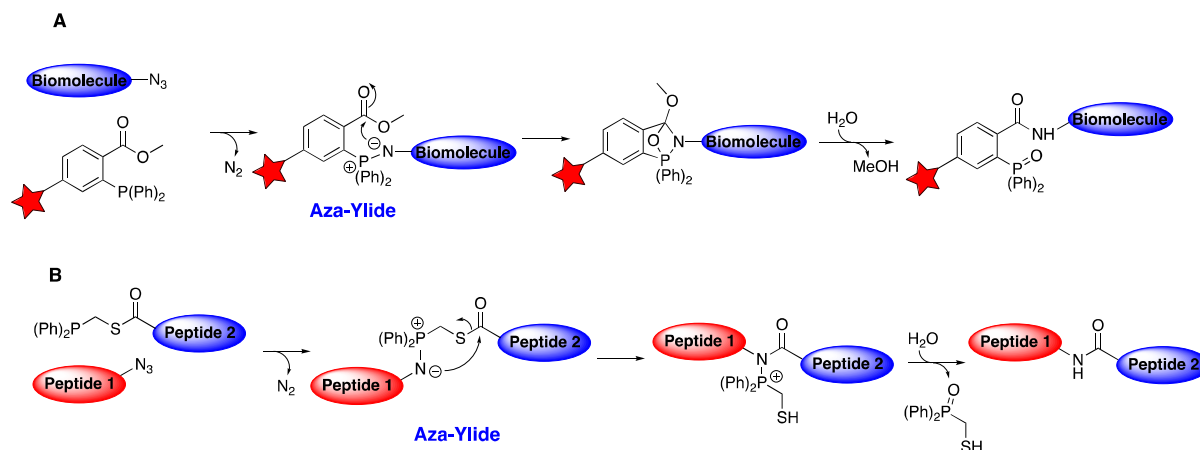


Scheme 20. Native chemical ligation methods. A. NCL of two peptides, a) thioesterification b) S-N acyl transfer. B. Expressed Protein Ligation (EPL), a) intein catalysed partial splicing b) native chemical ligation. C. Protein *trans*-splicing (PTS), a) association of two halves of the split intein b) intein catalysed protein splicing

NCL technique has rapidly found its application in biomolecule labelling experiments. Nakamura and co-workers reported that using stable isotope  $^{15}\text{N}$  labelling of C terminal domain of RNA polymerase  $\alpha$  subunit using NCL followed by NMR analysis revealed structural analysis of larger proteins (>50 kDa) is achievable using isotope labelling via chemical ligation.<sup>132</sup> Previously, structural determination of proteins over 25 kDa by NMR spectroscopy was limited due to degeneracy of the chemical shifts. More recent studies on the labelling of proteins using NCL include the investigation of protein-protein interaction using dual labelling. Wu and co-workers have showed that dual labelling of Rab7 GTPase with fluorescein and coumarin via NCL and oxime ligation can be done in one pot. Moreover, they demonstrated the possibility of studying protein refolding and protein-protein interaction with the help of a dual labelling using fluorescence resonance energy transfer (FRET) technique.<sup>133</sup> As NCL does not require the insertion of label domains in proteins, it is superior to other protein fluorescent labelling methods. As every technique has its drawbacks, NCL labelling technique is inferior to other bioorthogonal labelling such as CuAAC in terms of reaction kinetics which makes it unsuitable for experiments that require fast coupling.<sup>134</sup>

### 1.5.3.3 Staudinger ligation

In search for better bioorthogonal groups, azide functionality has emerged as one of the most suitable for this purpose due to its small size, overall neutrality and absence in almost all biological systems.<sup>4</sup> The utilisation of azide group as a chemical reporter in bioorthogonal ligation was first introduced by Bertozzi and co-workers in 2000.<sup>135</sup> Their strategy was fundamentally based on previously known azide reduction by phosphines discovered by Staudinger and Meyer back in 1919.<sup>136</sup> This ligation of azide and phosphine strategy was later termed as a Staudinger ligation. The mechanism of Staudinger ligation relies on an ester group (electrophilic trap) that is vulnerable to nucleophilic attack from aza - ylide intermediate to form a cyclic amide bond which later can be hydrolysed to give native amide bond. (Scheme 21. A)



Scheme 21. Staudinger ligation mechanism. A. Classical Staudinger ligation with a tagged phosphine. B. Peptide coupling using traceless Staudinger ligation.

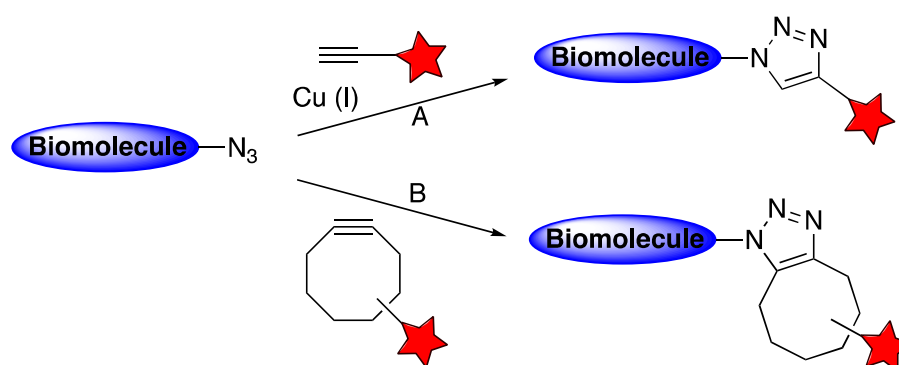
Staudinger ligation strategy was further employed in peptide coupling reactions which was named as a traceless Staudinger ligation. Traceless refers to the fact that after the peptide coupling took place, there is no phosphine oxide moiety present in the coupled peptide.<sup>137</sup> Raines and co-workers adapted this strategy in combination with native chemical ligation concept using thioester chemistry for peptide coupling reactions (Scheme 21. B).<sup>138</sup> The research group of Bertozzi have published numerous papers describing the possibility of studying the metabolism of azide tagged unnatural sugars and their assembly into cell membrane glycans or other glycoproteins through metabolic labelling of azide tagged sugars with a fluorescent probe that undergo Staudinger ligation reaction.<sup>139-144</sup> The main drawback of Staudinger ligation is that the phosphine moiety can be oxidised under physiological conditions.

#### 1.5.3.4 Alkynes and azides in Bioorthogonal ligation and Click Chemistry

The term “click chemistry” was first coined by Sharpless and co-workers in 2001 and it was envisioned that it will lead to an innovative approach to chemical synthesis of molecules. The reaction has to proceed rapidly with a high yield under ambient conditions to form a single desired product.<sup>145</sup> As described above, azide functionality best suits for click chemistry requirements and therefore are exploited for most of the click reactions.

Alternative to Staudinger ligation, azides are also able to participate in cycloaddition reactions with alkenes and alkynes in a type of 1,3-dipolar cycloaddition that was first introduced by Huisgen in 1950s, but to complete the reaction high temperatures or pressures are required

which are not compatible with biological systems.<sup>146</sup> In 2002, the research groups of Sharpless and Meldal have independently reported the improvement of this reaction with the aid of copper (I) catalyst (Scheme 22, A).<sup>147, 148</sup> Since their report, Cu (I) catalysed 1,3-dipolar cycloaddition of azide and alkyne (CuAAC) was extensively studied and improved. Reaction rate can be increased if reactive groups are polarised, therefore it is common to introduce an electron withdrawing group close to an alkyne. The rate also can be enhanced when using specific ligands that chelates to copper and stabilises it.<sup>149, 150</sup>



Scheme 22. 1,3-dipolar azide alkyne cycloaddition reaction. A. Copper catalysed cycloaddition (CuAAC). B. Strain promoted cycloaddition (SPAAC).

The cycloaddition between azide and terminal alkynes can also be catalysed by ruthenium (II) to yield 1,5-disubstituted 1,2,3-triazole products instead of 1,4-disubstituted in the case of CuAAC.<sup>151</sup> Because ruthenium catalyst is expensive as well as sensitive to water and air, its application is limited. Hong and co-workers<sup>152</sup> have recently reported the utilisation of nickel catalyst to achieve 1,5-disubstituted cycloaddition product. They have shown that nickel catalysed azide alkyne cycloaddition (NiAAC) proceeds both in water and organic solvents which overcomes the limitation of ruthenium catalyst.

In terms of mechanism, Fokin and co-workers suggested that ruthenium catalysed cycloaddition reaction starts with the displacement of ligands by alkyne and azide molecules to produce activated complex. This activated complex is then converted to ruthenacycle via the oxidative coupling of alkyne and azide. The ruthenacycle further undergoes reductive elimination to produce triazole complex which collapses to produce triazole and regenerating the catalyst.<sup>153</sup> (Figure 13, A). According to Fokin and co-workers, the copper catalysed cycloaddition reaction starts with  $\sigma$ -bound copper acetylide complexed with  $\pi$ -bound copper reversibly coordinates

azide molecule to produce azide complex. This azide complex is then converted to azide intermediate through nucleophilic attack at N-3 of the azide by  $\beta$ -carbon of acetylide. The intermediate undergoes ring closure to form triazolide which further collapses to catalyst and cycloaddition product.<sup>154</sup> (Figure 13, B) Hong and co-workers suggested that the mechanism of NiAAC starts with the formation of nickel catalyst coordinated azide and alkyne. It follows the C-N bond formation which determines regioselectivity resulting in cycloaddition complex. In the final stage, cycloaddition complex collapses to produce copper cyclised product and free catalyst via reductive elimination.<sup>152</sup> (Figure 13, C)

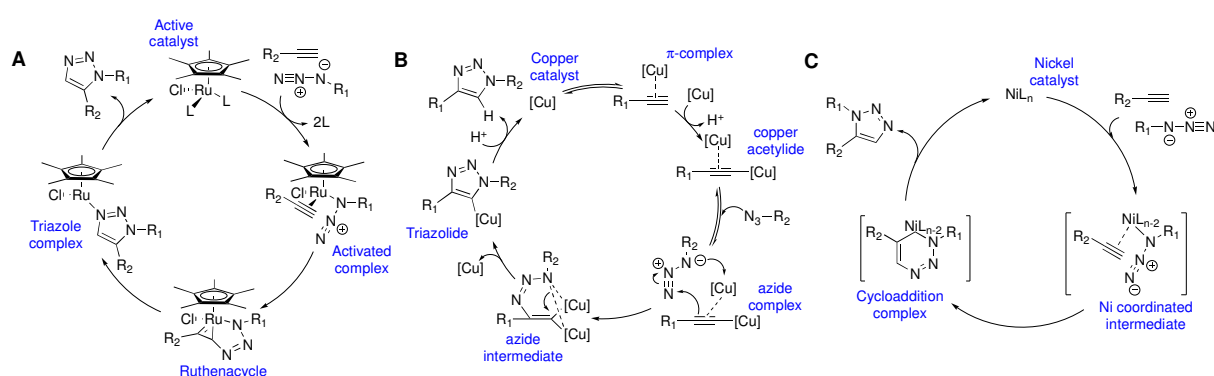


Figure 13. Mechanism of metal catalysed azide alkyne cycloaddition. A) Ruthenium catalysed cycloaddition. B) Copper catalysed cycloaddition C) Nickel catalysed cycloaddition

Although CuAAC gained popularity in organic synthesis, materials chemistry and biological chemistry etc., its use in living systems is hampered due to the toxicity of copper (I). Free copper (I) ions promote the generation of reactive oxygen and nitrogen species.<sup>155</sup> To overcome the toxicity caused by copper (I) catalyst, Bertozzi and co-workers have elegantly used a different approach for alkyne azide cycloaddition reaction using strain promotion<sup>5</sup> (Scheme 22, B), hence circumvents the requirement of copper catalysis. The concept of accelerating reaction rate by strain promotion had been reported back in early 20<sup>th</sup> century for the reaction between azide and cycloalkene<sup>156</sup> and it was further studied by Krebs and co-workers during 1950s when they have reported the dramatic rate increase for reaction between phenylazide and cyclooctyne.<sup>157</sup> In their study, Bertozzi and co-workers reported that using strain promoted azide alkyne cycloaddition (SPAAC) strategy was possible for labelling cell surface glycans with no cytotoxic effects.<sup>5</sup> Further studies continue in search for a strained alkyne to enhance reaction kinetics and biocompatibility.

### 1.5.3.5 Click Chemistry using alkene and azide

As alkynes proved to be suitable for cycloaddition reactions, the research on alkene cycloaddition with azides has been performed simultaneously since they also share similar reactivity towards dipolar reactants. Rutjes and co-workers reported in 2007 that a oxanorbornadiene containing alkene underwent cycloaddition reaction with azide functionality and used this strategy for a labelling study.<sup>158</sup>

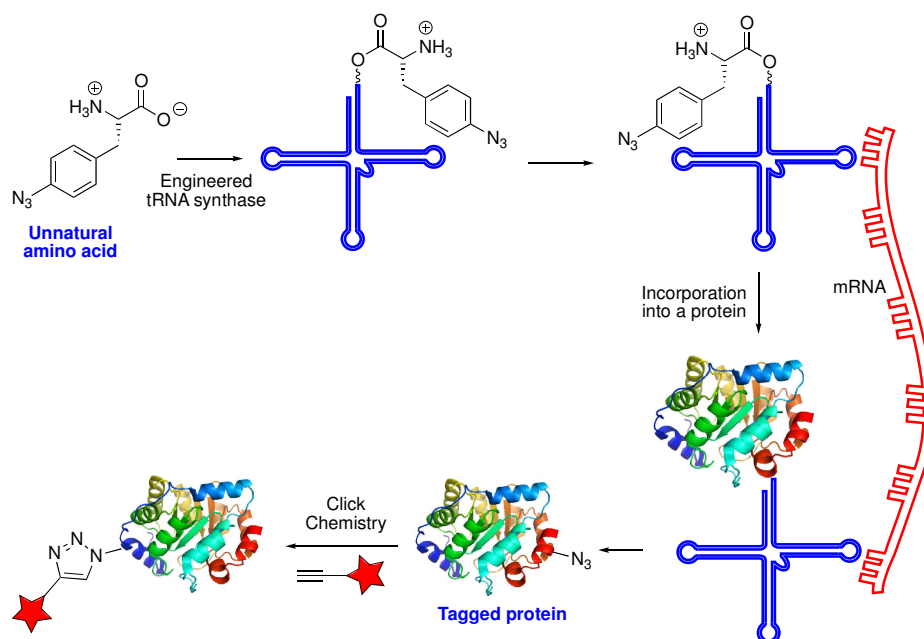
Apart from in vivo labelling research, both strain promoted and metal catalysed azide alkene cycloaddition strategy has been used in variety of studies including total synthesis of organic molecules<sup>159, 160</sup> polymer chemistry<sup>161</sup> and biological chemistry.<sup>162</sup>

## 1.5.4 Click Chemistry (bioorthogonal ligation) in metabolic labelling

All of the bioorthogonal reactions discussed above particularly azide alkyne cycloaddition found immense practical applications in metabolic labelling studies. They are used to label wide variety of biomolecules including proteins, carbohydrates, lipids and nucleic acids. In this section the applications of bioorthogonal ligation (i.e. click chemistry) in labelling studies will be discussed.

### 1.5.4.1 Click Chemistry in protein labelling

Azide and alkyne functionality as a tag can be easily introduced in molecules via chemical synthesis but introduction in proteins poses a challenge due to its structural complexity. Tirell and co-workers have pioneered in this field by elegantly using inability of certain tRNA synthases to differentiate between natural and unnatural amino acids that are close in structural properties (Scheme 23).<sup>163</sup> With this method, a range of bioorthogonal functionalities have been metabolically incorporated into proteins in both bacteria and eukaryotes using homopropargylglycine, homoallylglycine, azidohomoalanine, azidophenylalanine as well as alkynylphenylalanine.<sup>164-166</sup> More recently alkyne or azide tagged lysine residues have successfully been incorporated into a recombinant protein of *Methanosarcina barkeri* and labelled using CuAAC.<sup>167</sup> Later the SPAAC strategy was also successfully employed for site specific protein labelling using unnatural amino acids.<sup>168</sup>



Scheme 23. Labelling of protein using unnatural amino acids and genetically engineered tRNA synthase.

Although this method is a powerful tool for protein labelling, it suffers the drawback of needing specifically engineered tRNA synthase for a specific amino acids to be incorporated. This means that every time a new unnatural amino acid needs to be incorporated, the tRNA synthase has also to be engineered for that.

More recent studies, however, allowed the development of a new type of tRNA synthase that can tolerate variety of bioorthogonal functionalities. For example, Liu and co-workers succeeded in incorporating 6 different tyrosine and 12 phenylalanine derivatives in *E.coli*.<sup>169</sup>

Another example of protein labelling with azide or alkyne functionality is the labelling of a virus surface. Finn and co-workers demonstrated labelling of tagged lysine or cysteine residues on surface coat protein of Cowpea mosaic virus (CPMV).<sup>170, 171</sup>

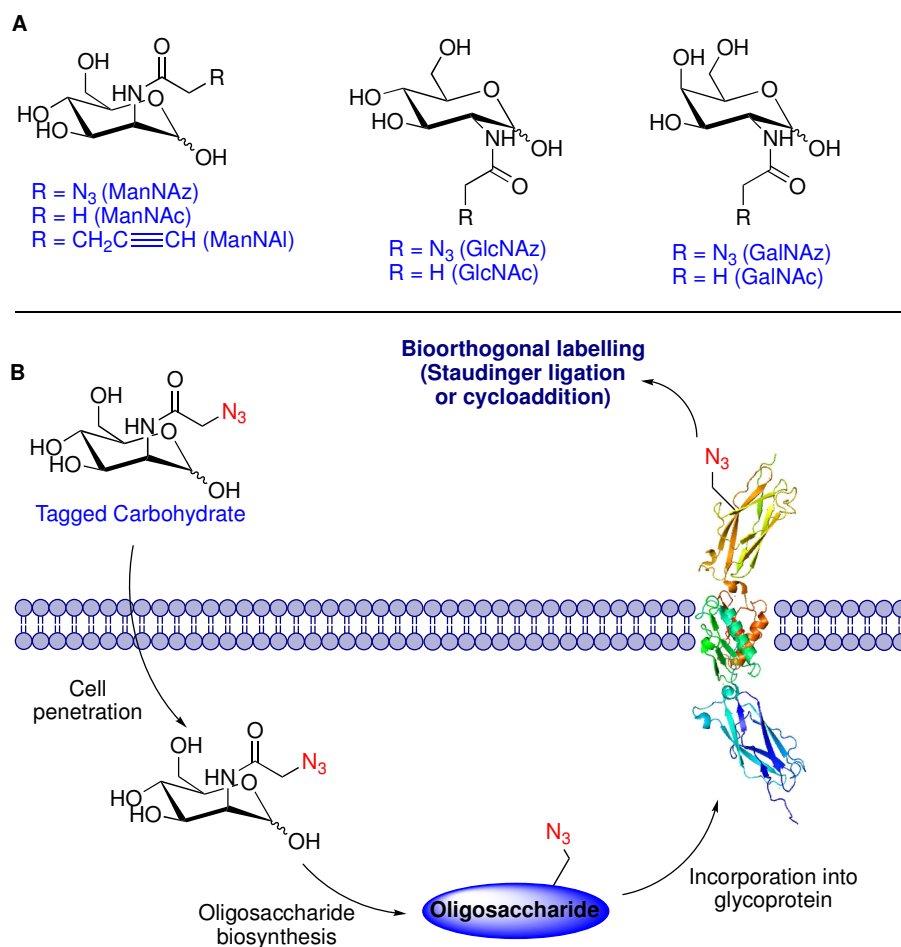
Click chemistry involving labelling technique was adapted for activity based protein profiling (ABPP) methods. ABPP is a chemical proteomic method that uses active site directed covalent binding probes with wide selectivity (i.e. specific or class of enzymes) to visualise the activity of proteins in cells, tissues and fluid samples. Although standard gel electrophoresis and mass spectrometry techniques are useful to quantify proteins, the number of posttranslational modifications have limited their use for the investigation of active protein fractions in a complex in vivo systems. ABPP was developed to address this limitation.<sup>172</sup> In 2003, Cravatt

and Overkleeft research groups reported the utilisation of azide functionalised small molecules that target certain enzymes.<sup>173, 174</sup> Later alkyne functionalised fluorophosphonates were proven to be efficient in profiling serine proteases with greater affinity than traditional probes due to their small size that enables easy cell permeability.<sup>175, 176</sup> Most activity based probes exploits the covalent binding to the active site of an enzyme but some enzymes such as kinases do not possess the required feature for covalent bonding with probes. To target this type of enzyme families, a non-covalent binding small molecule can be modified with photocrosslinking groups to facilitate covalent binding of a probe tagged with azide or alkyne functionality.<sup>177</sup>

#### 1.5.4.2 Click chemistry in carbohydrate labelling

Compared to proteins, carbohydrates are amenable to modifications by metabolic labelling with biosynthetic precursor. These precursors can be unnatural sialic acid, *N*-acetylgalactosamine (GalNAc), *N*-acetylglucosamine (GlcNAc), *N*-acetylmannosamine (ManNAc) and fucose (Fuc) etc (Scheme 24, A). Modification of these precursors with click chemistry functionality and further successful labelling of incorporated biomolecules was first demonstrated by Bertozzi and co-workers in 2000 when they employed *N*-azidoacetylmannosamine (ManNAz). This was better incorporated into sialic acid via the cell's biosynthetic machinery and later installed on the cell surface within glycoproteins where they can be efficiently detected with a fluorescent conjugate delivered by Staudinger ligation strategy.<sup>127, 135</sup> Later they showed that when ManNAz is preacetylated, it passes cell membrane efficiently and hydrolyse to ManNAc. Since they did not inhibit the production of endogenous ManNAc it was not possible to label completely all sialic acids on the cell surface (Scheme 24, B).<sup>178</sup> Moreover, azide functionalised modified carbohydrates (ManNAz, GalNAz etc.) successfully incorporated into glycoconjugates of zebrafish and mice.<sup>179</sup>

Not only azide functionality was used in glycan labelling studies but also alkyne was studied as a tag for biosynthetic carbohydrate precursor. Chang *et al*<sup>180</sup> have reported the possibility of using preacetylated *N*-(4-pentynoyl) mannosamine (ManNAI) as a tagged sugar for sialic acid biosynthesis.



Scheme 24. Labelling of carbohydrates using click chemistry. A. Examples of modified carbohydrates, B. Simple illustration of oligosaccharide engineering technique.

They observed that this molecule is well tolerated by mice as there was no toxicity sign. When compared to ManNAz, the labelling was 25 % more efficient.<sup>180, 181</sup>

It is obvious that if CuAAC reaction can be used to efficiently label glycoconjugates on cell surface, the possibility of SPAAC would also be exploited. In their study, Bertozzi and co-workers, showed that variety of cyclooctynes are amenable for in vivo labelling of glycoproteins on cell surface derived from preacetylated ManNAz. Nevertheless, they observed that Staudinger ligation with phosphine reagent produced more labelling than SPAAC and the distribution of phosphine reagent in different organs of a mice was greater than cyclooctynes.<sup>182</sup> More recent studies revealed the possibility of quantification of labelling efficiency of cell surface sialic acids derived from ManNAz. Using  $^{153}\text{Eu}$  and  $^{10}\text{B}$  isotopes and inductively coupled plasma mass spectrometry (ICPMS) technique, Liang et al., have demonstrated the quantification of cell surface sialic acid with the help of SPAAC was possible. The isotopes

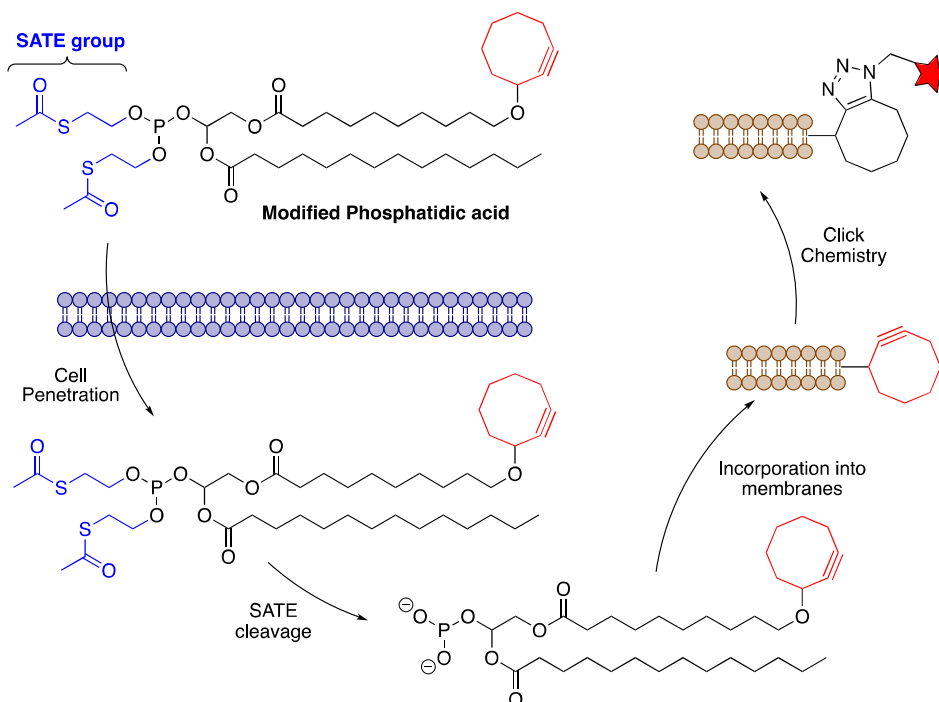
were conjugated to an alkyne reagent that undergoes click reaction with azide tagged sialic acids on the cell surface. The limit of detection of these clicked compounds were higher due to the isotopes.<sup>183</sup>

Proteomic research has also adapted oligosaccharide engineering technique to globally and site specifically analyse the sialated proteins on cell surface. Weixuan et al., demonstrated that metabolic based click mediated (SPAAC) proteomic analysis of normal and cancer cell surface sialated glycoproteins was possible and found that *N*-sialoglycoproteins are up-regulated in invasive cancer cells. The strategy they employed was the incorporation of ManNAz into *N*-sialoglycoproteins which was further clicked with cyclooctyne conjugated with biotin. After the digestion of the protein, biotinylated residue is enriched using avidin and analysed by mass spectrometry.<sup>184, 185</sup>

The click chemistry for carbohydrate labelling is also used in many other metabolic processes. One example is that it has an application for visualising bacteria. In their study, Vauzeilles and co-workers, showed that gram-negative bacterial membrane inner core is susceptible to metabolic incorporation of a modified precursor. They selected 3-deoxy-D-mannooctulosonic (KDO) acid as a target molecule as it is an essential compound for gram-negative bacterial membrane lipopolysaccharide constituents. Obtained by chemical synthesis, the azide functionalised KDO was sufficient enough to be incorporated into the target biomolecule and the visualisation of bacterial membrane was achieved by CuAAC with a fluorescent probe.<sup>186</sup> Continued with this bacterial labelling experiments, Vauzeilles and co-workers later applied their strategy to distinguish bacterial species. A pandemic deadly bacterial species *Legionella pneumophila* can be differentiated efficiently from other bacterial strains based on its metabolic pathway (known as Leg pathway) for the synthesis of a membrane lipopolysaccharides from a unique monosaccharide (2,4-diacetamido-2,4,6-trideoxy-D-mannopyranose) precursor. An azide functionalised analogue of this precursor was successfully incorporated into cell membrane lipopolysaccharides as visualised by fluorescence probe after CuAAC. They also proved that this strategy can differentiate the pathogen from other species as they do not utilize the unique monosaccharide. Moreover, this strategy is faster than traditional method of identification of bacterial species like a culture on Petri dishes that could last several days.<sup>187</sup>

### 1.5.4.3 Click Chemistry in lipid labelling

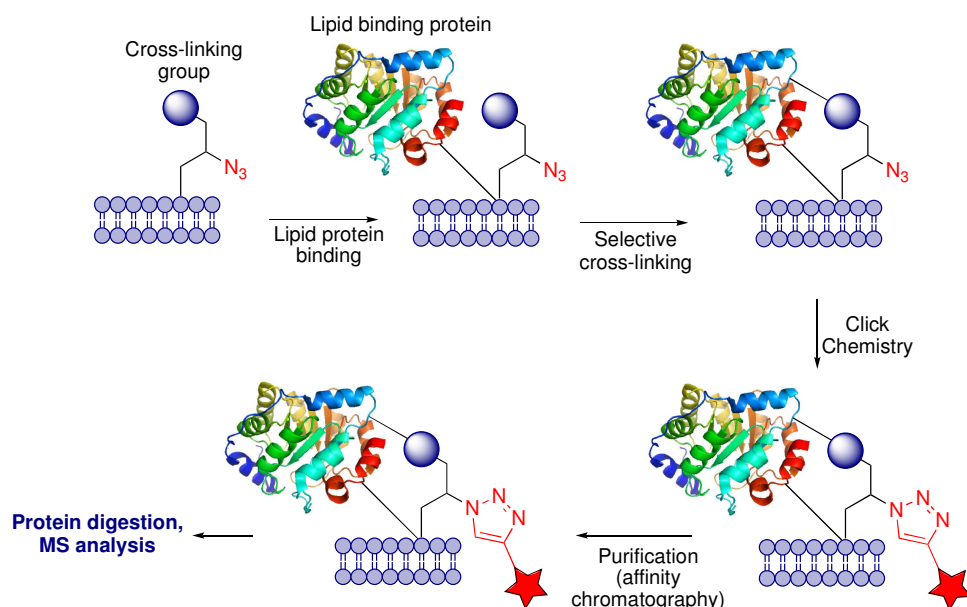
Like carbohydrates, lipids are also biomolecules that are not susceptible to genetic modification for metabolic studies as in the case of proteins. Lipids were therefore also studied using metabolic labelling approaches and the utilisation of bioorthogonal ligation in metabolic labelling studies has been extended since 2000s.



Scheme 25. Labelling of lipid with the tagged phosphatidic acid reported by Schultz and co-workers.

Early studies conducted by Schultz and co-workers showed the feasibility of dynamic studies of a lipid through fluorescence labelling *in vivo* using SPAAC click chemistry. They reported the incorporation of tagged phosphatidic acid (PA) into cell membrane as judged by fluorescence after clicking. PA is an important biomolecules that is involved in numerous processes such as signal transduction in skeletal muscle,<sup>188</sup> stimulation of DNA synthesis<sup>189</sup> and regulation of phospholipid synthesis<sup>190</sup>. To enhance the cell permeability of tagged PA, S-acetylthioethyl (SATE) groups were added to the phosphate moiety. This group facilitates the cell penetration after which it is cleaved by endogenous esterases releasing the free phosphate moiety. This resulting molecule does not leak from cell as it no longer possess cell permeability.<sup>191</sup> (Scheme 25)

Salic and co-workers also demonstrated that tagged choline with a terminal alkyne group can be efficiently incorporated into phospholipids and therefore could be used to visualise its cell distribution particularly into the biosynthesis of membranes of different cell organelles such as endoplasmic reticulum, mitochondria and golgi as well as surface of cell membrane.<sup>192</sup>



*Scheme 26. Strategy of identification of novel lipid binding proteins using cross-linker and click chemistry.*

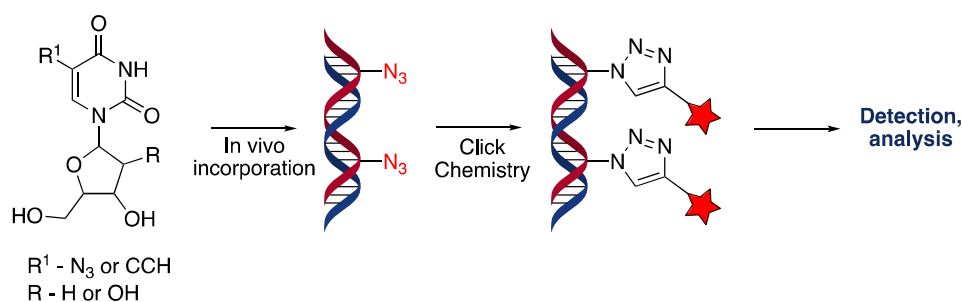
Apart from numerous imaging studies<sup>193-195</sup>, another possible application of lipid labelling is the identification of new lipid binding proteins. In their study, Bong and co-workers, showed that phosphatidylserine (PS) analogue could serve to identify novel PS receptors.<sup>196</sup> The strategy employed in this study seems similar to affinity based protein labelling technique because they employed the chemically synthesised analogue of PS bearing a photoaffinity cross-linker and azide group. Once the unknown receptor binds to the modified PS, the photoaffinity crosslinker establishes a covalent bond with the receptor upon activation and this covalently bonded (i.e., captured) receptor can be further labelled with click chemistry followed by purification and subjected to proteomics analysis.<sup>197</sup> (Scheme 26)

Recent studies demonstrated that this approach can also be applied to the identification of novel proteins based on protein-protein interactions. Particularly, S-palmitoylated proteins were tagged with bifunctional (contains cross-linker and bioorthogonal functionality) fatty acids and

Peng et al, with this method, identified novel proteins that interact with S-palmitoylated proteins.<sup>198</sup>

#### 1.5.4.4 Click Chemistry in nucleic acid labelling

The studies centred on the modification of DNA and RNA with clickable tag have been also an interesting subject along with carbohydrates, proteins and lipids. There have been number of studies performed in this area since the start of utilisation of click chemistry in metabolic labelling.<sup>199, 200</sup>



Scheme 27. Labelling of DNA synthesis using click chemistry.

Early studies include the research by Seo et al. on a single stranded DNA. They have demonstrated that alkyne and azide labelled DNA strand can be efficiently labelled with fluorescence dye in vitro.<sup>201</sup> Later studies conducted by Mitchison and co-workers showed that alkyne modified uridine analogue incorporates into a replicated DNA in vivo and could be imaged via fluorescence tagged click (CuAAC) labelling (Scheme 27). This method was superior to previously used techniques because i) it does not require DNA denaturation therefore preserves structural complexity ii) tagging agents (azide or alkyne) are very small and penetrate tissue very efficiently.<sup>202</sup> This strategy was also applied to RNA imaging experiments.<sup>203</sup>

Later studies showed SPAAC can also be introduced to label nucleic acids.<sup>204-206</sup> More recent studies showed an elegant way to label single stranded DNA or RNA with sequence specificity. In their report, Freisinger and co-workers, demonstrated that labelling of a single stranded DNA with a reactive strand bearing a reactive chemical group (tagged with alkyne in this case). Upon annealing the two strands, a nucleotide in the target strand forms a covalent bond with the

reactive group tagged with an alkyne residue that could be clicked with a fluorescence dye afterwards.<sup>207</sup>

To summarise, labelling of biomolecules has been the central tool to elucidate and understand the metabolism in living systems. Since the beginning of 20<sup>th</sup> century, scientists exploited many different ways to elucidate metabolic pathways. The discovery of isotopes had a huge impact on metabolic labelling studies as it is very sensitive to detection and does not alter chemical properties of a labelled molecule. Early studies were performed with both radio and stable isotopes for metabolic labelling of inorganic molecules and organic molecules such as amino acids.

Bioorthogonal ligation has emerged as a powerful tool in metabolic labelling studies in the late 1990s. This strategy relies on chemical functionalities that exclusively react with each other in the presence of variety of chemical functionalities that biological systems possess. Early developments in this field was the salvation of previously described reactions such as reduction of azide using phosphines that was reported in the mid 20<sup>th</sup> century.

During the intense developments in the field of bioorthogonal ligation reactions, azide and alkyne functionalities have emerged as a novel tool. The cycloaddition of azide and alkyne was bioorthogonal and these functions are almost completely absent in biological systems which makes them valuable tool to study metabolism.

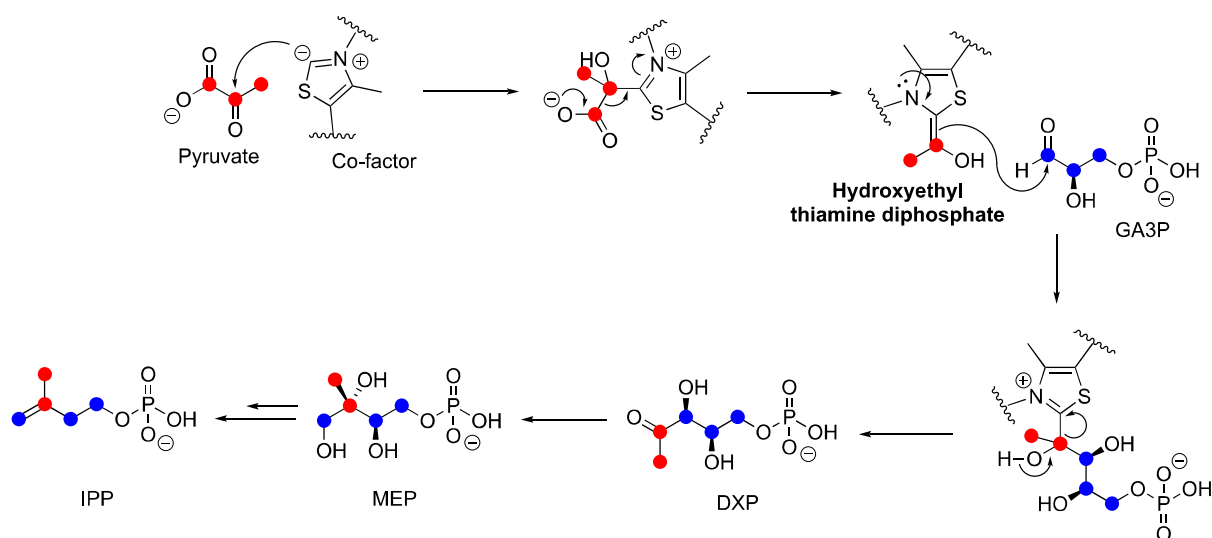
Later the term “click chemistry” was born in the beginning of 21<sup>st</sup> century. Although click chemistry has applications in variety of chemical fields, its utilisation in biological chemistry heralded the tremendous advancement in metabolic labelling. Click chemistry has been employed in proteins, carbohydrates and lipids as well as many other biomolecules’ metabolic labelling studies. The metabolic labelling studies using click chemistry still continues and there are many more to discover.

# CHAPTER-2

Metabolic labelling of  
the MEP pathway

## 2.1 Introduction

Most of the MEP pathway enzymes and their products have been determined using metabolic labelling studies. Since the discovery of initial enzymes in the pathway, much of further pathway elucidation was achieved with isotope labelling (both radio and stable isotope) studies.<sup>69, 71, 84, 99</sup> For example, the confirmation of the MEP pathway precursors as glyceraldehyde-3-phosphate and pyruvate was achieved with <sup>13</sup>C labelling experiments using *E.coli* mutants altered in the metabolism of triose phosphate by Rohmer *et al.* In their study, they found that C<sub>2</sub> and C<sub>3</sub> subunits derived from pyruvate and a triose phosphate respectively (Scheme 28). Stable isotope <sup>13</sup>C labelling and analysis by <sup>13</sup>C NMR of ubiquinone revealed further that C-1, C-2 and C-4 atoms of IPP derived from glyceraldehyde 3-phosphate phosphate and C-3 and C-5 atoms originated from C<sub>2</sub> subunit of pyruvate when *E.coli* mutants were fed with labelled pyruvate or labelled glycerol.<sup>53</sup>



Scheme 28. <sup>13</sup>C labelling experiments to identify the first intermediates of the MEP pathway. Red and blue dots represent labelled atoms of pyruvate and glyceraldehyde 3-phosphate (GA3P) respectively.<sup>53</sup>

Discovery of MEP pathway enzymes using either isotopic labelling or genetic screening methods have been presented in Chapter 1 and therefore will not be further discussed.

Metabolic labelling of the MEP pathway using bioorthogonal chemistry would be a strategy to monitor the activity of this pathway and its end products as well as studying the effect of small molecules, including potential antibacterial agents, on bacterial metabolism. Through labelling

of the MEP pathway, we could also develop a tool for rapid identification of specific bacteria that exclusively utilises this pathway. To the best of our knowledge, bioorthogonal labelling experiments was so far never attempted for studying this pathway. In this study, we aimed at applying bioorthogonal ligation (click chemistry) to further investigate the MEP pathway as this method is simple and easy for detection and analysis.

For this purpose, the main intermediate of this pathway, MEP, was selected to be modified with click functionality *i.e* with an azide group. Previous study using synthetic deuterium labelled 2-C-methyl-D-erythritol (ME, **9**) showed that it could be incorporated into ubiquinone when *E.coli* was incubated in the presence of the  $^{13}\text{C}$  labelled ME.<sup>63</sup> Based on this result we anticipated that if azide functionalised ME can be synthesised chemically and used in feeding experiments, bacteria would take it up and incorporate it into their isoprenoids. The position of the azide group, however, has to be decided. Indeed the ME analogue that has the azide functionality installed on a position where IspD enzyme does not take it up and does not convert it, then the labelling experiment would fail. Luckily Poulter and co-workers have recently published a paper in which they showed that 2-C-ethyl-D-erythritol phosphate (EEP, **11**) can be converted by the IspD enzyme.<sup>208</sup> As mentioned in Chapter 1, an azide group is very small and we assumed if IspD could convert EEP, it would also turnover ME analogue where azido group is attached to C-5 atom of ME. We, therefore, decided to introduce an azide group on C-5 atom of ME to synthesise an azido analogue (ME-N<sub>3</sub>, **10**) as a metabolic reporter for the MEP pathway. (Figure 14)

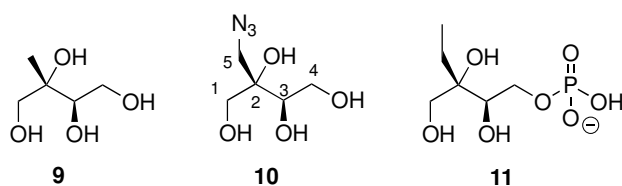
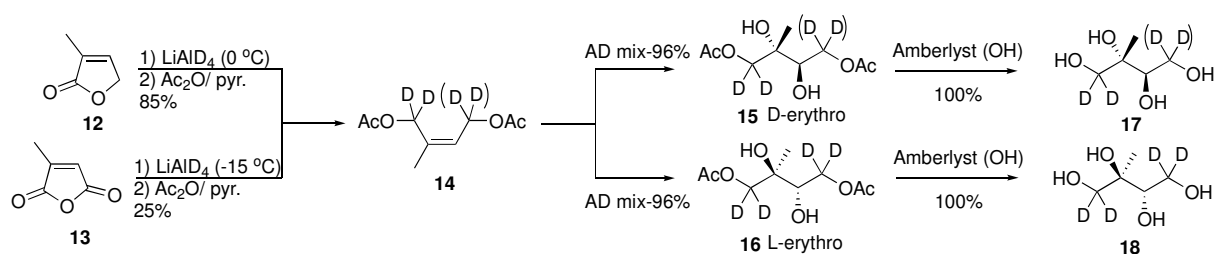


Figure 14. Structures of erythritol derivatives.

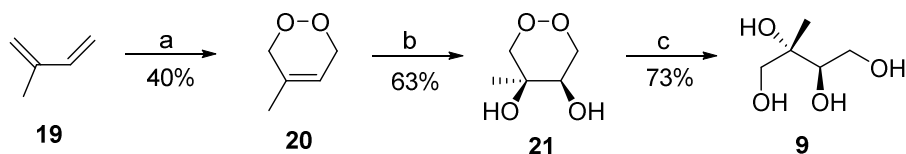
## 2.2 Synthesis of ME-N<sub>3</sub>

To date, the synthesis of methylerythritol and its derivatives (especially MEP) has been described by several research groups. Initial synthesis of ME for MEP pathway elucidation was conducted by Duvold *et al.*<sup>63</sup> They reported the synthesis of deuterium labelled D and L isomers of ME in 3 steps starting from 3-methylfuran-2-one **12**. The compound **12** was reduced with deuterated LiAlD<sub>4</sub>, followed by treatment with acetic anhydride to yield corresponding unsaturated diacetate **14**. Sharpless enantioselective dihydroxylation of **14** produced ME diacetate **15** in good yield. Hydrolysis of acetate groups was then achieved with basic ion exchange resin to afford the final deuterated ME **17** in quantitative yield. (Scheme 29)



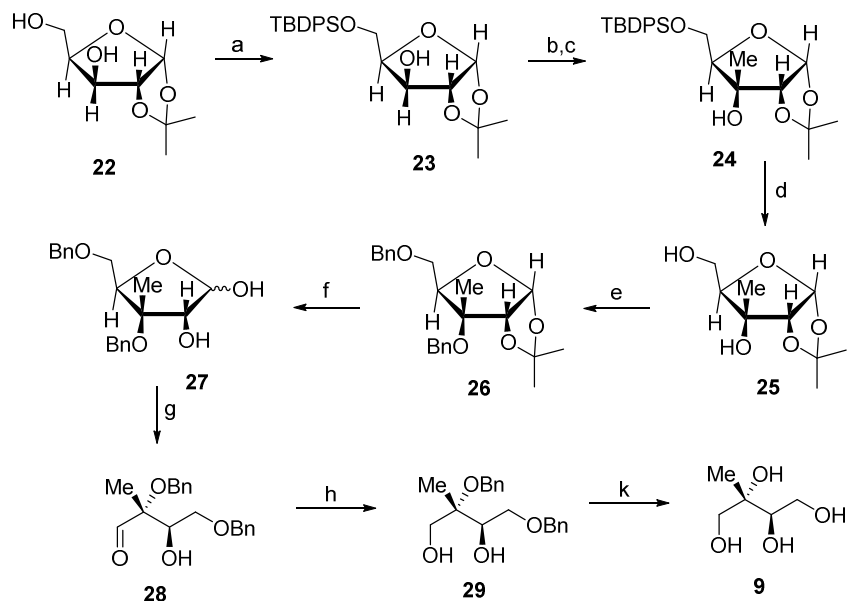
Scheme 29. Synthetic approach for deuterium labelled D and L isomers of ME reported by Duvold *et al.*

Another synthetic approach reported by Tiekink and co-workers also describes the synthesis of ME in 3 steps starting from butadiene **19** (Scheme 30). Using the photo-oxidation, they were able to obtain methylated dioxin **20** from a corresponding butadiene **19** in moderate yield. Similar to Duvold *et al.*, the Sharpless asymmetric dihydroxylation was performed on molecule **20** to generate dihydroxy-dioxane **21** by employing AD mix which contains 2 mol % K<sub>2</sub>OsO<sub>4</sub> and 5 mol % phtalazine ligand. This AD mix enhanced the reaction rate and yield. Next the reduction of peroxide linkage was achieved with palladium catalysed hydrogenation which gave ME **9** in good yield. They achieved the synthesis of ME starting from a butadiene derivative in three steps with an overall yield of 25%.<sup>209</sup>



Scheme 30. ME synthesis through 1,2-dioxin. a) O<sub>2</sub>; b) K<sub>2</sub>O<sub>8</sub>, NMO, MeCN; c) Pd/C, H<sub>2</sub>, MeOH.

Rohmer and co-workers also reported the synthesis of tritium labelled ME starting from commercially available 1,2-*O*-isopropylidene- $\alpha$ -D-xylofuranose **22** in 8 steps with overall yield of 43%.<sup>210</sup> In the first step, they introduced silyl protecting group on primary alcohol group of starting material **22** to produce protected alcohol **23** in 88% yield. Oxidation of secondary alcohol **23** was achieved using Swern oxidation and without further purification, the methyl group was immediately introduced using Grignard reaction to lead to molecule **24** with the desired configuration in 95% yield.

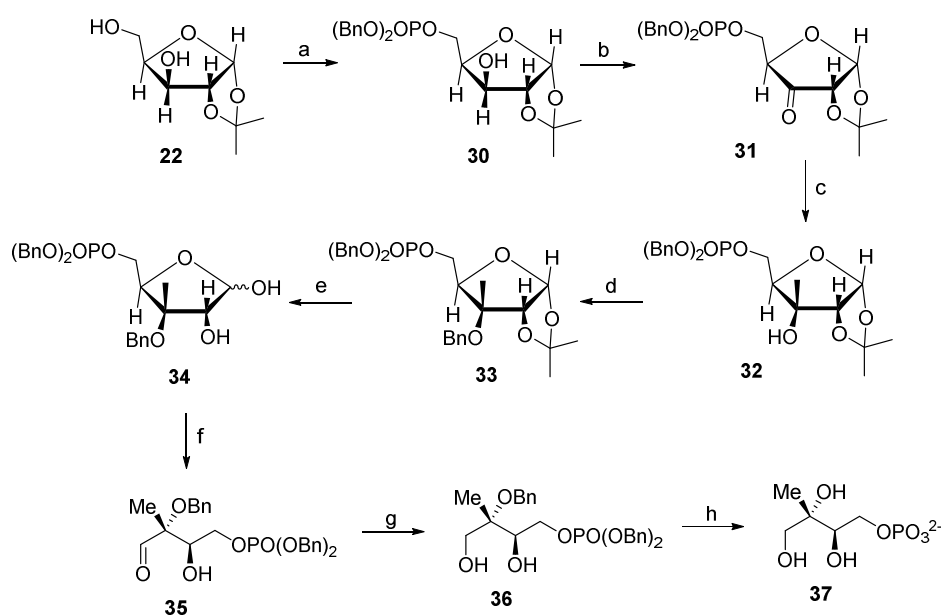


Scheme 31. Synthesis of ME starting from 1,2-*O*-isopropylidene- $\alpha$ -D-xylofuranose. a) TBDPSCl, DMAP, TEA, DCM; b) (COCl)<sub>2</sub>, DMSO, TEA, THF; c) MeMgCl; d) (*n*-Bu)<sub>4</sub>NF, THF; e) NaH, BnBr, DMSO; f) TFA:H<sub>2</sub>O (9:1); g) NaIO<sub>4</sub>, MeOH:H<sub>2</sub>O (1:1); h) NaBH<sub>4</sub>, *i*-Propanol; k) H<sub>2</sub>, Pd/C, EtOH

After cleavage of silyl protecting group with standard fluorine reagent, they protected two alcohol groups with benzyl protecting groups. They have chosen benzyl protecting group

because it was stable under high acidic condition and can be cleaved easily by hydrogenolysis at the last step with no requirement of purification. Benzylation reaction was achieved to produce molecule **26** in 83% yield. Next, the isopropylidene acetal was cleaved under acidic conditions. The resulting hemiacetals were subjected to oxidative cleavage with sodium metaperiodate to produce aldehyde **28** in 90% yield. Reduction of aldehyde by sodium borohydride gave molecule **29** in 92 % yield. The final step conducted under standard catalytic hydrogenation using palladium catalyst to give synthetic ME in excellent 98% yield. The synthetic scheme employed by Rohmer and co-workers is illustrated above (Scheme 31).

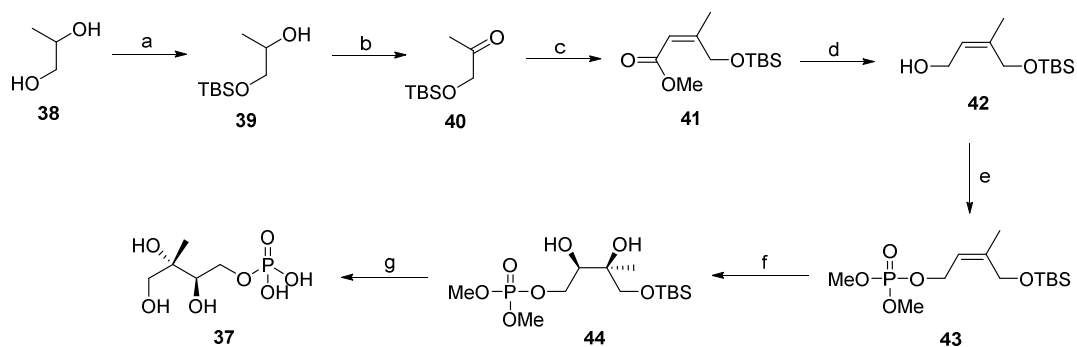
Rohmer and co-workers also adopted their synthetic scheme to prepare MEP starting from similar commercially available carbohydrate.<sup>211</sup> Their synthetic route to MEP is illustrated below in Scheme 32.



Scheme 32. Synthesis of MEP starting from 1,2-O-isopropylidene- $\alpha$ -D-xylofuranose. a)  $(\text{BnO})_2\text{P}(\text{O})\text{Cl}$ , pyridine; b) PDC, AcOH, 3A MS, DCM; c)  $\text{MeMgCl}$ , THF; d) benzyl 2,2,2-trichloroacetimidate,  $\text{CF}_3\text{SO}_3\text{H}$ , *c*-Hex/DCM (2/1); e) aq. TFA; f)  $\text{NaIO}_4$ ,  $\text{MeOH}:\text{H}_2\text{O}$ ; g)  $\text{NaBH}_4$ ,  $\text{MeOH}$ ; h)  $\text{H}_2$ , Pd/C, EtOH.

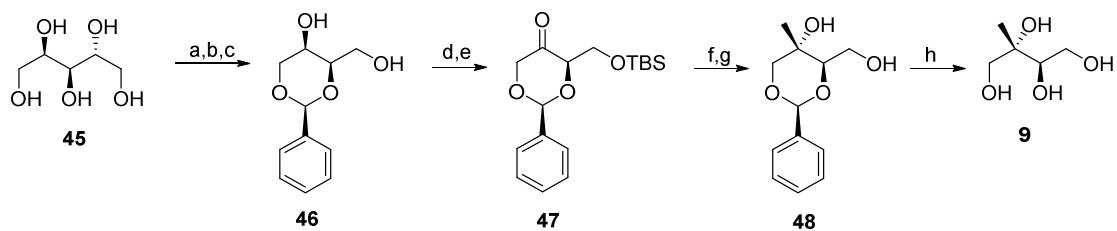
Poulter and co-workers have also been working on the synthetic accessibility to ME and MEP for many years. They first reported the synthetic approach for IspC enzyme product MEP in 7 steps. Starting from commercially available propanediol **38** that was treated with 1 eq of TBSCl, they obtained mono-silylated alcohol **39** in good yield. Subsequent oxidation with ruthenium catalyst TPAP in the presence of NMO gave ketone **40**. The ketone **40** then underwent Horner-

Wadsworth-Emmons reaction to give (*Z*)-dominant olefin **41**. They reported that raising the reaction temperature to  $-40\text{ }^{\circ}\text{C}$  did not affect the yield but *E/Z* selectivity was reduced (more *E* isomers produced). The stereoisomers were readily separated by flash chromatography at this stage or after the introduction of phosphate moiety. The ester was then reduced with DIBAL and subsequent treatment with dimethyl chlorophosphate resulted in phosphoester **43** which was further dihydroxylated with AD mix (Sharpless asymmetric dihydroxylation) to give molecule **44**. They observed that during the dihydroxylation, standard AD mix condition promoted migration of the phosphate moiety to the secondary or tertiary alcohol group. Therefore, basic conditions with  $\text{NaHCO}_3$  buffering was used to prevent this migration. Deprotection of the phosphate moiety was achieved with bromotrimethylsilane and the TBS group was cleaved at the same time with  $\text{HCl}$  to give MEP **37**.<sup>212</sup> (Scheme 33)



Scheme 33. Synthesis of MEP starting from a propanediol. a)  $\text{TBSCl}$ , *N*-ethyl-diisopropylamine,  $\text{DCM}$ ; b)  $\text{TPAP}$ ,  $\text{NMO}$ ,  $\text{DCM}$ ; c)  $\text{KH}$ , bis-(2,2,2-trifluoroethyl)methoxycarbonylmethyl phosphonate,  $\text{THF}$ ; d)  $\text{DIBAL}$ ,  $\text{DCM}$ ; e) dimethyl chlorophosphate,  $\text{DMAP}$ ,  $\text{DCM}$ ; f)  $\text{AD-mix } \beta$ ,  $t\text{-BuOH}/\text{H}_2\text{O}$ ,  $\text{NaHCO}_3$ ; g)  $\text{TMSBr}$ ,  $\text{H}_2\text{O}$ ,  $\text{HCl}$

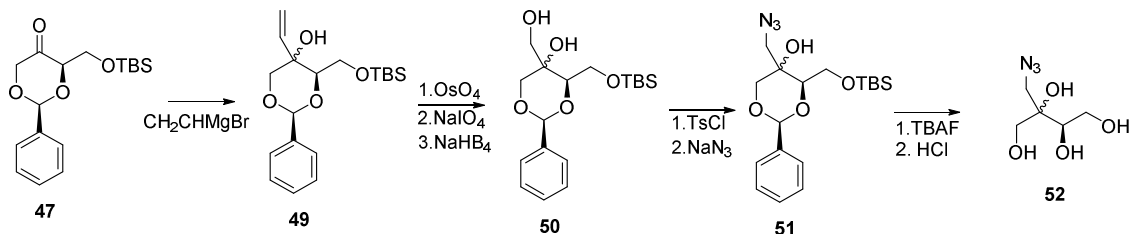
Later Coates and co-workers have reported another approach that entails a main intermediate dioxanone (Scheme 34). Starting from commercial D-arabitol **45**, in three steps the diol **46** was obtained in good yield. It is then converted to ketone using  $\text{TPAP}$  and the resulting ketone is susceptible to Grignard reaction using methyl magnesium bromide to obtain the desired stereo isomer **48** dominantly. The resulting methylated diol is then subjected to catalytic hydrogenation using palladium to give the ME in 60 % yield. By passing through the dioxanone **47** intermediate, this synthetic approach allowed them to access not only ME but also gave possibility to synthesise MEP.<sup>213</sup>



Scheme 34. ME synthesis via dioxanone. a) PhCHO, HCl; b) NaIO<sub>4</sub>, MeOH/H<sub>2</sub>O; c) NaHB<sub>4</sub>, MeOH/H<sub>2</sub>O; d) TBSCl, Imidazole, DCM; e) TPAP, NMO, DCM; f) MeMgBr, Et<sub>2</sub>O; g) TBAF, THF; h) H<sub>2</sub>, Pd(OH)/C

We decided to utilise the dioxanone approach for the synthesis of ME-N<sub>3</sub> because it is versatile, the starting material and reagents are affordable and the chemistry involved is known. Our initial strategy was to attach an oxymethyl group to ketone intermediate **47** to access protected azido alcohol **51** (Scheme 35). The stereochemistry of the quaternary carbon atom of ME-N<sub>3</sub> seemed not to be so important as IspD enzyme only takes the (*S*) isomer and rejects (*R*) isomer<sup>208</sup> therefore if we synthesise the mixture of two stereoisomers our goal should still be achieved.

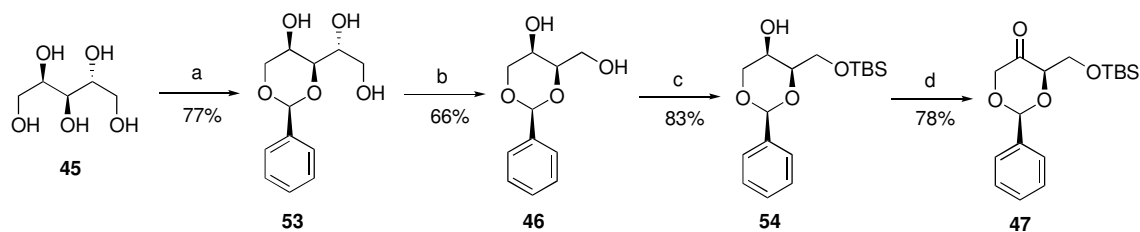
To introduce oxymethyl group on the ketone intermediate, Grignard reaction could be performed using vinyl magnesium bromide to obtain molecule **49** which after dihydroxylation of the double bond with OsO<sub>4</sub> and subsequent oxidative cleavage with NaIO<sub>4</sub> followed by reduction could yield oxymethylated molecule **50**. The alcohol of the oxymethyl group could be converted into a leaving group. Subsequent nucleophilic displacement of this latter with azide and cleavage of TBS and benzylidene acetal protecting groups under standard conditions could further generate ME-N<sub>3</sub>.



Scheme 35. Initial synthetic approach for ME-N<sub>3</sub>

The synthesis of ketone intermediate **47** started with the commercially available D-arabitol **45** as described by Coates and co-workers.<sup>214</sup> The synthesis of 1,3-benzylidene D-arabitol was originally reported by Hudson and co-workers in 1943. They achieved selective protection at 1,3 position of D-arabitol using anhydrous HCl gas passed through the mixture of D-arabitol and benzaldehyde.<sup>215</sup> Although it is described, in the original 1943 paper, that passing HCl gas through the mixture for 20 minutes was enough to achieve complete reaction, we found it insufficient. We found that it was best to keep stirring manually the reaction mixture (approximately 40 minutes) while passing the gas until the reaction mixture becomes a sticky solid mass that was left at room temperature for 18 h. We also noticed that no purification or recrystallization step was needed using this way and that continuous washing with Et<sub>2</sub>O while triturating the solid removes all excess of benzaldehyde yielding pure product. (Scheme 36)

After obtaining benzylidene protected pentose **53**, it was submitted to oxidative cleavage reaction followed by reduction with sodium borohydride to give diol **46** in good yield. The selective protection of the primary alcohol group was easily achieved with *tert*-butyl dimethyl silyl chloride in high yield. The oxidation of molecule **54** was achieved with ruthenium catalyst as described in good yield. We attempted the oxidation using cheaper reagents such as Dess-Martin, pyridinium chlorochromate or pyridinium dichromate because ruthenium catalyst was expensive. We observed that overnight reaction with PCC and PDC results in deprotection of benzylidene group and no ketone was generated. Dess-Martin periodinane worked but the reaction was sluggish. Oxidation reaction was monitored by IR spectroscopy as TLC was deceptive because of overlapping spots of alcohol and ketone. They could, however, be differentiated by staining the TLC with vanillin in which ketone produces brownish spot but the completion of the reaction could not be determined therefore IR was preferred. It should be mentioned that ketone **47** was not stable at room temperature overnight and thus must be submitted to the next reaction immediately after purification. Luckily oxidation catalysed by ruthenium in the presence of 4 Å molecular sieves proceeds clean and fast. Moreover, no purification of **47** was needed. Indeed the reaction mixture was only filtered through a pack of silica gel and after evaporation of the solvent a clean ketone was obtained (95 % pure) as judged by <sup>1</sup>H NMR. We also noticed the cleavage of benzylidene protecting group in the presence of the ruthenium catalysed reaction but this can be minimised by dropping the temperature down to 0 °C and keeping the temperature until the reaction is complete.



Scheme 36. Synthesis of intermediate ketone. a) HCl, PhCHO, 18 h, r.t.; b) NaIO<sub>4</sub>, NaBH<sub>4</sub>, MeOH/H<sub>2</sub>O, 2 h, 0 °C – r.t.; c) TBSCl, Imidazole, DCM, 3 h, 0 °C – r.t.; d) TPAP, NMO, 4Å MS, DCM, 0.5 h, 0 °C.

The ketone intermediate in hand, the Grignard reaction with vinyl magnesium bromide was attempted to synthesise molecule **49**. Initial attempts using commercial Grignard reagent with various conditions failed. *In situ* generation of Grignard reagent using vinyl bromide with metal magnesium and subsequent addition of ketone also did not proceed. Failure to generate Grignard reagent and to accomplish the synthesis of vinyl alcohol **49** led us to revise our initial synthetic plan.

Coates research group had also published a paper that described epoxide formation reactions from ketone intermediate.<sup>9</sup> We decided to follow this procedure to obtain an epoxide intermediate which later can be regioselectively opened by a nucleophilic substitution by azide. After cleavage of protecting groups with standard reagents, the synthesis of ME-N<sub>3</sub> could be achieved.

Following the published result, ketone **47** was converted into an olefin **55** under standard Wittig reaction condition in good yield (Scheme 37). The epoxide ring formation was accomplished by employing *m*-CPBA but this reaction yields two stereoisomers (*S,R*) **56** and (*R,R*) **57** that are separable by flash column chromatography. Although Coates and co-workers reported the ratio of the two isomers to be 2 : 1 (**57** : **56**), we found that, the ratio was approximately 1.4 : 1 (**57** : **56**) as judged by <sup>1</sup>H NMR of the crude reaction mixture (Figure 15). The reaction favours (*R,R*) isomer over (*S,R*) (Scheme 37) and it can be explained by steric hindrance caused by the bulky silyl protecting group.<sup>214</sup>

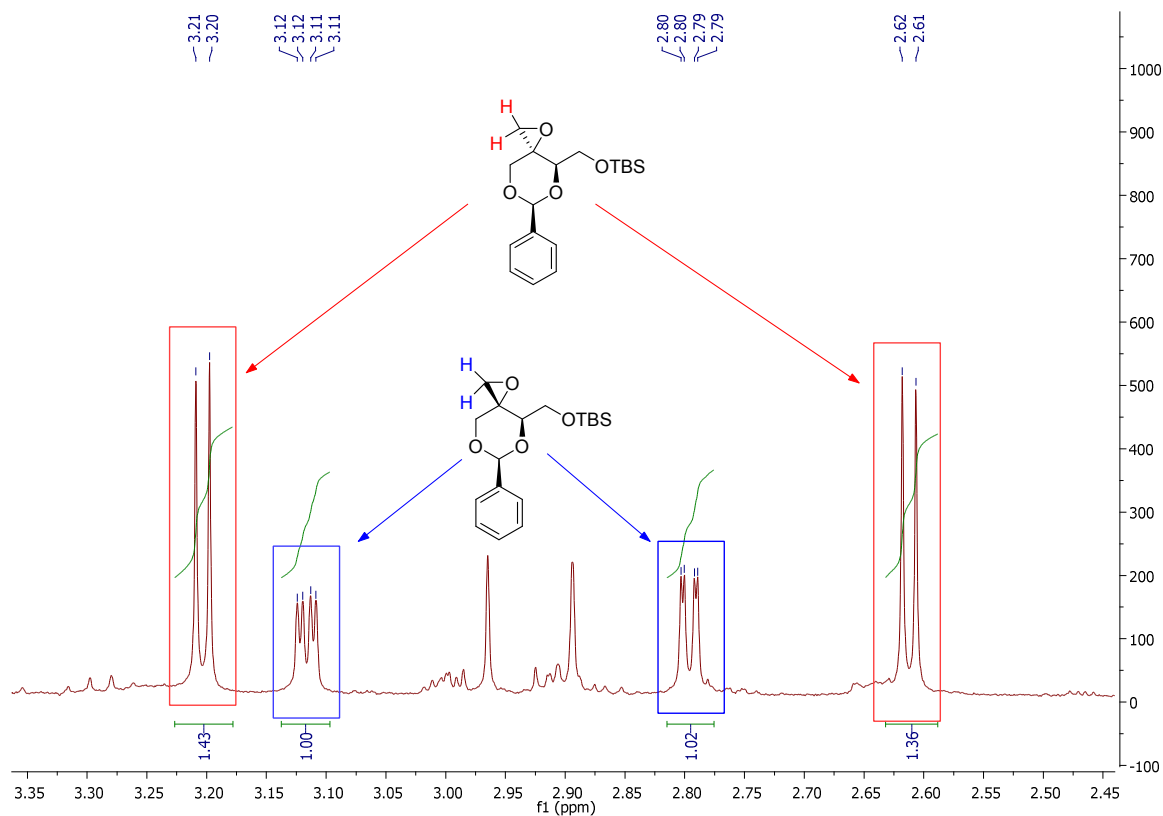
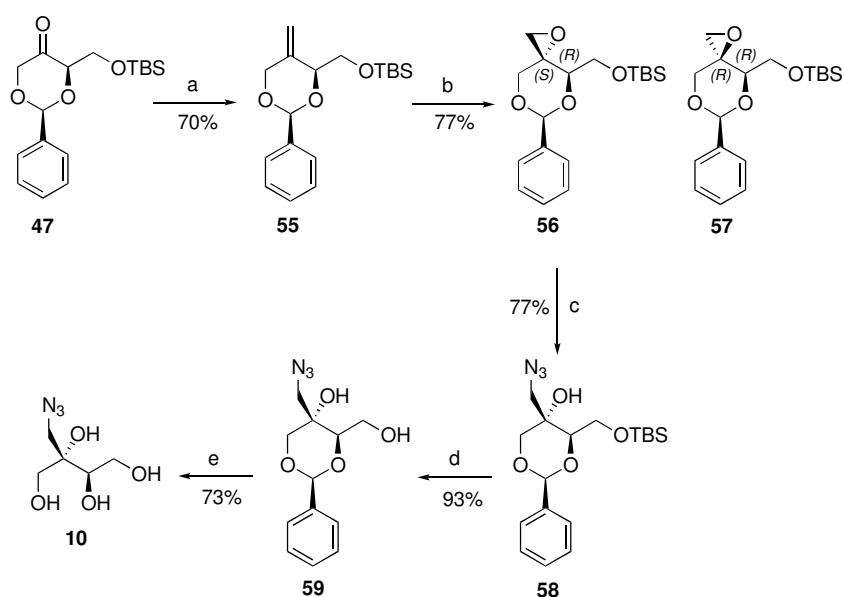


Figure 15.  $^1\text{H}$  NMR spectra of crude mixture of epoxidation reaction. Corresponding protons are highlighted in colours.

Initial reactions did not produce comparable yield as in the publication<sup>214</sup> when reproduced. The yield was lower and the reaction did not reach completion. Prolonging the reaction time from overnight to approximately six days, however, resulted in completion but byproducts formed which were difficult to separate. The main byproduct was benzaldehyde which indicates that the cleavage of benzylidene protecting group occurs the reaction time was increased. It was observed that if commercial *m*-CPBA was purified before the reaction, the cleavage of benzylidene group decreased but was not completely eliminated as judged by TLC. Commercial *m*-CPBA powder contains roughly 10% *m*-chlorobenzoic acid and water as stabilisers to prevent any danger of explosion by pure *m*-CPBA.<sup>216</sup> We thought that the stabilising components (acid and water) most likely triggered the benzylidene cleavage. We, therefore, first washed commercial *m*-CPBA with phosphate buffer<sup>216</sup> to remove residual *m*-chlorobenzoic acid and obtained dry and pure *m*-CPBA as judged by  $^1\text{H}$  NMR. As epoxidation proceeds, *m*-CPBA converts into *m*-chlorobenzoic acid which was insoluble in reaction solvent DCM at 30 °C. Therefore after every two days of reaction, the reaction mixture was filtered through a glass filter to remove *m*-chlorobenzoic acid to minimise benzylidene acetal cleavage.



Scheme 37. Synthesis of ME-N<sub>3</sub> via epoxide intermediate. a) *n*-BuLi, (Ph)<sub>3</sub>PCH<sub>2</sub>Br, THF, 18 h, -75 °C – r.t.; b) *m*-CPBA, DCM, 6 d, r.t.; c) NaN<sub>3</sub>, NH<sub>4</sub>Cl, DMF, 2 h, 60 °C; d) TBAF, THF, 0 °C – r.t.; e) DOWEX, MeOH, 72 h

After obtaining the two epoxide isomers, we continued the synthesis on the desired (*S,R*) isomer **56**. Every steps beyond epoxidation have not been described for these molecules and therefore we also first continued the synthesis on the (*R,R*) isomer **57** in order to test the reactions and optimise them. Epoxide ring opening reaction was accomplished by the nucleophilic azide to afford azido alcohol **58** in good yield. This reaction reaches completion fairly quickly.

Deprotection of silyl group was achieved under standard conditions using TBAF to obtain azido diol **59** in high yield. The final step in our synthetic pathway was reductive ring opening of the benzylidene acetal which was easily achieved by catalytic hydrogenation using palladium catalyst<sup>217-219</sup> in good to high yield. Under these conditions, however, the azide functionality is susceptible to reduction and to convert into an amine group.<sup>220-222</sup> Therefore we used an acidic ion exchange resin to hydrolyse the acetal to afford our target molecule ME-N<sub>3</sub> (**10**) in good yield. One might assume it would be impossible to purify the product using conventional silica gel column chromatography as it contains four hydrophilic hydroxyl groups but we managed to achieve purification using silica gel with DCM : MeOH (9 : 1) ratio of eluent system. As ME-N<sub>3</sub> is not UV active, TLC staining with vanillin was preferred during the purification step.

### 2.3 Synthesis of BCN-TMPP

To detect the metabolic labelling product of ME-N<sub>3</sub>, we decided to utilise SPAAC over CuAAC due to toxicity related to copper catalyst. Bicyclo[6.1.0]nonyne (BCN, **60**) (Figure 16) was chosen for SPAAC reaction compartment because, first, it was readily accessible in our lab and, second, conjugating BCN to a detectable probe was easy to achieve using known chemistry. For detection and analysis of labelled metabolite, we could attach variety of probes including fluorescence or mass spectroscopic probes to BCN moiety. Although fluorescence detection and imaging has been extensively used in labelling sugars (Chapter 1), we decided to utilise a probe suitable for mass spectroscopic analysis in our study because of availableness of the required instrumentation in our laboratory. Enhancement of signal detection during MS analysis is vital to efficiently detect tagged metabolites and therefore we decided to attach a tris(2,4,6-trimethoxyphenyl)phosphine (TMPP) probe to BCN moiety via ethylenediamine linker to synthesise BCN-TMPP molecule **62** (Figure 16).

TMPP probe had been used for MS analysis in metabolic labelling studies. For example, Northen and co-workers demonstrated that neutral lipids in serum extracts can be efficiently detected at an attomole range (under normal conditions they are not detectable by ESI-MS) when they were chemically derivatised with an activated TMPP probe as it carries a permanent positive charge that increases sensitivity in positive ESI-MS analysis.<sup>7</sup> Evans and co-workers also reported an increase of sensitivity in the detection of organic acids such as maleic, sorbic and fumaric acids in plasma when these molecules were derivatised with TMPP probe.<sup>6</sup>

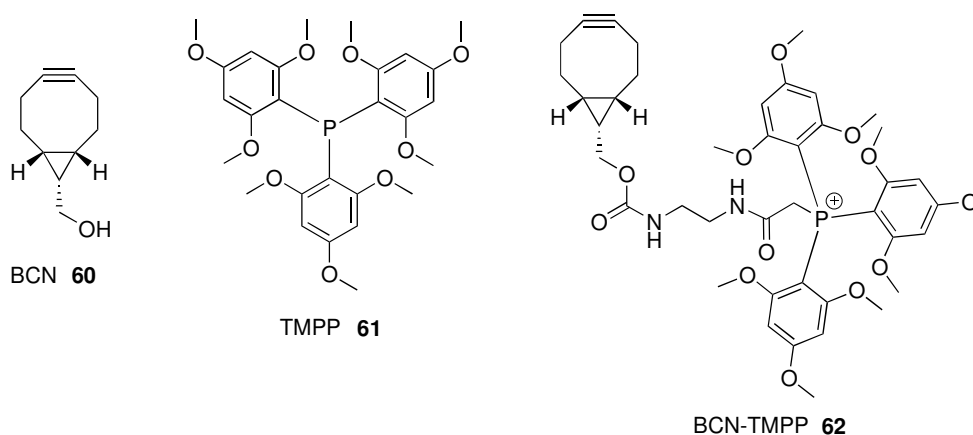
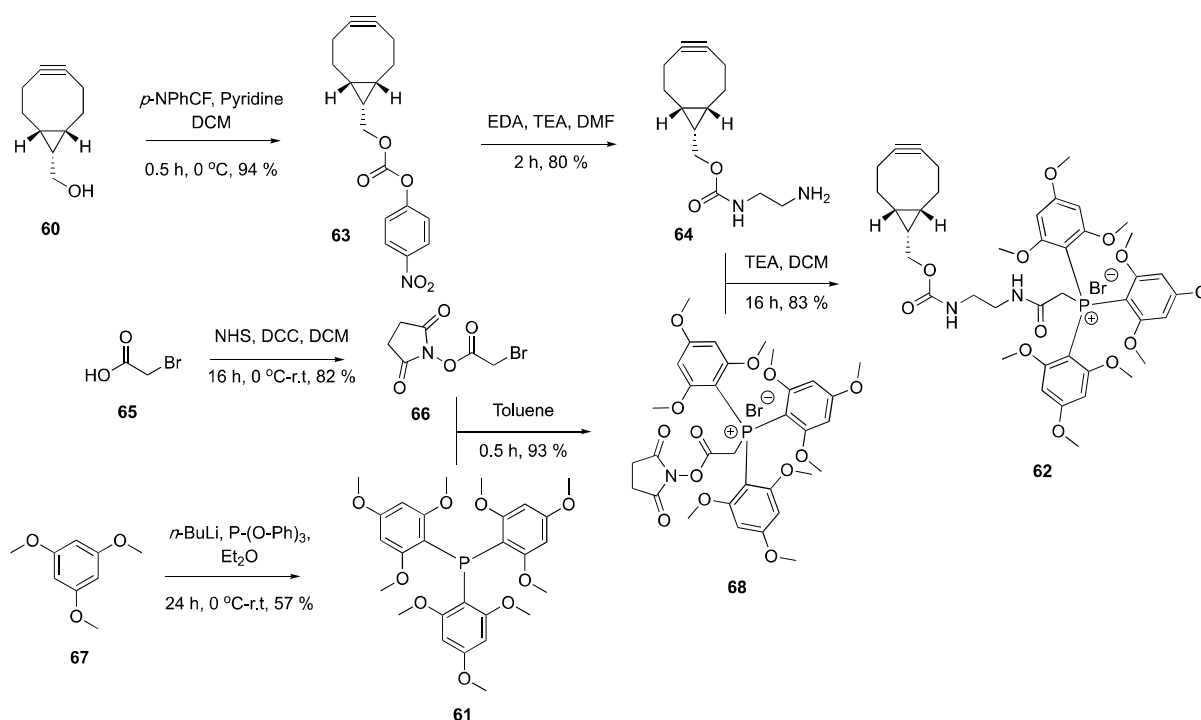


Figure 16. Structure of BCN, TMPP and BCN-TMPP molecules

Tagging biomolecules with a TMPP probe for MS analysis was also adapted for proteomic studies using MS analysis. In proteomic research, peptide derivatisation with TMPP brought two major advantages. First, as it carries a permanent positive charge, it increases the detection of peptides that are otherwise not detectable. Second, because it is hydrophobic due to trimethoxy phenyl groups, it shifts the retention time of derivatised peptides during LC analysis circumventing overlap with non-derivatised peptides and hence allowing to efficiently detect them.<sup>223-226</sup> As MEP pathway intermediates are mainly hydrophilic, hydrophobicity of TMPP probe could also increase the efficiency of detection during LC-MS analysis.

The synthesis of BCN-TMPP was achieved through convergent synthetic pathway (Scheme 38) compared to ME-N<sub>3</sub> which was synthesised through a linear approach. As mentioned above, BCN alcohol **60** was readily accessible in our laboratory and it was converted into its activated form **63** by reacting with *p*-nitrophenyl chloroformate in an excellent yield. The activated BCN **63** was then reacted with solution of ethylene diamine to afford molecule **64** in good yield. On the other hand, TMPP probe was synthesised based on literature report starting from trimethoxy phenyl **67** in the presence of a strong base and triphenyl phosphite.<sup>227</sup>



Scheme 38. Synthetic pathway to BCN-TMPP **62**

The TMPP **61** was then activated with the bromoacetic acid ester **66** to afford activated TMPP **68** in excellent yield. The final step was the coupling of activated TMPP **68** with the ethylene diamine (EDA) link attached to the BCN analogue **64** and this reaction was achieved in good yield under basic condition. Although BCN-TMPP is a charged molecule, we were able to achieve its purification using normal flash chromatography on silica gel.

## 2.4 Kinetic study of click reaction between ME-N<sub>3</sub> and BCN-TMPP

Before starting the *in vivo* incubation experiments of **10** using bacteria, it was necessary to determine the kinetics of the click reaction between molecule **10** and **62**. The kinetic study would provide information on the time of incubation needed and the quantity of BCN-TMPP required to click all tagged metabolites formed during the *in vivo* tests.

Kinetic experiments were performed using HPLC analysis in order to measure the concentration of clicked product over time for a reaction time of 10 hours (Figure 17). ME-N<sub>3</sub> was kept at 0.1 mM and BCN-TMPP varied between 0.1 – 1.6 mM (1 – 16 times ratio).

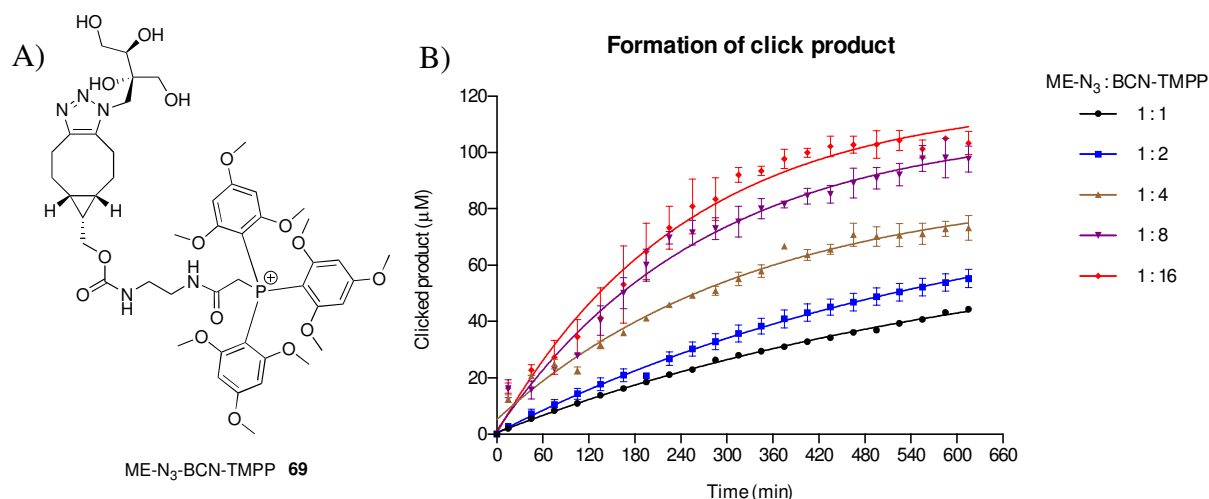


Figure 17. Click reaction kinetics. A) Structure of the clicked product ME-N<sub>3</sub>-BCN-TMPP **69**. B) Formation of ME-N<sub>3</sub>-BCN-TMPP. 20 % MeCN in PBS 0.1 M (pH 7.5), 25 °C.

The second order rate constant was determined to be 12.58 M<sup>-1</sup>min<sup>-1</sup> (0.21 M<sup>-1</sup>s<sup>-1</sup>) (Experimental part, page 129). The second order rate constant was 1.5 times higher when compared to the literature report (0.14 M<sup>-1</sup>s<sup>-1</sup>) for BCN derivative.<sup>228</sup> The kinetic constant of

the reaction depends on the conditions and therefore can be varied. For example, Delft and co-workers have obtained  $0.29 \text{ M}^{-1}\text{s}^{-1}$  for BCN when the reaction was performed in a more polar solvent (MeCN : H<sub>2</sub>O / 1 : 2) compared to the less polar solvent (MeCN : H<sub>2</sub>O / 3 : 1) that resulted  $0.14 \text{ M}^{-1}\text{s}^{-1}$ .<sup>228</sup> This could explain why we obtained higher kinetic constant compared to Delft and co-workers' result because we performed the reaction 20 % MeCN containing aqueous PBS (0.1 M, pH = 7.5) solution. We found that sixteen equivalents of BCN-TMPP was sufficient enough for complete reaction after 10 hours.

## 2.5 Limit of detection of ME-N<sub>3</sub>-BCN-TMPP by LC-MS

Our next goal was to determine the limit of detection (LOD) of the clicked product **69** using LC-MS analysis. By conducting this experiment, we would acquire a knowledge about the quantity of ME-N<sub>3</sub> that should be administered to the bacterial culture for metabolic incorporation. If we incubate less amount of ME-N<sub>3</sub> than the limit of detection of our LC-MS instrument, then we would not be able to detect a tagged metabolite. It was, therefore, crucial to determine the LOD of clicked product using our LC-MS instrument.

To determine the limit of detection, we performed the test in the following two conditions. i) click reaction in phosphate buffer (pH = 7.5) and ii) in a bacterial lysate. Since our goal was to label bacterial metabolism inside the bacteria, it was required to have optimised detection conditions in bacterial lysate. Compared to a buffer system, a bacterial lysate contains bacterial endogenous chemical constituents that could affect the click reaction and its product detection. Therefore, we needed to determine the amount of clicked product **69** that could be detected in a bacterial lysate.

We prepared an *E.coli* lysate for LOD determination to know if the obtained LOD will be comparable to the test in buffer. An *E.coli* culture was incubated with the natural substrate ME and after incubation and resuspension in PBS buffer, the mixture was sonicated to obtain the bacterial lysate.

The LC-MS analysis of the synthesised clicked product **69** under the developed LC-MS conditions led to m/z 493 Da (Figure 18) rather than whole molecular mass of **69** (987 Da). We could anticipate additional protonation as the eluent system contained 0.05 % formic acid and this result was consistent in both buffer system and bacterial lysate.



For example, in PBS (pH=7.5), the MS peak intensity of clicked product **69** was 990 in the reaction mixture where 0.01  $\mu\text{M}$  ME-N<sub>3</sub> and 0.2  $\mu\text{M}$  BCN-TMPP were reacted. On the other hand, the MS peak intensity of clicked product **69** was 250 in the reaction mixture where 0.01  $\mu\text{M}$  ME-N<sub>3</sub> and 0.2  $\mu\text{M}$  BCN-TMPP were reacted in bacterial lysate. In both cases (buffer and the lysate), we found that LOD was 0.01  $\mu\text{M}$  ME-N<sub>3</sub>. Even when the single ion recording mode (MS detector searches for a predefined single mass and ignores other masses) was used on apparatus, we were not able to detect the clicked product signal below 0.01  $\mu\text{M}$  ME-N<sub>3</sub> range. (Experimental part, page 130)

Although TMPP tag enhances signal during MS analysis and it has been successfully applied for this purpose on many different studies by increasing detection range,<sup>6,7</sup> LOD would depend on many factors such as machine's sensitivity and injection volume etc.

## 2.6 LC-MS analysis of ME-N<sub>3</sub> incorporation in *E.coli*

We further carried out the metabolic labelling experiments of the MEP pathway with molecule **10** as probe using *E.coli* (MG1655) strain. Synthetic ME can be incorporated into *E.coli* and used in the MEP pathway as previously reported in the group.<sup>85</sup> *E.coli* was cultured in M9 media in the presence of 10 mM of ME-N<sub>3</sub> for 22 hours under shaking (200 rpm). The bacteria were further harvested by centrifugation. Bacterial lysate was obtained after resuspension of the cells in buffer (PBS, pH = 7.5) followed by sonication. The proteins were removed by precipitation using acetonitrile.<sup>229</sup> We anticipated that incorporated azide tagged metabolites' concentration would range from 0.02 – 0.06  $\mu\text{M}$ <sup>85</sup> due to previous [<sup>3</sup>H]-ME labelled experiments. Based on our kinetic results we further incubated the bacterial lysate with 20 equivalents of BCN-TMPP overnight and analysed the samples by LC-MS.

As clicked product **69** gives m/z 493 (+2 charged) signal during LC-MS analysis, we could exploit this overall +2 charge feature to search for BCN-TMPP clicked MEP pathway products that have a molecular mass higher than 1250 Da as our MS detector was unable to detect higher masses than 1250 Da.

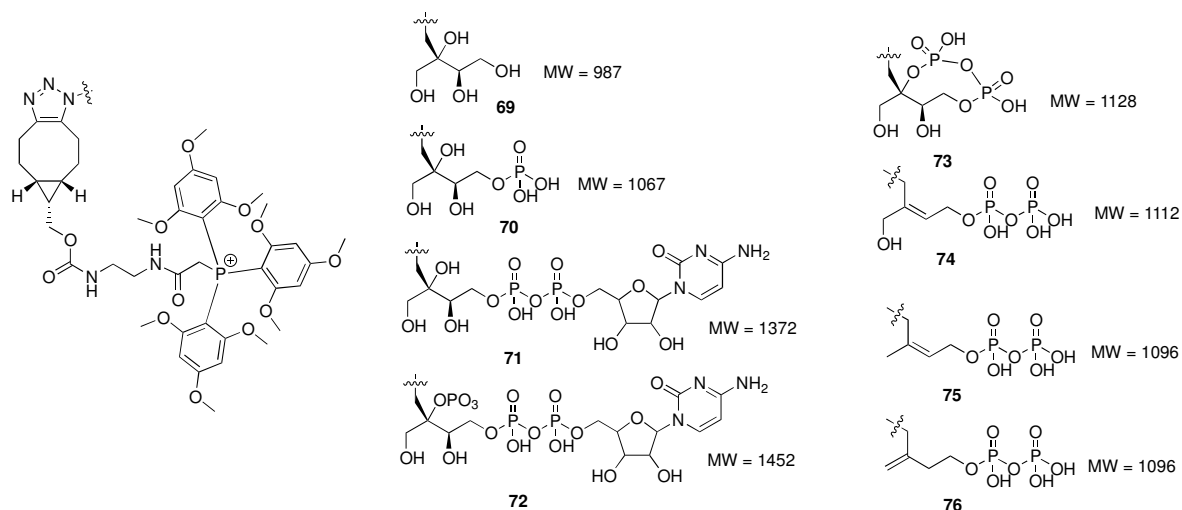


Figure 20. Structure and molecular weight (MW) of MEP pathway products clicked with BCN-TMPP

Initially we screened for the molecular weights of MEP pathway products clicked with BCN-TMPP that are given in Figure 20 except for the masses of products **71** and **72** that have a higher molecular weight than the MS detector sensitivity. As synthesised click product **69** is protonated during the analysis, we also screened possible +2 charged products. Unfortunately, we did not observe any signal corresponding to the possible products. This negative result might be due to the fragmentation of the products during the analysis and therefore possible fragmentations were searched using SIR mode.

From the literature research, we found two possible fragmentation patterns for endogenous diphosphate molecules. The first possible fragmentation is cleavage of phosphodiester bond to release phosphate moiety (**78**,  $\text{PO}_3$ ).<sup>230, 231</sup> Another possible fragmentation is the loss of water from diphosphate moiety to produce molecule **79** (Figure 21).<sup>232, 233</sup> During our search for possible fragmented products, we observed a signal corresponding to 1078 Da with a retention time of 2.34 min that could arise from molecule **80** (Figure 21).

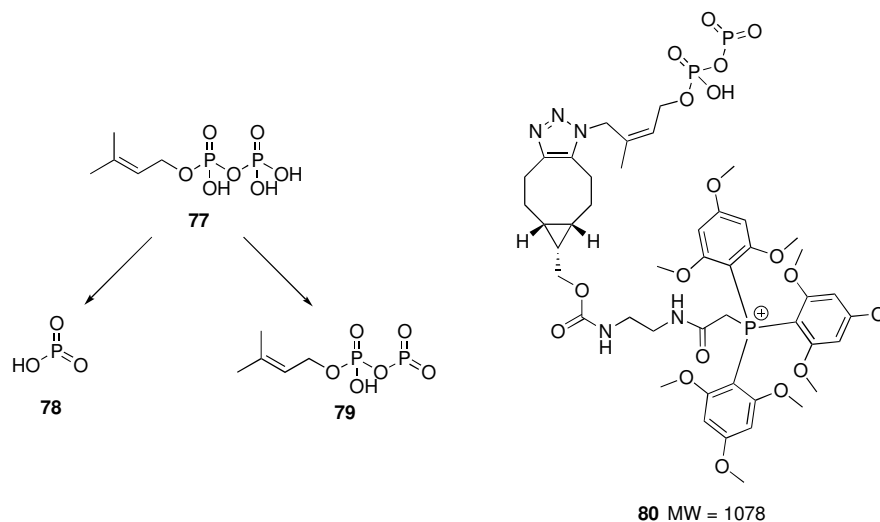


Figure 21. Fragmentation of DMAPP during MS analysis and structure of possible fragmented clicked product.

The control experiment that was performed using lysate from *E.coli* incubated with synthetic ME did not produce a signal at the same retention time (2.34 min) showing that this peak might not be an artefact (Figure 22). As no other possible clicked products were detected, we needed to validate this result by comparing the retention time of the peak that might correspond to fragmented product **80** with the retention time obtained for the clicked product formed by synthetic N<sub>3</sub>-DMAPP with BCN-TMPP.

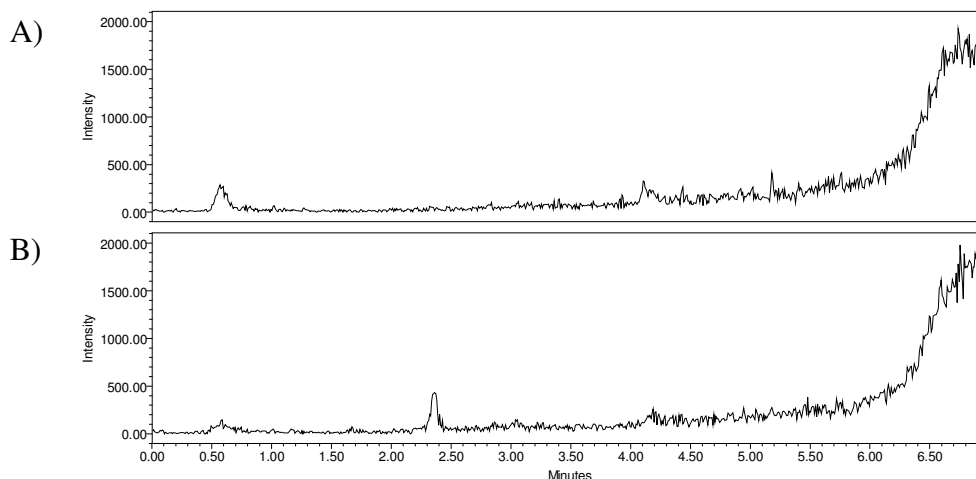
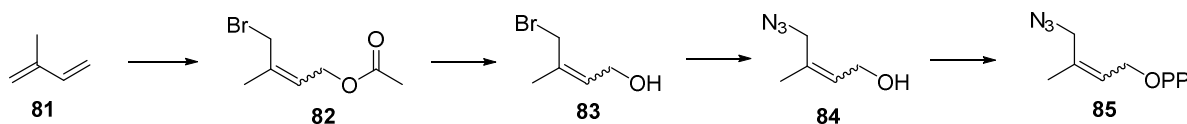


Figure 22. Chromatogram of MS analysis of the bacterial extract after incubation of ME or ME-N<sub>3</sub> in *E.coli* using SIR mode. A) ME incubated in bacterial culture (control experiment). B) ME-N<sub>3</sub> incubated in bacterial culture. Peak at 2.34 min might correspond to fragmented molecule **80**.

Therefore, the synthesis of azide tagged dimethyl allyl diphosphate ( $N_3$ -DMAPP) was performed. Once the product in hand, we would be able to click it with BCN-TMPP and analyse the adduct by LC-MS in order to confirm that *E.coli* transformed ME- $N_3$  into  $N_3$ -DMAPP.

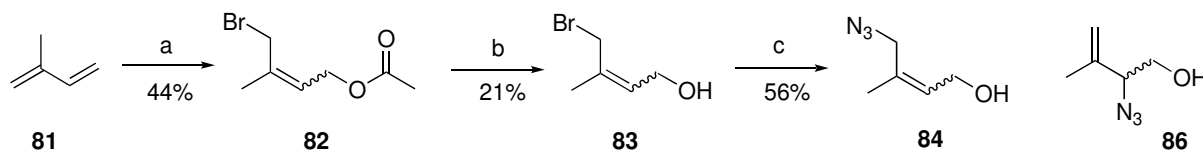
## 2.7 Synthesis and LC-MS analysis of $N_3$ -DMAPP

Our synthetic approach to  $N_3$ -DMAPP was to start with the commercially available isoprene (**81**) (Scheme 39). Isoprene can be converted into bromo acetyl ester **82** in one step followed by deacetylation and displacement of bromine by azide. The resulting azido alcohol **84** can be diphosphorylated to give  $N_3$ -DMAPP **85** (Scheme 39)



Scheme 39. Possible synthesis of  $N_3$ -DMAPP starting from isoprene.

The synthesis started with isoprene to obtain molecule **82** in moderate yield and the acetyl group was cleaved in the presence of a base to give bromo alcohol **83** in low yield. Although the first step produces mixture of *E/Z* isomers, the products were not separated as our goal was to determine the LC retention time of synthetic  $N_3$ -DMAPP clicked with BCN-TMPP.

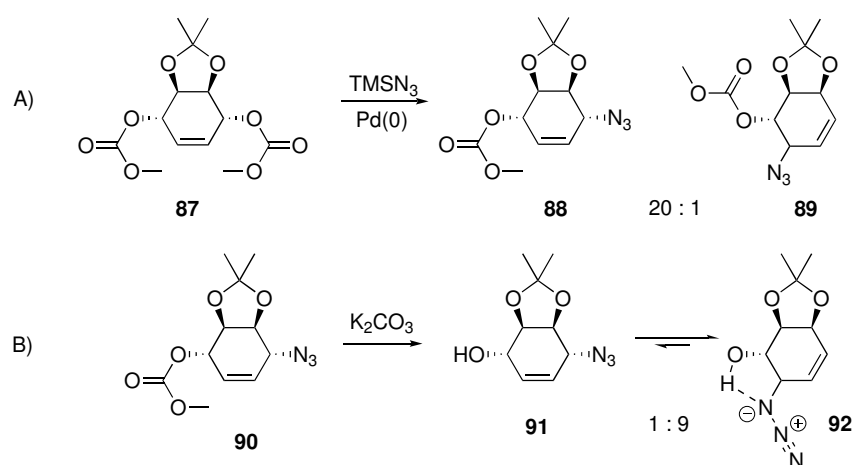


Scheme 40. Synthesis of azido alcohol **84**. a) NBS, AcOH, *p*-TSA, 2 h, 80 °C – r.t.; b)  $K_2CO_3$ , MeOH, 2 h, r.t.; c)  $NaN_3$ , DMF, 1 h, r.t.

The ratio between *E/Z* isomers of **82** was 8 : 2 according to  $^1H$  NMR analysis (literature, 7 : 3)<sup>234</sup> and the two isomers were inseparable by chromatography. Deacetylation was achieved in

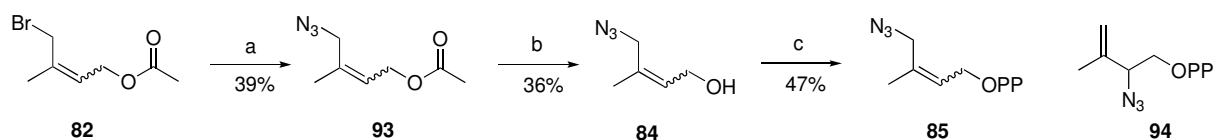
21 % yield with standard procedure with a base to afford *E/Z* isomers of bromo alcohol **83**. The bromo alcohol **83** then underwent a nucleophilic substitution reaction with sodium azide in DMF and the reaction generated two products as judged by TLC.  $^1\text{H}$  NMR analysis revealed that azide group was shifted intramolecularly and gave product **86** as a major product (Scheme 40). The ratio between azido alcohol **84** : **86** was 3 : 7 according to  $^1\text{H}$  NMR analysis. Another problem was that azido alcohol **84** was unstable and therefore spontaneously converts into azido alcohol **86** over time. Therefore it was impossible to obtain pure compound **84** as azide group shifts during purification process. In fact, intramolecular rearrangement of allylic azide group was already reported. From the literature research we found that this type of rearrangement is called Winstein rearrangement. It was first reported in 1960 by Winstein and co-workers who observed the rapid equilibration of allylic azides when azide ion was used as a trap for cationic intermediates for solvolysis of allylic halides.<sup>235</sup>

The ratio between the two allylic azido alcohols can be explained by intramolecular hydrogen bonding. Pulley and co-workers reported that [3,3]-sigmatropic rearrangement of 1,4-allylic azide product **88** occurred less if the reaction is performed in an appropriate condition using palladium catalyst (Scheme 41, A). They were able to achieve ratio of 20 : 1 for 1,4-product **88** and rearranged 1,2-product **89** respectively. They assumed that if carbonate group was hydrolysed to free the alcohol group, the formation of rearranged 1,2-product could be favoured thermodynamically as free hydroxyl group can make hydrogen bonding with shifted azide functionality. When the hydroxyl group was released under basic condition, 1 : 9 (**91** : **92**) ratio was observed and it proves that the thermodynamic product was rearranged 1,2-isomer **92** due to intramolecular hydrogen bonding (Scheme 41, B).<sup>236</sup>



Scheme 41. Rearrangement observed by Pulley and co-workers.

Based on the study of Pulley and co-workers, we decided to introduce the azide group before deacetylation of the hydroxyl group in order to prevent azide shift due to hydrogen bonding.<sup>237</sup> The bromo ester **82** was transformed into azido ester **93** in moderate yield (Scheme 42). As expected, the [3,3]-sigmatropic rearrangement of azide group was not observed. The azido ester was then submitted to deacetylation under basic condition which provided azido alcohol **84** also in moderate yield. However, the sigmatropic rearrangement occurs during the purification step.



Scheme 42. Synthesis of  $N_3$ -DMAPP. a)  $\text{NaN}_3$ , Acetone/ $\text{H}_2\text{O}$ , 10 min, r.t.; b)  $\text{K}_2\text{CO}_3$ , MeOH, 0.5 h, r.t.; c)  $\text{CNCCl}_3$ ,  $\text{Et}_3\text{N}$ ,  $\text{H}_3\text{PO}_4$ , MeCN, 0.5 h, 0 °C – r.t.

**84** was, therefore, submitted to diphosphorylation reaction using  $\text{H}_3\text{PO}_4$ . Phosphorylation by  $\text{H}_3\text{PO}_4$  in the presence of  $\text{CCl}_3\text{CN}$  and  $\text{Et}_3\text{N}$  produces mono, di and triphosphorylated products that can be separated by flash chromatography on silica gel using 28 %  $\text{NH}_4\text{OH}$  solution, water and isopropanol (3 : 1 : 6) as eluent system. After lyophilisation, a white solid mass was obtained which was partly insoluble in water. This insoluble material was some small amount of silica gel that dissolved in water (in eluent system) and eluted from the column. The initial white solid was therefore redissolved in a small amount of water and filtered to remove insoluble silica gel and the filtrate was lyophilised again.

The phosphorylation reaction yielded  $N_3$ -DMAPP **85** with *E/Z* isomer 7 : 3 (according to integration of  $\text{H}_1$  and  $\text{H}_2$ ) ratio as well as azide shifted DMAPP **94** with ratio of 1 : 1 to (*E*)- $N_3$ -DMAPP (according to integration of  $\text{H}_1$  and  $\text{H}_3$  or  $\text{H}_4$ ). (Figure 23)

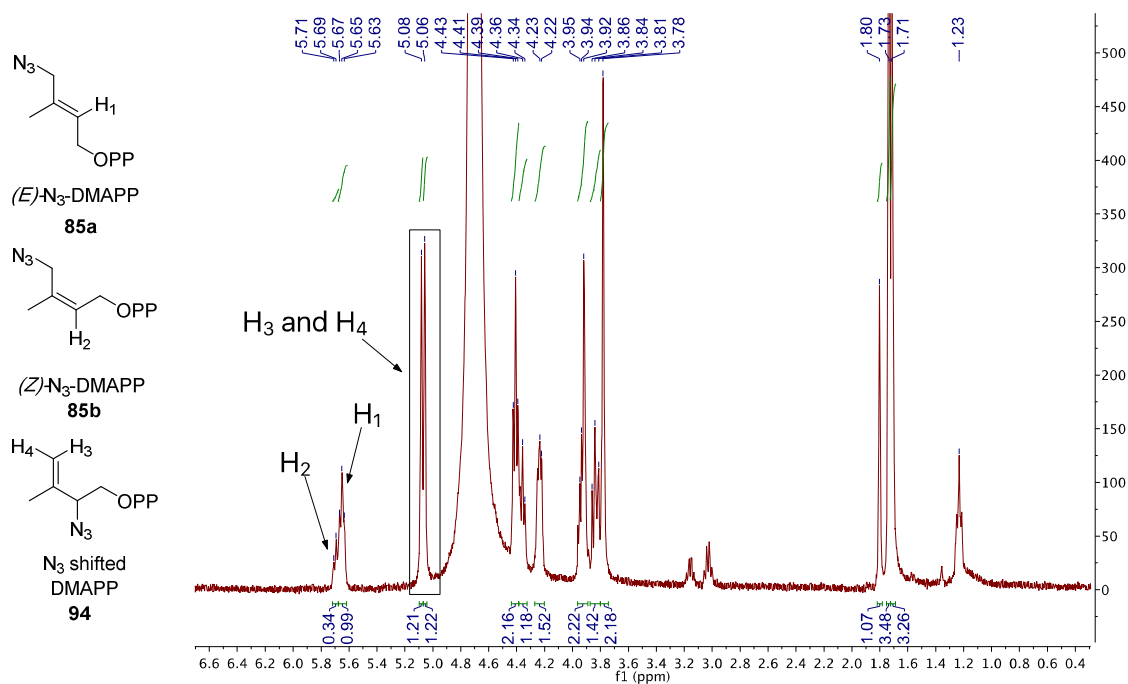


Figure 23.  $^1H$  NMR spectra and structure of  $E/Z$  and azide shifted  $N_3$ -DMAPP.

Once synthetic  $N_3$ -DMAPP **85** was obtained, the click reaction with BCN-TMPP was performed. The LC-MS analysis of the clicked product **75** was carried out under the same conditions as described previously. LC-MS analysis led to a non-protonated molecular mass of 1096 Da and a protonated +2 charged moiety mass of 548 Da as expected. (Figure 24)

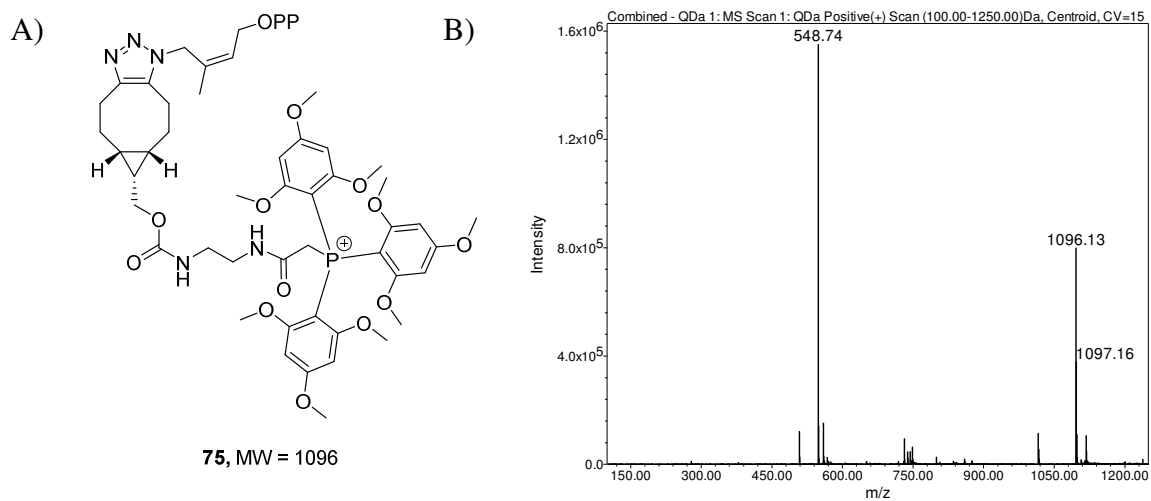


Figure 24. A) Structure of  $N_3$ -DMAPP and BCN-TMPP clicked product, B) Mass spectra of molecule **75**

Unfortunately, we did not detect any relevant peak at retention time of 2.34 min when clicked product **75** was scanned using SIR mode - 1078 Da (Figure 25). This result proves that our assumption was wrong. We could see that clicked product **75** did not fragment during the LC-MS analysis from Figure 24, B. If our assumption would be correct, we would see a peak at 2.34 min that should correspond to the suggested fragmented molecule **80** (Figure 22, B)

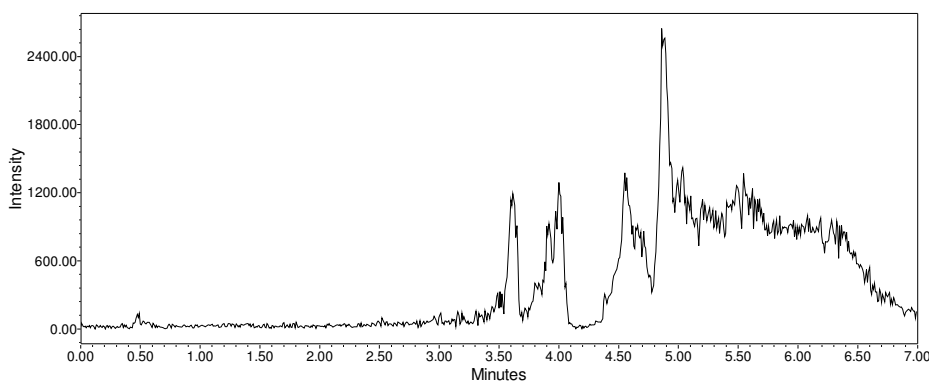


Figure 25. MS scan (SIR mode – 1078 Da) of molecule **75**.

Although we did not succeed in detecting ME-N<sub>3</sub> incorporated metabolites of *E.coli*, detection of N<sub>3</sub>-DMAPP using BCN-TMPP was possible, showing that the detection of an azide tagged MEP pathway intermediate using bioorthogonal chemistry and the LC-MS instrumentation the team.

## 2.8 ME-N<sub>3</sub> incorporation study using mutant *E.coli* EcAB4-5

The inability to detect ME-N<sub>3</sub> metabolites could be explained by the fact that these metabolites might be present in quantities that were too low to be detected by our LC-MS instrument. In order to increase the amount of ME-N<sub>3</sub> metabolites of the MEP pathway, we decided to perform the previous incubation experiment using an *E.coli* EcAB4-5 mutant that lacks *gcpE* gene *i.e* has no IspG enzyme. Therefore MEP pathway does not proceed beyond ME-cPP (Scheme 9) production in this mutant.<sup>85</sup> If synthetic ME-N<sub>3</sub> incorporates into the MEP pathway in this mutant, it can only be metabolised until N<sub>3</sub>-ME-cPP **98**. Therefore, with this mutant only N<sub>3</sub>-MEP **95**, N<sub>3</sub>-ME-CDP **96**, N<sub>3</sub>-MEP-CDP **97** and N<sub>3</sub>-ME-cPP (Figure 26) can form which limits the number of metabolites and the masses to be detected. We also envisioned to detect N<sub>3</sub>-ME-

cPP because it should accumulate and therefore be present in a higher concentration over other azide tagged intermediates. After incubation of *E.coli* EcAB4-5 with ME-N<sub>3</sub> followed by the preparation of the bacterial extracts explained previously, we screened for possible azide tagged products **95**, **96**, **97** and **98** but no expected signal corresponding to the masses of the metabolites was detected by LC-MS analysis.

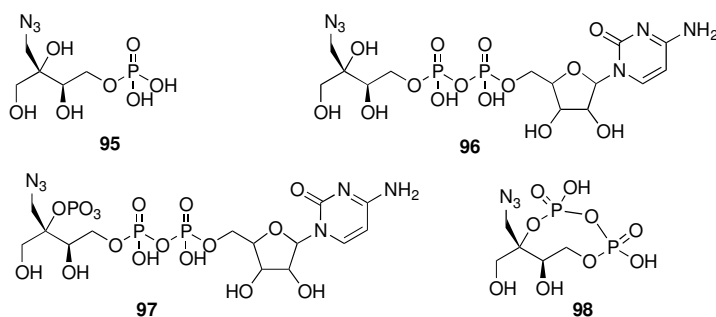


Figure 26. Structure of azide tagged MEP pathway metabolites that could be produced from ME-N<sub>3</sub> in *E.coli* EcAB4-5 mutant

This negative result could be due to the fact that ME-N<sub>3</sub> might not be incorporated in *E.coli*. It is known that *E.coli* uses the sorbitol phosphotransferase complex<sup>238</sup> to incorporate ME but ME-N<sub>3</sub> might not be passing the *E.coli* membranes. Another reason might be that ME-N<sub>3</sub> is inhibiting the MEP pathway.

We also observed that *E.coli* EcAB4-5 mutant did not grow very fast in the presence of ME-N<sub>3</sub>. Therefore, we hypothesised that ME-N<sub>3</sub> might inhibit cell growth. We measured the growth curves of both *E.coli* MG1655 and EcAB4-5 mutant (Figure 27). After overnight incubation, the cultures reached plateau but the OD<sub>600</sub> (Optical Density at 600 nm) did not differ in the presence or absence of ME-N<sub>3</sub>.

MG1655 culture reached plateau after 23 h for all concentrations of ME-N<sub>3</sub> tested but, when the incubation was further continued until 25 h, we did not see any significant change in OD (Figure 27). For EcAB4-5 mutant, the OD<sub>600</sub> steadily rise until OD<sub>600</sub> ≈ 2.0 in 23 h. Compared to MG1655 mutant, EcAB4-5 mutant led to a small drop in OD<sub>600</sub> when the incubation was continued for more than 23 h.

From these experiments, ME-N<sub>3</sub> does not seem to inhibit the growth of the *E.coli* EcAB4-5 and MG1655.

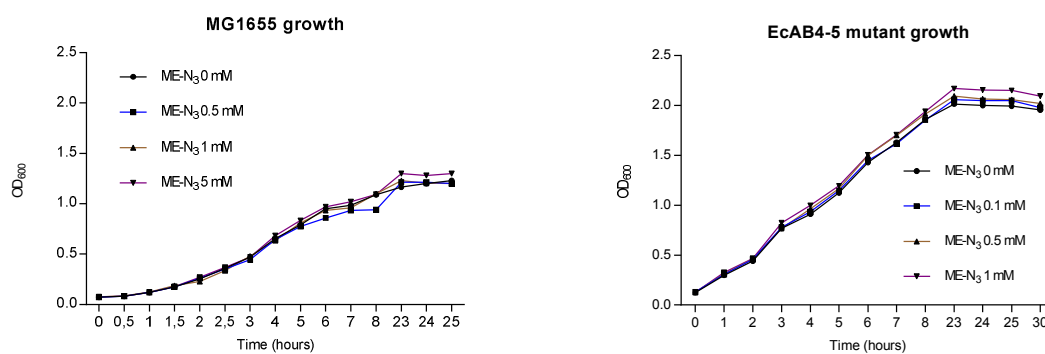


Figure 27. Growth curves of *E. coli* MG1655 (performed in M9 media) and *EcAB4-5* mutant (performed in LB media).

In the next chapter, we investigated whether ME-N<sub>3</sub> incorporates into the MEP pathway if it is phosphorylated. By studying IspD, the third enzyme of the MEP pathway, using phosphorylated ME-N<sub>3</sub> could reveal if ME-N<sub>3</sub> can be incorporated into the MEP pathway.

To summarise, we have successfully synthesised ME-N<sub>3</sub> through a multistep linear synthetic approach in 9 steps with an overall yield of 12 %. As a click reaction compartment, we have also synthesised BCN-TMPP through a convergent synthetic pathway with an overall yield of 62 %.

After synthesis of ME-N<sub>3</sub> and BCN-TMPP, we have determined click reaction kinetics and the limit of detection using LC-MS analysis. The second order rate constant of the click reaction between ME-N<sub>3</sub> and BCN-TMPP was 1.5 times higher than the literature report. This difference might be due to differences in experimental conditions. With the help of TMPP probe attached to BCN we were able to detect a clicked molecule in the range of 10 nM using our LC-MS apparatus. We assumed this LOD range was sufficient to detect a tagged metabolite based on previous literature reports. Although some researchers found that TMPP probe increases detection range, it also depends on LC-MS equipment and of the experimental conditions.

When *E.coli* was incubated with ME-N<sub>3</sub>, any clicked metabolite was detected using LC-MS analysis. Through searching possible fragmented metabolites using MS, we detected a signal that was hypothesised to be azide tagged DMAPP fragment. To validate this result, N<sub>3</sub>-DMAPP was synthesised in 4 steps starting from isoprene. The click reaction between the synthetic sample of N<sub>3</sub>-DMAPP and BCN-TMPP led to a different signal as the one we assumed to be N<sub>3</sub>-DMAPP fragment. This result proved that our hypothesis about the possible fragment was wrong. We also performed a similar incubation study using an *E.coli* strain that is deficient in IspG, an enzyme of the MEP pathway. If the mutant incorporates ME-N<sub>3</sub>, we should detect certain metabolites but, even in this case, any relevant signal of expected metabolites was detected by LC-MS analysis.

Inability to detect any MEP pathway metabolite using mass spectroscopy draws the question that ME-N<sub>3</sub> might not enter *E.coli* or it might not be metabolised? From all these experiments, we can not conclude on ME-N<sub>3</sub> cell permeability or incorporation. However, the concentration of ME-N<sub>3</sub> incorporated into the bacteria might be too low to allow its detection by LC-MS. In the case if *E.coli* would incorporate ME-N<sub>3</sub>, further experiments would consist in concentrating the bacterial lysate to have sufficient amount of tagged metabolites and using a more sensitive MS instrument.

# CHAPTER-3

## Kinetic Studies of IspD enzyme

### 3.1 Introduction to enzyme kinetics

Enzymes like other catalysts increase the reaction rate. If we consider a simple enzymatic reaction that converts one substrate into one product, the reaction can be written as follows.



First a free enzyme (E) binds to a substrate (S) to form an enzyme substrate complex (ES) after which the enzyme catalyses the transformation to form an enzyme product complex (EP). Once the product (P) is formed, it is released from the complex to free the enzyme for the next catalytic conversion. The formation of the ES complex during an enzymatic reaction was first reported by Leonor Michaelis and Maud Leonora Menten in 1913.<sup>239</sup> In their paper, they described that the initial rate of the reaction was proportional to enzyme-substrate (ES) complex concentration. Initially, they hypothesised that an enzyme catalysis occurs via ES complex formation and proved their hypothesis by fitting experimental data to the now famous Michaelis-Menten equation (1) where  $v$  – reaction rate,  $V_{max}$  – maximum velocity,  $[S]$  – substrate concentration and  $K_m$  – Michaelis constant.<sup>240</sup> The relationship between reaction rate and substrate concentration was actually first pointed out by the French chemist Victor Henri in early 1900s.<sup>241</sup>

$$v = \frac{V_{max} [S]}{K_m + [S]} \quad (1) \qquad \frac{1}{v} = \frac{1}{V_{max}} \left( 1 + \frac{K_m}{[S]} \right) \quad (1')$$

In 1925, the British scientists George Briggs and John Haldane proposed a modification of the Michaelis-Menten theory that assumes E and S are always in a rapid equilibrium with ES. What, Haldane and Briggs, reported was that as soon as E and S are mixed, ES concentration reaches a constant value after a certain time and therefore steady state approximation can be used in Michaelis-Menten kinetics.<sup>242</sup>

$V_{max}$  is the maximum reaction rate at a saturating substrate concentration and  $K_m$  represents the substrate concentration at which the half of  $V_{max}$  can be achieved. (Figure 28). Single substrate enzymatic reactions generally tend to obey Michaelis-Menten kinetics.  $V_{max}$  and  $K_m$  values can be determined using GraphPad Prism (graphic analysis software) by plotting reaction rate versus substrate concentration and fitting the data to equation (1) and  $V_{max}$  and  $K_m$  values can also be estimated using the double reciprocal plot with equation (1').

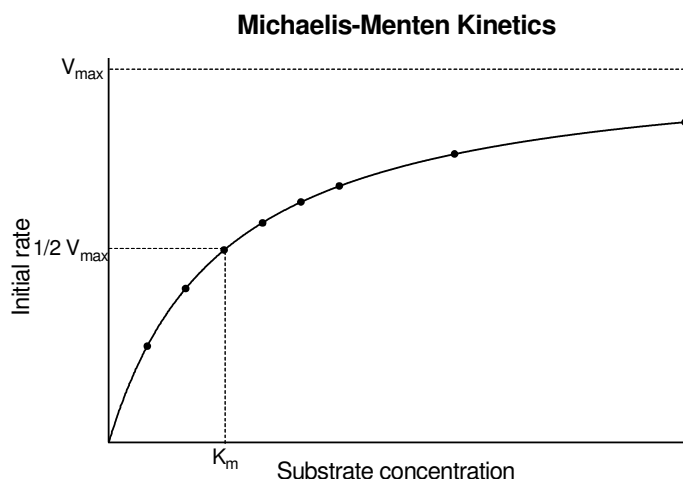
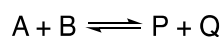


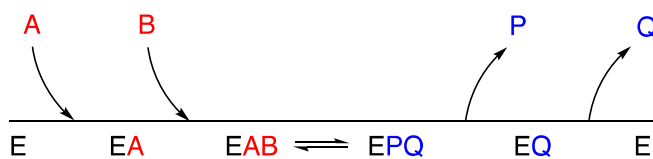
Figure 28. Michaelis-Menten equation fitted curve. Initial rate as a function of substrate concentration.

For two substrates (bisubstrate) enzymatic reactions, the kinetic analysis becomes simple when one substrate concentration is fixed and the other substrate concentration is varied. Performing enzymatic tests under this condition and analysis of the data using equation (1) yields kinetic constants. For example, general bisubstrate reaction can be written as follows:



Substrates A and B are converted to products P and Q by the enzyme. If we want to determine kinetic constants of the enzyme for substrate A, then we should perform enzymatic reaction where [B] is constant and [A] is varied. Fitting the data to equation (1) will provide  $V_{\max}$  value of the enzyme, and the  $K_m$  for substrate A, and vice versa.<sup>243</sup>

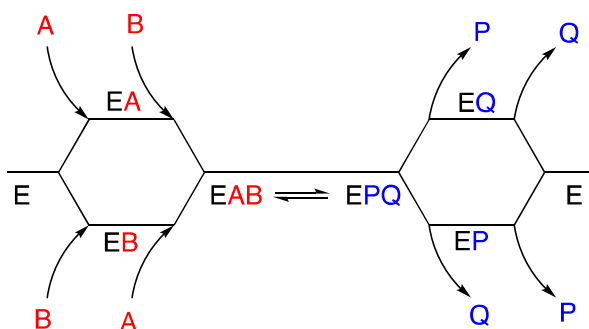
The mechanism of a bisubstrate reaction can be different depending on how substrates bind to the enzyme. According to nomenclature by Cleland, bisubstrate enzymes possess two mechanisms, namely sequential and ping-pong.<sup>244</sup> The mechanism where both substrates must be added to the enzyme before any product release is called sequential mechanism.



Scheme 43. Ordered sequential mechanism

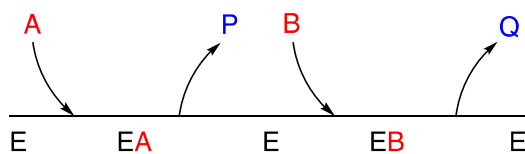
The sequential mechanism can be divided into two sub-mechanisms: ordered and random. If the substrates are added to the enzyme in an obligatory order, the mechanism is called ordered (Scheme 43). In Scheme 43, the enzymatic reaction is represented by the horizontal line and substrate addition and product release are indicated by arrows. Enzyme substrate and product complexes are labelled below the horizontal line. The product A must be taken up by the enzyme first followed by B. Once the ternary complex (EAB) is formed, the product release is also ordered by releasing product P first, followed by product Q. This system is also called ordered bi bi system according to Cleland nomenclature.<sup>244</sup>

If substrates do not follow a specific order to bind to the enzyme as in ordered bi bi system, then the mechanism is called random sequential mechanism or random bi bi system. Either the substrate A or B can be first added to the enzyme followed by the addition of the second substrate A or B. Either the products P or Q can be first released from the ternary complex (EPQ) followed by the release of the second product P or Q to release the free enzyme (Scheme 44).



Scheme 44. Random sequential mechanism

If one or more products are released before all substrates are added to the enzyme, the mechanism is called ping-pong (Scheme 45).

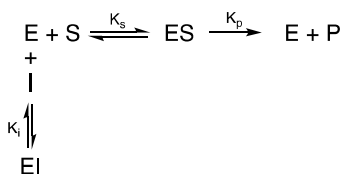


Scheme 45. Ping pong mechanism

### 3.1.1 Enzyme inhibition kinetics

Compounds which decrease the enzyme catalysed reaction rate are called inhibitors. According to Cleland nomenclature, there are three different types of inhibition mechanisms, namely competitive, non-competitive and uncompetitive, based on how the inhibitor binds to the enzyme.<sup>245</sup> If the replot of slope and intercept deduced from a double-reciprocal analysis of steady state inhibition kinetics are a linear functions of the inhibitor concentration, then the inhibition is called linear. Double reciprocal plot is obtained by plotting inverse of initial velocity ( $1/V_0$ ) as a function of the inverse of the substrate concentration ( $1/[S]$ ). Double reciprocal equation can be obtained by taking reciprocal of both sides of the equation.

In competitive inhibition mechanism, both substrate and inhibitor compete for the same active site of the enzyme (Scheme 46). Once the ES complex is formed, it does not bind the inhibitor.



Scheme 46. Competitive inhibition. *I* – Inhibitor,  $K_i$  – inhibition constant and *EI* -enzyme-inhibitor complex.

The reaction rate of a competitive inhibition mechanism and its double-reciprocal form is given in equation (2) and (3) respectively.

$$v = \frac{V_{\max}[S]}{K_m \left(1 + \frac{[I]}{K_i}\right) + [S]} \quad (2) \quad \frac{1}{v} = \frac{K_m}{V_{\max}} \left(1 + \frac{[I]}{K_i}\right) \frac{1}{[S]} + \frac{1}{V_{\max}} \quad (3)$$

Competitive inhibition mechanism can be determined graphically using double-reciprocal analysis by plotting  $1/v$  as a function of  $1/[S]$  for several inhibitor concentrations. The obtained lines intersect on the vertical axis for competitive inhibition pattern (Figure 29). From Figure 29 it can be seen that for competitive inhibition, the apparent  $V_{\max}$  is not affected by the inhibitor but the apparent  $K_m$  value increases when inhibitor concentration increases.



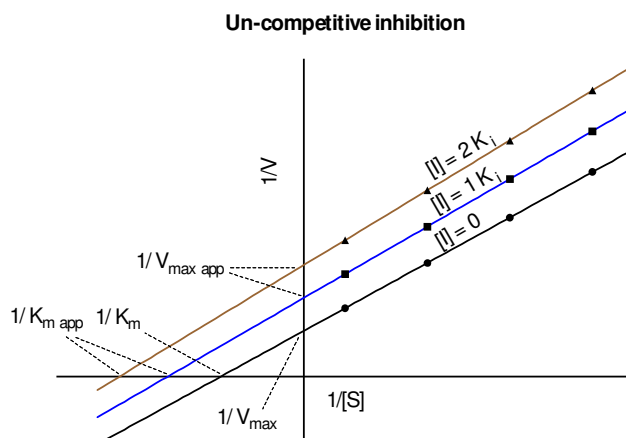
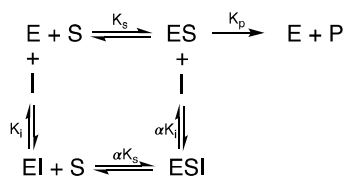


Figure 30. Double-reciprocal analysis of uncompetitive inhibition mechanism.

In the case of non-competitive inhibition, the inhibitor can bind to both free enzyme (E) and enzyme substrate complex (ES). Once the ternary complex ESI forms, reaction does not produce products. Sometimes non-competitive inhibition can be referred to mixed type inhibition because it resembles both competitive as inhibitor can bind to free enzyme and uncompetitive as inhibitor can bind to ES complex. The mechanism for non-competitive inhibition is illustrated in Scheme 48.



Scheme 48. Non-competitive inhibition.  $\alpha$ -factor by which  $K_i$  changes when the inhibitor binds to the ES complex.

The rate equation for non-competitive or mixed type inhibition and its double-reciprocal form is given in equation (6) and (7).

$$v = \frac{V_{\max}[S]}{K_m \left(1 + \frac{[I]}{K_i}\right) + [S] \left(1 + \frac{[I]}{\alpha K_i}\right)} \quad (6) \quad \frac{1}{v} = \frac{K_m}{V_{\max}} \left(1 + \frac{[I]}{K_i}\right) \frac{1}{[S]} + \frac{1}{V_{\max}} \left(1 + \frac{[I]}{\alpha K_i}\right) \quad (7)$$

The double-reciprocal plot in the case of non-competitive inhibition at different fixed inhibitor concentrations provides lines that intersect on the horizontal axis when  $K_i$  value equals to  $\alpha K_i$  value. This situation is sometimes referred as pure non-competitive inhibition. If  $K_i$  is smaller or greater than  $\alpha K_i$ , then lines intersect below or above the horizontal axis respectively but left of the vertical axis.<sup>245</sup> This situation is sometimes referred to mixed type inhibition (Figure 31). In mixed type inhibition mechanism, both apparent  $V_{\max}$  and  $K_m$  values are affected by the inhibitor. When  $\alpha > 1$ , the inhibitor preferentially binds to the free enzyme and if,  $\alpha < 1$ , the inhibitor preferentially binds to the ES complex.<sup>246</sup>

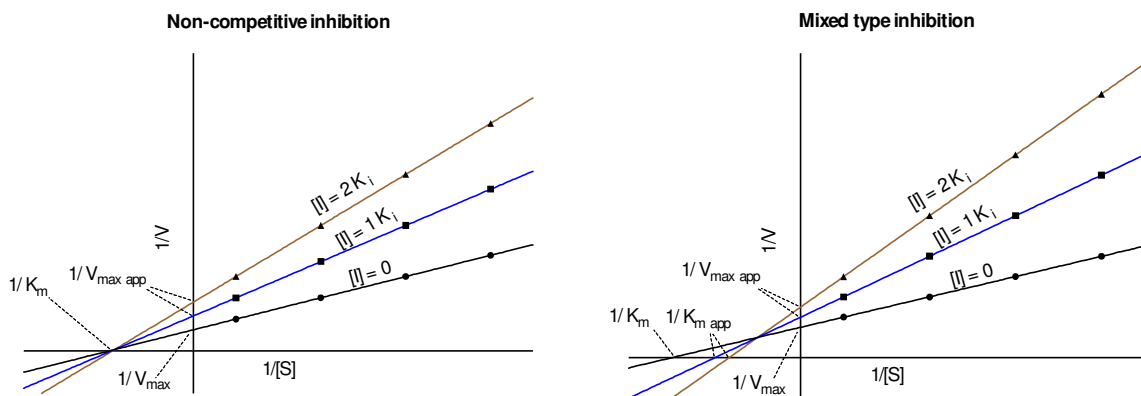


Figure 31. Double-reciprocal analysis for pure non-competitive and an example of mixed type inhibition.

### 3.2 Synthesis of MEP-N<sub>3</sub>

Since metabolic labelling studies on the MEP pathway using synthetic ME-N<sub>3</sub> were not successful, we decided to check whether IspD could convert ME-N<sub>3</sub> labelled chemical reporter supposing it would be previously incorporated in *E.coli* and phosphorylated. *E.coli* IspD could be purified successfully in our laboratory. IspD converts MEP *i.e* the phosphorylated ME into

CDP-ME (Figure 32). Therefore, we planned to verify if MEP-N<sub>3</sub> could be an alternate substrate of IspD. If MEP-N<sub>3</sub> would not be converted by IspD *in vitro*, it would explain why we were unable to detect any labelled metabolites in the previous LC-MS analysis.

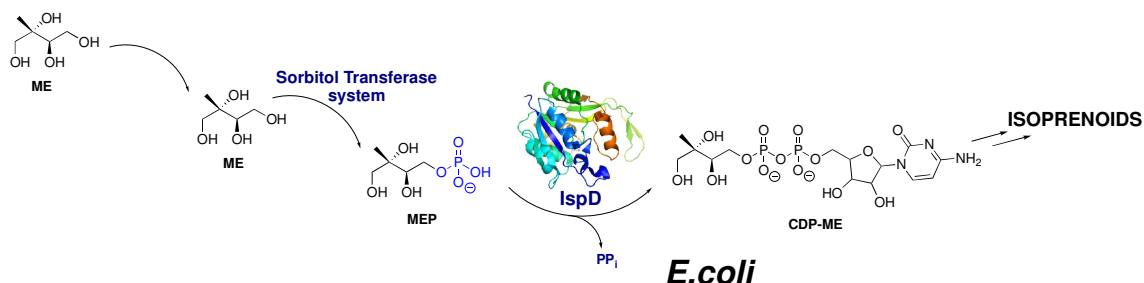
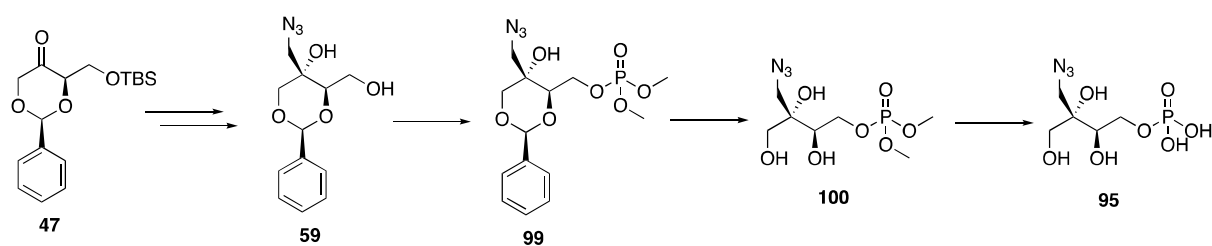


Figure 32. Illustration of ME conversion into MEP and CDP-ME by IspD.

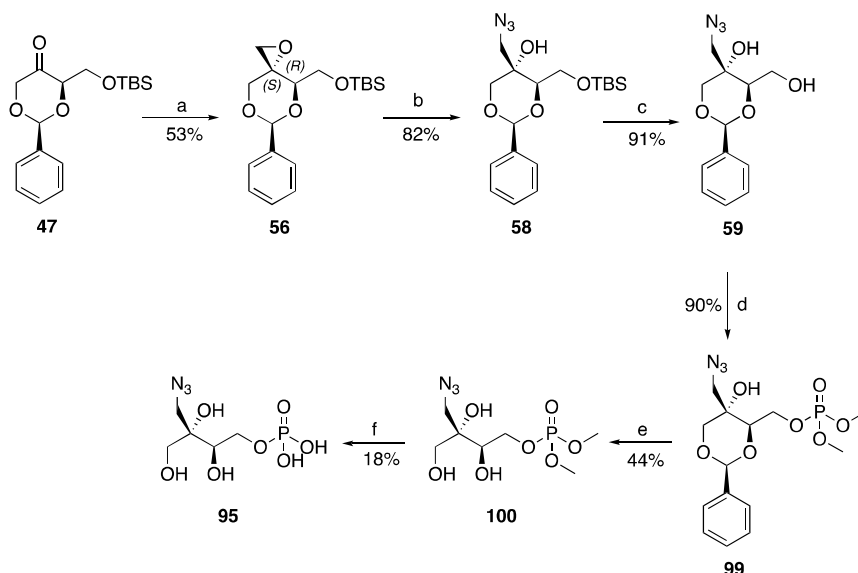
To achieve this work, the synthesis of MEP-N<sub>3</sub> is required. Our synthetic plan to obtain MEP-N<sub>3</sub> was based on our synthesis of ME-N<sub>3</sub> in which azido diol **59** was produced. The primary alcohol group of **59** can be selectively phosphorylated. From ketone intermediate **47** it was possible to synthesise the target molecule MEP-N<sub>3</sub> (Scheme 49). After introduction of the phosphate group to the azido diol, the cleavage of the protecting groups will afford the desired MEP-N<sub>3</sub>.



Scheme 49. Planned synthetic route to MEP-N<sub>3</sub>.

During the synthesis of MEP-N<sub>3</sub>, we found that it was possible to obtain epoxide **56** selectively and directly from the ketone **47** via a Corey-Chaykovsky reaction. This reaction was first discovered by E. J. Corey and Michael Chaykovsky in the 1960s and uses either dimethylsulfonium methylide or dimethylsulfoxonium methylide to add a methylene

functionality onto an electrophilic unsaturated bonds such as C=O, C=N, C=S or C=C.<sup>247-249</sup> The Corey-Chaykovsky reaction replaced two steps: olefination by a Wittig reaction and epoxidation by *m*-CPBA (Scheme 37 in chapter 2).



Scheme 50. Synthesis of MEP-N<sub>3</sub>. a) (CH<sub>3</sub>)<sub>3</sub>SOI, NaH, DMSO, 10 min, r.t.; b) NaN<sub>3</sub>, NH<sub>4</sub>Cl, DMF, 2 h, 60 °C; c) TBAF, THF, 0 °C – r.t.; d) (CH<sub>3</sub>O)<sub>2</sub>POCl, DMAP, DCM, 2 h, 0 °C; e) DOWEX (H<sup>+</sup>), MeOH, 48 h, r.t.; f) (CH<sub>3</sub>)<sub>3</sub>SiBr, H<sub>2</sub>O, DCM, 0 °C – r.t.

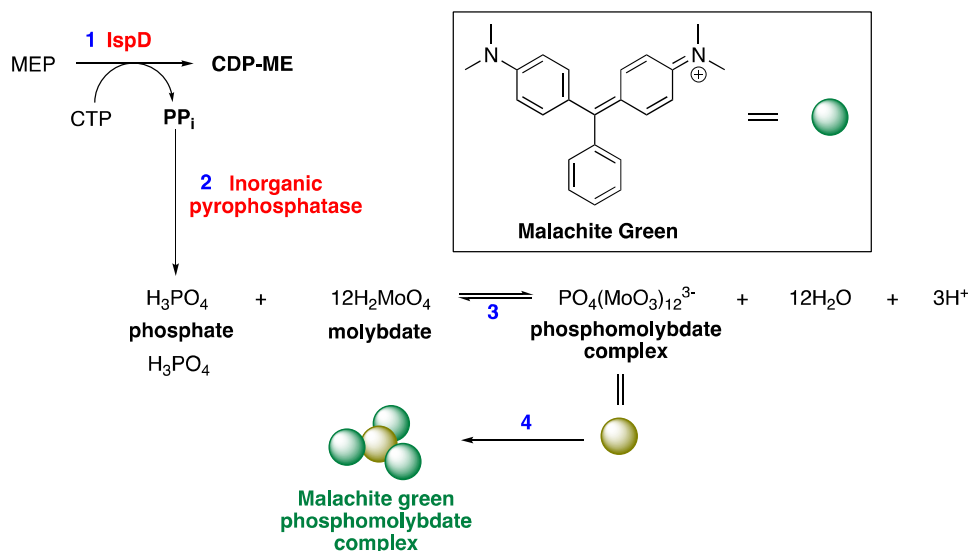
The synthesis of MEP-N<sub>3</sub> started with a Corey-Chaykovsky reaction yielding to the single epoxide isomer **56** (Scheme 50). The Corey-Chaykovsky reaction yielded selectively *S,R*-isomer **56** over *R,R*-isomer **57** due to steric hindrance from bulky silyl protecting group. The epoxide ring opening using NaN<sub>3</sub> and deprotection of primary alcohol group was performed as described previously in good yield. Introduction of the protected phosphate moiety on the primary alcohol group was achieved in good yield. Hydrolysis of the benzylidene acetal was achieved with acidic resin as described previously in moderate yield over two days to give phosphorylated molecule **100**. The final deprotection step of the phosphate group was most challenging as the reaction produced many side products and hence yielded the desired product **95** in low yield at 18 %. This demethylation of phosphate moiety using silyl reagent is sometimes referred as McKenna reaction.<sup>250</sup> The synthesis of MEP-N<sub>3</sub> was achieved in six steps starting from the ketone intermediate **47** with an overall yield of 3 %.

### 3.3 Investigation of the kinetics of IspD.

#### 3.3.1 MEP-N<sub>3</sub>: a substrate of IspD?

In order to check if MEP-N<sub>3</sub> is a substrate of IspD, we first need to develop an enzymatic assay for this enzyme that will first allow to determine the kinetic constants of IspD using MEP and CTP as substrates. Once the test in hand, MEP will be replaced by MEP-N<sub>3</sub>.

To determine the kinetic constants of IspD in the presence of its natural substrates, we decided to utilise the previously described colorimetric assay by Imperial and co-workers<sup>251</sup>. This test is simple and frequently used for phosphate quantification. During the IspD enzymatic reaction, two products, CDP-ME and diphosphate, are released. This colorimetric assay relies on the determination of the absorbance of phosphate complexed with malachite green ammonium molybdate. The assay, therefore, deliberately contains inorganic pyrophosphatase which hydrolyses the diphosphate produced by IspD into two molecules of phosphate. These two phosphate molecules will form a complex with the dye reagent – malachite green ammonium molybdate in solution (Scheme 51) that can be quantified using UV visible spectroscopy.



Scheme 51. Principle of the colorimetric assay. 1) Diphosphate (PP<sub>i</sub>) is produced by IspD 2) Diphosphate is hydrolysed into two molecules of phosphate by inorganic pyrophosphatase. 3) Phosphate forms a complex with molybdate. 4) Phosphomolybdate complex forms the secondary complex with malachite green.

Although Soyenkoff, in 1947, was first to report that malachite green colour change in the presence of phosphomolybdate,<sup>252</sup> in 1966, Itaya and Ui reported the colorimetric quantification of inorganic phosphates at microgramme scale using malachite green.<sup>253</sup> Since then, this principle has been applied for quantification of inorganic phosphates in biological and non-biological samples up to nanomolar range.<sup>254-257</sup>

We first determined the kinetic constants ( $V_{\max}$  and  $K_m$ ) of purified IspD using MEP at varied concentrations and CTP at a fixed concentration. In order to determine these kinetic values, it was required to optimise the IspD reaction conditions such as incubation time and enzyme concentration. We initially performed the reactions using 0.48  $\mu\text{g}$  of purified IspD and measured the time course of phosphate production using the colorimetric assay (Figure 33). This experiment will determine if the enzyme concentration is suitable for further kinetic experiments.

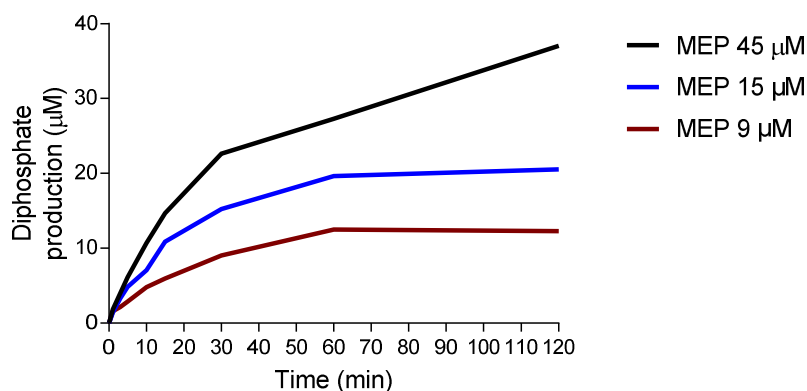


Figure 33. Time course measurement of diphosphate production by IspD.

Conditions:  $\text{MgCl}_2$  (1 mM), CTP (0.2 mM), DTT (1 mM), Inorganic pyrophosphatase (133 mU/mL), *E.coli* IspD – 0.48  $\mu\text{g}$  in 400  $\mu\text{L}$  Tris HCl (50 mM, pH = 8)

The amount of IspD (in a volume of 400  $\mu\text{L}$ ) was actually 4 times higher than Imperial and co-workers used in their assay.<sup>251</sup> Our key criteria for the determination of a suitable enzyme concentration was that no more than 10 % of substrate would be converted by the enzyme in a reasonable time before the released phosphate was quenched with the dye reagent. From the time course measurement test (Figure 33) we found that 10 % substrate conversion was achieved in 3 minutes and it was too fast for the kinetic experiments. After reducing the enzyme quantity, it was found that 0.06  $\mu\text{g}$  enzyme is suitable for the kinetic experiments but we also

noticed that diluting the enzyme stock (17.48 mg/mL) over 800 times (0.0218 mg/mL) leads to a decrease in IspD activity. While we were trying to optimise these conditions, we also noticed that refreezing the leftover of pyrophosphatase resulted in loss of activity of this enzyme. Imperial and co-workers used 44 mU/mL pyrophosphatase in their assay but we needed to use three times higher (133 mU/mL) amounts for the kinetic assays. 0.06  $\mu\text{g}$  IspD and 133 mU/mL of pyrophosphatase in a volume of 400  $\mu\text{L}$ , 8 minutes of reaction time at 30  $^{\circ}\text{C}$  yielded approximately 10 % conversion of MEP when the released phosphate was quantified using a malachite green solution. Therefore, all further kinetic experiments were conducted with these optimised conditions.

When velocity of the IspD reaction was plotted against MEP concentration and the results fitted according to Michaelis-Menten equation (1), the following graph was obtained (Figure 34). An apparent  $K_m$  value of  $41 \pm 6 \mu\text{M}$  was determined for MEP. Imperial and co-workers who used the same method found an apparent  $K_m$  value of  $61 \pm 14 \mu\text{M}$ <sup>251</sup> which is in agreement with our result.

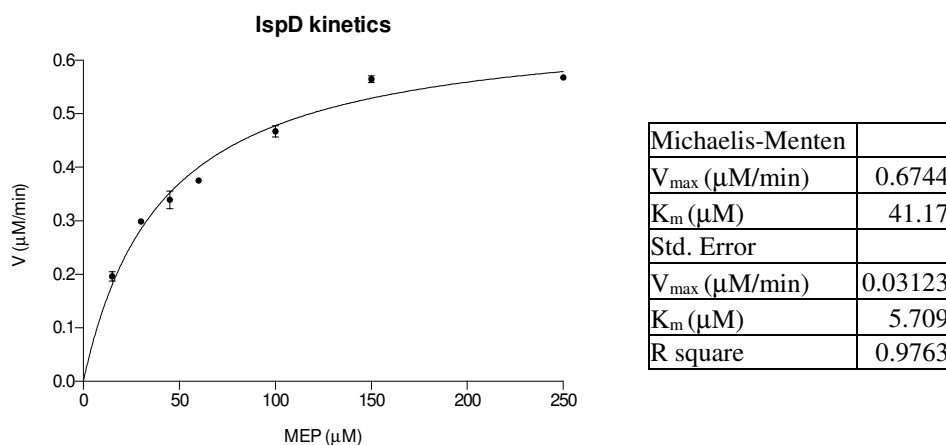


Figure 34. IspD kinetics using varied MEP concentrations.

Conditions:  $\text{MgCl}_2$  (1 mM), CTP (0.2 mM), DTT (1 mM), Inorganic pyrophosphatase (133 mU/mL), *E. coli* IspD – 0.065  $\mu\text{g}$  in 400  $\mu\text{L}$  Tris HCl (50 mM, pH = 8)

When IspD was first discovered to catalyse MEP transformation into CDP-ME and diphosphate by Zenk and co-workers, they found a  $K_m$  value of  $3.14 \mu\text{M}$ <sup>69</sup> for MEP which is 10 times lower than our result but they used an assay based on cascade of reactions conducive to the reduction of  $\text{NADP}^+$ .

Cane and co-workers reported the *E.coli* IspD kinetic analysis and described an apparent  $K_m$  value of  $370 \pm 60 \mu\text{M}^{14}$  for wild type *E.coli* using  $^{14}\text{C}$ -MEP and a PhosphorImager to quantify the radioactive  $^{14}\text{C}$ -CDP-ME. Their result was nearly 10 times higher than our finding. These two last reports are different from our result but the data were obtained using different methodologies.

In order to determine the  $K_m$  of CTP for IspD the same experiment as mentioned above was performed except that the CTP concentration was varied between 30 to 450  $\mu\text{M}$  and MEP concentration was fixed to 250  $\mu\text{M}$ . We found an apparent  $K_m$  value of  $90 \pm 10 \mu\text{M}$  for CTP (Figure 35). Imperial and co-workers found  $K_m$  value of  $58 \pm 6 \mu\text{M}$  for CTP<sup>251</sup> and our finding is slightly higher than what they determined even we used a similar method. The team of Cane, on the other hand, obtained a  $K_m$  value of  $760 \pm 60 \mu\text{M}^{14}$  which is approximately 8 times higher than our findings. Zenk and co-workers reported a  $K_m$  value of  $131 \mu\text{M}^{69}$  for CTP and our finding is in close range to their value.

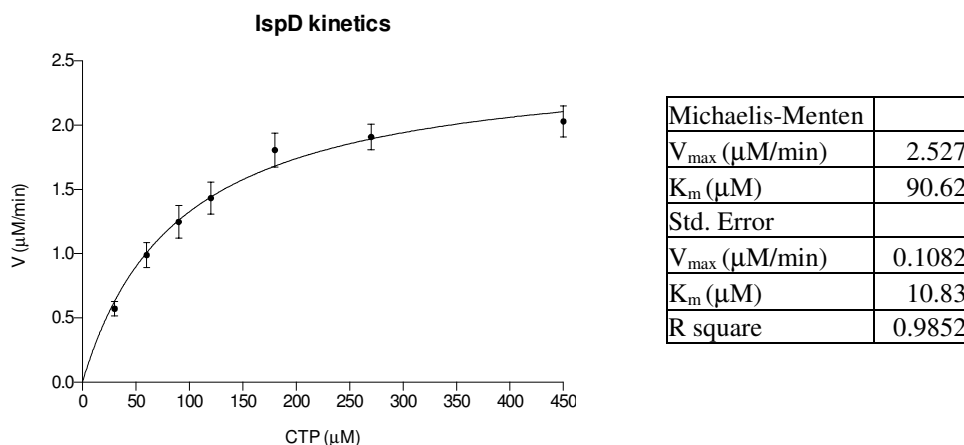


*Figure 35. IspD kinetics using varied CTP concentrations.*

*Conditions: MgCl<sub>2</sub> (1 mM), MEP (0.25 mM), DTT (1 mM), Inorganic pyrophosphatase (133 mU/mL), E.coli IspD – 0.065  $\mu\text{g}$  in 400  $\mu\text{L}$  Tris HCl (50 mM, pH = 8)*

MEP-N<sub>3</sub> kinetic studies using IspD were performed under similar conditions. During the initial attempts using the colorimetric assay, we found that MEP-N<sub>3</sub> was indeed a substrate of IspD but the rate of the reaction was very slow. We further validated that IspD catalyses the conversion of MEP-N<sub>3</sub> into CDP-ME-N<sub>3</sub> using LC-MS analysis after clicking CDP-ME-N<sub>3</sub> with BCN-TMPP. The click reaction produced molecule **71** (chapter 2, Figure 20). As we usually detect +2 charged adduct for clicked products during LC-MS analysis, the clicked

product **71** gave  $m/z$  686 Da (MW = 1372 Da). MS signal corresponds to clicked product **71** is given in Figure 36.

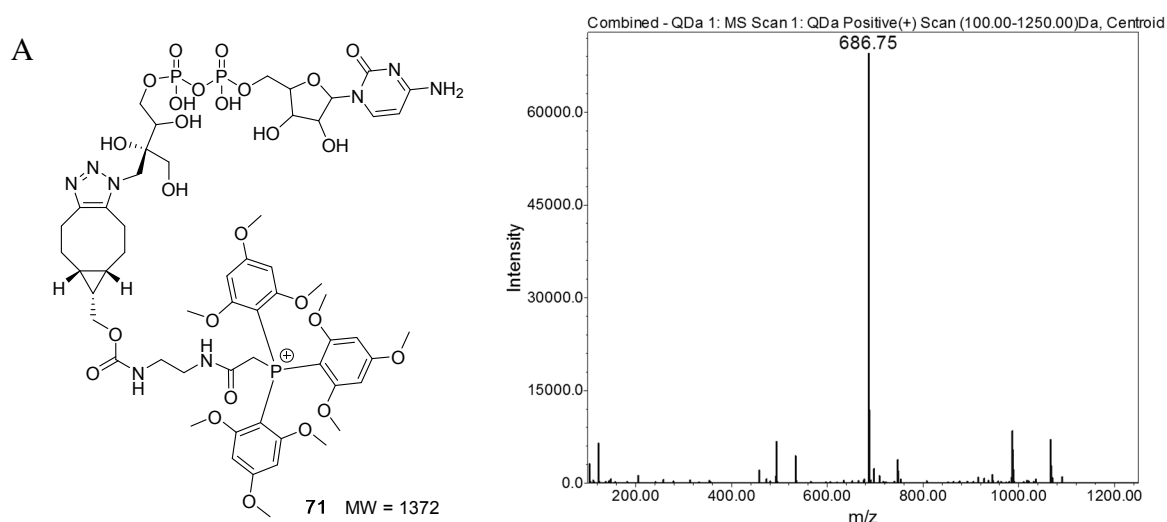


Figure 36. LC-MS analysis of MEP-N<sub>3</sub> conversion by IspD. A. Structure of clicked product **71**. B. MS spectra of product **71**

To determine Michaelis-Menten kinetic parameters ( $K_m$  and  $V_{max}$ ), the velocity should reach a plateau but the rate of the initial assays did not reach a plateau below 1 mM MEP-N<sub>3</sub> concentration.

We, therefore, increased the MEP-N<sub>3</sub> concentration to 3 mM in order to verify if the IspD rate could reach a plateau but these larger concentrations resulted in substrate inhibition, hence declining IspD reaction rate. Substrate inhibition is in fact very common among enzymes. When an enzyme is inhibited by its substrate, the normal Michaelis-Menten kinetics equation (1) should not be applied to calculate the kinetic constants. Instead, it should be fitted into equation (8).<sup>258-260</sup>

$$v = \frac{V_{max}[S]}{K_m + [S]} \quad (1) \quad v = \frac{V_{max}[S]}{K_m + [S] \left(1 + \frac{[S]}{K_i}\right)} \quad (8)$$

When the data were fitted to equation (8), using MEP-N<sub>3</sub> as a varied substrate, the following result was obtained (Figure 37).

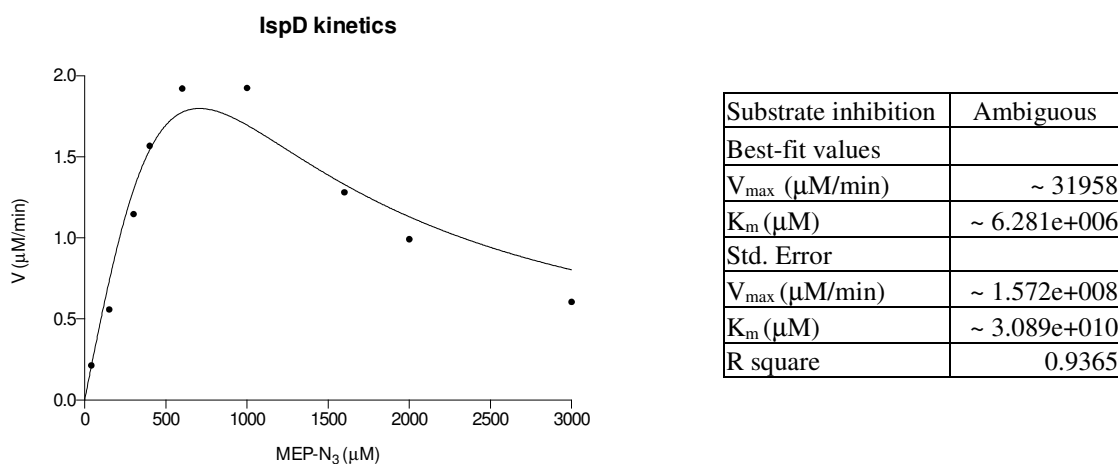


*Figure 37. IspD kinetics using varied MEP-N<sub>3</sub> concentrations.*

*Conditions: MgCl<sub>2</sub> (1 mM), MEP (0.25 mM), DTT (1 mM), Inorganic pyrophosphatase (133 mU/mL), E.coli IspD – 42  $\mu\text{g}$  in 400  $\mu\text{L}$  Tris HCl (50 mM, pH = 8)*

The data analysis resulted in very high values of  $K_m$  and  $V_{max}$  (Figure 37) that were incoherent. These results might be due to the fact that the graph might lack points and that more data should have been produced. Due to a limited supply of MEP-N<sub>3</sub> and shortage of time, we did not attempt to perform further experiments with additional MEP-N<sub>3</sub> concentrations.

It was noted that for 300  $\mu\text{M}$  MEP-N<sub>3</sub>, the reaction rate (0.0341  $\mu\text{mol}/\text{min}/\text{mg}$ ) of IspD was approximately 100 times less than the rate (3.47  $\mu\text{mol}/\text{min}/\text{mg}$ ) of IspD in presence of 250  $\mu\text{M}$  MEP. (Reaction rate is in  $\mu\text{mol}/\text{min}/\text{mg}$  units.  $\mu\text{mol}$  - diphosphate, min - reaction time, mg - IspD quantity). This means that MEP-N<sub>3</sub> is a poor substrate of IspD compared to MEP.

We also observed that IspD rate declined if MEP-N<sub>3</sub> was added to the reaction where MEP was used as a natural substrate. IspD reaction rate was decreased by 18 % in the presence of 25  $\mu\text{M}$  of MEP-N<sub>3</sub> when compared to the reaction in which no MEP-N<sub>3</sub> was added (Figure 38). This result prompted us to further investigate if MEP-N<sub>3</sub> is an inhibitor of IspD.

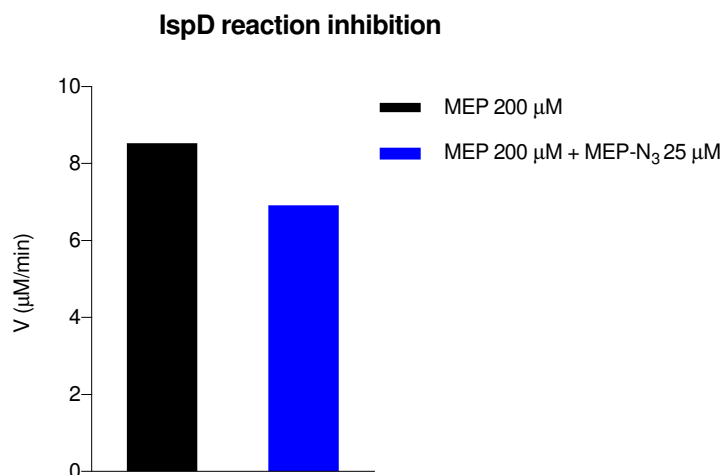


Figure 38. Comparison of IspD reaction in the presence or in the absence of MEP-N<sub>3</sub>.

### 3.3.2 MEP-N<sub>3</sub>: an inhibitor of IspD?

After MEP-N<sub>3</sub> was found to be inhibiting the IspD reaction, a more detailed kinetic analysis was performed in order to determine the  $K_i$  (inhibition constant) value and the mode of inhibition of MEP-N<sub>3</sub>. For this purpose, several IspD assays were carried out by fixing one substrate concentration and varying the concentration of other substrate for different MEP-N<sub>3</sub> concentrations.

First, IspD reaction rates were measured in the presence of 0, 20, 40 and 60 μM of MEP-N<sub>3</sub> with CTP concentration fixed at 200 μM and MEP concentration varied between 15 – 250 μM. We chose these MEP-N<sub>3</sub> concentrations based on initial attempts that suggested a  $K_i$  value around 40 μM. Indeed, the tests should be preferentially performed at 0, 0.5, 1 and 1.5  $K_i$  concentrations for MEP-N<sub>3</sub>. At 60 μM of MEP-N<sub>3</sub>, the reaction rate was declined by approximately 60 %. The velocity was plotted as a function of MEP concentration at a fixed MEP-N<sub>3</sub> concentration as shown in Figure 39.

The data were first fitted to equation (1). The  $V_{max}$  was decreasing when the concentration of MEP-N<sub>3</sub> increased and the apparent  $K_m$  was increasing as the concentration of MEP-N<sub>3</sub> was increasing.

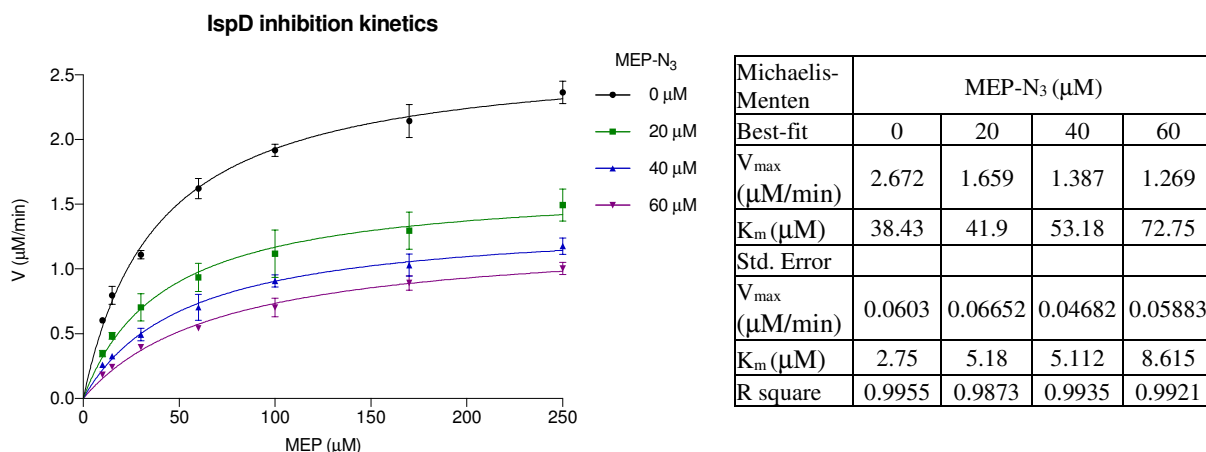
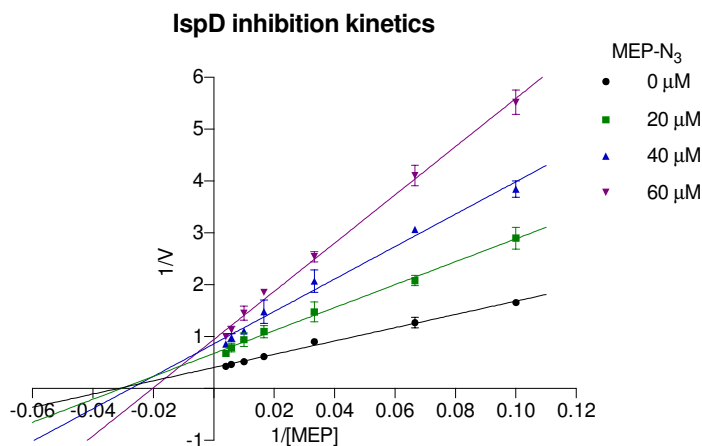


Figure 39. IspD inhibition by MEP-N<sub>3</sub> (MEP as a varied substrate).

Conditions: MgCl<sub>2</sub> (1 mM), CTP (0.2 mM), DTT (1 mM), Inorganic pyrophosphatase (133 mU/mL), *E. coli* IspD – 0.065 μg in 400 μL Tris HCl (50 mM, pH = 8)

As discussed early in this chapter, the double reciprocal plot of the data will inform on the type of inhibition mechanism that occurs. When the data were plotted in double reciprocal form (1/Velocity against 1/[MEP]), we obtained the following graph (Figure 40).



Best-fit values ± SE	MEP-N <sub>3</sub> (0 μM)	MEP-N <sub>3</sub> (20 μM)	MEP-N <sub>3</sub> (40 μM)	MEP-N <sub>3</sub> (60 μM)
Slope	12,79 ± 0,428	22,1 ± 0,722	31,27 ± 1,576	46,51 ± 1,196
Y-intercept = 1/V <sub>max</sub> (app)	0,4052 ± 0,02045	0,6759 ± 0,0345	0,8597 ± 0,07529	0,9436 ± 0,05715
X-intercept = 1/K <sub>m</sub> (app)	-0,03167	-0,03058	-0,02749	-0,02029
R square	0,9944	0,9947	0,9875	0,9967

Figure 40. IspD inhibition by MEP-N<sub>3</sub> in double reciprocal form ([MEP] was varied), [CTP] = 200 μM, IspD - 0.065 μg.

After analysing the data using a linear regression, it can be observed from the graph that both  $V_{\max}$  and  $K_m$  values have changed and that the lines cross each other at some point left of the vertical axis. This result suggests that the inhibition mechanism was neither competitive nor un-competitive but was non-competitive. As the intersection of the lines was not on the horizontal axis, we assumed that the inhibition mechanism was mixed type inhibition in which the inhibitor can bind either to the free enzyme or to the enzyme substrate complex.

Using a secondary plot of the double reciprocal analysis by plotting slope and y-axis intercept against inhibitor concentration, we could determine  $K_i$  and  $\alpha K_i$  values graphically.<sup>261</sup> The inhibition constant ( $K_i$ ) value can be estimated when slope replot is analysed by linear regression and the intersecting point of the line on the horizontal axis represents the  $-K_i$  value. We obtained a  $K_i$  value of 21  $\mu\text{M}$  for MEP- $\text{N}_3$  with IspD when MEP was the varied substrate (Figure 41).

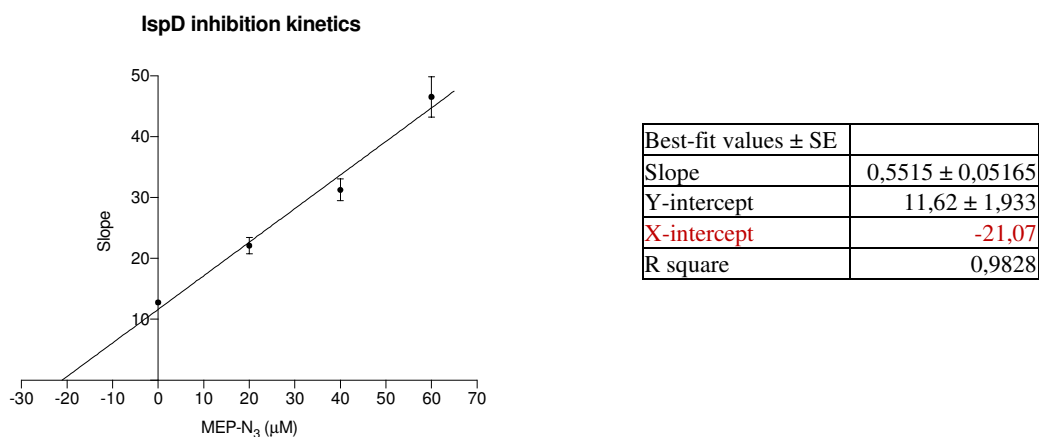


Figure 41. Slope replot of double reciprocal analysis (MEP as a varied substrate).  $x$ -intercept =  $-K_i$

By replotting y-intercept of double reciprocal plot as a function of inhibitor concentration,  $\alpha K_i$  value can be calculated. From this secondary plot, an  $\alpha K_i$  value of 54  $\mu\text{M}$  was obtained (Figure 42). From these findings, we can observe that  $\alpha = 2.5$  and according to Copeland, as mentioned before, it indicates that the inhibitor preferentially binds to the free enzyme rather than to the enzyme MEP complex and this behaviour features competitive inhibition characteristic.<sup>246</sup>

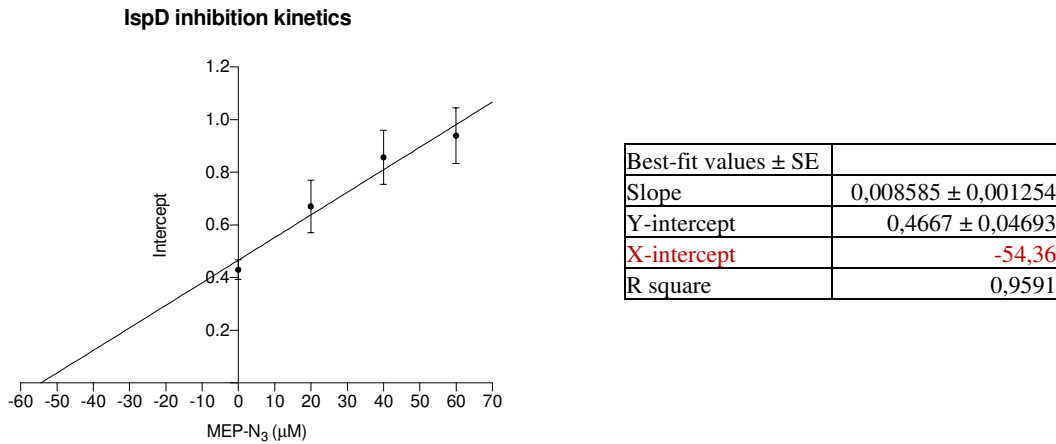


Figure 42. Intercept replot of double reciprocal analysis (MEP as a varied substrate).  $x$ -intercept =  $-\alpha K_i$

The same experiments were carried out by varying the CTP concentration instead of the MEP concentration using several fixed MEP- $N_3$  concentrations. CTP was varied between 50 – 240  $\mu$ M and MEP was fixed at 250  $\mu$ M. Initial experiments suggested a  $K_i$  value at approximately 60  $\mu$ M and therefore MEP- $N_3$  concentration of 0, 30, 60 and 90  $\mu$ M which corresponded to 0, 0.5, 1 and 1.5  $K_i$  values were chosen. At these inhibitor concentrations, we obtained the results described in Figure 43.

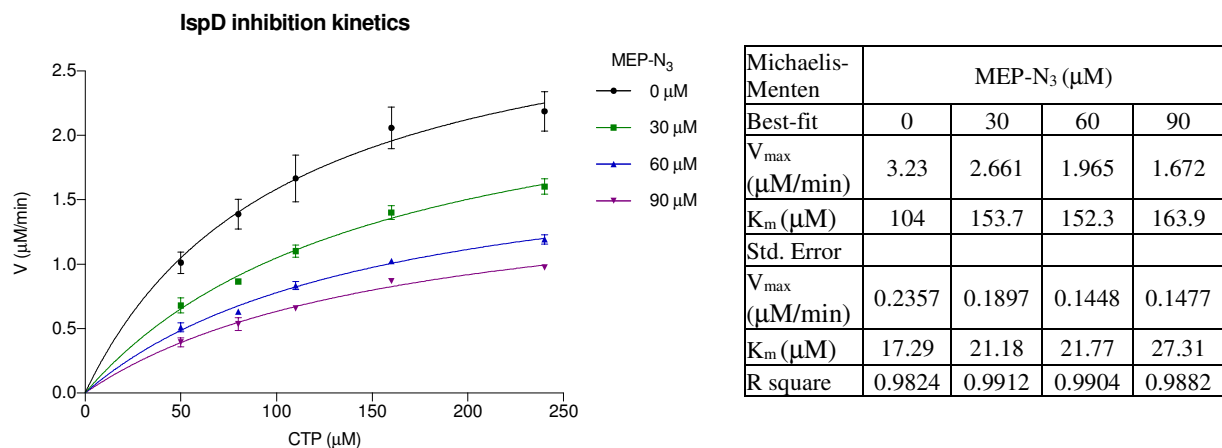


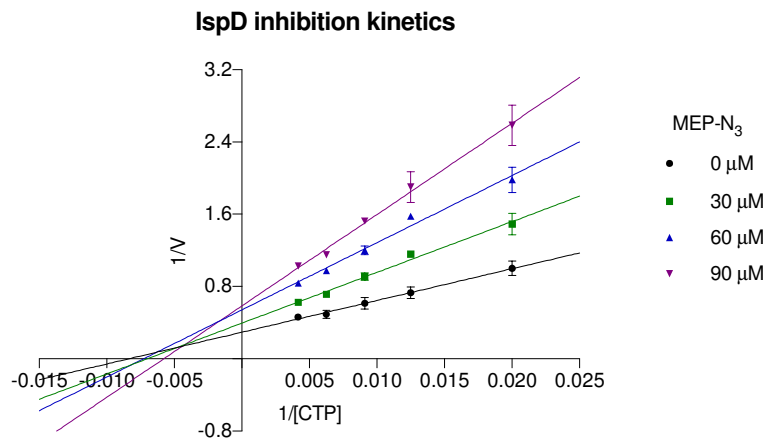
Figure 43. IspD inhibition by MEP- $N_3$  (CTP as a varied substrate).

Conditions:  $MgCl_2$  (1 mM), MEP (0.25 mM), DTT (1 mM), Inorganic pyrophosphatase (133 mU/mL), *E. coli* IspD – 0.065  $\mu$ g in 400  $\mu$ L Tris HCl (50 mM, pH = 8)

Initially, we attempted to perform this experiment with assays where CTP varied between 25 – 400  $\mu\text{M}$  but in this range the minimum and maximum points were unreliable due to fluctuations ( $\text{OD}_{630}$  values were too low for  $[\text{CTP}] = 25 \mu\text{M}$  and too high for  $[\text{CTP}] = 400 \mu\text{M}$ ). Therefore, we excluded first and last points and performed the experiment with assays containing 50 – 240  $\mu\text{M}$  CTP and, in this case, the fluctuations were negligible. At 90  $\mu\text{M}$  MEP- $\text{N}_3$ , the reaction rate had fallen by nearly 50 %.

When the data were plotted according to the Michaelis-Menten equation,  $V_{\text{max}}$  decreased as inhibitor concentration arose and  $K_m$  value increased when inhibitor concentration increased. This is indicative of mixed type inhibition pattern and therefore we could expect the double reciprocal analysis to be similar to the previous experiment in which MEP concentration varied.

The double reciprocal plot generated lines that intersect with each other left of the vertical axis and above the horizontal axis as expected (Figure 44). Therefore, MEP- $\text{N}_3$  also inhibits IspD in mixed type inhibition pattern when CTP was the variable substrate. Similar to the previous inhibition study, by plotting slope and intercept of double reciprocal plot,  $K_i$  and  $\alpha K_i$  values could be determined respectively.



Best-fit values $\pm$ SE	MEP- $\text{N}_3$ (0 $\mu\text{M}$ )	MEP- $\text{N}_3$ (30 $\mu\text{M}$ )	MEP- $\text{N}_3$ (60 $\mu\text{M}$ )	MEP- $\text{N}_3$ (90 $\mu\text{M}$ )
Slope	$35,14 \pm 1,442$	$56,21 \pm 3,374$	$74,38 \pm 5,76$	$101,2 \pm 4,157$
Y-intercept	$0,2947 \pm 0,01701$	$0,3951 \pm 0,03979$	$0,5421 \pm 0,06793$	$0,586 \pm 0,04903$
X-intercept	$-0,008387$	$-0,007028$	$-0,007288$	$-0,005792$
R square	0,995	0,9893	0,9823	0,995

Figure 44. IspD inhibition by MEP- $\text{N}_3$  in double reciprocal form ( $[\text{CTP}]$  varied), IspD - 0.065  $\mu\text{g}$ .

Secondary plot of the slope as a function of inhibitor concentration yielded a  $K_i$  value of 47  $\mu\text{M}$  for MEP- $\text{N}_3$  as indicated by the x-axis crossing point after using a linear regression (Figure 45).

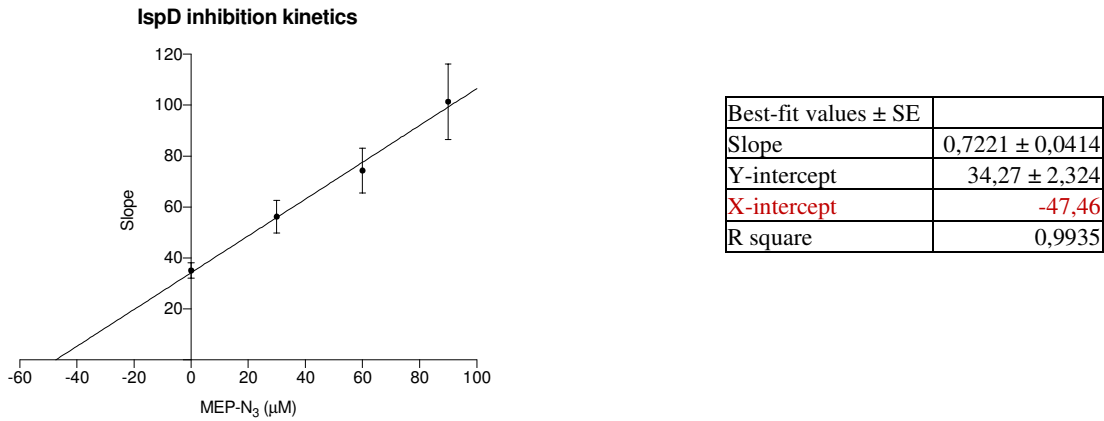


Figure 45. Slope replot of double reciprocal analysis (CTP as a varied substrate).  $x$ -intercept =  $-K_i$

On the other hand, replotting the intercept of double reciprocal analysis produced an  $\alpha K_i$  value of 105  $\mu\text{M}$  for MEP- $\text{N}_3$  when CTP was the variable substrate. (Figure 46)

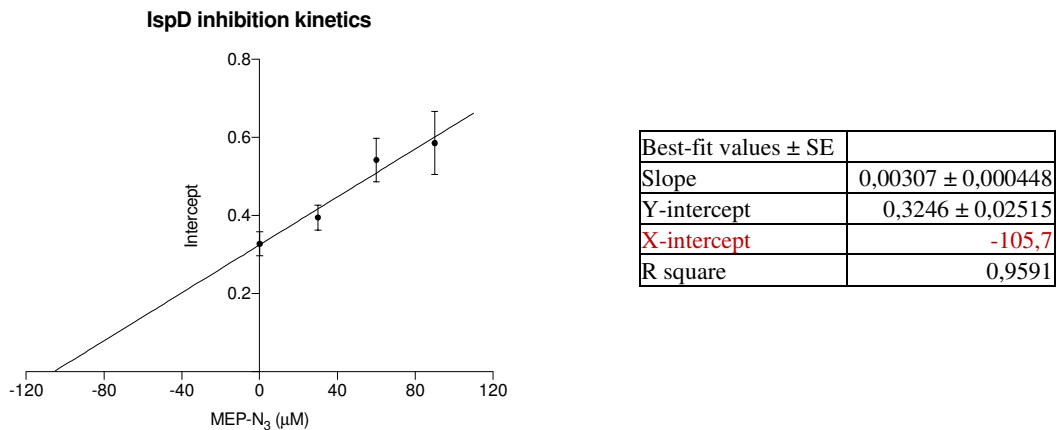


Figure 46. Intercept replot of double reciprocal analysis (CTP as a varied substrate).  $x$ -intercept =  $-\alpha K_i$

From the secondary plot of slope and intercept, we found  $\alpha = 2.2$  and, similar to the result when MEP varied, it indicates that the inhibitor preferentially binds to the free enzyme rather than the enzyme CTP complex.

MEP-N<sub>3</sub> was a non-competitive inhibitor of IspD when both natural substrates were varied. Together these results might suggest that MEP-N<sub>3</sub> competes for the MEP binding site which is plausible as it is a MEP analogue but MEP-N<sub>3</sub> might also bind close to the CTP binding site. The structure of *E.coli* IspD in the presence of MEP could not be solved yet. Only a substrate free structure of *E.coli* IspD<sup>262</sup> or in complex with CTP<sup>10</sup> or in complex with CDP-ME<sup>10</sup> is available in the literature. In collaboration with Dr Jean-Luc Ferrer and Dr Franck Borel (IBS, Grenoble), we attempted to solve the crystal structure of the IspD-MEP-N<sub>3</sub> complex in order to evidence the mode of binding of MEP-N<sub>3</sub> to IspD. The crystallisation trials of IspD in the presence of MEP-N<sub>3</sub> led to some crystals but unfortunately the obtained crystals did not diffract. One can consider that lower the K<sub>i</sub> value, better the inhibitory effect. Throughout our literature search on inhibitors of IspD, we found numerous inhibitors that have been described for IspD of different organisms such as *Arabidopsis thaliana*,<sup>263-265</sup> *Plasmodium vivax*<sup>265</sup> and *Mycobacterium smegmatis*<sup>266</sup> with IC<sub>50</sub> values of up to nanomolar range. However, inhibitors of *E.coli* IspD are scarce.

For *E.coli* IspD, the first inhibitor D-erythritol 4-phosphate **102** was a substrate and displayed IC<sub>50</sub> = 1.38 mM. It led to a reduced IspD reaction rate when compared to MEP (Figure 47). Later the L-erythritol 4-phosphate **101** was synthesised enzymatically using *Brucella abortus* and led to a K<sub>i</sub> value of 240 ± 17 mM.<sup>12</sup> Interestingly fosmidomycin **103**, the only inhibitor of MEP pathway currently in clinical trial<sup>267</sup>, was also reported to be an inhibitor of IspD although its main target is DXR. Odom and co-workers observed an increase of MEP level and decrease of CDP-ME level when *Plasmodium falciparum*, the malarial parasite, was treated with fosmidomycin and this result raised a question whether molecule **103** had an effect on IspD or not. The authors further purified *E.coli* IspD and tested fosmidomycin as an inhibitor. In fact, fosmidomycin could be shown to inhibit *E.coli* IspD activity and an IC<sub>50</sub> = 20.4 ± 3.3 mM was measured.<sup>268</sup>

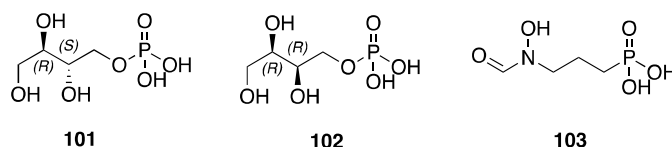


Figure 47. Structure of *E.coli* IspD enzyme inhibitors.

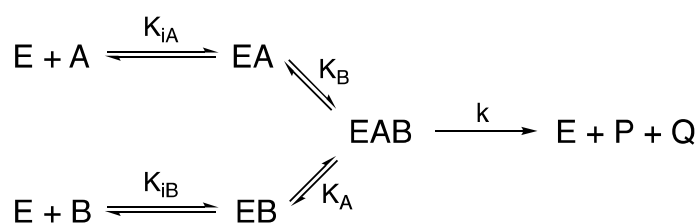
One could argue that comparing  $K_i$  and  $IC_{50}$  is not reasonable as  $IC_{50}$  value depends on concentration of substrates used in the experiment. However, researchers have compared these two values using the so-called Cheng-Prusoff equations. In their paper published in 1973, Yung-chi Cheng and William H. Prusoff described the equations for conversion between  $K_i$  and  $IC_{50}$  values based on enzymatic reaction mechanisms and inhibition patterns.<sup>269</sup> They described that if the bisubstrate reaction follows either ordered or random sequential mechanism and the inhibition is in non-competitive pattern, then  $IC_{50}$  value does not depend on the inhibitor concentration but equals to  $K_i$  value. Some pulse-chase experiments<sup>14</sup> suggested that *E.coli* IspD follows an ordered sequential mechanism (see chapter 1, section 1.4.3). As we found MEP-N<sub>3</sub> to be an inhibitor of *E.coli* IspD in non-competitive or mixed type pattern,  $K_i$  values could be compared to  $IC_{50}$  according to Cheng and Prusoff. When we directly compare our  $K_i$  values with the previously reported  $IC_{50}$  and  $K_i$  values, MEP-N<sub>3</sub> was found to be possessing highest inhibitory activity among the known inhibitors of *E.coli* IspD. Therefore, MEP-N<sub>3</sub> is the most potent *E.coli* IspD inhibitor known to date.

### 3.3.3 Investigation of the mechanism catalysed by IspD

Cane and co-workers have investigated the mechanism of IspD from *E.coli* by using a pulse-chase experiment in which radiolabelled MEP or CTP was first mixed with IspD followed by the addition of unlabelled MEP or unlabelled CTP to conduct the reaction. After quantification of the formed [<sup>14</sup>C] CDP-ME using PhosphorImager, the results revealed that CTP binds first to IspD followed by MEP.<sup>14</sup> This work highlights that IspD catalysis follows a sequential mechanism where substrates bind to the enzyme in an orderly fashion.

The bisubstrate enzyme mechanism can also be determined using steady state kinetic analysis by measuring the velocity of different assays in which one of the substrate is fixed at different constant concentrations and the concentration of the other is varied. Double reciprocal plot ( $1/V$  against  $1/[S]_A$  where  $S_A$  is the varied substrate) for different fixed concentrations of  $S_B$  will allow to determine the mechanism. If the lines from the double reciprocal plot intersect at one point, it is indicative of sequential mechanism and if the lines do not intersect but are parallel, it indicates the mechanism is ping-pong.<sup>246</sup> According to a British scientist Keith Dalziel, by plotting slopes and intercepts of initial double reciprocal plots against a substrate concentration, one can also determine the kinetic parameters ( $K_m$  and  $V_{max}$ ).<sup>270</sup>

If we assume that IspD reaction is sequential, the binding of the substrates to the enzyme must be sequential. For example, free enzyme (E) first binds to substrate A (CTP) forming EA (E-CTP) complex and substrate B (MEP) is then bound to the E-CTP complex forming the ternary complex EAB (E-CTP-MEP). This complex then collapses to the products P (CDP-ME) and Q (PP<sub>i</sub>). Another possibility is E first binds to B (MEP) forming EB (E-MEP) complex which later forms EBA (E-MEP-CTP) complex upon substrate A (CTP) addition. This complex then collapses to P (CDP-ME) and Q (PP<sub>i</sub>). (Scheme 52)



Scheme 52. Substrate binding to the enzyme for sequential mechanism

According to Dalziel, a typical rate equation of sequential mechanism in double reciprocal form can be written as shown in equation (9 and 9') where **A** is CTP, **B** is MEP, **K<sub>A</sub>** is the dissociation constant of EB (E-MEP) complex for A (CTP), **K<sub>B</sub>** is the dissociation constant of EA (E-CTP) complex for B (MEP), **K<sub>iB</sub>** is the Michaelis constant of E for B (MEP) and **K<sub>iA</sub>** is the Michaelis constant of E for A (CTP) in our case. (Scheme 52).

$$\frac{1}{v} = \frac{1}{V_{max}} \left( 1 + \frac{K_A}{[A]} + \frac{K_B}{[B]} + \frac{K_{iA}K_B}{[A][B]} \right) \quad (9) \quad \frac{1}{v} = \frac{1}{V_{max}} \left( 1 + \frac{K_A}{[A]} + \frac{K_B}{[B]} + \frac{K_{iB}K_A}{[A][B]} \right) \quad (9')$$

When substrate A is varied

When substrate B is varied

If 1/V as a function of 1/[A] is plotted as a primary plot (when A is a varied substrate), then equation (9) can be expressed as equation (10). On the other hand, if 1/V as a function of 1/[B] is plotted (when B is a varied substrate) then equation (9') can be expressed as equation (10')

$$\frac{1}{v} = \frac{1}{V_{max}} \left( K_A + \frac{K_{iA}K_B}{[B]} \right) \frac{1}{[A]} + \frac{1}{V_{max}} \left( 1 + \frac{K_B}{[B]} \right) \quad (10)$$

$$\frac{1}{v} = \frac{1}{V_{max}} \left( K_B + \frac{K_{iB}K_A}{[A]} \right) \frac{1}{[B]} + \frac{1}{V_{max}} \left( 1 + \frac{K_A}{[A]} \right) \quad (10')$$

When substrate A is varied, it can be seen that slope (highlighted in blue) of primary graph is  $(1/V_{max}) * (K_A + (K_{iA}K_B)/[B])$  and the intercept (highlighted in red) is  $(1/V_{max}) * (1 + K_B/[B])$  from equation (10). When substrate B is varied, it can be seen that slope of primary plot is  $(1/V_{max}) * (K_B + (K_{iA}K_B)/[A])$  and intercept is  $(1/V_{max}) * (1 + K_A/[A])$  from equation (10').

If slopes of the primary plot are replotted (secondary plot) as a function of  $1/[B]$  (when A is varied), then equation (11) is obtained. On the other hand, the equation (11') could be obtained when slopes of primary plot are replotted as a function of  $1/[A]$  (when B is varied).

$$Slope = \left( \frac{K_{iA}K_B}{V_{max}} \right) \frac{1}{[B]} + \frac{K_A}{V_{max}} \quad (11)$$

$$Slope = \left( \frac{K_{iB}K_A}{V_{max}} \right) \frac{1}{[A]} + \frac{K_B}{V_{max}} \quad (11')$$

If intercepts of the primary plot are replotted (secondary plot) as a function of  $1/[B]$  (when A is varied), then equation (12) is obtained. On the other hand, the equation (12') could be obtained when intercepts of primary plot are replotted as a function of  $1/[A]$  (when B is varied).

$$Intercept = \left( \frac{K_B}{V_{max}} \right) \frac{1}{[B]} + \frac{1}{V_{max}} \quad (12)$$

$$Intercept = \left( \frac{K_A}{V_{max}} \right) \frac{1}{[A]} + \frac{1}{V_{max}} \quad (12')$$

From equation 12 and 12', we observe that y-intercept of linear regression of secondary plot is equal to  $1/V_{max}$  therefore  $V_{max}$  values of the kinetic experiment for both cases where A and B is varied can be calculated. Since the slope of this linear regression is equal to  $K_{B(A)}/V_{max}$ , we can deduce  $K_B$  or  $K_A$  values. Once  $K_A$  or  $K_B$  and  $V_{max}$  values are calculated,  $K_{iA}$  and  $K_{iB}$  values could be determined as the slope of linear regression of the secondary plot of slopes (equation 11 and 11') is equal to  $K_{iA(B)}K_{B(A)}/V_{max}$ . (Figure 48)

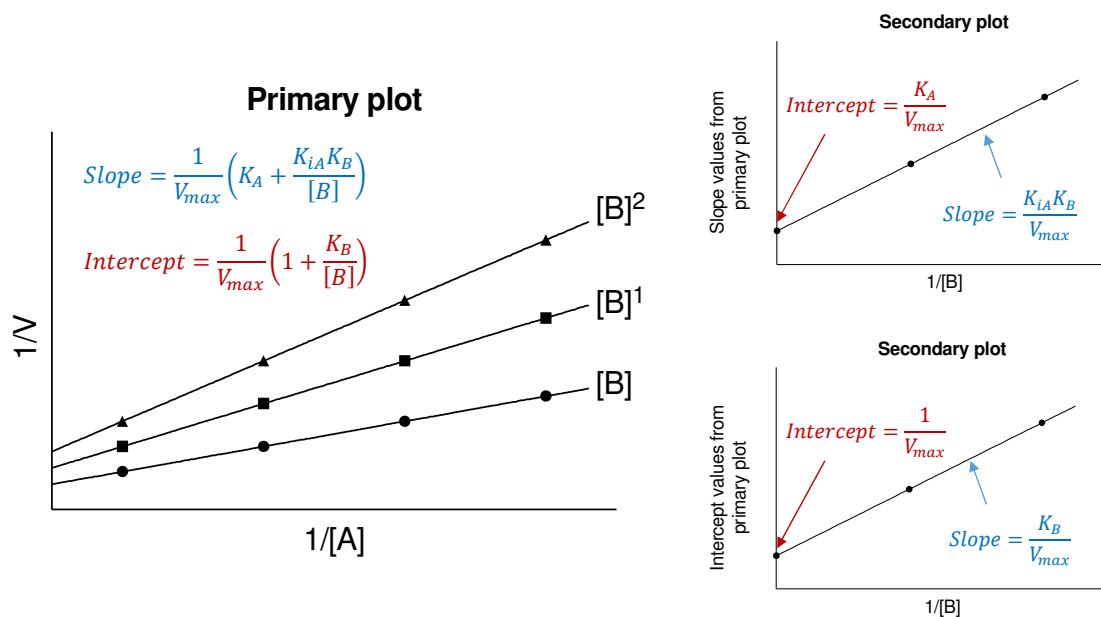
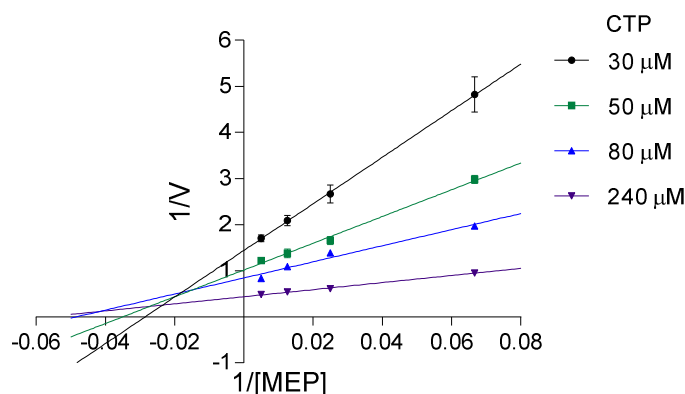


Figure 48. Determination of  $V_{max}$  and  $K_m$  values using Dalziel's method when A is varied substrate. In a similar manner  $K_{iB}$  and  $K_A$  values can be determined when B is varied substrate.

To the best of our knowledge, *E. coli* IspD mechanism has never been determined using a steady state kinetic analysis. Only pulse-chase experiment as well as X-ray crystallography were used to illustrate the mechanism. We, therefore, investigated *E. coli* IspD mechanism by using a steady state kinetic analysis. For this purpose, we performed the kinetic experiments by first varying MEP between 15 – 200  $\mu\text{M}$  and fixing CTP at 30, 50, 80 and 240  $\mu\text{M}$ . Upon producing the double reciprocal plot ( $1/V$  against  $1/[\text{MEP}]$ ) of the obtained data and linear regression analysis, we found series of lines that intersect with each other left of the y-axis and above the x-axis (Figure 49). This feature suggests that the mechanism is sequential rather than ping-pong.

Since kinetic parameters can be estimated from this double reciprocal plot, we plotted corresponding secondary plots to obtain the kinetic values for comparison to our previous values that were obtained using the classical Michaelis-Menten model.



Best-fit values $\pm$ SE	CTP (30 $\mu$ M)	CTP (50 $\mu$ M)	CTP (80 $\mu$ M)	CTP (240 $\mu$ M)
Slope	50,57 $\pm$ 0,6467	29,04 $\pm$ 1,585	17,46 $\pm$ 2,266	7,682 $\pm$ 0,3628
Y-intercept	1,44 $\pm$ 0,02343	1,016 $\pm$ 0,05744	0,8439 $\pm$ 0,08211	0,4356 $\pm$ 0,01314
X-intercept	-0,02848	-0,03498	-0,04832	-0,05671
R square	0,9997	0,9941	0,9674	0,9956

Figure 49. Double reciprocal plot of Michaelis-Menten kinetics of IspD (MEP as a varied substrate)  
 Conditions: MgCl<sub>2</sub> (1 mM), DTT (1 mM), Inorganic pyrophosphatase (133 mU/mL), E.coli IspD – 0.065  $\mu$ g in 400  $\mu$ L Tris HCl (50 mM, pH = 8)

As mentioned above, if we replot the slopes of primary double reciprocal plot (Figure 49) as a function of 1/[CTP] and analyse the plot by linear regression, the following graph was obtained (Figure 50). The slope from this graph is equal to  $K_{iB} * K_A / V_{max}$ .

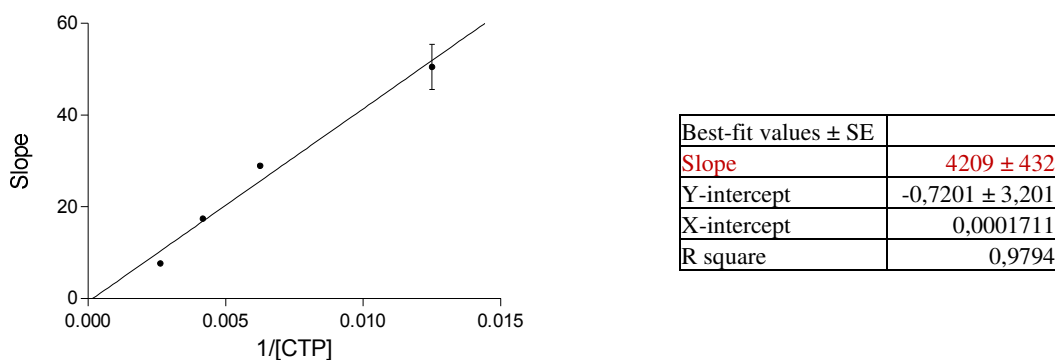


Figure 50. Slope replot of double reciprocal analysis (MEP as a varied substrate).

As described above,  $V_{max}$  and  $K_A$  values can be determined by replotting the intercepts of primary plot as a function of 1/[CTP] (Figure 51). The y-intercept of this graph is equal to  $1/V_{max}$  and the slope is equal to  $K_A/V_{max}$ .

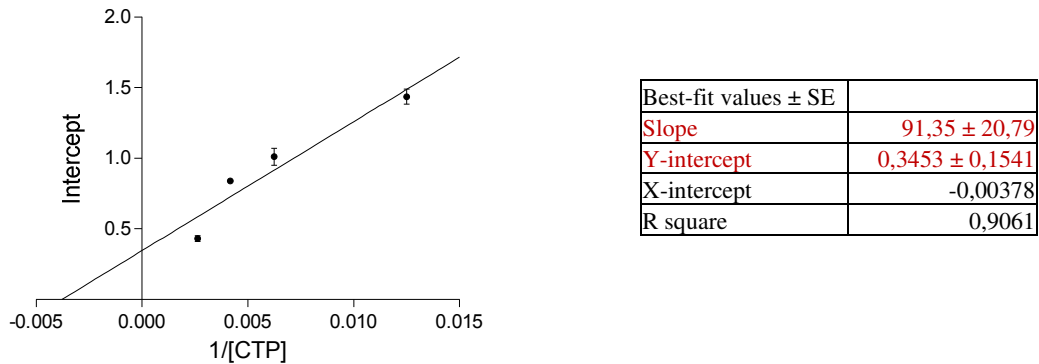
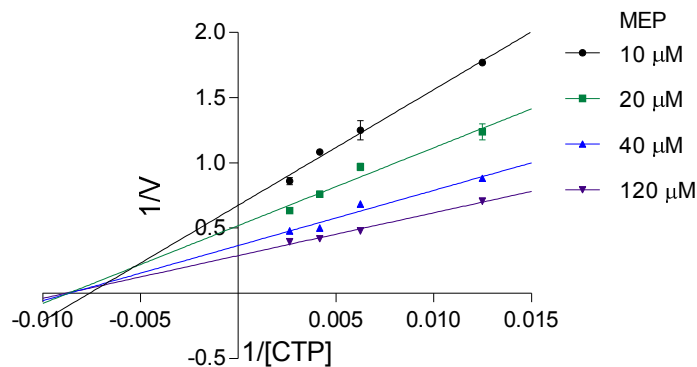


Figure 51. Intercepts replot of primary double reciprocal plot (MEP as a varied substrate).

From intercept replot (Figure 51), one could estimate that  $V_{\max} = 2.9 \mu\text{M}/\text{min}$  (y-intercept =  $1/V_{\max}$ ) and  $K_A = 264.9 \mu\text{M}$  (Slope =  $K_A/V_{\max}$ ). Using  $K_A$  and  $V_{\max}$  values, we could estimate that  $K_{iB} = 46 \mu\text{M}$  (Figure 50) and this corresponds to  $K_m$  value of MEP for IspD. Previously we had determined a  $K_m$  value of  $40 \mu\text{M}$  for MEP with IspD using Michaelis-Menten equation (Figure 34). The  $K_m$  value obtained by Dalziel's method was in agreement with Michaelis-Menten kinetic analysis.



Best-fit values $\pm$ SE	CTP (30 $\mu\text{M}$ )			
Slope	88,7 $\pm$ 6,221	59,71 $\pm$ 8,603	42,33 $\pm$ 6,426	32,8 $\pm$ 2,566
Y-intercept	0,6752 $\pm$ 0,04609	0,5194 $\pm$ 0,06374	0,3661 $\pm$ 0,04761	0,2895 $\pm$ 0,01901
X-intercept	-0,007612	-0,008698	-0,00865	-0,008824
R square	0,9903	0,9601	0,9559	0,9879

Figure 52. Double reciprocal plot of Michaelis-Menten kinetics of IspD (CTP as a varied substrate)  
 Conditions:  $\text{MgCl}_2$  (1 mM), DTT (1 mM), Inorganic pyrophosphatase (133 mU/mL), *E. coli* IspD – 0.065  $\mu\text{g}$  in 400  $\mu\text{L}$  Tris HCl (50 mM, pH = 8)

Similarly, we performed the experiments with CTP varied between 80 – 380  $\mu\text{M}$  and MEP fixed at 10, 20, 40 and 120  $\mu\text{M}$ . The double reciprocal plot resulted in series of lines intersecting left of y-axis and top of x-axis (Figure 52). Since the lines were intersecting for both double reciprocal plots (MEP and CTP varied), IspD catalyses the reaction according to a sequential mechanism. Sequential mechanism can be either ordered where substrates bind to the enzyme in orderly fashion or random where substrates bind to the enzyme randomly without any specific order.

By replotting slopes of primary plot as a function of  $1/[\text{MEP}]$ , the following graph was obtained (Figure 53). The slope of this graph equals to  $K_{iA} * K_B / V_{\text{max}}$ .

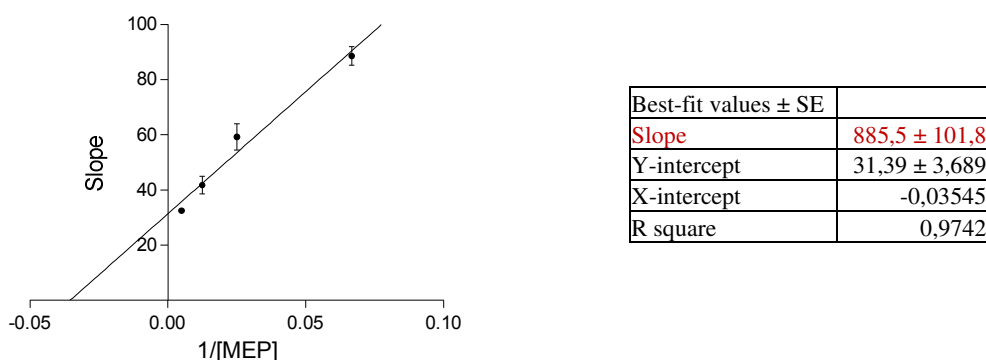


Figure 53. Slope replot of double reciprocal analysis (CTP as a varied substrate).

$V_{\text{max}} = 3.3 \mu\text{M}/\text{min}$  and  $K_B = 20 \mu\text{M}$  was obtained from the intercept replot (Figure 54). Using these values  $K_{iA}$  value determined to be  $149 \mu\text{M}$ . We found  $K_m$  value for CTP to be  $90 \mu\text{M}$  in our previous study using Michaelis-Menten equation and it is 1.6 times lower than the value determined by Dalziel's method ( $149 \mu\text{M}$ ).

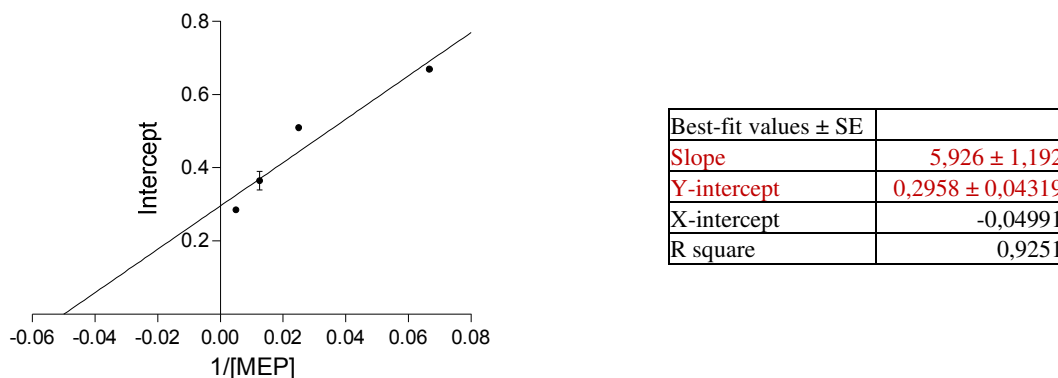
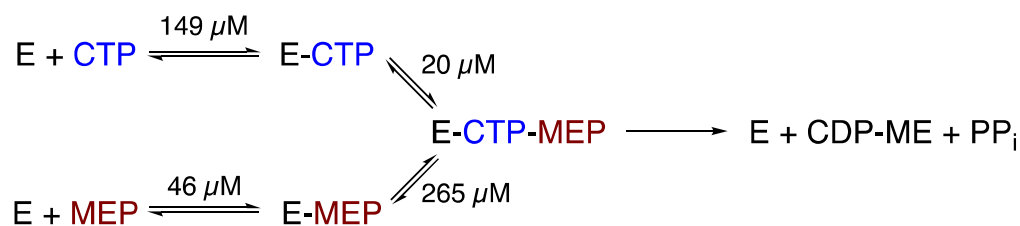


Figure 54. Intercept replot of double reciprocal analysis (CTP as a varied substrate).

The assay for determination of kinetic parameters using Dalziel's method is summarised in Scheme 53. We have found following  $K_m$  values for IspD: 149  $\mu\text{M}$  ( $K_{iA}$ ) for CTP and 46  $\mu\text{M}$  ( $K_{iB}$ ) for MEP. On the other hand, dissociation constant of E-CTP complex for MEP ( $K_B$ ) was 20  $\mu\text{M}$  and dissociation constant of E-MEP complex for CTP ( $K_A$ ) was 265  $\mu\text{M}$ . This would mean that if CTP binds to the free enzyme first, the affinity of MEP for E-CTP complex would be increased (low dissociation constant). If MEP binds to the free enzyme first, the affinity of CTP for E-MEP complex will be very low (high dissociation constant) and the E-MEP complex might not be productive and would dissociate. Therefore, these results are in agreement with ordered sequential mechanism in which CTP binds first to the IspD followed by MEP. To confirm this result, dead end inhibition studies<sup>271-273</sup> should be conducted.



Scheme 53. Determination of  $V_{max}$  and  $K_m$  values of MEP and CTP for IspD.

To summarise, IspD kinetic studies were carried out using a colorimetric assay.  $K_m$  value of IspD for MEP and CTP were found to be in agreement with literature reports.

We have successfully synthesised MEP-N<sub>3</sub> and showed that it is a substrate for IspD. IspD converts MEP-N<sub>3</sub> into the corresponding product as judged by LC-MS analysis. It was noticed that IspD reaction rate was diminished at higher concentrations of MEP-N<sub>3</sub> (>500  $\mu$ M) pointing that substrate inhibition occurred. Preliminary activity tests highlighted the potential inhibitory activity of MEP-N<sub>3</sub> on IspD.

More detailed kinetic studies showed that, MEP-N<sub>3</sub> was a mixed type inhibitor for both substrates. Mixed type inhibition pattern suggests that the inhibitor can bind to either free enzyme or enzyme substrate complex. MEP-N<sub>3</sub> preferentially binds to the free enzyme according to  $\alpha$  value. In terms of inhibition, we found that MEP-N<sub>3</sub> possesses highest inhibitory activity against *E.coli* IspD when compared to currently known inhibitors of this bacterial enzyme.

Although IspD reaction mechanism has been previously investigated by pulse-chase experiments, we further determined the mechanism of IspD using steady state kinetic analysis using a bisubstrate model. The double reciprocal plot of initial rate analysis showed series of lines that cross each other. This is indicative of sequential mechanism and it is in agreement with the result obtained by pulse-chase experiments. The kinetic parameters for both natural substrates are in the same range as those found using the classical Michaelis-Menten model. However, the dissociation constant of CTP for E-MEP complex and the dissociation constant of MEP for E-CTP complex suggest that CTP might first bind to the enzyme followed by MEP confirming the pulse-chase experiment. Therefore, IspD follows an ordered sequential mechanism with CTP binding first and dead end inhibition studies should be performed to further complete this study.

# CHAPTER-4

## Development of Novel ADC linkers

## 4.1 Introduction

Throughout the 20<sup>th</sup> century, chemotherapy was one of the main cancer treatment choices. In the beginning of the early stages of development of cytotoxic agents, the main concept for chemotherapy was that rapidly proliferating cancer cells would consume cytotoxic agents faster than normal cells. However, even if cancer cell death occurs, normal cells also die due to poor selectivity of cytotoxic agents. First class of anticancer agents include nitrogen mustard, chlorambucil and cyclophosphamide (Figure 55) which suppress cancer cell proliferation by alkylating DNA. In the second half of the last century, the combination of cytotoxic agents for cancer treatment was adopted but still it lacks selectivity for cancer cells over normal cells, resulting in numerous side effects.<sup>274</sup>

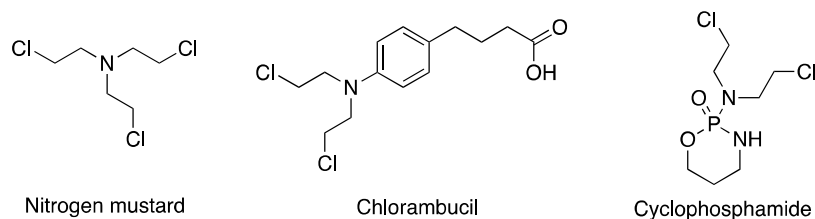


Figure 55. Examples of chemotherapy agents.

The ideal chemotherapy for cancer treatment should possess high selectivity for cancer cells thus the concept of targeted chemotherapy had emerged as a promising method to fight against cancer. Monoclonal antibody (mAb) is one of the main targeted anticancer treatment. The fundamental of mAb treatment is to obtain an antibody that specifically targets an antigen which is mostly expressed on the surface of tumour cell. These antigens can be cell surface glycoprotein, protein or carbohydrates. mAb mostly acts through antibody dependent cellular cytotoxicity (ADCC), for example by activating natural killer cells to target tumour cells, or mAb can alter signal transduction within tumour cell.<sup>275-277</sup> Initially mAb was efficient in terms of selectivity, but mAb were often obtained in low yield and in a mixture of non-specific antibodies for tumour cells but later researchers figured out to selectively produce specific mAb in high quantity.<sup>8</sup>

Using mAb, researchers were able to deliver cytotoxic agents selectively to tumour cells so the new concept antibody drug conjugate (ADC) was born. The first generation ADC includes

anticancer drugs methotrexate, vinblastine and doxorubicin (Figure 56) attached to mAb and since then ADC have been developed intensively.

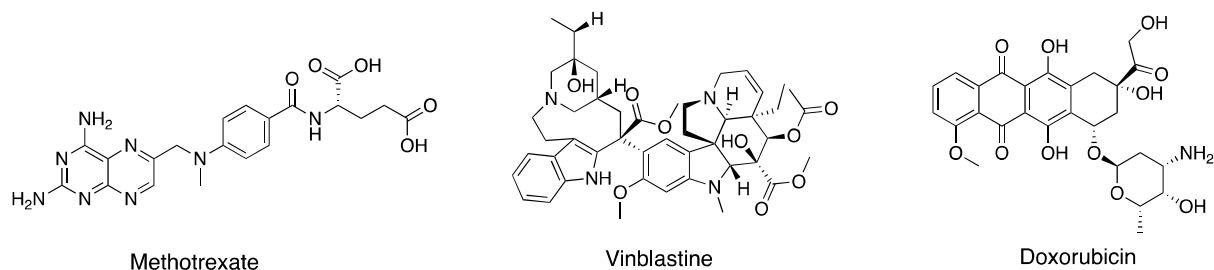
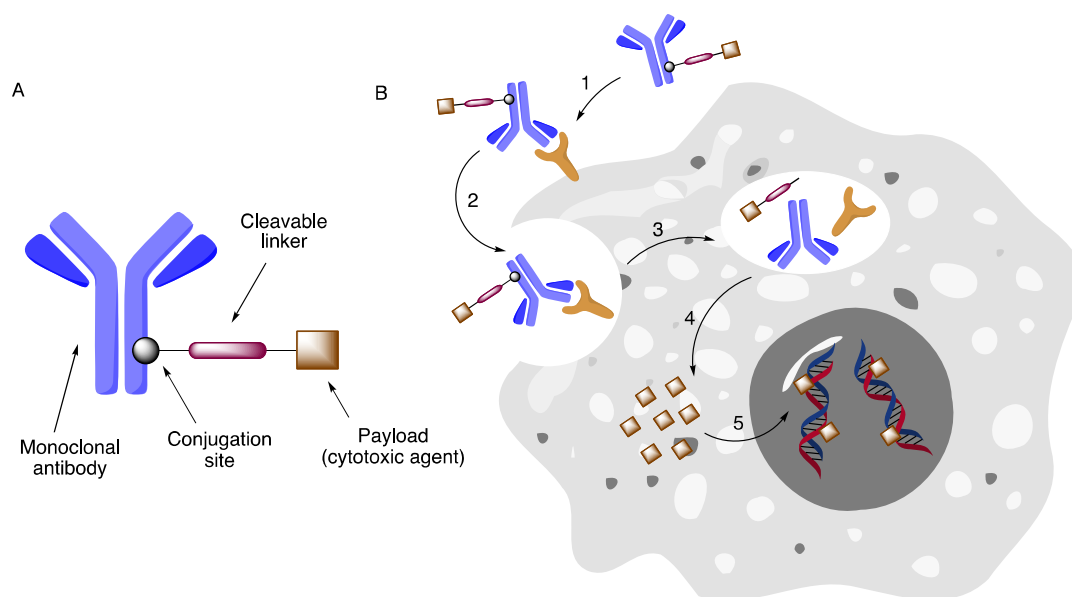


Figure 56. Examples of anticancer drugs

ADC consist of three constituents – mAb, a linker and a payload (anticancer drugs). A linker is one important thing for successful ADC technique. An ideal linker should possess following features; First, a good stability in the plasma. If the linker is not stable enough in blood circulation the cytotoxic payload will prematurely be released and the efficiency of ADC treatment would fall. Secondly, the linker has to be cleaved rapidly and release the payload once the ADC is internalised inside the tumour cell. Lastly, but not least, a linker has to be hydrophilic otherwise it tends to aggregate before the internalisation.<sup>278</sup> The general structure and mechanism of action of ADC is illustrated in Figure 57. The linker can be either cleavable or non-cleavable and in the case of non-cleavable linker, the linker and payload size should be considered because some non-cleavable linkers might interfere payload interaction with its target.

The cleavable linker releases the payload due to extracellular or intracellular environments such as pH or redox potential or it can be cleaved by intracellular lysosomal activity. Currently, there are several types of cleavable linkers including hydrazone, disulphide, diphosphate and cathepsin B cleavable linker.



*Figure 57. Structure and mechanism of ADC. A) General structure of ADC. B) General mechanism of ADC technique. 1. ADC binds to a cell surface antigen. 2. Internalisation of ADC-antigen complex by endocytosis into the tumour cell. 3. ADC-antigen complex is degraded by lysosomal processing. 4. Cytotoxic payload is released after lysosomal degradation. 5. Payload binds to its target which are mostly nucleic acid or microtubule to disrupt tumour cell proliferation resulting in cell death.*

Hydrazone linkers relies on cleavage upon exposition to acidic environment of endosomes or lysosomes (pH 4.8 - 6).<sup>279, 280</sup> The disulphide linker, on the other hand, releases the payload by reduction with glutathione which is more abundant in intracellular environment compared to extracellular environment thus disulphide linker stays stable in the circulation. Upon internalisation and lysosomal degradation, higher concentration of glutathione triggers disulphide bond reduction and cleavage.<sup>281</sup> More recently, a diphosphate diester linker was reported to have a better stability in the blood circulation, better solubility due to anionic feature of diphosphate and smooth cleavage occurs upon internalisation. After internalisation, the linker is cleaved by an enzyme during endosomal and lysosomal process but the enzyme is currently unknown.<sup>282</sup>

Non-cleavable linkers are linked to mAb and payload via stable covalent bond that is not susceptible to lysosomal degradation hence remains with the payload after internalisation. mAb has to be completely degraded by lysosomal process to release the payload.<sup>283</sup>

In terms of conjugating mAb to a linker attached to the payload, chemical and enzymatic processes are employed. In chemical conjugation technique, a linker is attached to an amino acid residue on the surface of antibody through a controlled chemical reaction. When antibody

is conjugated to a payload, the term Drug to Antibody Ratio (DAR) raises and in general higher DAR can result in aggregation, toxicity if payload is released prematurely and has other drawbacks.

One of the most used chemical conjugation site is lysine side chain amine on mAb (Figure 58, A). This method relies on amide bond formation between amine and activated carboxylic acid. Generally, there are approximately 80 lysine residues on a typical mAb and 10 of them are chemically accessible making DAR to be higher than preferred. Some lysine residues play a critical role in recognition of antigen on cancer cell surface by antibody, therefore if these lysine residues are conjugated to payload, the efficiency of ADC would fall.<sup>278</sup>

Cysteine is another possible conjugation site but, in general, there are no free cysteine thiol groups on antibody surface and all of them exist in disulphide bond (Figure 58, B). Under mild conditions these disulphide bonds can be selectively reduced to release the free thiol groups which will be reactive towards certain functionalities attached to the linker. Due to the low number of disulphide bond present on antibody, cysteine conjugation is superior to lysine conjugation in terms of DAR ratio.<sup>284</sup>

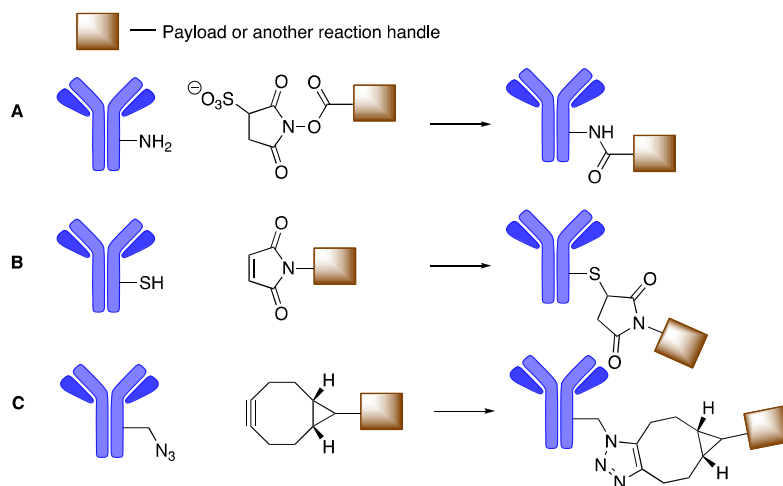


Figure 58. Examples of chemical conjugation. A) Lysine residue is reacted with activated carboxylic acid ester. B) Thiol group liberated by reduction of disulphide bond reacts with maleimide functionality. C) Non-natural amino acid residue containing azide group reacts with BCN moiety to form clicked product.

Another conjugation method using chemical reaction is to introduce a non-natural amino acid residue to an antibody by genetic engineering and later attach the payload (Figure 58, C). In

most cases, un-natural amino acids bearing bioorthogonal functionality such as azide, alkyne or carbonyl, *etc* are installed on an antibody via genetic engineering.<sup>285</sup>

Apart from chemical conjugation methods, mAbs are also susceptible to enzymatic conjugation methods. These enzymes can modify on either native or genetically modified antibodies with site specific reactions therefore enzymatic conjugation method allows controlled DAR.<sup>278</sup>

In search for a better bioconjugating agent, in 2014, Koniev *et al*, reported that APN (3-Arylpropionitrile) derivative to be a novel and promising tagging agent for cysteine moiety. They exploited APN derivative selectivity for thiols over other functional groups in protein as well as its stability in plasma and found APN derivative to be superior to maleimide which is widely used in cysteine modification.<sup>286</sup> In the following contexts, we studied APN analogues as novel bioconjugating agents for specifically thiol to thiol and amine to thiol conjugation methods. This work is described in the following papers. I contributed to the synthesis of *p*-(maleimide)-phenylpropionitrile (MAPN) and sodium 4-((4-(cyanoethynyl)benzoyl)oxy)-2,3,5,6-tetrafluorobenzenesulfonate (CBTF) (Figure 59).

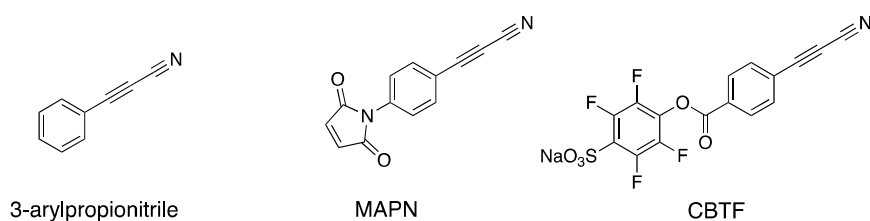


Figure 59. Structure of APN and its derivatives.

# General conclusion and perspectives

## General conclusion

The aim of this project was to investigate the MEP pathway using metabolic labelling. For this purpose bioorthogonal ligation (click chemistry) was used. ME-N<sub>3</sub> was synthesised in 9 steps with an overall yield of 12 %. For click reaction, BCN-TMPP was synthesised through a convergent synthetic pathway with an overall yield of 62 %. After synthesis of ME-N<sub>3</sub> and BCN-TMPP, the determination of click reaction kinetics and the limit of detection of the clicked product using LC-MS were determined. The second order rate constant of the click reaction between ME-N<sub>3</sub> and BCN-TMPP was found to be 0.21 M<sup>-1</sup>s<sup>-1</sup>. With the help of TMPP probe attached to BCN the clicked molecule was detectable using LC-MS starting from 10 nM ME-N<sub>3</sub>. We assumed this limit of detection range was sufficient to detect a tagged metabolite based on previous literature reports.

When *E.coli* was incubated with ME-N<sub>3</sub>, no clicked metabolite was detected using LC-MS analysis. Through searching possible fragmented metabolites, we detected a signal that was hypothesised to be azide tagged DMAPP fragment. To validate this hypothesis, N<sub>3</sub>-DMAPP was synthesised in 4 steps starting from isoprene. The click reaction between N<sub>3</sub>-DMAPP and BCN-TMPP produced a product which led to a different MS spectrum and a different retention time compared to the one we assumed to be N<sub>3</sub>-DMAPP fragment. This result proved that our hypothesis about the possible fragment was wrong. We also performed a similar incubation study on an *E.coli* strain that is deficient in IspG, an enzyme of the MEP pathway. If the mutant incorporates ME-N<sub>3</sub>, we should detect only a very limited number of metabolites but, even in this case, any relevant signal of expected metabolites was detected by LC-MS analysis.

Inability to detect any MEP pathway metabolite using LC-MS draws the question that ME-N<sub>3</sub> might not enter bacteria or might not be metabolised. At this stage, we could not conclude on ME-N<sub>3</sub> cell permeability or incorporation. However, the concentration of ME-N<sub>3</sub> incorporated into the bacteria might be too low to allow its detection by LC-MS. If *E.coli* incorporates ME-N<sub>3</sub>, further experiments would consist in concentrating the bacterial lysate to have sufficient amount of tagged metabolites and using a more sensitive MS instrument for detection of the compounds.

In order to reveal if ME-N<sub>3</sub> could enter the MEP pathway, we have successfully synthesised MEP-N<sub>3</sub>. IspD (the third enzyme of the MEP pathway) converted MEP-N<sub>3</sub> into the ME-N<sub>3</sub>-CDP in the presence of CTP as judged by LC-MS analysis. It was noticed that IspD reaction

rate was diminished at higher concentrations of MEP-N<sub>3</sub> (>500 μM) pointing that substrate inhibition occurred.

More detailed kinetic studies showed that MEP-N<sub>3</sub> was a mixed type inhibitor for both substrates of IspD: MEP and CTP. Although mixed type inhibition pattern suggests that the inhibitor can bind to either free enzyme or enzyme substrate complex, MEP-N<sub>3</sub> preferentially binds to the free enzyme according to the  $\alpha K_i$  value obtained. In terms of inhibition potency, we found that MEP-N<sub>3</sub> possesses highest inhibitory activity ( $K_i = 21 \mu\text{M}$ ) against *E.coli* IspD when compared to currently known inhibitors of *E.coli* IspD. We, therefore, can conclude that ME-N<sub>3</sub> was not a good tagged metabolic precursor for labelling the MEP pathway as it was an inhibitor of the third enzyme of the MEP pathway. It is also not clear if ME-N<sub>3</sub> enters *E.coli* cell.

Although IspD reaction mechanism has been previously investigated by using pulse-chase experiments, we further determined the mechanism of IspD using steady state kinetic analysis using a bisubstrate model. The double reciprocal plot of initial rate analysis showed series of lines that cross each other. This is indicative of sequential mechanism and it is in agreement with the result obtained by pulse-chase experiments. The kinetic parameters for both natural substrates were 40 μM for MEP and 90 μM for CTP. However, the value of the dissociation constant of CTP from E-MEP complex (265 μM) and the value of the dissociation constant of MEP from E-CTP complex (20 μM) suggest that CTP might first bind to the enzyme followed by MEP confirming the pulse-chase experiment. Therefore, IspD follows an ordered sequential mechanism with CTP binding first but dead end inhibition studies should be performed to further complete this study.

For the development of novel ADC linker, an APN analogue CBTF was prepared in good yield and found to be superior in terms of stability in the plasma over commercially available reagent SMCC (succinimidyl 4-(N-maleimidomethyl)cyclohexane 1-carboxylate) and this makes CBTF a new conjugating agent suitable for purposes in which stability is a key requirement. MAPN, an another analogue of APN with hetero biofunctionality was successfully prepared and applied for thiol-to-thiol heteroconjugation. It showed clean and complete conversion to a single desired product with higher efficiency when compared to a commercial reagent *p*-phenylenedimaleimide.

## Perspective

ME-N<sub>3</sub> was revealed to be a poor probe for metabolic labelling studies of the MEP pathway. However, it is still unclear if this molecule enters *E.coli* cells. In order to investigate if ME-N<sub>3</sub> is capable of crossing the bacterial membranes, one solution would be to synthesise [<sup>3</sup>H]-ME-N<sub>3</sub> using a similar protocol as described for [<sup>3</sup>H]-ME<sup>210</sup> and check if the EcAB4-5 mutant accumulates some MEP pathway intermediates. Such experiments were already performed using [<sup>3</sup>H]-ME and led to the detection of [<sup>3</sup>H]-ME-cPP.<sup>85</sup> However, as MEP-N<sub>3</sub> was shown to be a poor substrate but also an inhibitor of IspD, other molecules should be synthesised that are suitable for bioorthogonal ligation.

As we learnt that allylic azides can undergo 1,4-sigmatropic rearrangement, the position of azide functionality has to be carefully considered. To avoid sigmatropic rearrangement at DMAPP and IPP production stage, azide could be attached at C-1 (**105**) and C-4 (**104**) of MEP molecule. To facilitate the cell permeability of the azide tagged molecule, cleavable hydrophobic residues could be attached to the phosphate moiety as it was unclear if ME-N<sub>3</sub> (**10**) could enter bacterial cell membranes. For example, molecule **106** could be synthesised for better cell permeability. (Figure 60)

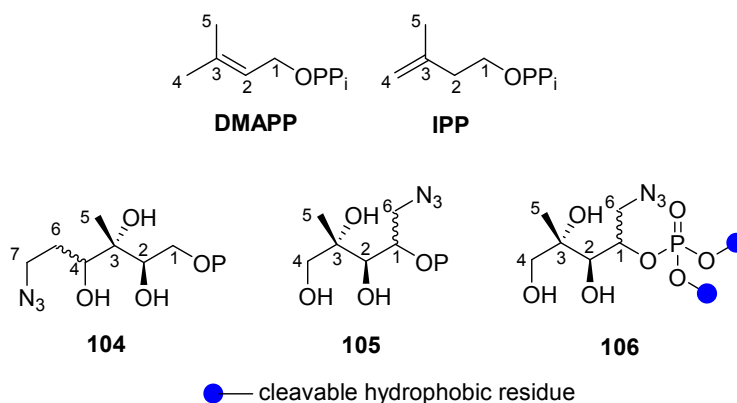


Figure 60. Possible azide tagged MEP analogues for further metabolic studies.

In addition to synthesising other azide tagged ME analogues, the labelling experiment could be improved at the detection stage. Instead of analysing the cell lysate directly using LC-MS, the concentration of the lysate prior to LC-MS analysis could be performed.

In reported work a solid phase extraction had been applied<sup>287</sup> to increase the detection of the native MEP pathway intermediates using ultra performance liquid chromatography mass spectroscopy analysis and the limit of detection discovered was similar to our result. As most of the MEP pathway intermediates are phosphorylated, such an anion exchange solid phase extraction could be added to our protocol to partially purify and concentrate the azide labelled MEP intermediates that could accumulate to increase the detection limit we obtained.

Concerning other methods of detection of metabolic intermediates of the MEP pathway, attempts were previously performed using  $^{31}\text{P}$  NMR to measure methylerythritol cyclodiphosphate (ME-cPP) in spinach leaves that accumulated in presence of strong illumination or  $\text{Cd}^{2+}$ . However, this method allowed only the detection of methylerythritol cyclodiphosphate that reaches, under stress conditions, quantities as high as  $1\ \mu\text{mol}$  per gramme of leaves.<sup>288, 289</sup>

During this work, we also accessed to the best inhibitor of *E.coli* IspD known to date. The  $K_i$  obtained are in the  $\mu\text{M}$  range. We could improve our inhibitor by using fragment growing. In collaboration with Dr Jean-Luc Ferrer and Dr Franck Borel (IBS, Grenoble, France), preliminary docking experiments using the structure of *E.coli* IspD – ME-CDP complex<sup>10</sup> showed that MEP- $\text{N}_3$  docks close to the CDP part of the ME-CDP with the azido moiety pointing towards the cytosine base (Figure 61). One could imagine to perform *in situ* click experiments using a library of nucleotides containing an alkyne functionality. If successful, such experiment should lead to a molecule having a better affinity for the enzyme and hence improved inhibition properties. The discovery of new inhibitors of *E.coli* IspD should lead to the development of new antibacterial agents to overcome the problem of resistance we are facing today.

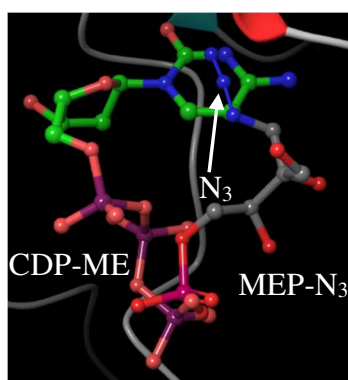


Figure 61. MEP- $\text{N}_3$  molecule docked in IspD with ME-CDP

# Experimental Section

## General experimental condition

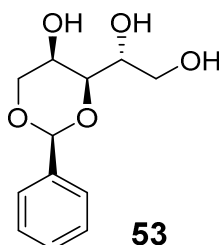
All chemicals and solvents were purchased from commercial suppliers. Reactions were performed under N<sub>2</sub> atmosphere unless otherwise stated. TLC was performed on Merck TLC Silica gel 60 F<sub>254</sub> aluminium sheets and revealed under 254 nm or with stains (vanillin and KMnO<sub>4</sub>). NMR spectra were recorded on Bruker Avance 400 and 500 MHz spectrometers. IR spectra were recorded on Nicolet 380 FT-IR spectrometer. UV visible spectrophotometer was recorded on Genesys 10 UV machine. Specific optical rotation was determined on Jasco P-2000 polarimeter instrument conditioning with standard compound Fmoc-Ser(tBu)-OH (CAS: 71989-33-8) 0.1 % solution, + 25°. LC-MS analysis was conducted on Waters Alliance 2690 LC system (C<sub>18</sub> column) coupled with Waters ACQUITY QDa mass detector. HPLC analysis was conducted on Shimadzu Nexera LC 20AD system on C<sub>18</sub> column.

LC-MS conditions: Solution A (H<sub>2</sub>O, 0.05 % Formic acid), Solution B (MeCN). Gradient as follows: 0 min 95 % A and 5 % B; 0-5 min, 5 % A and 95 % B; 5-6 min, 5 % A and 95 % B; 6-7 min, 95 % A and 5 % B. Detection at 254 nm in positive mode.

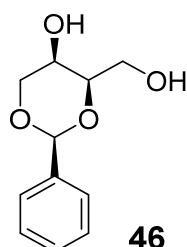
HPLC conditions: Solution A (H<sub>2</sub>O, 0.05 % Formic acid), Solution B (MeCN). Gradient as follows: 0 min 95 % A and 5 % B; 0-10 min, 5 % A and 95 % B; 10-12.5 min, 5 % A and 95 % B; 12.5-15 min, 95 % A and 5 % B. Detection at 254 nm.

NMR spectra chemical shifts were referenced as following: <sup>1</sup>H-NMR CDCl<sub>3</sub> δ = 7.26 ppm, CD<sub>3</sub>OD δ = 3.31 ppm, D<sub>2</sub>O δ = 4.79 ppm. <sup>13</sup>C-NMR CDCl<sub>3</sub> δ = 77.16 ppm, CD<sub>3</sub>OD δ = 49 ppm.

## Synthesis of molecules described in Chapter 2 and 3

1-((2S,4R)-5-hydroxy-2-phenyl-1,3-dioxan-4-yl)ethane-1,2-diol (**53**)

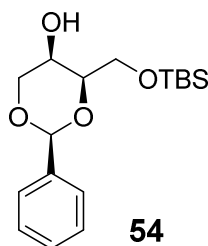
Benzaldehyde (1.2 eq, 15.6 g, 147 mmol) was added to **45** (1 eq, 18 g, 118 mmol). HCl gas that was generated by dripping a solution of concentrated HCl to a solution of concentrated H<sub>2</sub>SO<sub>4</sub>. The gas was passed to the reaction mixture with manual stirring until the mixture become a very viscous syrup. It was then left to stand at room temperature.<sup>290</sup> After 18 h, the solid mass was broken down and triturated with Et<sub>2</sub>O (50 mL) and saturated NaHCO<sub>3</sub> (80 mL) to remove the excess of benzaldehyde and to neutralize the remaining HCl. Resulting white crystals were washed with Et<sub>2</sub>O (4 x 100 mL) to give 22 g of **53** (77 %) as a white solid. <sup>1</sup>H NMR (400 MHz, MeOD) δ (ppm): 7.54 – 7.50 (m, 2H), 7.37 – 7.32 (m, 3H), 5.60 (s, 1H), 4.21 (dd, *J* = 12.1, 1.8 Hz, 1H), 4.13 (dd, *J* = 12.1, 1.8 Hz, 1H), 3.89 – 3.88 (m, 2H), 3.80 (s, 1H), 3.79 – 3.76 (m, 1H), 3.68 – 3.64 (m, 1H); <sup>13</sup>C NMR (101 MHz, MeOD) δ (ppm): 139.91, 129.72, 128.96, 127.39, 102.55, 80.04, 73.80, 70.96, 64.08, 63.94.

(2S,4R)-4-(hydroxymethyl)-2-phenyl-1,3-dioxan-5-ol (**46**)

A solution of **53** (1 eq, 18.6 g, 77.4 mmol) in MeOH (250 mL) was stirred and cooled to 0 °C and then cold aqueous (50 mL) solution of NaIO<sub>4</sub> (1.1 eq, 18.2 g, 85.2 mmol) was added

dropwise. The reaction mixture was stirred for 20 minutes during which period TLC (10 : 90, EtOH : CH<sub>2</sub>Cl<sub>2</sub>) indicated no trace of starting material. The white precipitate was filtered and washed with 10 mL of MeOH. The filtrate containing the aldehyde was further stirred and NaBH<sub>4</sub> (1.1 eq, 3.22 g, 85.2 mmol) in water (2 mL) was added dropwise at 0 °C. The resulting milky suspension was stirred for an hour at zero degree. After completion, MeOH was evaporated under reduced pressure and saturated NH<sub>4</sub>Cl (150 mL) was added. The mixture was extracted with DCM (4 x 150 mL) and the organic layer was dried over MgSO<sub>4</sub> and evaporated. The resulting solid was recrystallized (DCM : Acetone, 70 : 30) to give 10.3 g of diol **46** (66 %) as white crystals. <sup>1</sup>H NMR (400 MHz, MeOD) δ (ppm): δ 7.57 – 7.54 (m, 2H), 7.38 – 7.32 (m, 3H), 5.60 (s, 1H), 4.15 (dd, *J* = 12.1, 1.7 Hz, 1H), 4.11 (dd, *J* = 12.1, 1.6 Hz, 1H), 4.02 (ddd, *J* = 6.8, 5.5, 1.6 Hz, 1H), 3.81 (dd, *J* = 11.6, 6.8 Hz, 1H), 3.76 (dd, *J* = 11.6, 5.5 Hz, 1H), 3.61 (dd, *J* = 1.7, 1.6 Hz, 1H); <sup>13</sup>C NMR (101 MHz, MeOD) δ (ppm): 139.88, 129.75, 128.95, 127.54, 102.72, 81.43, 73.69, 64.86, 63.05.

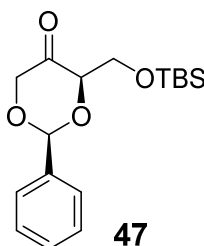
**(2S,4R)-4-(((tert-butyldimethylsilyloxy)methyl)-2-phenyl-1,3-dioxan-5-ol (54)**



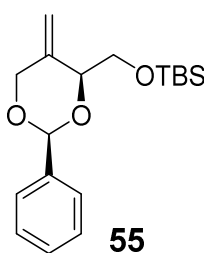
A solution of **46** (1 eq, 4.4 g, 20.9 mmol) and imidazole (1.1 eq, 1.56 g, 22.9 mmol) in anhydrous DCM (150 mL) was stirred and cooled at 0 °C as TBDMSCl (1.2 eq, 3.96 g, 26.3 mmol) in anhydrous DCM (10 mL) was added dropwise over 5 min. The resulting milky suspension was stirred for 3 h at room temperature and the reaction was monitored by TLC (3 : 7, EtOAc : *c*-Hexane). After completion, ethanolamine (6.6 mL, 109 mmol) was added to scavenge the excess of TBDMSCl, and the suspension was stirred 20 min further. Water (200 mL) was added and the product was extracted with DCM (4 x 100 mL). Combined organic layers were dried over MgSO<sub>4</sub> and concentrated under reduced pressure. The residue was purified by flash chromatography (Acetone : *c*-Hexane, 20 : 80) to give 5.6 g of alcohol **54** (83 %) as a white solid. <sup>1</sup>H NMR (400 MHz, CDCl<sub>3</sub>) δ (ppm): 7.53 – 7.49 (m, 2H), 7.41 – 7.34 (m, 3H), 5.59 (s, 1H), 4.27 (dd, *J* = 11.9, 1.9 Hz, 1H), 4.09 (dd, *J* = 11.9, 1.3 Hz, 1H), 4.00 (ddd, *J*

= 6.6, 5.2, 1.3 Hz, 1H), 3.93 (dd,  $J = 10.1, 6.6$  Hz, 1H), 3.82 (dd,  $J = 10.1, 5.2$  Hz, 1H), 3.73 (dd,  $J = 10.1, 1.3$  Hz, 1H), 2.86 (d,  $J = 10.1$  Hz, 1H), 0.92 (s, 9H), 0.10 (s, 3H), 0.10 (s, 3H);  $^{13}\text{C}$  NMR (101 MHz,  $\text{CDCl}_3$ )  $\delta$  (ppm): 137.95, 129.12, 128.36, 126.11, 101.57, 79.97, 72.84, 63.86, 62.57, 26.00, 18.45, -5.24, -5.28.

**(2S,4R)-4-(((tert-butyldimethylsilyloxy)methyl)-2-phenyl-1,3-dioxan-5-one (47)**

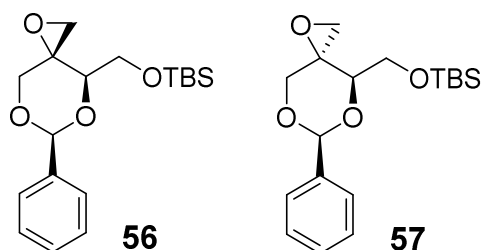


To a solution of alcohol **54** (1 eq, 500 mg, 1.54 mmol) in anhydrous DCM (5 mL) containing 4A MS (500 mg per mmol) was added 4-methylmorpholine N-oxide (1.5 eq, 270 mg, 2.31 mmol) and tetrapropylammonium perruthenate (0.1 eq, 54.2 mg, 0.154 mmol) as solids and the reaction was monitored by IR. After 30 min, the reaction mixture was diluted with ether (10 mL) and the resulting solution was filtered through silica (50 g). Silca gel was further eluted with ether (50 mL) and combined organic solvents were evaporated under reduced pressure to give colourless oil which was purified by flash chromatography (EtOAc : *n*-Hexane, 20 : 80) to yield 390 mg of ketone **47** (78 %) as a colourless oil.  $^1\text{H}$  NMR (400 MHz,  $\text{CDCl}_3$ )  $\delta$  (ppm): 7.60 – 7.54 (m, 2H), 7.45 – 7.37 (m, 3H), 5.94 (s, 1H), 4.54 (td,  $J = 3.2, 0.9$  Hz, 1H), 4.45 (dd,  $J = 17.7, 0.9$  Hz, 1H), 4.43 (dd,  $J = 17.7, 0.9$  Hz, 1H), 4.13 (dd,  $J = 10.1, 2.8$  Hz, 1H), 4.09 (dd,  $J = 10.1, 1.9$  Hz, 1H), 0.91 (s, 9H), 0.10 (s, 3H), 0.08 (s, 3H);  $^{13}\text{C}$  NMR (101 MHz,  $\text{CDCl}_3$ )  $\delta$  (ppm): 205.19, 137.33, 129.33, 128.44, 126.35, 99.28, 84.26, 72.73, 62.93, 25.93, 18.43, -5.16, -5.28.

**tert-butyl dimethyl(((2S,4S)-5-methylene-2-phenyl-1,3-dioxan-4-yl)methoxy)silane (**55**)**

A suspension of methyltriphenylphosphonium bromide (3 eq, 6.2 g, 17.6 mmol) in anhydrous THF was stirred and cooled to  $-75\text{ }^{\circ}\text{C}$ . Then n-BuLi (3 eq, 2.5 M, 7.03 mL, 17.6 mmol) was added dropwise and the mixture turned yellow. The mixture was brought to room temperature and stirred further 30 minutes. The mixture was cooled to  $-75\text{ }^{\circ}\text{C}$  again while ketone **47** (1 eq, 1.8 g, 5.86 mmol) in anhydrous THF (3 mL) was added dropwise then the solution was warmed to room temperature. After completion, reaction was quenched with cold water (10 mL) and the product was extracted with ether (4 x 40 mL). The organic layer was dried over  $\text{MgSO}_4$ , evaporated and the residue was purified by flash chromatography (EtOAc : c-Hexane, 20 : 80) to give 1.3 g of olefin **55** (70 %) as a pale yellow oil.  $^1\text{H}$  NMR (400 MHz,  $\text{CDCl}_3$ )  $\delta$  (ppm): 7.52 – 7.47 (m, 2H), 7.39 – 7.32 (m, 3H), 5.71 (s, 1H), 5.17 (s, 1H), 5.06 (s, 1H), 4.49 (s, 2H), 4.44 (t,  $J = 5.3$  Hz, 1H), 4.06 (dd,  $J = 10.5, 6.2$  Hz, 1H), 3.93 (dd,  $J = 10.5, 5.3$  Hz, 1H), 0.90 (s, 8H), 0.09 (s, 3H), 0.07 (s, 3H);  $^{13}\text{C}$  NMR (101 MHz,  $\text{CDCl}_3$ )  $\delta$  (ppm): 140.37, 138.29, 128.97, 128.32, 126.35, 110.21, 101.17, 78.64, 71.95, 63.97, 26.01, 18.43, -5.08, -5.2.

**tert-butyl dimethyl(((3*S*,4*R*,6*S*)-6-phenyl-1,5,7-trioxaspiro[2.5]octan-4-yl)methoxy)silane (56) and tert-butyl dimethyl(((3*R*,4*R*,6*S*)-6-phenyl-1,5,7-trioxaspiro[2.5]octan-4-yl)methoxy)silane (57)**



Purified *m*-CPBA (1.5 eq, 242 mg, 1.4 mmol) was added to a solution of olefin **55** (1 eq, 300 mg, 0.936 mmol) in DCM (12 mL) at 0 °C then the temperature was raised to 30 °C gradually and maintained. The reaction mixture was stirred for 6 days and monitored by TLC (EtOAc : *c*-Hexane, 10 : 90). After completion, saturated aq. NaHCO<sub>3</sub> (50 mL) was added to the reaction and the product was extracted with DCM (4 x 20 mL) the combined organic layers were washed with brine (30 mL) then dried over MgSO<sub>4</sub> and evaporated. The residue was purified by flash chromatography (EtOAc : *c*-Hexane, 5 : 95) to give 110 mg of epoxide **56** and 130 mg of epoxide **57** as colourless oil (combined yield : 77 %). Data for epoxide **56**: <sup>1</sup>H NMR (400 MHz, CDCl<sub>3</sub>) δ (ppm): 7.53 (m, 2H), 7.40 – 7.35 (m, 3H), 5.73 (s, 1H), 4.23 – 4.18 (m, 2H), 3.77 (d, *J* = 11.5 Hz, 1H), 3.73 – 3.70 (m, 2H), 3.12 (dd, *J* = 4.4, 1.8 Hz, 1H), 2.80 (dd, *J* = 4.4, 0.9 Hz, 1H), 0.89 (s, 9H), 0.05 (s, 3H), 0.04 (s, 3H); <sup>13</sup>C NMR (101 MHz, CDCl<sub>3</sub>) δ (ppm): 137.68, 129.05, 128.32, 126.32, 101.04, 79.59, 71.41, 61.31, 52.65, 52.28, 25.98, 18.46, -5.09, -5.13. Data for epoxide **57**: <sup>1</sup>H NMR (400 MHz, CDCl<sub>3</sub>) δ (ppm): 7.55 – 7.51 (m, 2H), 7.40 – 7.34 (m, 3H), 5.72 (s, 1H), 4.49 (d, *J* = 12.5 Hz, 1H), 4.43 (dd, *J* = 7.5, 4.4 Hz, 1H), 3.75 (dd, *J* = 7.5, 10.4 Hz, 1H), 3.71 (d, *J* = 12.5 Hz, 1H), 3.63 (dd, *J* = 10.4, 4.4 Hz, 1H), 3.20 (d, *J* = 4.6 Hz, 1H), 2.61 (d, *J* = 4.6 Hz, 1H), 0.88 (s, 9H), 0.05 (d, *J* = 0.9 Hz, 6H); <sup>13</sup>C NMR (101 MHz, CDCl<sub>3</sub>) δ (ppm): 137.83, 129.20, 128.39, 126.44, 101.61, 78.24, 72.78, 61.23, 54.63, 47.48, 26.00, 18.33, -5.27, -5.38.

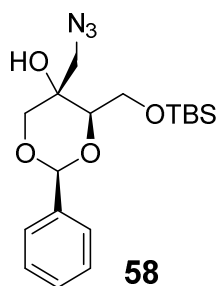
Obtention of **56** by Corey-Chaykovsky reaction.<sup>291</sup> To a solution of trimethylsulfoxonium iodide (1.1 eq., 793 mg, 3.61 mmol) in dry DMSO (11 mL) was added pre-crushed NaH (1.1 eq., 144 mg, 3.61 mmol) and the mixture was stirred for 5 minutes. Ketone **47** (1 eq., 1057 mg, 3.28 mmol) in THF (2 mL) was added dropwise to the mixture and stirred at r.t for 10 min monitored by TLC. (EtOAc / *c*Hexane : 1 / 9). The reaction was quenched with slow addition of water (10 mL) and extracted with DCM (5 x 50 mL) and combined organic layers were dried

over magnesium sulphate and evaporated. The residue was purified by flash chromatography (EtOAc / cHexane : 1 / 9) to give 582 mg of epoxide **56** as colourless oil (53 %).

Purification of commercial *m*-CPBA: Commercial *m*-CPBA (5 g) dissolved in DCM (100 mL) was washed with Phosphate buffer pH = 7.5 (150 mL x 3) and washed with brine (50 mL) during which time organic layer became weak yellow. The organic layer was dried over MgSO<sub>4</sub> then concentrated until white needle like crystals started to appear. Crystals were filtered and washed with DCM (10 mL) dropwise carefully to remove yellow colour. Filtrate was concentrated again and the process was repeated until small amount of organic layer left.

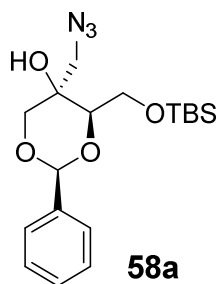
Phosphate buffer preparation: 0.1 M KH<sub>2</sub>PO<sub>4</sub> (100 mL) + 0.1 M NaOH.(81.8 mL).

**(2S,4R,5S)-5-(azidomethyl)-4-(((tert-butyldimethylsilyl)oxy)methyl)-2-phenyl-1,3-dioxan-5-ol (58)**



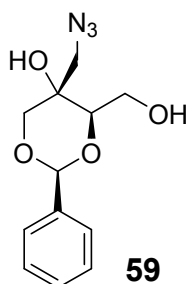
To a solution of epoxide **56** (1 eq, 150 mg, 0.446 mmol) in DMF (2.5 mL) was added NH<sub>4</sub>Cl (1.5 eq., 35.8 mg, 0.669 mmol) and NaN<sub>3</sub> (4 eq., 115 mg, 1.78 mmol) and the mixture was stirred at 60 °C for 2 h.<sup>292</sup> water (5 mL) was added and the mixture was extracted with EtOAc (4 x 15 mL) and combined organic layers were washed with water, brine then dried over MgSO<sub>4</sub> and evaporated. The residue was purified by flash chromatography (EtOAc : c-Hexane, 2 : 8) to give 130 mg of compound **58** (77 %) as colourless oil. R<sub>f</sub> 0.48 (EtOAc : c-Hexane, 2 : 8), [α]<sub>D</sub><sup>20</sup> + 9.8 (c = 0.2, MeOH), <sup>1</sup>H NMR (400 MHz, CDCl<sub>3</sub>) δ (ppm): 7.44 (m, 2H), 7.39 – 7.35 (m, 3H), 5.55 (s, 1H), 4.32 (d, *J* = 11.2 Hz, 1H), 4.00 (dd, *J* = 9.6, 5.5 Hz, 1H), 3.94 (dd, *J* = 9.9, 5.5 Hz, 1H), 3.89 (dd, *J* = 9.6, 9.9 Hz, 2H), 3.77 (d, *J* = 11.2 Hz, 2H), 3.67 (dd, *J* = 11.2, 1.1 Hz, 1H), 3.61 (dd, *J* = 11.2, 1.1 Hz, 1H), 0.93 (s, 9H), 0.15 (s, 3H), 0.13 (s, 3H). <sup>13</sup>C NMR (101 MHz, CDCl<sub>3</sub>) δ (ppm): 137.29, 129.36, 128.47, 126.26, 102.32, 79.90, 72.19, 69.14, 62.96, 53.25, 25.92, 18.24, -5.50, -5.52. IR (neat) ν (cm<sup>-1</sup>) 3479 (OH), 2953, 2857, 2101 (N<sub>3</sub>), 1255.

**(2S,4R,5R)-5-(azidomethyl)-4-(((tert-butyldimethylsilyl)oxy)methyl)-2-phenyl-1,3-dioxan-5-ol (58a)**



The synthesis was performed as described for compound **58**. Colourless oil (51 %).  $R_f$  0.67 (EtOAc : *c*-Hexane, 2 : 8),  $[\alpha]_D^{20} + 26$  ( $c = 0.2$ , MeOH).  $^1\text{H NMR}$  (400 MHz,  $\text{CDCl}_3$ )  $\delta$  (ppm): 7.53 – 7.47 (m, 2H), 7.42 – 7.34 (m, 3H), 5.53 (s, 1H), 4.12 (d,  $J = 11.7$  Hz, 1H), 4.06 (dd,  $J = 10.6, 6.0$  Hz, 1H), 3.92 (d,  $J = 11.7$  Hz, 1H), 3.87 (dd,  $J = 6.0, 4.0$  Hz, 1H), 3.82 (dd,  $J = 10.6, 4.0$  Hz, 1H), 3.63 (d,  $J = 13.1$  Hz, 1H), 3.51 (s, 1H), 3.33 (d,  $J = 13.1$  Hz, 1H), 0.92 (s, 9H), 0.11 (s, 3H), 0.10 (s, 3H).  $^{13}\text{C NMR}$  (101 MHz,  $\text{CDCl}_3$ )  $\delta$  (ppm): 137.41, 129.17, 128.30, 126.07, 101.58, 80.38, 73.64, 69.61, 62.43, 53.75, 25.88, 18.27, -5.43. IR (neat)  $\nu$  ( $\text{cm}^{-1}$ ) 3455 (OH), 2953, 2928, 2856, 2102 ( $\text{N}_3$ ), 1252.

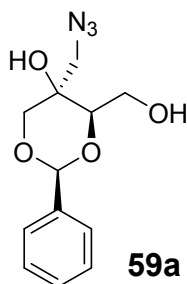
**(2S,4R,5S)-5-(azidomethyl)-4-(hydroxymethyl)-2-phenyl-1,3-dioxan-5-ol (59)**



To a solution of azido alcohol **58** (1 eq., 85 mg, 0.224 mmol) in anhydrous THF (4 mL) at 0 °C was added TBAF (1.05 eq., 1 M, 0.235 mL, 0.235 mmol) dropwise and the mixture stirred at room temperature for 30 minutes. Water (5 mL) was added and the product was extracted with ether (4 x 10 mL). Combined organic layers were dried over  $\text{MgSO}_4$  and evaporated to give 55 mg of compound **59** (93 %) as a colourless oil.  $R_f$  0.33 (EtOAc : *c*-Hexane, 4 : 6),  $[\alpha]_D^{20} - 8$  ( $c = 0.2$ , MeOH).  $^1\text{H NMR}$  (400 MHz,  $\text{CDCl}_3$ )  $\delta$  (ppm): 7.47 (m, 2H), 7.42 – 7.36 (m, 3H), 5.57

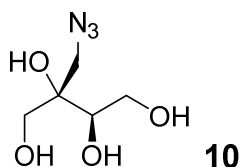
(s, 1H), 4.27 (d,  $J = 11.1$  Hz, 1H), 3.96 – 3.86 (m, 4H), 3.77 (dd,  $J = 12.6, 1.0$  Hz, 1H), 3.60 (dd,  $J = 11.1, 1.0$  Hz, 1H).  $^{13}\text{C}$  NMR (101 MHz,  $\text{CDCl}_3$ )  $\delta$  (ppm): 137.17, 129.50, 128.53, 126.30, 102.36, 82.03, 72.59, 68.06, 60.99, 53.22. IR (neat)  $\nu$  ( $\text{cm}^{-1}$ ) 3379 (OH), 2929, 2868, 2105 ( $\text{N}_3$ ).

**(2S,4R,5R)-5-(azidomethyl)-4-(hydroxymethyl)-2-phenyl-1,3-dioxan-5-ol (59a)**



The synthesis was performed in the as described for compound **59**. Colourless oil (95 %).  $R_f$  0.4 (EtOAc : *c*-Hexane, 5 : 5),  $[\alpha]_D^{20} + 47$  ( $c = 0.2$ , MeOH).  $^1\text{H}$  NMR (400 MHz,  $\text{CDCl}_3$ )  $\delta$  (ppm): 7.51 (dd,  $J = 6.6, 3.1$  Hz, 2H), 7.43 – 7.37 (m, 3H), 5.55 (s, 1H), 4.05 (d,  $J = 11.7$  Hz, 1H), 3.91 – 3.89 (m, 3H), 3.88 (d,  $J = 8.4$  Hz, 1H), 3.49 (s, 1H), 3.46 (d,  $J = 13.0$  Hz, 1H), 3.28 (d,  $J = 13.0$  Hz, 1H).  $^{13}\text{C}$  NMR (101 MHz,  $\text{CDCl}_3$ )  $\delta$  (ppm): 137.21, 129.50, 128.52, 126.18, 101.79, 80.85, 73.84, 69.49, 61.50, 53.42. IR (neat)  $\nu$  ( $\text{cm}^{-1}$ ) 3360 (OH), 2952, 2906, 2334, 2098 ( $\text{N}_3$ ).

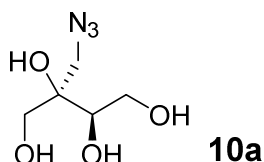
**(2S,3R)-2-(azidomethyl)butane-1,2,3,4-tetraol (10)**



To a solution of alcohol **59** (1 eq., 200 mg, 0.754 mmol) in MeOH (6 mL) was added DOWEX 50WX4-200 acidic resin (40 mg). The mixture was stirred at 30  $^{\circ}\text{C}$  for 72 h.<sup>292</sup> The reaction mixture was filtered and the filtrate was evaporated under vacuum overnight to remove volatile benzaldehyde. 97 mg of compound **10** (73 %) were obtained as a colourless viscous oil.  $R_f$  0.5 (DCM : MeOH, 9 : 1),  $[\alpha]_D^{20} - 4.1$  ( $c = 0.1$ , MeOH).  $^1\text{H}$  NMR (400 MHz, MeOD)  $\delta$  (ppm):

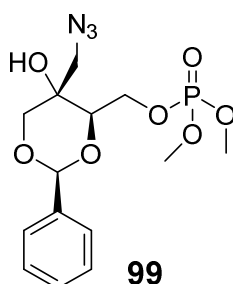
3.79 (dd,  $J = 10.4, 2.9$  Hz, 1H), 3.69 (m, 2H), 3.62 (d,  $J = 11.3$  Hz, 1H), 3.56 (d,  $J = 11.3$  Hz, 1H), 3.51 (d,  $J = 12.6$  Hz, 1H), 3.43 (d,  $J = 12.6$  Hz, 1H).  $^{13}\text{C}$  NMR (101 MHz, MeOD)  $\delta$  (ppm): 75.94, 72.92, 62.81, 62.13, 53.19. IR (neat)  $\nu$  ( $\text{cm}^{-1}$ ) 3351 (OH), 2105 ( $\text{N}_3$ ).

**(2R,3R)-2-(azidomethyl)butane-1,2,3,4-tetraol (10a)**



The synthesis was performed in the as described for compound **10**. Viscous oil (82 %).  $R_f$  0.42 (DCM : MeOH, 9 : 1),  $[\alpha]_D^{20} + 21.4$  ( $c = 0.1$ , MeOH).  $^1\text{H}$  NMR (400 MHz, MeOD)  $\delta$  (ppm): 3.79 (dd,  $J = 10.2, 2.9$  Hz, 1H), 3.70 – 3.63 (m, 2H), 3.63 (d,  $J = 11.3$  Hz, 1H), 3.60 (d,  $J = 11.3$  Hz, 1H), 3.50 (d,  $J = 12.6$  Hz, 1H), 3.40 (d,  $J = 12.6$  Hz, 1H).  $^{13}\text{C}$  NMR (101 MHz, MeOD)  $\delta$  (ppm): 75.94, 72.92, 62.81, 62.13, 53.19. IR (neat)  $\nu$  ( $\text{cm}^{-1}$ ) 3351 (OH), 2105 ( $\text{N}_3$ ).

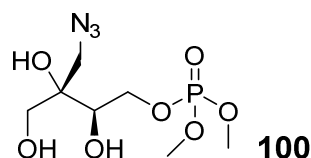
**((2S,4R,5S)-5-(azidomethyl)-5-hydroxy-2-phenyl-1,3-dioxan-4-yl)methyl dimethyl phosphate (59)**



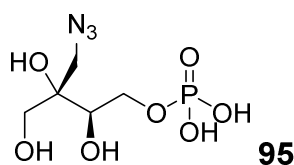
To a solution of alcohol **59** (1 eq., 453 mg, 1.71 mmol) in anhydrous DCM (2.2 mL) at 0 °C was added DMAP (1.5 eq., 312 mg, 2.56 mmol) followed by dropwise addition of dimethyl chlorophosphate (1.5 eq., 370 mg, 276  $\mu\text{L}$ , 2.56 mmol). The reaction was stirred for 2 hours (checked by TLC EtOAc : cHex, 5 : 5). After completion, the mixture was concentrated and chromatographed (EtOAc : cHex 5:5 to 7:3) to yield 574 mg compound **99** (90%) as a colourless oil.  $R_f$  0.4 (EtOAc : cHex, 5 : 5),  $[\alpha]_D^{20} + 10.16$  ( $c = 0.13$ , MeOH)  $^1\text{H}$  NMR (400 MHz,  $\text{CDCl}_3$ )  $\delta$  (ppm): 7.47 (m, 2H), 7.37 (m, 3H), 5.57 (s, 1H), 4.49 (ddd,  $J = 10.8, 7.2, 3.2$  Hz, 1H), 4.25

(d,  $J = 11.1$  Hz, 1H), 4.21 – 4.15 (m, 1H), 4.11 (dd,  $J = 7.2, 3.2$  Hz, 1H), 3.90 (d,  $J = 12.6$  Hz, 1H), 3.78 (d,  $J = 5.4$  Hz, 3H), 3.75 (d,  $J = 5.4$  Hz, 3H), 3.68 (d,  $J = 12.6$  Hz, 1H), 3.63 (d,  $J = 11.1$  Hz, 1H), 2.89 (s, 1H).  $^{13}\text{C}$  NMR (101 MHz,  $\text{CDCl}_3$ )  $\delta$  (ppm): 136.94, 129.25, 128.31, 126.11, 102.10, 82.03 (d,  $J = 6.5$  Hz), 72.68, 67.41, 65.43 (d,  $J = 5.4$  Hz), 54.56 (dd,  $J = 6.0, 2.7$  Hz), 52.71.  $^{31}\text{P}$  NMR (162 MHz,  $\text{CDCl}_3$ )  $\delta$  (ppm) 1.27. IR (neat)  $\nu$  ( $\text{cm}^{-1}$ ) 3310 (OH), 2950, 2847, 2100 ( $\text{N}_3$ ), 1450, 1254 (P=O), 1012

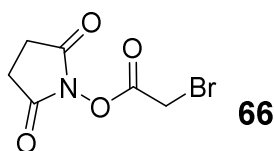
**(2R,3S)-4-azido-2,3-dihydroxy-3-(hydroxymethyl)butyl dimethyl phosphate (100)**



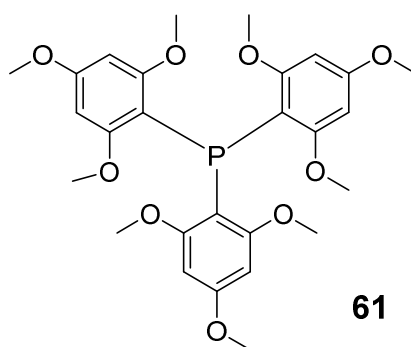
To a solution of phosphodimethyl ester **99** (1 eq., 90 mg, 0.241 mmol) in MeOH (1.92 mL) and water (0.3 mL) was added DOWEX 50WX4-200 (50 mg). The mixture was stirred until completion by TLC (MeOH : DCM, 1 : 9). The mixture was then filtered through a glass filter and purified by flash chromatography (MeOH : DCM, 1 : 9) to give 30 mg compound **100** (44%) as a colourless oil.  $R_f$  0.38 (DCM : M 5 : 5),  $[\alpha]_D^{20} +2.8$  ( $c = 0.3$ , MeOH).  $^1\text{H}$  NMR (400 MHz,  $\text{CDCl}_3$ )  $\delta$  (ppm): 4.37 (t,  $J = 9.8$  Hz, 1H), 4.27 (d,  $J = 3.9$  Hz, 1H), 4.20 (dd,  $J = 18.7, 9.4$  Hz, 1H), 3.99 (d,  $J = 7.6$  Hz, 1H), 3.92 (s, 1H), 3.81 (s, 3H), 3.78 (s, 3H), 3.73 (d,  $J = 10.8$  Hz, 1H), 3.62 (d,  $J = 10.8$  Hz, 1H).  $^{13}\text{C}$  NMR (101 MHz,  $\text{CDCl}_3$ )  $\delta$  (ppm): 75.75, 72.35 (d,  $J = 5.3$  Hz), 69.35 (d,  $J = 5.8$  Hz), 64.07, 54.94 (d,  $J = 3.4$  Hz), 54.88 (d,  $J = 3.2$  Hz), 53.08.  $^{31}\text{P}$  NMR (162 MHz,  $\text{CDCl}_3$ )  $\delta$  (ppm) 1.58. IR (neat)  $\nu$  ( $\text{cm}^{-1}$ ) 3350 (OH), 2099 ( $\text{N}_3$ ), 1445, 1241 (P=O), 1009, 849.

**(2R,3S)-4-azido-2,3-dihydroxy-3-(hydroxymethyl)butyl dihydrogen phosphate (95)**

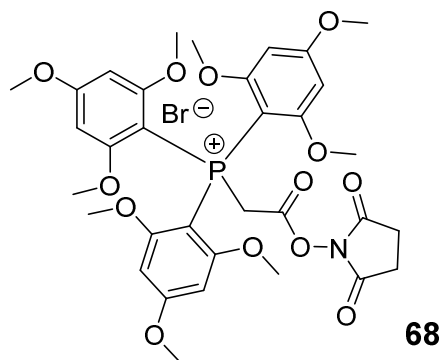
To a solution of phosphodimethyl ester **100** (1 eq., 30 mg, 0.105 mmol) in DCM (2 mL) was added bromotrimethylsilane (6 eq., 96.6 mg, 83.3  $\mu$ L, 0.631 mmol) in DCM (1 mL) dropwise at zero degrees and stirred for 0.5 h at zero degree and 0.5 h at rt. Solvent was evaporated and water (3 mL) was added and the mixture was further stirred 1 h at rt. Water was removed by lyophilisation and the residue was purified by flash chromatography on silica gel (*i*-PrOH : NH<sub>4</sub>OH (28%), H<sub>2</sub>O / 6 : 3 : 0.5) to yield MEP-N<sub>3</sub> (18%) as a white solid (di ammonium salt). *R*<sub>f</sub> 0.13 (*i*-PrOH : NH<sub>4</sub>OH (28%), H<sub>2</sub>O / 6 : 3 : 0.5),  $[\alpha]_D^{20} +4.5$  (*c* = 0.1, MeOH) <sup>1</sup>H NMR (500 MHz, D<sub>2</sub>O)  $\delta$  (ppm): 3.95 – 3.90 (m, 1H), 3.82 – 3.76 (m, 2H), 3.59 (d, *J* = 12.0 Hz, 1H), 3.56 (d, *J* = 12.0 Hz, 1H), 3.51 (d, *J* = 13.0 Hz, 1H), 3.43 (d, *J* = 13.0 Hz, 1H). <sup>13</sup>C NMR (126 MHz, D<sub>2</sub>O)  $\delta$  (ppm): 76.13, 71.74 (d, *J* = 6.9 Hz), 64.76 (d, *J* = 4.8 Hz), 62.25, 52.72. <sup>31</sup>P NMR (162 MHz, D<sub>2</sub>O)  $\delta$  (ppm) 2.79. IR (neat)  $\nu$  (cm<sup>-1</sup>) 3321 (OH), 2109 (N<sub>3</sub>), 1423, 1256 (P=O)

**2,5-dioxopyrrolidin-1-yl 2-bromoacetate (66)**

N-hydroxysuccinimide (1.2 eq., 0.994 g, 8.64 mmol) and bromoacetic acid (1 eq., 1 g, 0.518 mL, 7.2 mmol) were dissolved in anhydrous DCM (100 mL) and cooled to 0 °C. DCC (100 %, 1.48 g, 7.2 mmol) in anhydrous DCM (10 mL) was added to the mixture dropwise. The reaction mixture left for stirring overnight at room temperature.<sup>293</sup> The mixture was filtered and solvent was evaporated to give crude material which was purified by flash chromatography on silica gel (EtOAc : *n*Hex, 4 : 6) to give 1.39 g of compound **66** (82 %) as a white solid. <sup>1</sup>H NMR (500 MHz, CDCl<sub>3</sub>)  $\delta$  (ppm): 4.10 (s, 2H), 2.85 (s, 4H). <sup>13</sup>C NMR (126 MHz, CDCl<sub>3</sub>)  $\delta$  (ppm): 168.57, 163.09, 25.68, 21.32.

**tris(2,4,6-trimethoxyphenyl)phosphane (61)**

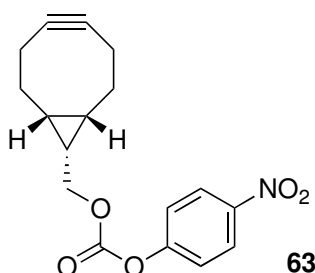
To a solution of 1,3,5-trimethoxybenzene (2 eq., 5 g, 29.7 mmol) in anhydrous Et<sub>2</sub>O (25 mL) was added *n*-BuLi (1.1 eq, 1.6 M, 20.4 mL, 32.7 mmol) dropwise at zero degree. The reaction mixture was stirred at 0 °C for 12 h and triphenyl phosphite (0.4 eq., 2.05 g, 1.73 mL, 6.6 mmol) was added dropwise at 0 °C and the mixture stirred for 12 h during which time temperature raised to room temperature.<sup>294</sup> Majority of the solvent was transferred and remaining solvent was evaporated. Residue was dissolved in hot EtOH (200 mL) and evaporated under reduced pressure until white precipitates started to appear. Precipitate was filtered and washed with EtOH (2 x 10 mL) and Et<sub>2</sub>O (2 x 10 mL) to give 1.99 g of compound **61** (57 %) as white crystals. <sup>1</sup>H NMR (400 MHz, CDCl<sub>3</sub>) δ (ppm): 6.02 (d, *J* = 2.6 Hz, 6H), 3.76 (s, 9H), 3.48 (s, 18H). <sup>13</sup>C NMR (101 MHz, CDCl<sub>3</sub>) δ (ppm): 163.28, 163.19, 160.81, 108.62, 108.43, 91.35, 56.14, 55.18. <sup>31</sup>P NMR (162 MHz, CDCl<sub>3</sub>) δ (ppm): -69.87.

**(2-((2,5-dioxopyrrolidin-1-yl)oxy)-2-oxoethyl)tris(2,4,6-trimethoxyphenyl) phosphonium bromide (68)**

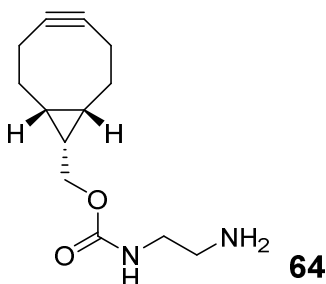
To a solution of bromoacetic acid *N*-hydroxysuccinimide ester (1.04 eq., 23.1 mg, 0.0977 mmol) in toluene (20 mL) was added a solution of tris(2,4,6-trimethoxyphenyl)phosphine (1

eq., 50 mg, 0.0939 mmol) in toluene (30 mL). The mixture left for standing at room temperature for 30 minutes.<sup>226</sup> The reaction mixture was diluted with cyclohexane and the white precipitates were filtered and washed with cyclohexane and dried under reduced pressure to give 60 mg of compound **68** (93 %) as a white solid. <sup>1</sup>H NMR (400 MHz, CDCl<sub>3</sub>) δ (ppm): 6.15 (d, *J* = 5.1 Hz, 6H), 4.47 (d, *J* = 14.7 Hz, 2H), 3.90 (s, 9H), 3.64 (s, 18H), 1.85 (s, 4H). <sup>13</sup>C NMR (101 MHz, CDCl<sub>3</sub>) δ (ppm): 168.83, 166.52, 164.02, 91.66, 91.58, 89.59, 56.56, 56.19, 25.74, 23.21. <sup>31</sup>P NMR (162 MHz, CDCl<sub>3</sub>) δ (ppm): -5.09

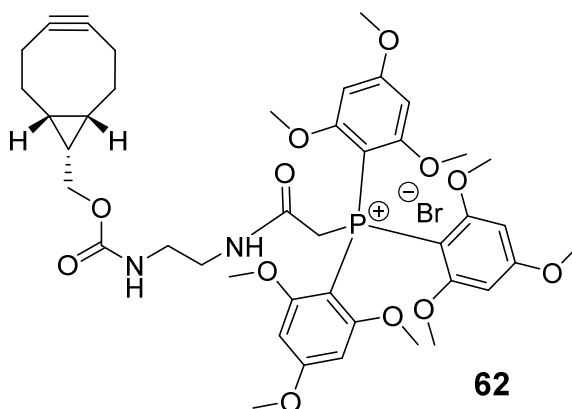
**((1*R*,8*S*,9*S*)-bicyclo[6.1.0]non-4-yn-9-yl)methyl (4-nitrophenyl) carbonate (**63**)**



To a solution of BCN **60** (1 eq., 300 mg, 2 mmol) and pyridine (5 eq., 789 mg, 0.808 mL, 9.99 mmol) in DCM (10 mL) was added para-nitrophenol chloroformate (1.5 eq., 603 mg, 3 mmol) at 0 °C and the solution was stirred for 30 minutes.<sup>295</sup> The mixture was quenched with saturated NH<sub>4</sub>Cl solution (30 mL) and extracted with DCM (4 x 30 mL). The organic layer was dried over MgSO<sub>4</sub> and concentrated under reduced pressure. The residue was purified by flash chromatography (EtOAc : *n*-Hexane, 1 : 9) to afford 590 mg of compound **63** (94 %) as a white solid. <sup>1</sup>H NMR (400 MHz, CDCl<sub>3</sub>) δ (ppm): 8.30 (d, *J* = 9.0 Hz, 2H), 7.40 (d, *J* = 9.0 Hz, 2H), 4.42 (d, *J* = 8.2 Hz, 2H), 2.37 – 2.21 (m, 6H), 1.62 – 1.54 (m, 2H), 1.52 – 1.43 (m, 1H), 1.09 – 1.04 (m, 2H). <sup>13</sup>C NMR (101 MHz, CDCl<sub>3</sub>) δ (ppm): 155.79, 152.72, 145.56, 125.45, 121.90, 98.86, 68.16, 29.22, 21.51, 20.70, 17.43.

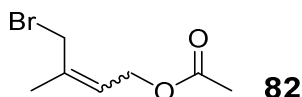
**((1R,8S,9s)-bicyclo[6.1.0]non-4-yn-9-yl)methyl (2-aminoethyl)carbamate (64)**

To a solution of ethylene diamine (10 eq., 190 mg, 0.212 mL, 3.17 mmol) and TEA (10 eq., 320 mg, 0.441 mL, 3.17 mmol) in anhydrous DMF (2 mL) was added a solution of (1R,8S,9s)-bicyclo[6.1.0]non-4-yn-9-ylmethyl (4-nitrophenyl) carbonate (1 eq., 100 mg, 0.317 mmol) in anhydrous DMF (2 mL) dropwise. The reaction was stirred 2h at room temperature and monitored by TLC (EtOAc : c-Hexane, 3 : 7). The solvent was evaporated under reduced pressure and 1M NaH<sub>2</sub>PO<sub>4</sub> (10 mL) was added. The mixture was extracted with DCM (4 x 10 mL). The aqueous layer was basified to pH 9 with a solution of 1M NaOH, then extracted with DCM (4 x 20 mL). The combined organic layers were dried over MgSO<sub>4</sub> and concentrated to afford 60 mg of compound **64** (80 %) as a yellow sticky solid. <sup>1</sup>H NMR (400 MHz, CDCl<sub>3</sub>) δ (ppm): 5.17 (s, 1H), 4.15 (d, *J* = 8.0 Hz, 2H), 3.25 (dd, *J* = 11.8, 5.9 Hz, 2H), 2.84 (t, *J* = 5.9 Hz, 2H), 2.28 – 2.20 (m, 6H), 1.94 (s, 2H), 1.58 – 1.55 (m, 2H), 1.36 – 1.32 (m, 1H), 0.97 – 0.90 (m, 2H). <sup>13</sup>C NMR (101 MHz, CDCl<sub>3</sub>) δ (ppm): 157.14, 98.93, 62.89, 43.60, 41.79, 29.19, 21.54, 20.25, 17.90.

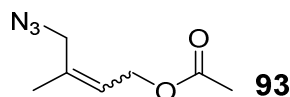
**(2-(((2-(((1R,8S,9s)-bicyclo[6.1.0]non-4-yn-9-yl)methoxy)carbonyl)amino)ethyl)amino)-2-oxoethyl)tris(2,4,6-trimethoxyphenyl)phosphonium bromide (62)**

To a solution of (1R,8S,9s)-bicyclo[6.1.0]non-4-yn-9-ylmethyl (2-aminoethyl)carbamate (1 eq., 60 mg, 0.254 mmol) in DCM (3 mL) was added TEA (27 mg, 0.0371 mL, 0.267 mmol) followed by addition of compound **68** (1 eq., 175 mg, 0.254 mmol). The reaction mixture was stirred at room temperature for 16 h. The solvent was removed under reduced pressure and the residue was purified by flash chromatography (DCM : c-Hexane : MeOH, 4 : 5 : 1) to give 170 mg of compound **62** (83 %) as a white solid.  $R_f$  0.35 (DCM : c-Hexane : MeOH, 4 : 5 : 1),  $^1\text{H}$  NMR (400 MHz,  $\text{CDCl}_3$ )  $\delta$  (ppm): 6.05 (d,  $J = 4.8$  Hz, 6H), 4.55 (d,  $J = 15.3$  Hz, 2H), 4.10 (d,  $J = 8.0$  Hz, 2H), 3.82 (s, 9H), 3.65 (s, 18H), 3.32 (s, 2H), 3.25 (s, 2H), 2.29 – 2.16 (m, 6H), 1.75 (s, 2H), 1.56 – 1.51 (m, 2H), 1.36 – 1.30 (m, 1H), 0.91 (t,  $J = 9.6$  Hz, 2H).  $^{13}\text{C}$  NMR (101 MHz,  $\text{CDCl}_3$ )  $\delta$  (ppm): 166.39, 165.32, 165.31, 163.87, 157.18, 99.07, 93.64, 92.55, 91.03, 90.96, 62.25, 56.23, 55.58, 40.56, 40.33, 29.26, 21.61, 20.25, 18.11. IR (neat)  $\nu$  ( $\text{cm}^{-1}$ ) 3216 (N-H), 3004, 2941, 2843 (C-H), 1592 (C=O), 1230 (C-O).

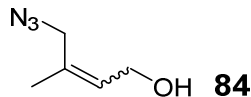
#### 4-bromo-3-methylbut-2-en-1-yl acetate (**82**)



To a solution of isoprene (1 eq., 5 g, 7.35 mL, 72.7 mmol) in acetic acid (72.8 mL) was added NBS<sup>234</sup> (0.75 eq., 9.7 g, 54.5 mmol) and the reaction mixture was stirred for 2 h. *p*-TSA (1.5 %, 0.188 g, 0.175 mL, 1.09 mmol) was added to the mixture and was first heated to 80 °C for 1 h then cooled to room temperature. The mixture was extracted with hexane (100 mL) washed with water and 1M NaOH, (50 mL) dried over  $\text{MgSO}_4$  then concentrated under reduced pressure to yield 6.6 g of compound **82** as a colourless oil (44 %). The product was subsequently submitted to azide introduction reaction without further purification. *E* isomer:  $^1\text{H}$  NMR (400 MHz,  $\text{CDCl}_3$ )  $\delta$  (ppm): 5.74 (t,  $J = 6.7$  Hz, 1H), 4.61 (d,  $J = 6.5$  Hz, 2H), 3.99 (s, 2H), 2.06 (s, 3H), 1.84 (s, 3H).  $^{13}\text{C}$  NMR (101 MHz,  $\text{CDCl}_3$ )  $\delta$  (ppm) 170.94, 137.41, 124.37, 61.07, 39.55, 21.02, 15.26. *Z* isomer:  $^1\text{H}$  NMR (400 MHz,  $\text{CDCl}_3$ )  $\delta$  (ppm): 5.54 (t,  $J = 6.7$  Hz, 1H), 4.61 (d, overlap 2H), 3.99 (s, 2H), 2.06 (s, overlap 3H), 1.90 (s, 3H).

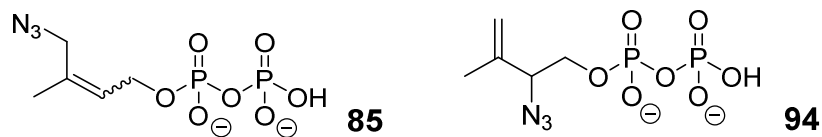
**4-azido-3-methylbut-2-en-1-yl acetate (93)**

To a solution of 4-bromo-3-methylbut-2-en-1-yl acetate (1 eq., 3.2 g, 15.5 mmol) in Acetone/H<sub>2</sub>O (56.8 mL) (3:1)<sup>296</sup> was added NaN<sub>3</sub> (1.5 eq., 1.51 g, 0.815 mL, 23.2 mmol) and the mixture was stirred for 10 minutes at room temperature. The mixture was diluted with DCM, washed with water, brine and dried over MgSO<sub>4</sub> and evaporated under reduced pressure. The crude was purified by flash chromatography R<sub>f</sub> - 0.47 (EtOAc : c-Hexane, 1 : 9) to give compound **93** as a colourless oil (39 %). (*E/Z* peaks overlapped) <sup>1</sup>H NMR (400 MHz, CDCl<sub>3</sub>) δ (ppm): 5.62 (td, *J* = 6.8, 1.2 Hz, 1H), 4.64 (d, *J* = 6.8 Hz, 2H), 3.72 (s, 2H), 2.06 (s, 3H), 1.77 (s, 3H). <sup>13</sup>C NMR (101 MHz, CDCl<sub>3</sub>) δ (ppm): 170.99, 135.61, 123.08, 60.70, 58.44, 21.05, 15.06.

**4-azido-3-methylbut-2-en-1-ol (84)**

To a solution of 4-azido-3-methylbut-2-en-1-yl acetate (1 eq., 1.18 g, 6.97 mmol) in MeOH (28.3 mL) was added K<sub>2</sub>CO<sub>3</sub> (1 eq., 0.964 g, 6.97 mmol) in water (2 mL) and the reaction stirred for 0.5 h at room temperature. The mixture was poured into a water and extracted with DCM (4 x 10 mL) then washed with water, dried over MgSO<sub>4</sub>. The solvent was removed under reduced pressure to give the crude product which was purified by flash chromatography R<sub>f</sub> - 0.4 (EtOAc : c-Hexane, 3 : 7) to afford 320 mg compound **84** (36 %) as a colourless oil (*E/Z* isomer 7:3). *E* isomer: <sup>1</sup>H NMR (400 MHz, CDCl<sub>3</sub>) δ (ppm): 5.68 (t, *J* = 6.6 Hz, 1H), 4.23 (d, *J* = 6.6 Hz, 2H), 3.71 (s, 2H), 1.73 (s, 3H). <sup>13</sup>C NMR (101 MHz, CDCl<sub>3</sub>) δ (ppm): 129.33, 128.26, 58.98, 58.64, 14.83. *Z* isomer: <sup>1</sup>H NMR (400 MHz, CDCl<sub>3</sub>) δ (ppm): 5.73 (t, *J* = 7.0 Hz, 1H), 4.17 (t, *J* = 7.0 Hz, 2H), 3.83 (s, 2H), 1.84 (s, 3H). <sup>13</sup>C NMR (101 MHz, CDCl<sub>3</sub>) δ (ppm): 129.43, 128.36, 58.58, 51.24, 22.43.

**4-azido-3-methylbut-2-en-1-yl diphosphate (85) and 2-azido-3-methylbut-3-en-1-yl diphosphate (94)**



To a solution of 4-azido-3-methylbut-2-en-1-ol (1 eq., 160 mg, 1.26 mmol) in MeCN (13 mL) were added  $\text{CNCCl}_3$  (25 eq., 4536 mg, 3.15 mL, 31.4 mmol) dropwise at zero degree and TEAP solution was added (3.15 mL x 3) in three portions dropwise with 5 minutes between each addition.  $\text{H}_3\text{PO}_4$  (Solution A) and  $\text{Et}_3\text{N}$  (Solution B) were mixed to produce TEAP solution. Preparation of solution A: 3.528 g of  $\text{H}_3\text{PO}_4$  was dissolved in minimum amount of water and diluted with MeCN to 10 mL. Preparation of solution B: 10.68 mL of  $\text{Et}_3\text{N}$  was diluted with MeCN to 20 mL. Preparation of TEAP solution: 18.75 mL of Solution B was added to Solution A (10 mL). Acetonitrile was evaporated to give viscous yellow oil which was purified by flash chromatography  $R_f - 0.23$  (i-Pr/ $\text{H}_2\text{O}$ / $\text{NH}_4\text{OH}$ : 6/0.5/3 - 6/1.5/3). TLC system i-Pr/ $\text{H}_2\text{O}$ / $\text{NH}_4\text{OH}$ : 6/0.5/3. Organic solvent was evaporated under reduced pressure and remaining aqueous solution was evaporated by lyophilisation to give 170 mg of compound **85** (*E/Z* isomer 7:3) with mixture of compound **94** as a white solid yielding total of 47 %. *Z* isomer:  $^1\text{H}$  NMR (400 MHz,  $\text{D}_2\text{O}$ )  $\delta$  (ppm): 5.82 (t,  $J = 7.2$  Hz, 1H), 4.56 (t,  $J = 7.2$  Hz, 2H), 4.02 (s, 2H), 1.89 (s, 3H). *E* isomer:  $^1\text{H}$  NMR (400 MHz,  $\text{D}_2\text{O}$ )  $\delta$  (ppm) 5.78 (t,  $J = 6.8$  Hz, 1H), 4.61 (t,  $J = 6.8$  Hz, 3H), 3.87 (s, 2H), 1.83 (s, 3H). Compound **94**.  $^1\text{H}$  NMR (400 MHz,  $\text{D}_2\text{O}$ )  $\delta$  (ppm): 5.18 (s, 1H), 5.17 (s, 1H), 4.39 (dd,  $J = 8.0, 4.6$  Hz, 1H), 4.16 – 4.11 (m, 1H), 4.05 – 3.96 (m, 1H), 1.81 (s, 3H).

### Kinetics of BCN-TMPP and $\text{ME-N}_3$

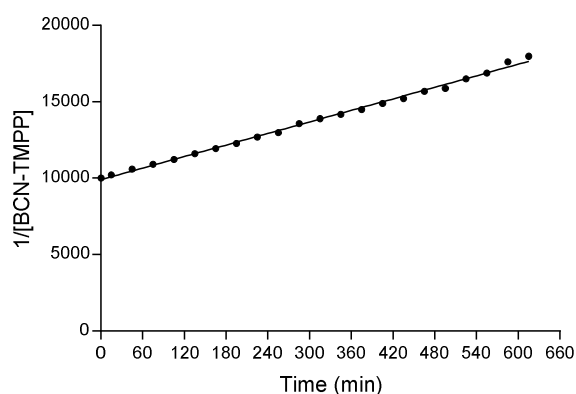
The formation of clicked product **69** was analysed by HPLC.  $\text{ME-N}_3$  concentration was fixed at 0.1 mM and varying BCN-TMPP concentration from 0.1 – 1.6 mM (*i.e.* 1-16 times ratio). Benzamide (2 mM) was used as an internal standard.

Preparation of the reaction between BCN-TMPP and  $\text{ME-N}_3$ : 20% MeCN in 0.1 M PBS (phosphate buffered saline). Stock concentrations:  $\text{ME-N}_3$  (10 mM), BCN-TMPP (10 mM), Benzamide (100 mM). The compounds were mixed according to the following table in a final volume of 1 mL.

Ratio ( $\text{ME-N}_3$ : BCN-TMPP)	1 : 1	1 : 2	1 : 4	1 : 8	1 : 16
BCN-TMPP ( $\mu\text{L}$ )	10	20	40	80	160
$\text{ME-N}_3$ ( $\mu\text{L}$ )	10	10	10	10	10
HPLC injection volume ( $\mu\text{L}$ )	20	20	20	10	10

The second order rate constant was determined as described in literature report. 1 : 1 ratio at 0.1 mM reaction was used to calculate the kinetic constant.<sup>297</sup>  $1/[\text{BCN-TMPP}]$  (M) as a function of time was plotted (values from average of two experiments). The results were fitted to a linear regression. Slope of linear regression corresponds to a second order rate constant ( $\text{M}^{-1}\text{min}^{-1}$ ).<sup>228,</sup>

297



Best-fit values	
Slope	$12.58 \pm 0.1698$
Y-intercept when X=0.0	$9905 \pm 60.31$
X-intercept when Y=0.0	-787,3
R square	0,9964

Figure 62. Second order rate constant determination

### Limit of Detection by LC-MS.

ME-N<sub>3</sub> 1 : 20 (eq) BCN-TMPP ratio was used for the determination of the limit of detection experiment in final volume of 150  $\mu$ L. ME-N<sub>3</sub> concentrations ( $\mu$ M): 100, 10, 1, 0.1, 0.01, 0.001, were prepared in either PBS 0.1 M (pH 7.5) buffer or bacterial lysate (*E.coli* MG1655) (The procedure to obtain the lysate is similar to ME-N<sub>3</sub> incorporation analysis study described below except ME (5 mL, 10 mM) was used instead of ME-N<sub>3</sub> (5 mL, 10 mM)). After addition of BCN-TMPP, the vials were left at room temperature overnight and then analysed by LC-MS (Single Ion Recording, SIR, mode) with 30  $\mu$ L injection volume. Triplicate experiments were performed. MS spectras (SIR mode for 493 Da) of clicked product **69** are shown in Figure 63 (LOD in bacterial lysate) and Figure 64 (LOD in PBS buffer).

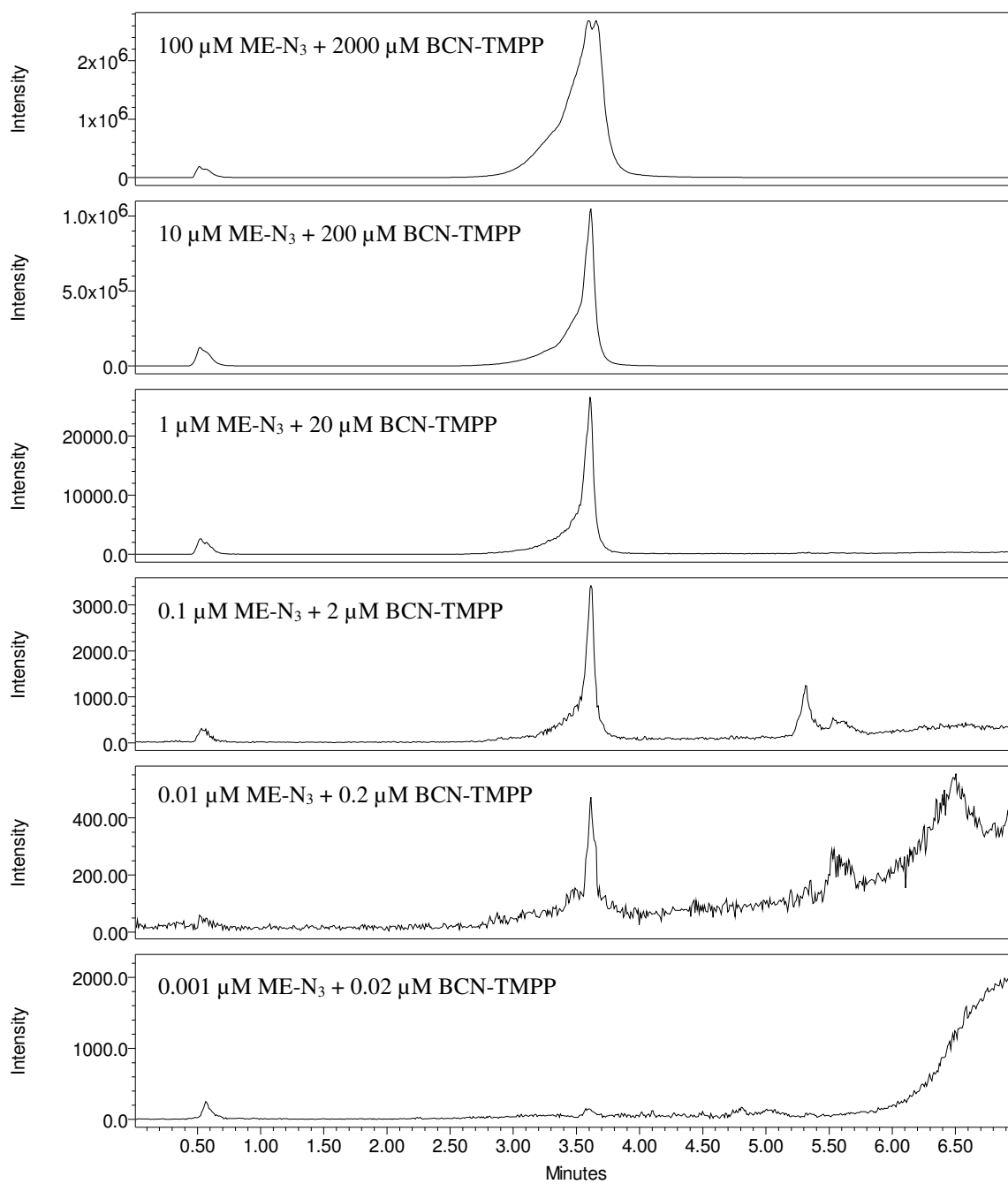


Figure 63. MS scans (SIR mode) of clicked product **69** in bacterial lysate for determination of LOD.

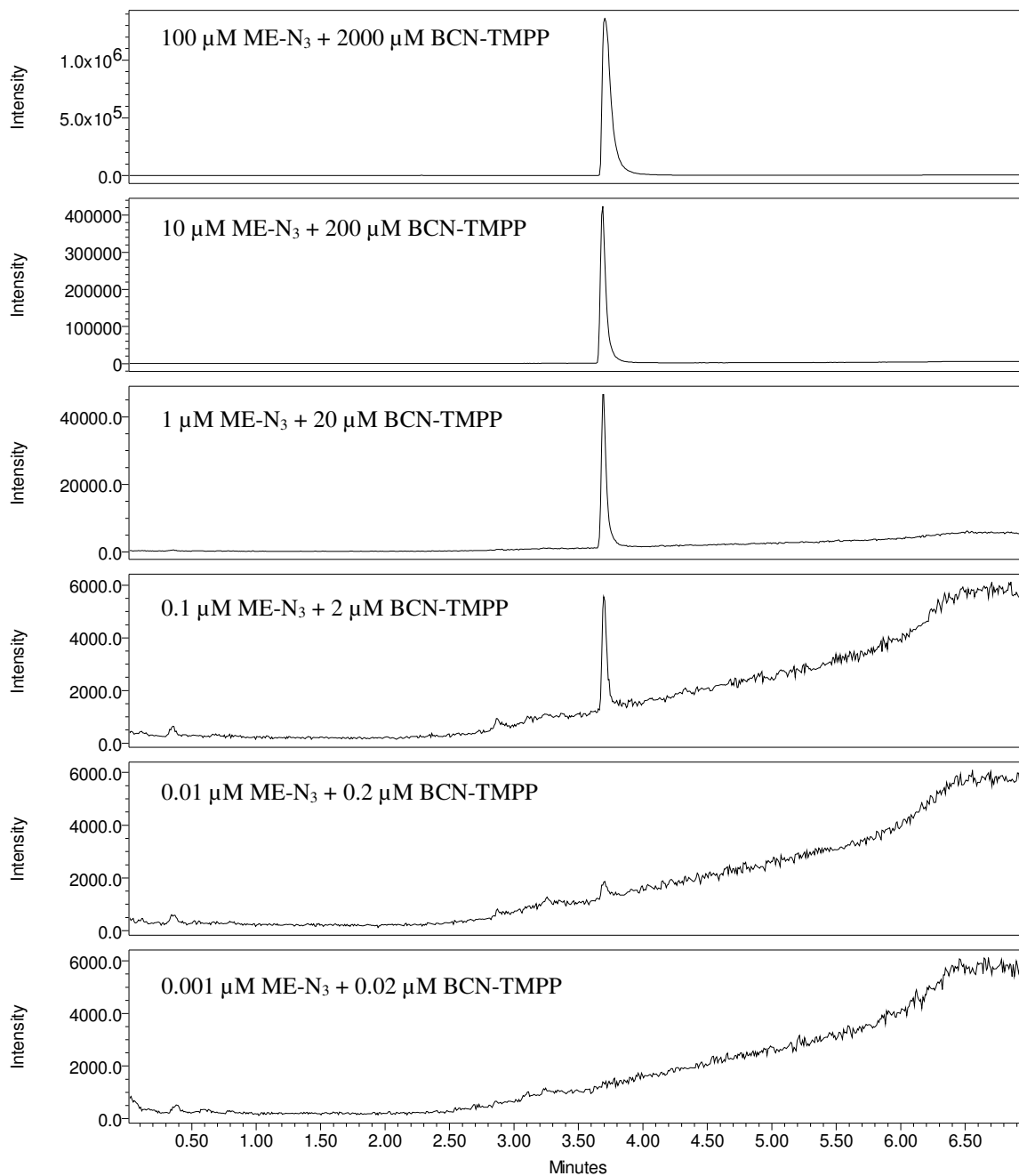


Figure 64. MS scans (SIR mode) of clicked product **69** in PBS for determination of LOD.

## LC-MS analysis of ME-N<sub>3</sub> incorporation

### *E.coli MG1655*

#### *ME-N<sub>3</sub> incubation*

ME-N<sub>3</sub> (5 mL, 10 mM) was added to M9 media (see below) that was inoculated with 500 µL of a preculture of *E.coli* (MG1655) in a final volume of 50 mL and incubated at 37 °C on 200 rpm shaking. After 22h, the culture was centrifuged to remove the media (13000 rpm, 10 min). Tris HCl buffer (3 mL, pH=7.5, 50 mM) was added to the bacterial pellet to resuspend it. Buffer (3 mL) was added to the mixture and it was centrifuged again (13000 rpm, 5 min). This process was repeated 3 times to wash the bacteria with Tris buffer. After washing, the bacteria were resuspended in 4 mL of Tris HCl buffer and sonicated (8 times for 30 seconds, 1 min cooling in between each sonication). The mixture was centrifuged (13000 rpm, 10 min) to remove cell debris. Supernatant was collected and MeCN (4 mL) was added to it (1 : 1 ratio to precipitate proteins)<sup>229</sup> and the mixture vortexed for 10 seconds and left to stand for 20 minutes at 0 °C. The mixture was centrifuged (10 min, 3500 rpm) and supernatant (i.e the lysate) was collected (final volume 8 mL). Incorporated azide tag was expected to be around 0.02 – 0.06 µM range based on previous study<sup>85</sup> and therefore BCN-TMPP was added to the lysate at a final concentration of 0.4 µM that was incubated overnight at room temperature. LC-MS analysis using injection volume of 30 µL and SIR mode was performed. Synthetic ME was used instead of ME-N<sub>3</sub> for control experiments.

#### *Preparation of M9 media:*

*M9 salts:* Na<sub>2</sub>HPO<sub>4</sub> (12.8 g), KH<sub>2</sub>PO<sub>4</sub> (3 g), NaCl (0.5 g), NH<sub>4</sub>Cl (1 g) were dissolved in 978 mL of distilled water and autoclaved at 121 °C for 20 minutes. Once the solution reaches 50 °C, a solution of glucose (20 mL, 20%) that was separately autoclaved at 121 °C for 20 minutes and 1 M MgSO<sub>4</sub> (2 mL), 1 M CaCl<sub>2</sub> (0,1 mL) and Thiamine (0.1 mL, 0.5 w/v) that were previously filtered on sterile Millex filters, 0.22 µm.

### *E.coli EcAB4-5*

#### *Growth of the mutant:*

Stock solutions of following compounds were prepared as follows: Chloramphenicol (170 mg) in EtOH (10 mL), Tetracycline (75 mg) in H<sub>2</sub>O (10 mL), Kanamycine (250 mg) in H<sub>2</sub>O (10

mL), Thiamine (50 mg) in 10mL H<sub>2</sub>O, Pyridoxol (30 mg) in 10 mL H<sub>2</sub>O, L-Arabinose (2 g) in 20 mL H<sub>2</sub>O and Tryptophan (102 mg) in H<sub>2</sub>O (10 mL). Each solution was transferred to an eppendorf tubes after filtration through filter (Millex, 0.22 µm) to sterilise solution and aliquot stock solutions were prepared. (1 g) of LB (Lysogeny broth) was dissolved in H<sub>2</sub>O (50 mL) and autoclaved at 121 °C for 20 min. After sterilisation: Chloramphenicol (5 µL), Tetracyclin (5 µL), Kanamycin (5 µL), Thiamine (5 µL), Pyridoxol (10 µL), Tryptophan (10 µL,) L-Arabinose (100 µL) and Mevalonic acid (488 mM, 10 µL) was added to sterilised LB medium (5 mL). *E.coli* EcAB4-5 strain stock (100 uL) was added to the previous medium that was further incubated at 37 °C on 200 rpm over the weekend.

#### *ME-N<sub>3</sub> incubation*

When OD<sub>600</sub> reached 0.7, bacteria were harvested by centrifugation (5000 rpm, 10 min) and washed with sterile LB media (50 mL) twice and then re-suspended in sterile LB media (3 mL) and transferred to LB media (50 mL) that contains all the components above mentioned except mevalonic acid and L-arabinose but instead 0.5 mM ME-N<sub>3</sub>. After 18 hours of growing, cells were harvested by centrifugation (5000 rpm, 10 min) and washed with Tris HCl 0.5 M (pH 7.5) four times and re-suspended in Tris buffer (4 mL). The cells were sonicated (8 x 30 seconds, 1 min break) and centrifuged (15000 rpm, 10 min). Supernatant was collected and MeCN (4 mL) was added. The mixture was vortexed for 10 seconds and left to stand at 0 °C for 20 minutes. Precipitated proteins were separated by centrifugation (3000 rpm, 10 min). The supernatant was aliquoted and analysed by LC-MS after addition of BCN-TMPP (same procedure as for *E.coli* MG1655). Synthetic ME was used instead of ME-N<sub>3</sub> for control experiments.

#### ***E.coli* mutant growth test using ME-N<sub>3</sub>**

##### *MG1655*

Sterile M9 media (5 mL) was inoculated with 100 µL of a stock of *E.coli* EcAB4-5. The suspension was incubated overnight at 37 °C 200 rpm. Next day, 0, 0.5, 1 or 5 mM ME-N<sub>3</sub> were added to a solution containing 300 µL of the previous preculture and M9 media (3.2 mL). Following amounts of H<sub>2</sub>O and ME-N<sub>3</sub> (10 mM) were added to prepare the mixture in a final volume of 7 mL.

ME-N <sub>3</sub> (mM)	<b>0</b>	<b>0.5</b>	<b>1</b>	<b>5</b>
ME-N <sub>3</sub> (μL)	0	350	700	3500
H <sub>2</sub> O (μL)	3500	3150	2800	0

OD<sub>600</sub> was measured every 30 min until 3 hours and every hour until 8 hours and 23, 24 and 25 hours.

#### *EcAB4-5*

To a sterile LB media (5 mL) was added Chloramphenicol (5 μL, 17 mg/mL stock), Tetracyclin (5 μL, 7.5 mg/mL stock), Kanamycin (5 μL, 25 mg/mL stock), Thiamine (5 μL, 5 mg/mL stock), Pyridoxol (10 μL, 3 mg/mL stock), Tryptophan (10 μL, 50 μM/mL stock), L-Arabinose (100 μL, 2 g/mL stock) and Mevalonic acid (10 μL, 488 mM stock). 100 μL of the stock of EcAB4-5 was added to this solution and the mixture incubated overnight at 37 °C, 200 rpm. Next day 0, 0.1, 0.5 or 1 mM ME-N<sub>3</sub> were prepared in the final volume of 10 mL containing 600 μL of the preculture in LB media (8.32 mL) and 80 μL of Mixture A. Following amounts of H<sub>2</sub>O and ME-N<sub>3</sub> (10 mM) were added to prepare the mixture.

ME-N <sub>3</sub> (mM)	<b>0</b>	<b>0.1</b>	<b>0.5</b>	<b>1</b>
ME-N <sub>3</sub> (μL)	0	100	500	1000
H <sub>2</sub> O (μL)	1000	900	500	0

Constituents of Mixture A: Chloramphenicol (10 μL, 17 mg/mL stock), Tetracyclin (10 μL, 7.5 mg/mL stock), Kanamycin (10 μL, 25 mg/mL stock), Thiamine (10 μL, 5 mg/mL stock), Pyridoxol (20 μL, 3 mg/mL stock), Tryptophan (20 μL, 50 μM/mL stock).

OD<sub>600</sub> was measured every hour until 8 hours and at 23, 24, 25 and 30 hours.

### **IspD Kinetics**

#### *Preparation of the dye reagent*

Ammonium molybdate (188 mg) was dissolved in H<sub>2</sub>O (2.5 mL) and added to malachite green solution (10 mL). Tween 20 (200 μL) was added and mixed to homogenous solution. Malachite green solution was prepared according to the literature report.<sup>255</sup> Conc. H<sub>2</sub>SO<sub>4</sub> (60 mL) was

slowly added to H<sub>2</sub>O (300 mL) and the solution left at room temperature to cool down. After cooling, malachite green powder (400 mg) was added to the solution and dissolved.

#### *Preparation of phosphate standard curve*

Commercially available phosphate standard solution (7.04 mM) was diluted to prepare stock solution of phosphate (40 μM). From this solution, 2, 4, 5, 10, 20 and 30 μM phosphate solutions were prepared in a total volume of 400 μL containing following compounds: MgCl<sub>2</sub> (1 mM), CTP (0.2 mM) (when MEP was varied) or 0.25 mM MEP (when CTP was varied), DTT (1 mM), Inorganic pyrophosphatase (133 mU/mL) in each vial. After addition of 100 μL dye reagent, vials were incubated at 30 °C for 10 minutes and OD<sub>630 nm</sub> was measured. Standard curve was linear between 5 – 30 μM.

#### *General reaction procedure:*

The tests were performed in Tris HCl (50 mM pH 8) in a total volume of 400 μL. The vials were incubated at 30 °C for 8 minutes before adding 100 μL of dye reagent. Incubation was further continued for 10 minutes after which OD<sub>630 nm</sub> was measured. A blank reaction containing similar components except IspD was performed at the same time and OD was subtracted. The concentration of phosphate was determined from phosphate standard curve.

#### ***MEP as a varied substrate.***

MEP was added at different concentrations between 15, 30, 45, 60, 100, 150 and 250 μM in a final total volume of 400 μL (Tris HCl 50 mM, pH =8) containing: MgCl<sub>2</sub> (1 mM), CTP (0.2 mM), DTT (1 mM), Inorganic pyrophosphatase (133 mU/mL). *E.coli* IspD (3 μL - 0.065 μg) was added to each vial to initiate the reaction.

#### *Determination of the concentration of MEP stock solution*

MEP salt (approximately 5 mg of MEP) was dissolved in H<sub>2</sub>O (400 μL) and lyophilised after freezing. This process was repeated until the MEP mass reaches constant value. 25 mM MEP stock solution was prepared using dry MEP in distilled water. From this stock solution, a 25 μM MEP solution was prepared in a final volume of 1 mL (Tris HCl, 50 mM, pH = 8, 5 mM MgCl<sub>2</sub>) containing 2.5 μL (112.25 μg) of alkaline phosphatase (44.9 mg/mL - Sigma Aldrich). 125 μM MEP solution was prepared in a similar manner. The two assay were incubated at 25 °C. At 2 h and 5 h, 400 μL from the reaction containing 25 μM MEP were spiked to 100 μL of

dye reagent. At 2 h and 5 h, 200  $\mu\text{L}$  from the reaction containing 125  $\mu\text{M}$  MEP were spiked to 200  $\mu\text{L}$  buffer (Tris HCl 50 mM, pH = 8) mixed and 100  $\mu\text{L}$  dye reagent was added. Incubation was further continued for 10 min at 37 °C and OD<sub>630</sub> nm was measured.

Standard curve was prepared from 40  $\mu\text{M}$  phosphate stock solution (prepared from commercial 7.04 mM solution). From this solution 2, 4, 5, 10, 20 and 30  $\mu\text{M}$  phosphate solutions were prepared in a total volume of 400  $\mu\text{L}$  in Tris HCl, 50 mM, pH = 8, 5 mM MgCl<sub>2</sub>. After addition of 100  $\mu\text{L}$  dye reagent, vials were incubated at 30 °C for 10 minutes and OD<sub>630</sub> nm was measured. Standard curve was linear between 5 – 30  $\mu\text{M}$ .

### ***CTP as a varied substrate***

CTP concentrations were varied between 30, 60, 90, 120, 180, 270 and 450  $\mu\text{M}$  in a final total volume of 400  $\mu\text{L}$  containing: MgCl<sub>2</sub> (1 mM), MEP (0.25 mM), DTT (1 mM), Inorganic pyrophosphatase (133 mU/mL). *E.coli* IspD (3  $\mu\text{L}$  - 0.065  $\mu\text{g}$ ) was added to each vial to initiate the reaction.

### ***Determination of the concentration of CTP stock solution***

Commercially available CTP salt (approximately 20 mg of CTP) was dissolved in H<sub>2</sub>O (400  $\mu\text{L}$ ) and lyophilised after freezing. This process was repeated until the CTP mass reaches constant value. 25  $\mu\text{M}$  CTP solution was prepared in a final volume of 1 mL (Tris HCl, 50 mM, pH 8, 5 mM MgCl<sub>2</sub>) containing 2.5  $\mu\text{L}$  (112.25  $\mu\text{g}$ ) alkaline phosphatase (44.9 mg/mL - Sigma Aldrich). 100  $\mu\text{M}$  CTP solution was prepared in a similar way. Mixtures were incubated at 25 °C. At 2 h and 5 h, 400  $\mu\text{L}$  from the reaction containing 25  $\mu\text{M}$  CTP were spiked to 100  $\mu\text{L}$  of dye reagent and 200  $\mu\text{L}$  from the reaction containing 100  $\mu\text{M}$  CTP were spiked to 200  $\mu\text{L}$  buffer (Tris HCl 50 mM, pH = 8) mixed and 100  $\mu\text{L}$  dye reagent was added. Incubation further continued for 10 min at 37 °C and OD<sub>630</sub> nm was measured.

Standard curve was prepared from 40  $\mu\text{M}$  phosphate stock solution (prepared from commercial 7.04 mM solution). From this solution 2, 4, 5, 10, 20 and 30  $\mu\text{M}$  phosphate solutions were prepared in total volume of 400  $\mu\text{L}$  in Tris HCl, 50 mM, pH 8, 5 mM MgCl<sub>2</sub>. After addition of 100  $\mu\text{L}$  dye reagent, vials were incubated at 30 °C for 10 minutes and OD<sub>630</sub> nm was measured. Standard curve was linear between 5 – 30  $\mu\text{M}$ .

***MEP-N<sub>3</sub> as a varied substrate***

MEP-N<sub>3</sub> solutions were prepared at following concentrations 40, 150, 300, 400, 600, 1000, 1600, 2000 and 3000  $\mu\text{M}$  in a final total volume of 388  $\mu\text{L}$  containing:  $\text{MgCl}_2$  (1 mM), CTP (0.2 mM), DTT (1 mM), Inorganic pyrophosphatase (133 mU/mL). *E.coli* IspD (12  $\mu\text{L}$  - 42  $\mu\text{g}$ ) in each vial was added to initiate the reaction. Concentration of MEP-N<sub>3</sub> was determined in a similar way as MEP and CTP.

***IspD inhibition by MEP-N<sub>3</sub>***

In order to test if MEP-N<sub>3</sub> inhibits IspD activity, two reactions were performed with MEP-N<sub>3</sub> 0  $\mu\text{M}$  and 25  $\mu\text{M}$ . Each reaction mixture contains:  $\text{MgCl}_2$  (1 mM), MEP (0.2 mM), CTP (0.2 mM), DTT (1 mM), Inorganic pyrophosphatase (133 mU/mL). *E.coli* IspD (3  $\mu\text{L}$  - 0.065  $\mu\text{g}$ ) was added to each vial to initiate the reaction. (Chapter 3, section 3.3.1)

**IspD Inhibition kinetics**

General reaction conditions are similar to IspD kinetic conditions.

***MEP as a varied substrate.***

MEP solutions were prepared at following concentrations 15, 30, 45, 60, 100, 150 and 250  $\mu\text{M}$  in a final total volume of 400  $\mu\text{L}$  containing:  $\text{MgCl}_2$  (1 mM), CTP (0.2 mM), DTT (1 mM), Inorganic pyrophosphatase (133 mU/mL). *E.coli* IspD (3  $\mu\text{L}$  - 0.065  $\mu\text{g}$ ) was added to each vial to initiate the reaction. MEP-N<sub>3</sub> concentrations were fixed at 0, 20, 40 and 60  $\mu\text{M}$ .

***CTP as a varied substrate***

CTP solutions were prepared at following concentrations 50, 80, 120, 160 and 240  $\mu\text{M}$  in a final total volume of 400  $\mu\text{L}$  containing:  $\text{MgCl}_2$  (1 mM), MEP (0.25 mM), DTT (1 mM), Inorganic pyrophosphatase (133 mU/mL). *E.coli* IspD (3  $\mu\text{L}$  - 0.065  $\mu\text{g}$ ) was added to each vial to initiate the reaction. MEP-N<sub>3</sub> concentrations were fixed at 0, 30, 60 and 90  $\mu\text{M}$ .

**IspD Mechanism determination**

General reaction conditions are similar to IspD kinetic conditions.

***MEP as a varied substrate.***

MEP solutions were prepared at following concentrations 15, 40, 80 and 200  $\mu\text{M}$  in a final total volume of 400  $\mu\text{L}$  containing:  $\text{MgCl}_2$  (1 mM), DTT (1 mM), Inorganic pyrophosphatase (133 mU/mL). *E.coli* IspD (3  $\mu\text{L}$  - 0.065  $\mu\text{g}$ ) was added to each vial to initiate the reaction. CTP concentrations were fixed at 30, 50, 80 and 240  $\mu\text{M}$ .

#### ***CTP as a varied substrate***

CTP solutions were prepared at following concentrations 80, 160, 240 and 380  $\mu\text{M}$  in a final total volume of 400  $\mu\text{L}$  containing:  $\text{MgCl}_2$  (1 mM), DTT (1 mM), Inorganic pyrophosphatase (133 mU/mL). *E.coli* IspD (3  $\mu\text{L}$  - 0.065  $\mu\text{g}$ ) was added to each vial to initiate the reaction. MEP concentrations were fixed at 10, 20, 40 and 120  $\mu\text{M}$ .

#### **MEP-N<sub>3</sub> as substrate of IspD by MS analysis**

MEP-N<sub>3</sub> (0.2 mM) was added to a mixture of CTP (1 mM),  $\text{MgCl}_2$  (5 mM), DTT (1 mM) in a final volume of 200  $\mu\text{L}$  buffer (Tris HCl, 50 mM pH = 8). *E.coli* IspD (34  $\mu\text{g}$ , stock 17 mg/mL) was added to initiate the reaction. The reaction mixture was incubated at 30 °C for 1 h. MeCN (200  $\mu\text{L}$ ) was added and left at 0 °C for 20 min to precipitate proteins. The precipitate was centrifuged 10 min (13000 rpm) and separated. BCN-TMPP (0.8 mM) was added and incubated at 37 °C overnight. The mixture was analysed by LC-MS (see the general experimental condition) using 10  $\mu\text{L}$  of injection volume.

#### **10 % conversion determination**

Reaction mixture A contains:  $\text{MgCl}_2$  (1 mM), CTP (0.2 mM), DTT (1 mM), Inorganic pyrophosphatase (133 mU/mL) was prepared in the final volume of 18336  $\mu\text{L}$  of Tris HCl (50 mM, pH = 8)

*45  $\mu\text{M}$  MEP reaction:* MEP (144  $\mu\text{L}$ , 1 mM stock) was added to a mixture A (3056  $\mu\text{L}$ ). *E.coli* IspD (11  $\mu\text{L}$ , stock 0.0437  $\mu\text{g}/\mu\text{L}$ ) was added to reaction tube to initiate the reaction. At 1, 3, 5, 10, 15, minutes, 400  $\mu\text{L}$  of samples were spiked and added to 100  $\mu\text{L}$  dye reagent and incubation continued further 10 min before  $\text{OD}_{630}$  was measured. At 30, 60, 120 minutes 200  $\mu\text{L}$  of samples were spiked and added to Tris HCl (200  $\mu\text{L}$ , 50 mM, pH = 8) followed by 100  $\mu\text{L}$  dye reagent and incubation continued further 10 min before  $\text{OD}_{630}$  was measured. Blanc reaction

was performed at the same time using same condition except Tris HCl (11  $\mu$ L, 50 mM, pH = 8) was added instead of IspD.

*15  $\mu$ M MEP reaction:* MEP (48  $\mu$ L, 1 mM stock) was added to mixture A (3056  $\mu$ L). *E.coli* IspD (11  $\mu$ L, stock 0.0437  $\mu$ g/ $\mu$ L) was added to reaction tube to initiate the reaction. At 1, 3, 5, 10, 15, 30, 60, minutes, 400  $\mu$ L of samples were spiked and added to 100  $\mu$ L dye reagent and incubation continued further 10 min before OD<sub>630</sub> was measured. At 120 minutes 200  $\mu$ L of samples were spiked and added to Tris HCl (200  $\mu$ L, 50 mM, pH = 8) followed by 100  $\mu$ L dye reagent and incubation continued further 10 min before OD<sub>630</sub> was measured. Blanc reaction was performed at the same time using same condition except Tris HCl (11  $\mu$ L, 50 mM, pH = 8) was added instead of IspD.

*9  $\mu$ M MEP reaction:* MEP (28  $\mu$ L, 1 mM stock) was added to mixture A (3056  $\mu$ L). *E.coli* IspD (11  $\mu$ L, stock 0.0437  $\mu$ g/ $\mu$ L) was added to reaction tube to initiate the reaction. At 1, 3, 5, 10, 15, 30, 60, minutes, 400  $\mu$ L of samples were spiked and added to 100  $\mu$ L dye reagent and incubation continued further 10 min before OD<sub>630</sub> was measured. At 120 minutes 200  $\mu$ L of samples were spiked and added to Tris HCl (200  $\mu$ L, 50 mM, pH = 8) followed by 100  $\mu$ L dye reagent and incubation continued further 10 min before OD<sub>630</sub> was measured. Blanc reaction was performed at the same time using same condition except Tris HCl (11  $\mu$ L, 50 mM, pH = 8) was added instead of IspD.

Standard curve was prepared from 40  $\mu$ M phosphate stock solution (prepared from commercial 7.04 mM solution). From this solution 2, 4, 5, 10, 20 and 30  $\mu$ M of solutions were prepared in total volume of 400  $\mu$ L in Tris HCl, (50 mM pH = 8). After addition of 100  $\mu$ L dye reagent, vials were incubated at 30 °C for 10 minutes and OD<sub>630</sub> nm was measured. Standard curve was linear between 5 – 30  $\mu$ M.

# References

- 1.
2. Rohmer, M., The discovery of a mevalonate-independent pathway for isoprenoid biosynthesis in bacteria, algae and higher plants. *Nat. Prod. Rep.*, **1999**, *16*, (5), 565-74.
3. Rohmer, M., Knani, M., Simonin, P., Sutter, B. and Sahm, H., Isoprenoid biosynthesis in bacteria: a novel pathway for the early steps leading to isopentenyl diphosphate. *Biochem. J.*, **1993**, *295*, (Pt 2), 517-524.
4. Griffin, R. J., The medicinal chemistry of the azido group. *Prog Med Chem*, **1994**, *31*, 121-232.
5. Agard, N. J., Prescher, J. A. and Bertozzi, C. R., A Strain-Promoted [3 + 2] Azide-Alkyne Cycloaddition for Covalent Modification of Biomolecules in Living Systems. *J. Am. Chem. Soc.*, **2004**, *126*, (46), 15046-15047.
6. Cartwright, A. J., Jones, P., Wolff, J.-C. and Evans, E. H., Detection of phosphorus tagged carboxylic acids using HPLC-SF-ICP-MS. *J. Anal. At. Spectrom.*, **2005**, *20*, (2), 75-80.
7. Woo, H.-K., Go, E. P., Hoang, L., Trauger, S. A., Bowen, B., Siuzdak, G. and Northen, T. R., Phosphonium labeling for increasing metabolomic coverage of neutral lipids using electrospray ionization mass spectrometry. *Rapid Commun. Mass Spectrom.*, **2009**, *23*, (12), 1849-1855.
8. Chari, R. V. J., Miller, M. L. and Widdison, W. C., Antibody- Drug Conjugates: An Emerging Concept in Cancer Therapy. *Angew. Chem. Int. Ed.*, **2014**, *53*, (15), 3796-3827.
9. Lagisetti, C., Urbansky, M. and Coates, R. M., The dioxanone approach to (2S,3R)-2-C-methylerythritol 4-phosphate and 2,4-cyclodiphosphate, and various MEP analogues. *J. Org. Chem.*, **2007**, *72*, (26), 9886-9895.
10. Richard, S. B., Bowman, M. E., Kwiatkowski, W., Kang, I., Chow, C., Lillo, A. M., Cane, D. E. and Noel, J. P., Structure of 4-diphosphocytidyl-2-C-methylerythritol synthetase involved in mevalonate-independent isoprenoid biosynthesis. *Nat. Struct. Biol.*, **2001**, *8*, (7), 641-648.
11. Herz, S., Wungsintaweekul, J., Schuhr, C. A., Hecht, S., Luttmann, H., Sagner, S., Fellermeier, M., Eisenreich, W., Zenk, M. H., Bacher, A. and Rohdich, F., Biosynthesis

- of terpenoids: YgbB protein converts 4-diphosphocytidyl-2C-methyl-D-erythritol 2-phosphate to 2C-methyl-D-erythritol 2,4-cyclodiphosphate. *Proc Natl Acad Sci U S A*, **2000**, *97*, (6), 2486-90.
12. Lillo, A. M., Tetzlaff, C. N., Sangari, F. J. and Cane, D. E., Functional expression and characterization of EryA, the erythritol kinase of *Brucella abortus*, and enzymatic synthesis of L-erythritol-4-phosphate. *Bioorg. Med. Chem. Lett.*, **2003**, *13*, (4), 737-9.
  13. Zhang, B., Watts, K. M., Hodge, D., Kemp, L. M., Hunstad, D. A., Hicks, L. M. and Odom, A. R., A Second Target of the Antimalarial and Antibacterial Agent Fosmidomycin Revealed by Cellular Metabolic Profiling. *Biochemistry.*, **2011**, *50*, (17), 3570-3577.
  14. Richard, S. B., Lillo, A. M., Tetzlaff, C. N., Bowman, M. E., Noel, J. P. and Cane, D. E., Kinetic Analysis of *Escherichia coli* 2-C-Methyl-d-erythritol-4-phosphate Cytidyltransferase, Wild Type and Mutants, Reveals Roles of Active Site Amino Acids. *Biochemistry.*, **2004**, *43*, (38), 12189-12197.
  15. Barton, D., Nakanishi, K. and Meth-Cohn, O., *Comprehensive Natural Products Chemistry: Isoprenoids including carotenoids and steroids*. Elsevier: 1999.
  16. Zhao, L., Chang, W.-c., Xiao, Y., Liu, H.-w. and Liu, P., Methylerythritol Phosphate Pathway of Isoprenoid Biosynthesis. *Annu. Rev. Biochem.*, **2013**, *82*, (1), 497-530.
  17. Perez-Gil, J. and Rodriguez-Concepcion, M., Metabolic plasticity for isoprenoid biosynthesis in bacteria. *Biochem. J.*, **2013**, *452*, 19-25.
  18. Heuston, S., Begley, M., Gahan, C. G. M. and Hill, C., Isoprenoid biosynthesis in bacterial pathogens. *Microbiology*, **2012**, *158*, (6), 1389-1401.
  19. Dickschat, J. S., Isoprenoids in three-dimensional space: the stereochemistry of terpene biosynthesis. *Nat. Prod. Rep.*, **2011**, *28*, (12), 1917-1936.
  20. Agranoff, B. W., Eggerer, H., Henning, U. and Lynen, F., Isopentenol Pyrophosphate Isomerase. *J. Am. Chem. Soc.*, **1959**, *81*, (5), 1254-1255.

21. Kaneda, K., Kuzuyama, T., Takagi, M., Hayakawa, Y. and Seto, H., An unusual isopentenyl diphosphate isomerase found in the mevalonate pathway gene cluster from *Streptomyces* sp strain CL190. *Proc. Natl. Acad. Sci. U.S.A.*, **2001**, 98, (3), 932-937.
22. Poulter, C. D. and Rilling, H. C., Prenyltransferase: the mechanism of the reaction. *Biochemistry.*, **1976**, 15, (5), 1079-1083.
23. Poulter, C. D., Argyle, J. C. and Mash, E. A., Prenyltransferase. New evidence for an ionization-condensation-elimination mechanism with 2-fluorogeranyl pyrophosphate. *J. Am. Chem. Soc.*, **1977**, 99, (3), 957-959.
24. Kellogg, B. A. and Poulter, C. D., Chain elongation in the isoprenoid biosynthetic pathway. *Curr. Opin. Chem. Biol.*, **1997**, 1, (4), 570-8.
25. Erickson, H. K. and Poulter, C. D., Chrysanthemyl diphosphate synthase. The relationship among chain elongation, branching, and cyclopropanation reactions in the isoprenoid biosynthetic pathway. *J. Am. Chem. Soc.*, **2003**, 125, (23), 6886-6888.
26. Christianson, D. W., Roots of biosynthetic diversity. *Science*, **2007**, 316, (5821), 60-61.
27. Ogura, K. and Koyama, T., Enzymatic Aspects of Isoprenoid Chain Elongation. *Chem. Rev.*, **1998**, 98, (4), 1263-1276.
28. Popjak, G. and Cornforth, J. W., Substrate stereochemistry in squalene biosynthesis: The first Ciba medal lecture. *Biochem. J.*, **1966**, 101, (3), 553 b4-568.
29. Thulasiram, H. V. and Poulter, C. D., Farnesyl diphosphate synthase: The art of compromise between substrate selectivity and stereoselectivity. *J. Am. Chem. Soc.*, **2006**, 128, (49), 15819-15823.
30. Ito, M., Kobayashi, M., Koyama, T. and Ogura, K., Stereochemical analysis of prenyltransferase reactions leading to (Z)- and (E)-polyprenyl chains. *Biochemistry.*, **1987**, 26, (15), 4745-50.
31. Tarshis, L. C., Proteau, P. J., Kellogg, B. A., Sacchettini, J. C. and Poulter, C. D., Regulation of product chain length by isoprenyl diphosphate synthases. *Proc Natl Acad Sci U S A*, **1996**, 93, (26), 15018-23.

32. Satterwhite, D. M., Wheeler, C. J. and Croteau, R., Biosynthesis of monoterpenes. Enantioselectivity in the enzymatic cyclization of linalyl pyrophosphate to (-)-endo-fenchol. *J. Biol. Chem.*, **1985**, *260*, (26), 13901-8.
33. Cane, D. E., Isoprenoid Biosynthesis - Stereochemistry of the Cyclization of Allylic Pyrophosphates. *Acc. Chem. Res.*, **1985**, *18*, (7), 220-226.
34. Nicolaou, K. C., Dai, W. M. and Guy, R. K., Chemistry and Biology of Taxol. *Angew. Chem. Int. Ed.*, **1994**, *33*, (1), 15-44.
35. Christianson, D. W., Structural biology and chemistry of the terpenoid cyclases. *Chem. Rev.*, **2006**, *106*, (8), 3412-3442.
36. Lin, X. Y., Hezari, M., Koeppe, A. E., Floss, H. G. and Croteau, R., Mechanism of taxadiene synthase, a diterpene cyclase that catalyzes the first step of taxol biosynthesis in Pacific yew. *Biochemistry.*, **1996**, *35*, (9), 2968-2977.
37. Bloch, K., The biological synthesis of cholesterol. *Science*, **1965**, *150*, (3692), 19-28.
38. Mizioroko, H. M., Enzymes of the mevalonate pathway of isoprenoid biosynthesis. *Arch. Biochem. Biophys.*, **2011**, *505*, (2), 131-43.
39. Boucher, Y., Kamekura, M. and Doolittle, W. F., Origins and evolution of isoprenoid lipid biosynthesis in archaea. *Mol. Microbiol.*, **2004**, *52*, (2), 515-27.
40. Grochowski, L. L., Xu, H. and White, R. H., Methanocaldococcus jannaschii uses a modified mevalonate pathway for biosynthesis of isopentenyl diphosphate. *J. Bacteriol.*, **2006**, *188*, (9), 3192-8.
41. Smit, A. and Mushegian, A., Biosynthesis of isoprenoids via mevalonate in Archaea: the lost pathway. *Genome Res*, **2000**, *10*, (10), 1468-84.
42. Chen, M. and Poulter, C. D., Characterization of thermophilic archaeal isopentenyl phosphate kinases. *Biochemistry.*, **2010**, *49*, (1), 207-17.
43. Vannice, J. C., Skaff, D. A., Keightley, A., Addo, J. K., Wyckoff, G. J. and Mizioroko, H. M., Identification in *Haloferax volcanii* of phosphomevalonate decarboxylase and

- isopentenyl phosphate kinase as catalysts of the terminal enzyme reactions in an archaeal alternate mevalonate pathway. *J. Bacteriol.*, **2014**, *196*, (5), 1055-63.
44. Vinokur, J. M., Korman, T. P., Cao, Z. and Bowie, J. U., Evidence of a novel mevalonate pathway in archaea. *Biochemistry.*, **2014**, *53*, (25), 4161-8.
  45. Anderson, D. G., Norgard, D. W. and Porter, J. W., The incorporation of mevalonic acid-2-C<sup>14</sup> and dimethylacrylic acid-3-C<sup>14</sup> into carotenes. *Arch. Biochem. Biophys.*, **1960**, *88*, 68-77.
  46. Goodwin, T. W., Studies in carotenogenesis. 25. The incorporation of <sup>14</sup>CO<sub>2</sub>, [2-<sup>14</sup>C] acetate and [2-<sup>14</sup>C]mevalonate into beta-carotene by illuminated etiolated maize seedlings. *Biochem. J.*, **1958**, *70*, (4), 612-7.
  47. Ramasarma, T. and Ramakrishnan, T., Incorporation of [2-<sup>14</sup>C]mevalonic acid and [2-<sup>14</sup>C]acetic acid into lipids of mycobacteria. *Biochem. J.*, **1961**, *81*, 303-8.
  48. Pandian, S., Saengchjan, S. and Raman, T. S., An alternative pathway for the biosynthesis of isoprenoid compounds in bacteria. *Biochem. J.*, **1981**, *196*, (3), 675-81.
  49. Flesch, G. and Rohmer, M., Prokaryotic hopanoids: the biosynthesis of the bacteriohopane skeleton. Formation of isoprenic units from two distinct acetate pools and a novel type of carbon/carbon linkage between a triterpene and D-ribose. *Eur. J. Biochem.*, **1988**, *175*, (2), 405-11.
  50. Arigoni, D., Sagner, S., Latzel, C., Eisenreich, W., Bacher, A. and Zenk, M. H., Terpenoid biosynthesis from 1-deoxy-D-xylulose in higher plants by intramolecular skeletal rearrangement. *Proc Natl Acad Sci U S A*, **1997**, *94*, (20), 10600-5.
  51. Schwarz, M. K. Terpen-Biosynthese in *Ginkgo biloba*: eine überraschende Geschichte. PhD thesis, ETH Zurich, 1994.
  52. Rohmer, M., Sutter, B. and Sahn, H., Bacterial sterol surrogates. Biosynthesis of the side-chain of bacteriohopanetetrol and of a carbocyclic pseudopentose from <sup>13</sup>C-labelled glucose in *Zymomonas mobilis*. *J. Chem. Soc., Chem. Commun.*, **1989**, (19), 1471-1472.
  53. Rohmer, M., Seemann, M., Horbach, S., BringerMeyer, S. and Sahn, H., Glyceraldehyde 3-phosphate and pyruvate as precursors of isoprenic units in an alternative non-

- mevalonate pathway for terpenoid biosynthesis. *J. Am. Chem. Soc.*, **1996**, *118*, (11), 2564-2566.
54. Sprenger, G. A., Schorken, U., Wiegert, T., Grolle, S., de Graaf, A. A., Taylor, S. V., Begley, T. P., Bringer-Meyer, S. and Sahm, H., Identification of a thiamin-dependent synthase in *Escherichia coli* required for the formation of the 1-deoxy-D-xylulose 5-phosphate precursor to isoprenoids, thiamin, and pyridoxol. *Proc Natl Acad Sci U S A*, **1997**, *94*, (24), 12857-62.
55. Xiang, S., Usunow, G., Lange, G., Busch, M. and Tong, L., Crystal structure of 1-deoxy-D-xylulose 5-phosphate synthase, a crucial enzyme for isoprenoids biosynthesis. *J. Biol. Chem.*, **2007**, *282*, (4), 2676-82.
56. Jordan, F., Current mechanistic understanding of thiamin diphosphate-dependent enzymatic reactions. *Nat. Prod. Rep.*, **2003**, *20*, (2), 184-201.
57. White, J. K., Handa, S., Vankayala, S. L., Merkler, D. J. and Woodcock, H. L., Thiamin Diphosphate Activation in 1-Deoxy-d-xylulose 5-Phosphate Synthase: Insights into the Mechanism and Underlying Intermolecular Interactions. *J. Phys. Chem. B*, **2016**, *120*, (37), 9922-34.
58. Matsue, Y., Mizuno, H., Tomita, T., Asami, T., Nishiyama, M. and Kuzuyama, T., The herbicide ketoclofomazone inhibits 1-deoxy-D-xylulose 5-phosphate synthase in the 2-C-methyl-D-erythritol 4-phosphate pathway and shows antibacterial activity against *Haemophilus influenzae*. *J. Antibiot.*, **2010**, *63*, (10), 583-8.
59. Eubanks, L. M. and Poulter, C. D., *Rhodobacter capsulatus* 1-deoxy-D-xylulose 5-phosphate synthase: steady-state kinetics and substrate binding. *Biochemistry.*, **2003**, *42*, (4), 1140-9.
60. Brammer, L. A. and Meyers, C. F., Revealing substrate promiscuity of 1-deoxy-D-xylulose 5-phosphate synthase. *Org. Lett.*, **2009**, *11*, (20), 4748-51.
61. Sisquella, X., de Pourcq, K., Alguacil, J., Robles, J., Sanz, F., Anselmetti, D., Imperial, S. and Fernandez-Busquets, X., A single-molecule force spectroscopy nanosensor for the identification of new antibiotics and antimalarials. *FASEB J.*, **2010**, *24*, (11), 4203-17.

62. Brammer, L. A., Smith, J. M., Wade, H. and Meyers, C. F., 1-Deoxy-D-xylulose 5-phosphate synthase catalyzes a novel random sequential mechanism. *J. Biol. Chem.*, **2011**, 286, (42), 36522-31.
63. Duvold, T., Cali, P., Bravo, J. M. and Rohmer, M., Incorporation of 2-C-methyl-D-erythritol, a putative isoprenoid precursor in the mevalonate-independent pathway, into ubiquinone and menaquinone of *Escherichia coli*. *Tetrahedron Lett.*, **1997**, 38, (35), 6181-6184.
64. Takahashi, S., Kuzuyama, T., Watanabe, H. and Seto, H., A 1-deoxy-D-xylulose 5-phosphate reductoisomerase catalyzing the formation of 2-C-methyl-D-erythritol 4-phosphate in an alternative nonmevalonate pathway for terpenoid biosynthesis. *Proc Natl Acad Sci U S A*, **1998**, 95, (17), 9879-84.
65. Murkin, A. S., Manning, K. A. and Kholodar, S. A., Mechanism and inhibition of 1-deoxy-D-xylulose-5-phosphate reductoisomerase. *Bioorg. Chem.*, **2014**, 57, 171-85.
66. Lauw, S., Illarionova, V., Bacher, A., Rohdich, F. and Eisenreich, W., Biosynthesis of isoprenoids: studies on the mechanism of 2C-methyl-D-erythritol-4-phosphate synthase. *FEBS J*, **2008**, 275, (16), 4060-73.
67. Li, H., Tian, J., Sun, W., Qin, W. and Gao, W. Y., Mechanistic insights into 1-deoxy-D-xylulose 5-phosphate reductoisomerase, a key enzyme of the MEP terpenoid biosynthetic pathway. *FEBS J*, **2013**, 280, (22), 5896-5905.
68. Zhou, J. W., Wu, R. B., Wang, B. J., Cao, Z. X., Yan, H. G. and Mo, Y. R., Proton-Shuttle-Assisted Heterolytic Carbon Carbon Bond Cleavage and Formation. *ACS Catalysis*, **2015**, 5, (5), 2805-2813.
69. Rohdich, F., Wungsintaweekul, J., Fellermeier, M., Sagner, S., Herz, S., Kis, K., Eisenreich, W., Bacher, A. and Zenk, M. H., Cytidine 5'-triphosphate-dependent biosynthesis of isoprenoids: YgbP protein of *Escherichia coli* catalyzes the formation of 4-diphosphocytidyl-2-C-methylerythritol. *Proc. Natl. Acad. Sci. U.S.A.*, **1999**, 96, (21), 11758-11763.
70. Kuzuyama, T., Takagi, M., Kaneda, K., Dairi, T. and Seto, H., Formation of 4-(cytidine 5'-diphospho)-2-C-methyl-D-erythritol from 2-C-methyl-D-erythritol 4-phosphate by 2-

- C-methyl-D-erythritol 4-phosphate cytidyltransferase, a new enzyme in the nonmevalonate pathway. *Tetrahedron Lett.*, **2000**, *41*, (5), 703-706.
71. Luttgen, H., Rohdich, F., Herz, S., Wungstaweekul, J., Hecht, S., Schuhr, C. A., Fellermeier, M., Sagner, S., Zenk, M. H., Bacher, A. and Eisenreich, W., Biosynthesis of terpenoids: YchB protein of *Escherichia coli* phosphorylates the 2-hydroxy group of 4-diphosphocytidyl-2C-methyl-D-erythritol. *Proc Natl Acad Sci U S A*, **2000**, *97*, (3), 1062-7.
72. Kuzuyama, T., Takagi, M., Kaneda, K., Watanabe, H., Dairi, T. and Seto, H., Studies on the nonmevalonate pathway: conversion of 4-(cytidine 5'-diphospho)-2-C-methyl-D-erythritol to its 2-phospho derivative by 4-(cytidine 5'-diphospho)-2-C-methyl-D-erythritol kinase. *Tetrahedron Lett.*, **2000**, *41*, (16), 2925-2928.
73. Miallau, L., Alphey, M. S., Kemp, L. E., Leonard, G. A., McSweeney, S. M., Hecht, S., Bacher, A., Eisenreich, W., Rohdich, F. and Hunter, W. N., Biosynthesis of isoprenoids: crystal structure of 4-diphosphocytidyl-2C-methyl-D-erythritol kinase. *Proc Natl Acad Sci U S A*, **2003**, *100*, (16), 9173-8.
74. Wada, T., Kuzuyama, T., Satoh, S., Kuramitsu, S., Yokoyama, S., Unzai, S., Tame, J. R. and Park, S. Y., Crystal structure of 4-(cytidine 5'-diphospho)-2-C-methyl-D-erythritol kinase, an enzyme in the non-mevalonate pathway of isoprenoid synthesis. *J. Biol. Chem.*, **2003**, *278*, (32), 30022-7.
75. Herz, S., Wungstaweekul, J., Schuhr, C. A., Hecht, S., Luttgen, H., Sagner, S., Fellermeier, M., Eisenreich, W., Zenk, M. H., Bacher, A. and Rohdich, F., Biosynthesis of terpenoids: YgbB protein converts 4-diphosphocytidyl-2C-methyl-D-erythritol 2-phosphate to 2C-methyl-D-erythritol 2,4-cyclodiphosphate. *Proc. Natl. Acad. Sci. U.S.A.*, **2000**, *97*, (6), 2486-2490.
76. Takagi, M., Kuzuyama, T., Kaneda, K., Watanabe, H., Dairi, T. and Seto, H., Studies on the nonmevalonate pathway: formation of 2-C-methyl-D-erythritol 2,4-cyclodiphosphate from 2-phospho-4-(cytidine 5'-diphospho)-2-C-methyl-D-erythritol. *Tetrahedron Lett.*, **2000**, *41*, (18), 3395-3398.

77. Kemp, L. E., Bond, C. S. and Hunter, W. N., Structure of 2C-methyl-D-erythritol 2,4-cyclodiphosphate synthase: an essential enzyme for isoprenoid biosynthesis and target for antimicrobial drug development. *Proc Natl Acad Sci U S A*, **2002**, 99, (10), 6591-6.
78. Richard, S. B., Ferrer, J. L., Bowman, M. E., Lillo, A. M., Tetzlaff, C. N., Cane, D. E. and Noel, J. P., Structure and mechanism of 2-C-methyl-D-erythritol 2,4-cyclodiphosphate synthase. An enzyme in the mevalonate-independent isoprenoid biosynthetic pathway. *J. Biol. Chem.*, **2002**, 277, (10), 8667-72.
79. Kishida, H., Wada, T., Unzai, S., Kuzuyama, T., Takagi, M., Terada, T., Shirouzu, M., Yokoyama, S., Tame, J. R. and Park, S. Y., Structure and catalytic mechanism of 2-C-methyl-D-erythritol 2,4-cyclodiphosphate (MECDP) synthase, an enzyme in the non-mevalonate pathway of isoprenoid synthesis. *Acta. Crystallogr. Sect. D.*, **2003**, 59, (Pt 1), 23-31.
80. Gabrielsen, M., Rohdich, F., Eisenreich, W., Grawert, T., Hecht, S., Bacher, A. and Hunter, W. N., Biosynthesis of isoprenoids: a bifunctional IspDF enzyme from *Campylobacter jejuni*. *Eur. J. Biochem.*, **2004**, 271, (14), 3028-35.
81. Testa, C. A., Lherbet, C., Pojer, F., Noel, J. P. and Poulter, C. D., Cloning and expression of IspDF from *Mesorhizobium loti*. Characterization of a bifunctional protein that catalyzes non-consecutive steps in the methylerythritol phosphate pathway. *Biochim. Biophys. Acta. Proteins and Proteomics*, **2006**, 1764, (1), 85-96.
82. Altincicek, B., Kollas, A. K., Sanderbrand, S., Wiesner, J., Hintz, M., Beck, E. and Jomaa, H., GcpE is involved in the 2-C-methyl-D-erythritol 4-phosphate pathway of isoprenoid biosynthesis in *Escherichia coli*. *J. Bacteriol.*, **2001**, 183, (8), 2411-6.
83. Campos, N., Rodriguez-Concepcion, M., Seemann, M., Rohmer, M. and Boronat, A., Identification of gcpE as a novel gene of the 2-C-methyl-D-erythritol 4-phosphate pathway for isoprenoid biosynthesis in *Escherichia coli*. *FEBS Lett.*, **2001**, 488, (3), 170-173.
84. Hecht, S., Eisenreich, W., Adam, P., Amslinger, S., Kis, K., Bacher, A., Arigoni, D. and Rohdich, F., Studies on the nonmevalonate pathway to terpenes: the role of the GcpE (IspG) protein. *Proc Natl Acad Sci U S A*, **2001**, 98, (26), 14837-42.

85. Seemann, M., Campos, N., Rodriguez-Concepcion, M., Hoeffler, J. F., Grosdemange-Billiard, C., Boronat, A. and Rohmer, M., Isoprenoid biosynthesis via the methylerythritol phosphate pathway: accumulation of 2-C-methyl-D-erythritol 2,4-cyclodiphosphate in a *gcpE* deficient mutant of *Escherichia coli*. *Tetrahedron Lett.*, **2002**, *43*, (5), 775-778.
86. Seemann, M., Campos, N., Rodriguez-Concepcion, M., Ibanez, E., Duvold, T., Tritsch, D., Boronat, A. and Rohmer, M., Isoprenoid biosynthesis in *Escherichia coli* via the methylerythritol phosphate pathway: enzymatic conversion of methylerythritol cyclodiphosphate into a phosphorylated derivative of (E)-2-methylbut-2-ene-1,4-diol. *Tetrahedron Lett.*, **2002**, *43*, (8), 1413-1415.
87. Wolff, M., Seemann, M., Grosdemange-Billiard, C., Tritsch, D., Campos, N., Rodriguez-Concepcion, M., Boronat, A. and Rohmer, M., Isoprenoid biosynthesis via the methylerythritol phosphate pathway. (E)-4-hydroxy-3-methylbut-2-enyl diphosphate: chemical synthesis and formation from methylerythritol cyclodiphosphate by a cell-free system from *Escherichia coli*. *Tetrahedron Lett.*, **2002**, *43*, (14), 2555-2559.
88. Seemann, M., Bui, B. T. S., Wolff, M., Tritsch, D., Campos, N., Boronat, A., Marquet, A. and Rohmer, M., Isoprenoid biosynthesis through the methylerythritol phosphate pathway: The (E)-4-hydroxy-3-methylbut-2-enyl diphosphate synthase (GcpE) is a [4Fe-4S] protein. *Angew. Chem. Int. Ed.*, **2002**, *41*, (22), 4337-4339.
89. Seemann, M., Wegner, P., Schunemann, V., Bui, B. T. S., Wolff, M., Marquet, A., Trautwein, A. X. and Rohmer, M., Isoprenoid biosynthesis in chloroplasts via the methylerythritol phosphate pathway: the (E)-4-hydroxy-3-methylbut-2-enyl diphosphate synthase (GcpE) from *Arabidopsis thaliana* is a [4Fe-4S] protein. *J. Biol. Inorg. Chem.*, **2005**, *10*, (2), 131-137.
90. Reikittke, I., Nonaka, T., Wiesner, J., Demmer, U., Warkentin, E., Jomaa, H. and Ermler, U., Structure of the E-1-hydroxy-2-methyl-but-2-enyl-4-diphosphate synthase (GcpE) from *Thermus thermophilus*. *FEBS Lett.*, **2011**, *585*, (3), 447-451.
91. Xu, W. Y., Lees, N. S., Adedeji, D., Wiesner, J., Jomaa, H., Hoffman, B. M. and Duin, E. C., Paramagnetic Intermediates of (E)-4-Hydroxy-3-methylbut-2-enyl Diphosphate

- Synthase (GcpE/IspG) under Steady-State and Pre-Steady-State Conditions. *J. Am. Chem. Soc.*, **2010**, *132*, (41), 14509-14520.
92. Wang, W. X., Li, J. K., Wang, K., Huang, C. C., Zhang, Y. and Oldfield, E., Organometallic mechanism of action and inhibition of the 4Fe-4S isoprenoid biosynthesis protein GcpE (IspG). *Proc. Natl. Acad. Sci. U.S.A*, **2010**, *107*, (25), 11189-11193.
93. Gustafson, C. E., Kaul, S. and Ishiguro, E. E., Identification of the Escherichia-Coli LytB Gene, Which Is Involved in Penicillin Tolerance and Control of the Stringent Response. *J. Bacteriol.*, **1993**, *175*, (4), 1203-1205.
94. McAteer, S., Coulson, A., McLennan, N. and Masters, M., The lytB gene of Escherichia coli is essential and specifies a product needed for isoprenoid biosynthesis. *J. Bacteriol.*, **2001**, *183*, (24), 7403-7407.
95. Cunningham, F. X., Jr., Lafond, T. P. and Gantt, E., Evidence of a role for LytB in the nonmevalonate pathway of isoprenoid biosynthesis. *J. Bacteriol.*, **2000**, *182*, (20), 5841-8.
96. Altincicek, B., Kollas, A. K., Eberl, M., Wiesner, J., Sanderbrand, S., Hintz, M., Beck, E. and Jomma, H., LytB, a novel gene of the 2-C-methyl-D-erythritol 4-phosphate pathway of isoprenoid biosynthesis in Escherichia coli. *FEBS Lett.*, **2001**, *499*, (1-2), 37-40.
97. Rohdich, F., Hecht, S., Gartner, K., Adam, P., Krieger, C., Amslinger, S., Arigoni, D., Bacher, A. and Eisenreich, W., Studies on the nonmevalonate terpene biosynthetic pathway: Metabolic role of IspH (LytB) protein. *Proc. Natl. Acad. Sci. U.S.A*, **2002**, *99*, (3), 1158-1163.
98. Altincicek, B., Duin, E. C., Reichenberg, A., Hedderich, R., Kollas, A. K., Hintz, M., Wagner, S., Wiesner, J., Beck, E. and Jomaa, H., LytB protein catalyzes the terminal step of the 2-C-methyl-D-erythritol-4-phosphate pathway of isoprenoid biosynthesis. *FEBS Lett.*, **2002**, *532*, (3), 437-40.
99. Rohdich, F., Zepeck, F., Adam, P., Hecht, S., Kaiser, J., Laupitz, R., Grawert, T., Amslinger, S., Eisenreich, W., Bacher, A. and Arigoni, D., The deoxyxylulose phosphate pathway of isoprenoid biosynthesis: studies on the mechanisms of the reactions catalyzed by IspG and IspH protein. *Proc Natl Acad Sci U S A*, **2003**, *100*, (4), 1586-91.

100. Wolff, M., Seemann, M., Bui, B. T. S., Frapart, Y., Tritsch, D., Estrabot, A. G., Rodriguez-Concepcion, M., Boronat, A., Marquet, A. and Rohmer, M., Isoprenoid biosynthesis via the methylerythritol phosphate pathway: the (E)-4-hydroxy-3-methylbut-2-enyl diphosphate reductase (LytB/IspH) from *Escherichia coli* is a [4Fe-4S] protein. *FEBS Lett.*, **2003**, *541*, (1-3), 115-120.
101. Seemann, M., Janthawornpong, K., Schweizer, J., Bottger, L. H., Janoschka, A., Ahrens-Botzong, A., Tambou, M. N., Rotthaus, O., Trautwein, A. X., Rohmer, M. and Schunemann, V., Isoprenoid Biosynthesis via the MEP Pathway: In Vivo Mossbauer Spectroscopy Identifies a [4Fe-4S](2+) Center with Unusual Coordination Sphere in the LytB Protein. *J. Am. Chem. Soc.*, **2009**, *131*, (37), 13184-13185.
102. Ahrens-Botzong, A., Janthawornpong, K., Wolny, J. A., Tambou, E. N., Rohmer, M., Krasutsky, S., Poulter, C. D., Schunemann, V. and Seemann, M., Biosynthesis of Isoprene Units: Mossbauer Spectroscopy of Substrate and Inhibitor Binding to the [4Fe-4S] Cluster of the LytB/IspH Enzyme. *Angew. Chem. Int. Ed.*, **2011**, *50*, (50), 11976-11979.
103. Faus, I., Reinhard, A., Rackwitz, S., Wolny, J. A., Schlage, K., Wille, H. C., Chumakov, A., Krasutsky, S., Chaignon, P., Poulter, C. D., Seemann, M. and Schunemann, V., Isoprenoid Biosynthesis in Pathogenic Bacteria: Nuclear Resonance Vibrational Spectroscopy Provides Insight into the Unusual [4Fe-4S] Cluster of the *E. coli* LytB/IspH Protein. *Angew. Chem. Int. Ed.*, **2015**, *54*, (43), 12584-12587.
104. Span, I., Grawert, T., Bacher, A., Eisenreich, W. and Groll, M., Crystal structures of mutant IspH proteins reveal a rotation of the substrate's hydroxymethyl group during catalysis. *J. Mol. Biol.*, **2012**, *416*, (1), 1-9.
105. Xu, W. Y., Lees, N. S., Hall, D., Welideniya, D., Hoffman, B. M. and Duin, E. C., A Closer Look at the Spectroscopic Properties of Possible Reaction Intermediates in Wild-Type and Mutant (E)-4-Hydroxy-3-methylbut-2-enyl Diphosphate Reductase. *Biochemistry.*, **2012**, *51*, (24), 4835-4849.
106. Wang, W. X., Wang, K., Liu, Y. L., No, J. H., Li, J. K., Nilges, M. J. and Oldfield, E., Bioorganometallic mechanism of action, and inhibition, of IspH. *Proc. Natl. Acad. Sci. U.S.A.*, **2010**, *107*, (10), 4522-4527.

107. Hamilton, J. G., The Use of Radioactive Tracers in Biology and Medicine. *Radiology*, **1942**, 39, (5), 541-572.
108. Manly, M. L. and Bale, W. F., The Metabolism of Inorganic Phosphorus of Rat Bones and Teeth as Indicated by the Radioactive Isotope. *J. Biol. Chem.*, **1939**, 129, (1), 125-134.
109. Copp, D. H. and Greenberg, D. M., Studies in Mineral Metabolism with the Aid of Artificial Radioactive Isotopes: VI. Cobalt. *Proc Natl Acad Sci U S A*, **1941**, 27, (3), 153-7.
110. Greenberg, D. M. and Campbell, W. W., Studies in Mineral Metabolism with the Aid of Induced Radioactive Isotopes: IV-Manganese. *Proc Natl Acad Sci U S A*, **1940**, 26, (7), 448-52.
111. Chiewitz. O and Hevesy. G, Radioactive Indicators in the Study of Phosphorus Metabolism in Rats. *Nature*, **1935**, 136, 754-755.
112. Paneth, F. A., Use of radioactive tracers in biological research. *Nature*, **1949**, 163, 388-390.
113. Bass, L. A., Wang, M., Welch, M. J. and Anderson, C. J., In vivo transchelation of copper-64 from TETA-octreotide to superoxide dismutase in rat liver. *Bioconjugate Chem.*, **2000**, 11, (4), 527-532.
114. Ferrara, K. W., Borden, M. A. and Zhang, H., Lipid-Shelled Vehicles: Engineering for Ultrasound Molecular Imaging and Drug Delivery. *Acc. Chem. Res.*, **2009**, 42, (7), 881-892.
115. Song, Y. J., Qu, C. F., Rizvi, S. M. A., Li, Y., Robertson, G., Raja, C., Morgenstern, A., Apostolidis, C., Perkins, A. C. and Allen, B. J., Cytotoxicity of PAI2, C595 and Herceptin vectors labeled with the alpha-emitting radioisotope Bismuth-213 for ovarian cancer cell monolayers and clusters. *Cancer. Lett.*, **2006**, 234, (2), 176-183.
116. Gallagher, B. M., Fowler, J. S., Gutterson, N. I., Macgregor, R. R., Wan, C. N. and Wolf, A. P., Metabolic Trapping as a Principle of Radiopharmaceutical Design - Some Factors

- Responsible for Biodistribution of [F-18] 2-Deoxy-2-Fluoro-D-Glucose. *J. Nucl. Med.*, **1978**, *19*, (10), 1154-1161.
117. Hu, Z. H., Zhao, M. X., Qu, Y. W., Zhang, X. J., Zhang, M. R., Liu, M. H., Guo, H. B., Zhang, Z. Y., Wang, J., Yang, W. D. and Tian, J., In Vivo 3-Dimensional Radiopharmaceutical-Excited Fluorescence Tomography. *J. Nucl. Med.*, **2017**, *58*, (1), 169-174.
118. MacVicar, R. and Burris, R. H., Studies on nitrogen metabolism in tomato with use of isotopically labeled ammonium sulfate. *J. Biol. Chem.*, **1948**, *176*, (2), 511-516.
119. Martin, D. K., Use of Isotopes in Biochemical Research Fundamental Aspects. *Annu. Rev. Biochem.*, **1947**, *16*, 631-654.
120. Ong, S. E. and Mann, M., A practical recipe for stable isotope labeling by amino acids in cell culture (SILAC). *Nat. Protoc.*, **2006**, *1*, (6), 2650-2660.
121. Ong, S. E., Blagoev, B., Kratchmarova, I., Kristensen, D. B., Steen, H., Pandey, A. and Mann, M., Stable isotope labeling by amino acids in cell culture, SILAC, as a simple and accurate approach to expression proteomics. *Mol. Cell. Proteomics.*, **2002**, *1*, (5), 376-386.
122. Zhang, H., Li, X. J., Martin, D. B. and Aebersold, R., Identification and quantification of N-linked glycoproteins using hydrazide chemistry, stable isotope labeling and mass spectrometry. *Nat. Biotechnol.*, **2003**, *21*, (6), 660-666.
123. Boersema, P. J., Raijmakers, R., Lemeer, S., Mohammed, S. and Heck, A. J. R., Multiplex peptide stable isotope dimethyl labeling for quantitative proteomics. *Nat. Protoc.*, **2009**, *4*, (4), 484-494.
124. Huskey, S. E. W., Forseth, R. R., Li, H. M., Jian, Z. G., Catoire, A., Zhang, J., Ray, T., He, H., Flarakos, J. and Mangold, J. B., Utilization of Stable Isotope Labeling to Facilitate the Identification of Polar Metabolites of KAF156, an Antimalarial Agent. *Drug Metab. Dispos.*, **2016**, *44*, (10), 1697-1708.

125. Huskey, S. E. W., Li, H. M., Catoire, A., Jian, Z. G., Zhang, J., Flarakos, J., Ray, T. and Mangold, J., Utilization of Stable Isotope Labeling to Facilitate the Identification of Very Polar Metabolites in Rat Urine. *Drug Metab. Rev.*, **2015**, *47*, 191-192.
126. Sletten, E. M. and Bertozzi, C. R., Bioorthogonal Chemistry: Fishing for Selectivity in a Sea of Functionality. *Angew. Chem. Int. Ed.*, **2009**, *48*, (38), 6974-6998.
127. Mahal, L. K., Yarema, K. J. and Bertozzi, C. R., Engineering chemical reactivity on cell surfaces through oligosaccharide biosynthesis. *Science*, **1997**, *276*, (5315), 1125-1128.
128. Hang, H. C. and Bertozzi, C. R., Ketone isosteres of 2-N-acetamidoglucosamines as substrates for metabolic cell surface engineering. *J. Am. Chem. Soc.*, **2001**, *123*, (6), 1242-1243.
129. Dawson, P. E., Muir, T. W., Clarklewis, I. and Kent, S. B. H., Synthesis of Proteins by Native Chemical Ligation. *Science*, **1994**, *266*, (5186), 776-779.
130. Wieland, T., Bokelmann, E., Bauer, L., Lang, H. U. and Lau, H., Über Peptidsynthesen. 8. Mitteilung Bildung von S-haltigen Peptiden durch intramolekulare Wanderung von Aminoacylresten. *Justus Liebigs Annalen der Chemie*, **1953**, *583*, (1), 129-149.
131. Muralidharan, V. and Muir, T. W., Protein ligation: an enabling technology for the biophysical analysis of proteins. *Nat. Methods.*, **2006**, *3*, (6), 429-438.
132. Yamazaki, T., Otomo, T., Oda, N., Kyogoku, Y., Uegaki, K., Ito, N., Ishino, Y. and Nakamura, H., Segmental isotope labeling for protein NMR using peptide splicing. *J. Am. Chem. Soc.*, **1998**, *120*, (22), 5591-5592.
133. Yi, L., Sun, H., Itzen, A., Triola, G., Waldmann, H., Goody, R. S. and Wu, Y. W., One-Pot Dual-Labeling of a Protein by Two Chemoselective Reactions. *Angew. Chem. Int. Ed.*, **2011**, *50*, (36), 8287-8290.
134. Freidel, C., Kaloyanova, S. and Peneva, K., Chemical tags for site-specific fluorescent labeling of biomolecules. *Amino Acids*, **2016**, *48*, (6), 1357-1372.
135. Saxon, E. and Bertozzi, C. R., Cell surface engineering by a modified Staudinger reaction. *Science*, **2000**, *287*, (5460), 2007-10.

136. Staudinger, H. and Meyer, J., Über neue organische Phosphorverbindungen III. Phosphinmethylderivate und Phosphinimine. *Helv. Chim. Acta*, **1919**, 2, (1), 635-646.
137. Soellner, M. B., Nilsson, B. L. and Raines, R. T., Reaction mechanism and kinetics of the traceless Staudinger ligation. *J. Am. Chem. Soc.*, **2006**, 128, (27), 8820-8.
138. Soellner, M. B., Tam, A. and Raines, R. T., Staudinger Ligation of Peptides at Non-Glycyl Residues. *J. Org. Chem.*, **2006**, 71, (26), 9824-9830.
139. Laughlin, S. T. and Bertozzi, C. R., Metabolic labeling of glycans with azido sugars and subsequent glycan-profiling and visualization via Staudinger ligation. *Nat. Protoc.*, **2007**, 2, (11), 2930-2944.
140. Saxon, E., Luchansky, S. J., Hang, H. C., Yu, C., Lee, S. C. and Bertozzi, C. R., Investigating cellular metabolism of synthetic azidosugars with the Staudinger ligation. *J. Am. Chem. Soc.*, **2002**, 124, (50), 14893-14902.
141. Prescher, J. A., Dube, D. H. and Bertozzi, C. R., Chemical remodelling of cell surfaces in living animals. *Nature*, **2004**, 430, (7002), 873-877.
142. Laughlin, S. T., Agard, N. J., Baskin, J. M., Carrico, I. S., Chang, P. V., Ganguli, A. S., Hangauer, M. J., Lo, A., Prescher, J. A. and Bertozzi, C. R., Metabolic labeling of glycans with azido sugars for visualization and glycoproteomics. *Glycobiology*, **2006**, 415, 230-250.
143. Vocadlo, D. J., Hang, H. C., Kim, E. J., Hanover, J. A. and Bertozzi, C. R., A chemical approach for identifying O-GlcNAc-modified proteins in cells. *Proc. Natl. Acad. Sci. U.S.A.*, **2003**, 100, (16), 9116-9121.
144. Dube, D. H., Prescher, J. A., Quang, C. N. and Bertozzi, C. R., Probing mucin-type O-linked glycosylation in living animals. *Proc. Natl. Acad. Sci. U.S.A.*, **2006**, 103, (13), 4819-4824.
145. Kolb, H. C., Finn, M. G. and Sharpless, K. B., Click Chemistry: Diverse Chemical Function from a Few Good Reactions. *Angew. Chem. Int. Ed. Engl.*, **2001**, 40, (11), 2004-2021.

146. Huisgen, R., Kinetics and Mechanism of 1,3-Dipolar Cycloadditions. *Angew. Chem. Int. Ed.*, **1963**, 2, (11), 633-645.
147. Rostovtsev, V. V., Green, L. G., Fokin, V. V. and Sharpless, K. B., A stepwise huisgen cycloaddition process: copper(I)-catalyzed regioselective "ligation" of azides and terminal alkynes. *Angew. Chem. Int. Ed. Engl.*, **2002**, 41, (14), 2596-9.
148. Tornøe, C. W., Christensen, C. and Meldal, M., Peptidotriazoles on solid phase: [1,2,3]-triazoles by regiospecific copper(i)-catalyzed 1,3-dipolar cycloadditions of terminal alkynes to azides. *J. Org. Chem.*, **2002**, 67, (9), 3057-64.
149. Chan, T. R., Hilgraf, R., Sharpless, K. B. and Fokin, V. V., Polytriazoles as Copper(I)-Stabilizing Ligands in Catalysis. *Org. Lett.*, **2004**, 6, (17), 2853-2855.
150. Rodionov, V. O., Presolski, S. I., Gardinier, S., Lim, Y.-H. and Finn, M. G., Benzimidazole and Related Ligands for Cu-Catalyzed Azide-Alkyne Cycloaddition. *J. Am. Chem. Soc.*, **2007**, 129, (42), 12696-12704.
151. Zhang, L., Chen, X., Xue, P., Sun, H. H. Y., Williams, I. D., Sharpless, K. B., Fokin, V. V. and Jia, G., Ruthenium-Catalyzed Cycloaddition of Alkynes and Organic Azides. *J. Am. Chem. Soc.*, **2005**, 127, (46), 15998-15999.
152. Kim, W. G., Kang, M. E., Lee, J. B., Jeon, M. H., Lee, S., Lee, J., Choi, B., Cal, P. M. S. D., Kang, S., Kee, J.-M., Bernardes, G. J. L., Rohde, J.-U., Choe, W. and Hong, S. Y., Nickel-Catalyzed Azide-Alkyne Cycloaddition To Access 1,5-Disubstituted 1,2,3-Triazoles in Air and Water. *J. Am. Chem. Soc.*, **2017**, 139, (35), 12121-12124.
153. Boren, B. C., Narayan, S., Rasmussen, L. K., Zhang, L., Zhao, H. T., Lin, Z. Y., Jia, G. C. and Fokin, V. V., Ruthenium-catalyzed azide-alkyne cycloaddition: Scope and mechanism. *J. Am. Chem. Soc.*, **2008**, 130, (28), 8923-8930.
154. Worrell, B. T., Malik, J. A. and Fokin, V. V., Direct Evidence of a Dinuclear Copper Intermediate in Cu(I)-Catalyzed Azide-Alkyne Cycloadditions. *Science*, **2013**, 340, (6131), 457-460.
155. Gaetke, L. M. and Chow, C. K., Copper toxicity, oxidative stress, and antioxidant nutrients. *Toxicology*, **2003**, 189, (1-2), 147-63.

156. Alder, K. and Stein, G., Über den sterischen Verlauf von Additions- und Substitutionsreaktionen. V. Der sterische Verlauf der Phenylazid-reaktion. *Justus Liebigs Annalen der Chemie*, **1935**, 515, (1), 185-200.
157. Wittig, G. and Krebs, A., Zur Existenz niedergliederiger Cycloalkine, I. *Chem. Ber.*, **1961**, 94, (12), 3260-3275.
158. van Berkel, S. S., Dirks, A. J., Debets, M. F., van Delft, F. L., Cornelissen, J. J. L. M., Nolte, R. J. M. and Rutjes, F. P. J. T., Metal-Free Triazole Formation as a Tool for Bioconjugation. *ChemBioChem*, **2007**, 8, (13), 1504-1508.
159. Zhou, Y. and Murphy, P. V., New Access to 1-Deoxynojirimycin Derivatives via Azide-Alkene Cycloaddition. *Org. Lett.*, **2008**, 10, (17), 3777-3780.
160. de Miguel, I., Velado, M., Herradon, B. and Mann, E., Synthetic studies on the application of the intramolecular azide-alkene 1,3-dipolar cycloaddition reaction in the construction of the core structure of complex alkaloids. *Tetrahedron*, **2016**, 72, (31), 4617-4625.
161. Peng, Y. H., Jiang, X. M., Chen, S. M., Wu, Q. S., Shen, J. and Wu, W. T., Synthesis and characterization of ammonia-responsive polymer microgels. *Polym. Chem.*, **2015**, 6, (48), 8331-8342.
162. Lin, F., Yu, J. Y., Tang, W., Zheng, J. K., Defante, A., Guo, K., Wesdemiotis, C. and Becker, M. L., Peptide-Functionalized Oxime Hydrogels with Tunable Mechanical Properties and Gelation Behavior. *Biomacromolecules*, **2013**, 14, (10), 3749-3758.
163. Link, A. J., Mock, M. L. and Tirrell, D. A., Non-canonical amino acids in protein engineering. *Curr. Opin. Biotechnol.*, **2003**, 14, (6), 603-609.
164. van Hest, J. C. M., Kiick, K. L. and Tirrell, D. A., Efficient incorporation of unsaturated methionine analogues into proteins in vivo. *J. Am. Chem. Soc.*, **2000**, 122, (7), 1282-1288.
165. Kiick, K. L., van Hest, J. C. M. and Tirrell, D. A., Expanding the scope of protein biosynthesis by altering the methionyl-tRNA synthetase activity of a bacterial expression host. *Angew. Chem. Int. Ed.*, **2000**, 39, (12), 2148-+.
166. Kirshenbaum, K., Carrico, I. S. and Tirrell, D. A., Biosynthesis of proteins incorporating a versatile set of phenylalanine analogues. *ChemBioChem*, **2002**, 3, (2-3), 235-237.

167. Nguyen, D. P., Lusic, H., Neumann, H., Kapadnis, P. B., Deiters, A. and Chin, J. W., Genetic Encoding and Labeling of Aliphatic Azides and Alkynes in Recombinant Proteins via a Pyrrolysyl-tRNA Synthetase/tRNA(CUA) Pair and Click Chemistry. *J. Am. Chem. Soc.*, **2009**, *131*, (25), 8720-+.
168. Kurra, Y., Odoi, K. A., Lee, Y. J., Yang, Y. Y., Lu, T. X., Wheeler, S. E., Torres-Kolbus, J., Deiters, A. and Liu, W. S. R., Two Rapid Catalyst-Free Click Reactions for In Vivo Protein Labeling of Genetically Encoded Strained Alkene/Alkyne Functionalities. *Bioconjugate Chem.*, **2014**, *25*, (9), 1730-1738.
169. Wang, Y. S., Fang, X. Q., Chen, H. Y., Wu, B., Wang, Z. Y. U., Hilty, C. and Liu, W. S. R., Genetic Incorporation of Twelve meta-Substituted Phenylalanine Derivatives Using a Single Pyrrolysyl-tRNA Synthetase Mutant. *ACS Chem. Biol.*, **2013**, *8*, (2), 405-415.
170. Wang, Q., Chan, T. R., Hilgraf, R., Fokin, V. V., Sharpless, K. B. and Finn, M. G., Bioconjugation by copper(I)-catalyzed azide-alkyne [3+2] cycloaddition. *J. Am. Chem. Soc.*, **2003**, *125*, (11), 3192-3193.
171. Rubino, F. A., Oum, Y. H., Rajaram, L., Chu, Y. and Carrico, I. S., Chemoselective Modification of Viral Surfaces via Bioorthogonal Click Chemistry. *J. Vis. Exp.*, **2012**, (66).
172. Martell, J. and Weerapana, E., Applications of Copper-Catalyzed Click Chemistry in Activity-Based Protein Profiling. *Molecules*, **2014**, *19*, (2), 1378-1393.
173. Speers, A. E., Adam, G. C. and Cravatt, B. F., Activity-based protein profiling in vivo using a copper(I)-catalyzed azide-alkyne [3+2] cycloaddition. *J. Am. Chem. Soc.*, **2003**, *125*, (16), 4686-4687.
174. Ovaa, H., van Swieten, P. F., Kessler, B. M., Leeuwenburgh, M. A., Fiebiger, E., van den Nieuwendijk, A. M. C. H., Galardy, P. J., van der Marel, G. A., Ploegh, H. L. and Overkleeft, H. S., Chemistry in living cells: Detection of active proteasomes by a two-step labeling strategy. *Angew. Chem. Int. Ed.*, **2003**, *42*, (31), 3626-3629.
175. Gillet, L. C. J., Namoto, K., Ruchti, A., Hoving, S., Boesch, D., Inverardi, B., Mueller, D., Coulot, M., Schindler, P., Schweigler, P., Bernardi, A. and Gil-Parrado, S., In-cell

- selectivity profiling of serine protease inhibitors by activity-based proteomics. *Mol. Cell. Proteomics.*, **2008**, 7, (7), 1241-1253.
176. Tully, S. E. and Cravatt, B. F., Activity-Based Probes That Target Functional Subclasses of Phospholipases in Proteomes. *J. Am. Chem. Soc.*, **2010**, 132, (10), 3264-+.
177. Overall, C. M. and Lopez-Otin, C., Strategies for MMP inhibition in cancer: Innovations for the post-trial era. *Nat. Rev. Cancer*, **2002**, 2, (9), 657-672.
178. Luchansky, S. J., Argade, S., Hayes, B. K. and Bertozzi, C. R., Metabolic functionalization of recombinant glycoproteins. *Biochemistry.*, **2004**, 43, (38), 12358-12366.
179. Laughlin, S. T., Baskin, J. M., Amacher, S. L. and Bertozzi, C. R., In vivo imaging of membrane-associated glycans in developing zebrafish. *Science*, **2008**, 320, (5876), 664-667.
180. Chang, P. V., Chen, X., Smyrniotis, C., Xenakis, A., Hu, T. S., Bertozzi, C. R. and Wu, P., Metabolic Labeling of Sialic Acids in Living Animals with Alkynyl Sugars. *Angew. Chem. Int. Ed.*, **2009**, 48, (22), 4030-4033.
181. Hsu, T. L., Hanson, S. R., Kishikawa, K., Wang, S. K., Sawa, M. and Wong, C. H., Alkynyl sugar analogs for the labeling and visualization of glycoconjugates in cells. *Proc. Natl. Acad. Sci. U.S.A.*, **2007**, 104, (8), 2614-2619.
182. Chang, P. V., Prescher, J. A., Sletten, E. M., Baskin, J. M., Miller, I. A., Agard, N. J., Lo, A. and Bertozzi, C. R., Copper-free click chemistry in living animals. *Proc. Natl. Acad. Sci. U.S.A.*, **2010**, 107, (5), 1821-1826.
183. Liang, Y., Jiang, X., Yuan, R., Zhou, Y., Ji, C. X., Yang, L. M., Chen, H. F. and Wang, Q., Metabolism-Based Click-Mediated Platform for Specific Imaging and Quantification of Cell Surface Sialic Acids. *Anal. Chem.*, **2017**, 89, (1), 538-543.
184. Chen, W. X., Smeekens, J. M. and Wu, R. H., Systematic and site-specific analysis of N-sialoglycosylated proteins on the cell surface by integrating click chemistry and MS-based proteomics. *Chem. Sci.*, **2015**, 6, (8), 4681-4689.

185. Smeekens, J. M., Chen, W. X. and Wu, R. H., Mass Spectrometric Analysis of the Cell Surface N-Glycoproteome by Combining Metabolic Labeling and Click Chemistry. *J. Am. Soc. Mass. Spectrom.*, **2015**, *26*, (4), 604-614.
186. Dumont, A., Malleron, A., Awwad, M., Dukan, S. and Vauzeilles, B., Click-Mediated Labeling of Bacterial Membranes through Metabolic Modification of the Lipopolysaccharide Inner Core. *Angew Chem Int Edit*, **2012**, *51*, (13), 3143-3146.
187. Pons, J. M., Dumont, A., Sautejeau, G., Fugier, E., Baron, A., Dukan, S. and Vauzeilles, B., Identification of Living *Legionella pneumophila* Using Species-Specific Metabolic Lipopolysaccharide Labeling. *Angew. Chem. Int. Ed.*, **2014**, *53*, (5), 1275-1278.
188. Hornberger, T. A., Chu, W. K., Mak, Y. W., Hsiung, J. W., Huang, S. A. and Chien, S., The role of phospholipase D and phosphatidic acid in the mechanical activation of mTOR signaling in skeletal muscle. *Proc. Natl. Acad. Sci. U.S.A*, **2006**, *103*, (12), 4741-4746.
189. Knauss, T. C., Jaffer, F. E. and Abboud, H. E., Phosphatidic-Acid Modulates DNA-Synthesis, Phospholipase-C, and Platelet-Derived Growth-Factor Messenger-Rnas in Cultured Mesangial Cells - Role of Protein-Kinase-C. *J. Biol. Chem.*, **1990**, *265*, (24), 14457-14463.
190. Carman, G. M. and Henry, S. A., Phosphatidic acid plays a central role in the transcriptional regulation of glycerophospholipid synthesis in *Saccharomyces cerevisiae*. *J. Biol. Chem.*, **2007**, *282*, (52), 37293-37297.
191. Neef, A. B. and Schultz, C., Selective Fluorescence Labeling of Lipids in Living Cells. *Angew. Chem. Int. Ed.*, **2009**, *48*, (8), 1498-1500.
192. Jao, C. Y., Roth, M., Welti, R. and Salic, A., Metabolic labeling and direct imaging of choline phospholipids in vivo. *Proc. Natl. Acad. Sci. U.S.A*, **2009**, *106*, (36), 15332-15337.
193. Jao, C. Y., Roth, M., Welti, R. and Salic, A., Biosynthetic Labeling and Two-Color Imaging of Phospholipids in Cells. *ChemBioChem*, **2015**, *16*, (3), 472-476.

194. Ngo, J. T., Adams, S. R., Deerinck, T. J., Boassa, D., Rodriguez-Rivera, F., Palida, S. F., Bertozzi, C. R., Ellisman, M. H. and Tsien, R. Y., Click-EM for imaging metabolically tagged nonprotein biomolecules. *Nat. Chem. Biol.*, **2016**, *12*, (6), 459-U128.
195. Hu, F. H., Lamprecht, M. R., Wei, L., Morrison, B. and Min, W., Bioorthogonal chemical imaging of metabolic activities in live mammalian hippocampal tissues with stimulated Raman scattering. *Sci. Rep.*, **2016**, *6*.
196. Bandyopadhyay, S. and Bong, D., Synthesis of Trifunctional Phosphatidylserine Probes for Identification of Lipid-Binding Proteins. *Eur. J. Org. Chem.*, **2011**, (4), 751-758.
197. Best, M. D., Rowland, M. M. and Bostic, H. E., Exploiting Bioorthogonal Chemistry to Elucidate Protein-Lipid Binding Interactions and Other Biological Roles of Phospholipids. *Acc. Chem. Res.*, **2011**, *44*, (9), 686-698.
198. Peng, T. and Hang, H. C., Bifunctional Fatty Acid Chemical Reporter for Analyzing S-Palmitoylated Membrane Protein-Protein Interactions in Mammalian Cells. *J. Am. Chem. Soc.*, **2015**, *137*, (2), 556-559.
199. Weisbrod, S. H. and Marx, A., Novel strategies for the site-specific covalent labelling of nucleic acids. *Chem. Commun.*, **2008**, (44), 5675-5685.
200. El-Sagheer, A. H. and Brown, T., Click chemistry with DNA. *Chem. Soc. Rev.*, **2010**, *39*, (4), 1388-1405.
201. Seo, T. S., Li, Z. M., Ruparel, H. and Ju, J. Y., Click chemistry to construct fluorescent oligonucleotides for DNA sequencing. *J. Org. Chem.*, **2003**, *68*, (2), 609-612.
202. Salic, A. and Mitchison, T. J., A chemical method for fast and sensitive detection of DNA synthesis in vivo. *Proc. Natl. Acad. Sci. U.S.A.*, **2008**, *105*, (7), 2415-2420.
203. Jao, C. Y. and Salic, A., Exploring RNA transcription and turnover in vivo by using click chemistry. *Proc. Natl. Acad. Sci. U.S.A.*, **2008**, *105*, (41), 15779-15784.
204. Merkel, M., Peewasan, K., Arndt, S., Ploschik, D. and Wagenknecht, H. A., Copper-Free Postsynthetic Labeling of Nucleic Acids by Means of Bioorthogonal Reactions. *ChemBioChem*, **2015**, *16*, (11), 1541-1553.

205. Qiao, X., Ding, S., Liu, F., Kucera, G. L. and Bierbach, U., Investigating the cellular fate of a DNA-targeted platinum-based anticancer agent by orthogonal double-click chemistry. *J. Biol. Inorg. Chem.*, **2014**, *19*, (3), 415-426.
206. Marks, I. S., Kang, J. S., Jones, B. T., Landmark, K. J., Cleland, A. J. and Taton, T. A., Strain-Promoted "Click" Chemistry for Terminal Labeling of DNA. *Bioconjugate Chem.*, **2011**, *22*, (7), 1259-1263.
207. Egloff, D., Oleinich, I. A., Zhao, M., Konig, S. L. B., Sigel, R. K. O. and Freisinger, E., Sequence-Specific Post-Synthetic Oligonucleotide Labeling for Single-Molecule Fluorescence Applications. *ACS Chem. Biol.*, **2016**, *11*, (9), 2558-2567.
208. Krasutsky, S. G., Urbansky, M., Davis, C. E., Lherbet, C., Coates, R. M. and Poulter, C. D., Synthesis of Methylerythritol Phosphate Analogues and Their Evaluation as Alternate Substrates for IspDF and IspE from *Agrobacterium tumefaciens*. *J. Org. Chem.*, **2014**, *79*, (19), 9170-9178.
209. Robinson, T. V., Pedersen, D. S., Taylor, D. K. and Tiekink, E. R. T., Dihydroxylation of 4-Substituted 1,2-Dioxines: A Concise Route to Branched Erythro Sugars. *J. Org. Chem.*, **2009**, *74*, (14), 5093-5096.
210. Hoeffler, J. F., Grosdemange-Billiard, C. and Rohmer, M., Synthesis of tritium labelled 2-C-methyl-D-erythritol, a useful substrate for the elucidation of the methylerythritol phosphate pathway for isoprenoid biosynthesis. *Tetrahedron Lett.*, **2000**, *41*, (25), 4885-4889.
211. Hoeffler, J. F., Pale-Grosdemange, C. and Rohmer, M., Chemical synthesis of enantiopure 2-C-methyl-D-erythritol 4-phosphate, the key intermediate in the mevalonate-independent pathway for isoprenoid biosynthesis. *Tetrahedron*, **2000**, *56*, (11), 1485-1489.
212. Koppisch, A. T., Blagg, B. S. J. and Poulter, C. D., Synthesis of 2-C-methyl-D-erythritol 4-phosphate: The first pathway-specific intermediate in the methylerythritol phosphate route to isoprenoids. *Org. Lett.*, **2000**, *2*, (2), 215-217.

213. Urbansky, M., Davis, C. E., Surjan, J. D. and Coates, R. M., Synthesis of Enantiopure 2-C-Methyl-d-erythritol 4-Phosphate and 2,4-Cyclodiphosphate from d-Arabitol. *Org. Lett.*, **2004**, 6, (1), 135-138.
214. Lagisetti, C., Urbansky, M. and Coates, R. M., The Dioxanone Approach to (2S,3R)-2-C-Methylerythritol 4-Phosphate and 2,4-Cyclodiphosphate, and Various MEP Analogues. *J. Org. Chem.*, **2007**, 72, (26), 9886-9895.
215. Haskins, W. T., Hann, R. M. and Hudson, C. S., The Isomeric 1,3- and 2,3-Benzylidene-D-arabitol. *J. Am. Chem. Soc.*, **1943**, 65, (9), 1663-1667.
216. Aggarwal, V. K., Gultekin, Z., Grainger, R. S., Adams, H. and Spargo, P. L., (1R,3R)-2-methylene-1,3-dithiolane 1,3-dioxide: a highly reactive and highly selective chiral ketene equivalent in cycloaddition reactions with a broad range of dienes. *J. Chem. Soc. Perkin Trans. I*, **1998**, (17), 2771-2781.
217. Degoricija, L., Carnahan, M. A., Johnson, C. S., Kim, T. and Grinstaff, M. W., Synthesis and characterization of bola-type amphiphilic dendritic macromolecules. *Macromolecules*, **2006**, 39, (26), 8952-8958.
218. Akita, H., Nozawa, M. and Shimizu, H., Synthesis of decalin type chiral synthons based on enzymatic functionalisation and their application to the synthesis of (-)-ambrox and (+)-zonarol. *Tetrahedron-Asymmetry*, **1998**, 9, (10), 1789-1799.
219. Jiang, J., Kuo, C.-L., Wu, L., Franke, C., Kallemeijn, W. W., Florea, B. I., van Meel, E., van der Marel, G. A., Codée, J. D. C., Boot, R. G., Davies, G. J., Overkleeft, H. S. and Aerts, J. M. F. G., Detection of Active Mammalian GH31  $\alpha$ -Glucosidases in Health and Disease Using In-Class, Broad-Spectrum Activity-Based Probes. *ACS Cent. Sci.*, **2016**, 2, (5), 351-358.
220. Corey, E. J. and Link, J. O., A General, Catalytic, and Enantioselective Synthesis of Alpha-Amino-Acids. *J. Am. Chem. Soc.*, **1992**, 114, (5), 1906-1908.
221. Arai, N., Onodera, N. and Ohkuma, T., Efficient chemoselective hydrogenation of organic azides catalyzed by palladium nanoparticles with alkyne-derived homogeneous supports. *Tetrahedron Lett.*, **2016**, 57, (37), 4183-4186.

222. Sello, G., Orsini, F., Bernasconi, S. and Di Gennaro, P., Synthesis of enantiopure 2-amino-1-phenyl and 2-amino-2-phenyl ethanols using enantioselective enzymatic epoxidation and regio- and diastereoselective chemical aminolysis. *Tetrahedron-Asymmetry*, **2006**, *17*, (3), 372-376.
223. Gallien, S., Perrodou, E., Carapito, C., Deshayes, C., Reyrat, J.-M., Van Dorsselaer, A., Poch, O., Schaeffer, C. and Lecompte, O., Ortho-proteogenomics: Multiple proteomes investigation through orthology and a new MS-based protocol. *Genome. Res.*, **2009**, *19*, (1), 128-135.
224. Bertaccini, D., Vaca, S., Carapito, C., Arsène-Ploetze, F., Van Dorsselaer, A. and Schaeffer-Reiss, C., An Improved Stable Isotope N-Terminal Labeling Approach with Light/Heavy TMPP To Automate Proteogenomics Data Validation: dN-TOP. *J. Proteome. Res.*, **2013**, *12*, (6), 3063-3070.
225. Huang, Z.-H., Wu, J., Roth, K. D. W., Yang, Y., Gage, D. A. and Watson, J. T., A Picomole-Scale Method for Charge Derivatization of Peptides for Sequence Analysis by Mass Spectrometry. *Anal. Chem.*, **1997**, *69*, (2), 137-144.
226. Huang, Z.-H., Shen, T., Wu, J., Gage, D. A. and Watson, J. T., Protein Sequencing by Matrix-Assisted Laser Desorption Ionization–Postsource Decay–Mass Spectrometry Analysis of the N-Tris(2,4,6-trimethoxyphenyl)phosphine-Acetylated Tryptic Digests. *Anal. Biochem.*, **1999**, *268*, (2), 305-317.
227. Wada, M. and Higashizaki, S., A highly basic triphenylphosphine, [2,4,6-(MeO)3C6H2]3P. *J. Chem. Soc., Chem. Commun.*, **1984**, (7), 482-483.
228. Dommerholt, J., Schmidt, S., Temming, R., Hendriks, L. J. A., Rutjes, F. P. J. T., van Hest, J. C. M., Lefeber, D. J., Friedl, P. and van Delft, F. L., Readily Accessible Bicyclononynes for Bioorthogonal Labeling and Three-Dimensional Imaging of Living Cells. *Angew. Chem. Int. Ed.*, **2010**, *49*, (49), 9422-9425.
229. Polson, C., Sarkar, P., Incledon, B., Raguvaran, V. and Grant, R., Optimization of protein precipitation based upon effectiveness of protein removal and ionization effect in liquid chromatography-tandem mass spectrometry. *J. Chromatogr. B*, **2003**, *785*, (2), 263-275.

230. Luo, B., Groenke, K., Takors, R., Wandrey, C. and Oldiges, M., Simultaneous determination of multiple intracellular metabolites in glycolysis, pentose phosphate pathway and tricarboxylic acid cycle by liquid chromatography–mass spectrometry. *J. Chromatogr. A*, **2007**, *1147*, (2), 153-164.
231. Henneman, L., van Cruchten, A. G., Denis, S. W., Amolins, M. W., Placzek, A. T., Gibbs, R. A., Kulik, W. and Waterham, H. R., Detection of nonsterol isoprenoids by HPLC–MS/MS. *Anal. Biochem.*, **2008**, *383*, (1), 18-24.
232. Burke, R. M., Pearce, J. K., Boxford, W. E., Bruckmann, A. and Dessent, C. E. H., Stabilization of excess charge in isolated adenosine 5'-triphosphate and adenosine 5'-diphosphate multiply and singly charged anions. *J. Phys. Chem. A*, **2005**, *109*, (43), 9775-9785.
233. Jauhainen, M., Mönkkönen, H., Räikkönen, J., Mönkkönen, J. and Auriola, S., Analysis of endogenous ATP analogs and mevalonate pathway metabolites in cancer cell cultures using liquid chromatography–electrospray ionization mass spectrometry. *J. Chromatogr. B*, **2009**, *877*, (27), 2967-2975.
234. Van, T. N. and De Kimpe, N., New Synthesis of the Alkaloid Polonicumtoxin C. *Tetrahedron*, **2000**, *56*, (40), 7969-7973.
235. Gagneux, A., Winstein, S. and Young, W. G., Rearrangement of allylic azides. *J. Am. Chem. Soc.*, **1960**, *82*, (22), 5956-5957.
236. Trost, B. M. and Pulley, S. R., On the Flexibility of Allylic Azides as Synthetic Intermediates. *Tetrahedron Lett.*, **1995**, *36*, (48), 8737-8740.
237. Feldman, A. K., Colasson, B., Sharpless, K. B. and Fokin, V. V., The allylic azide rearrangement: Achieving selectivity. *J. Am. Chem. Soc.*, **2005**, *127*, (39), 13444-13445.
238. Testa, C. A., Cornish, R. A. and Poulter, C. D., The sorbitol phosphotransferase system is responsible for transport of 2-C-methyl-D-erythritol into *Salmonella enterica* serovar typhimurium. *J. Bacteriol.*, **2004**, *186*, (2), 473-480.
239. Michaelis, L. and Menten, M., L., Die kinetik der invertinwirkung. *Biochem. Z.*, **1913**, *49*, 333-369.

240. Johnson, K. A. and Goody, R. S., The Original Michaelis Constant: Translation of the 1913 Michaelis-Menten Paper. *Biochemistry.*, **2011**, *50*, (39), 8264-8269.
241. Henri, V., *Lois générales de l'action des diastases*. Hermann: Paris, 1903.
242. Briggs, G. E. and Haldane, J. B., A Note on the Kinetics of Enzyme Action. *Biochem. J.*, **1925**, *19*, (2), 338-9.
243. Chang, R., *Physical Chemistry for the Biosciences*. University Science Books. USA: 2005.
244. Cleland, W. W., The kinetics of enzyme-catalyzed reactions with two or more substrates or products. I. Nomenclature and rate equations. *Biochim. Biophys. Acta*, **1963**, *67*, 104-37.
245. Cleland, W. W., The kinetics of enzyme-catalyzed reactions with two or more substrates or products. II. Inhibition: nomenclature and theory. *Biochim. Biophys. Acta*, **1963**, *67*, 173-87.
246. Copeland, R. A., Evaluation of enzyme inhibitors in drug discovery. A guide for medicinal chemists and pharmacologists. *Methods Biochem. Anal.*, **2005**, *46*, 1-265.
247. Corey, E. J. and Chaykovsky, M., Dimethyloxosulfonium Methylide ((CH<sub>3</sub>)<sub>2</sub>SOCH<sub>2</sub>) and Dimethylsulfonium Methylide ((CH<sub>3</sub>)<sub>2</sub>SCH<sub>2</sub>). Formation and Application to Organic Synthesis. *J. Am. Chem. Soc.*, **1965**, *87*, (6), 1353-1364.
248. Corey, E. J. and Chaykovsky, M., Concerning the reaction of sulfonium methylides with conjugated carbonyl compounds. *Tetrahedron Lett.*, **1963**, *4*, (4), 169-171.
249. Corey, E. and Chaykovsky, M., Dimethylsulfoxonium methylide. *J. Am. Chem. Soc.*, **1962**, *84*, (5), 867-868.
250. Błażewska, K. M., McKenna Reaction—Which Oxygen Attacks Bromotrimethylsilane? *J. Org. Chem.*, **2014**, *79*, (1), 408-412.
251. Bernal, C., Palacin, C., Boronat, A. and Imperial, S., A colorimetric assay for the determination of 4-diphosphocytidyl-2-C-methyl-d-erythritol 4-phosphate synthase activity. *Anal. Biochem.*, **2005**, *337*, (1), 55-61.

252. Soyenkoff, B., A micromethod of phosphate determination. *J. Biol. Chem.*, **1947**, *168*, (2), 447-457.
253. Itaya, K. and Ui, M., A new micromethod for the colorimetric determination of inorganic phosphate. *Clin. Chim. Acta*, **1966**, *14*, (3), 361-366.
254. Carter, S. G. and Karl, D. W., Inorganic phosphate assay with malachite green: An improvement and evaluation. *J. Biochem. Bioph. Methods*, **1982**, *7*, (1), 7-13.
255. Baykov, A. A., Evtushenko, O. A. and Avaeva, S. M., A malachite green procedure for orthophosphate determination and its use in alkaline phosphatase-based enzyme immunoassay. *Anal. Biochem.*, **1988**, *171*, (2), 266-270.
256. Van Veldhoven, P. P. and Mannaerts, G. P., Inorganic and organic phosphate measurements in the nanomolar range. *Anal. Biochem.*, **1987**, *161*, (1), 45-48.
257. Cogan, E. B., Birrell, G. B. and Griffith, O. H., A Robotics-Based Automated Assay for Inorganic and Organic Phosphates. *Anal. Biochem.*, **1999**, *271*, (1), 29-35.
258. Hill, G. A. and Robinson, C. W., Substrate Inhibition Kinetics - Phenol Degradation by *Pseudomonas-Putida*. *Biotechnol. Bioeng.*, **1975**, *17*, (11), 1599-1615.
259. Daugulis, A. J. and Swaine, D. E., Examination of Substrate and Product Inhibition-Kinetics on the Production of Ethanol by Suspended and Immobilized Cell Reactors. *Biotechnol. Bioeng.*, **1987**, *29*, (5), 639-645.
260. Furman, P. A., Painter, G., Wilson, J. E., Cheng, N. and Hopkins, S., Substrate-Inhibition of the Human-Immunodeficiency-Virus Type-1 Reverse-Transcriptase. *Proc. Natl. Acad. Sci. U.S.A.*, **1991**, *88*, (14), 6013-6017.
261. Segel, I. H., *Enzyme kinetics : Behavior and Analysis of Rapid Equilibrium and Steady State Enzyme Systems*. Wiley: New York, 1975.
262. Kemp, L. E., Bond, C. S. and Hunter, W. N., Structure of a tetragonal crystal form of *Escherichia coli* 2-C-methyl-D-erythritol 4-phosphate cytidyltransferase. *Acta. Crystallogr. Sec. D. Biol. Crystallogr.*, **2003**, *59*, 607-610.

263. Witschel, M. C., Hoffken, H. W., Seet, M., Parra, L., Mietzner, T., Thater, F., Niggeweg, R., Rohl, F., Illarionov, B., Rohdich, F., Kaiser, J., Fischer, M., Bacher, A. and Diederich, F., Inhibitors of the Herbicidal Target IspD: Allosteric Site Binding. *Angew. Chem. Int. Ed.*, **2011**, *50*, (34), 7931-7935.
264. Witschel, M., Rohl, F., Niggeweg, R. and Newton, T., In search of new herbicidal inhibitors of the non-mevalonate pathway. *Pest Manag. Sci.*, **2013**, *69*, (5), 559-563.
265. Kunfermann, A., Witschel, M., Illarionov, B., Martin, R., Rottmann, M., Hoffken, H. W., Seet, M., Eisenreich, W., Knolker, H. J., Fischer, M., Bacher, A., Groll, M. and Diederich, F., Pseudilins: Halogenated, Allosteric Inhibitors of the Non-Mevalonate Pathway Enzyme IspD. *Angew. Chem. Int. Ed.*, **2014**, *53*, (8), 2235-2239.
266. Gao, P., Yang, Y. H., Xiao, C. L., Liu, Y. S., Gan, M. L., Guan, Y., Hao, X. Q., Meng, J. Z., Zhou, S., Chen, X. J. and Cui, J. F., Identification and validation of a novel lead compound targeting 4-diphosphocytidyl-2-C-methylerythritol synthetase (IspD) of mycobacteria. *Eur. J. Pharmacol.*, **2012**, *694*, (1-3), 45-52.
267. Fernandes, J. F., Lell, B., Agnandji, S. T., Obiang, R. M., Bassat, Q., Kremsner, P. G., Mordmüller, B. and Grobusch, M. P., Fosmidomycin as an antimalarial drug: a meta-analysis of clinical trials. *Future Microbiol.*, **2015**, *10*, (8), 1375-1390.
268. Zhang, B., Watts, K. M., Hodge, D., Kemp, L. M., Hunstad, D. A., Hicks, L. M. and Odom, A. R., A second target of the antimalarial and antibacterial agent fosmidomycin revealed by cellular metabolic profiling. *Biochemistry*, **2011**, *50*, (17), 3570-7.
269. Yung-Chi, C. and Prusoff, W. H., Relationship between the inhibition constant (KI) and the concentration of inhibitor which causes 50 per cent inhibition (I50) of an enzymatic reaction. *Biochem. Pharmacol.*, **1973**, *22*, (23), 3099-3108.
270. Purich, D. L., *Enzyme Kinetics: Catalysis & Control, A Reference of Theory and Best-Practice Methods*. Academic Press, Elsevier: 2010.
271. Leventhal, P. S. and Bertics, P. J., Kinetic-Analysis of Protein-Kinase-C - Product and Dead-End Inhibition Studies Using Adp, Poly(L-Lysine), Nonhydrolyzable Atp Analogs, and Diadenosine Oligophosphates. *Biochemistry.*, **1991**, *30*, (5), 1385-1390.

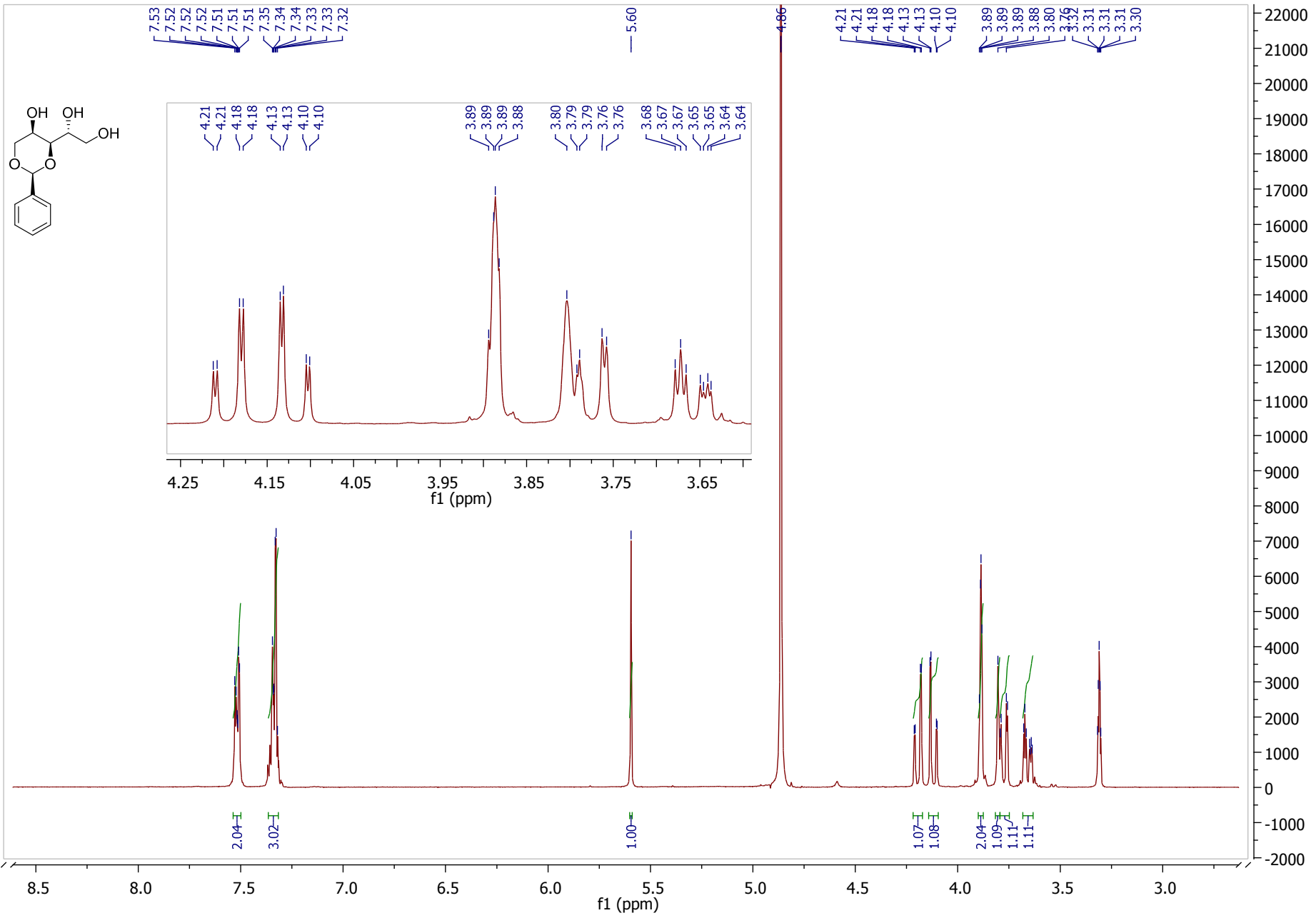
272. Northrop, D. B. and Cleland, W. W., The Kinetics of Pig Heart Triphosphopyridine Nucleotide-Isocitrate Dehydrogenase: II. Dead-end and multiple inhibition studies. *J. Biol. Chem.*, **1974**, *249*, (9), 2928-2931.
273. Bar-Tana, J. and Cleland, W. W., Rabbit Muscle Phosphofructokinase: II. Product and dead-end inhibition. *J. Biol. Chem.*, **1974**, *249*, (4), 1271-1276.
274. DeVita, V. T. and Chu, E., A History of Cancer Chemotherapy. *Cancer. Res.*, **2008**, *68*, (21), 8643-8653.
275. Adams, G. P. and Weiner, L. M., Monoclonal antibody therapy of cancer. *Nat. Biotechnol.*, **2005**, *23*, (9), 1147-1157.
276. Nicodemus, C. F. and Berek, J. S., Monoclonal antibody therapy of ovarian cancer. *Expert. Rev. Anticancer. Ther.*, **2005**, *5*, (1), 87-96.
277. Schalhorn, A., Monoclonal antibodies in cancers - Monoclonal antibodies in the therapy of advanced colorectal cancer. *Arzneimittel-Forschung-Drug Research*, **2005**, *55*, (11), 709-710.
278. Tsuchikama, K. and An, Z., Antibody-drug conjugates: recent advances in conjugation and linker chemistries. *Protein & Cell*, **2016**, 1-14.
279. Greenfield, R. S., Kaneko, T., Daves, A., Edson, M. A., Fitzgerald, K. A., Olech, L. J., Grattan, J. A., Spitalny, G. L. and Braslawsky, G. R., Evaluation *in Vitro* of Adriamycin Immunoconjugates Synthesized Using an Acid-sensitive Hydrazone Linker. *Cancer. Res.*, **1990**, *50*, (20), 6600-6607.
280. Rao N, V., Mane, S., Kishore, A., Das Sarma, J. and Shunmugam, R., Norbornene Derived Doxorubicin Copolymers as Drug Carriers with pH Responsive Hydrazone Linker. *Biomacromolecules*, **2012**, *13*, (1), 221-230.
281. Zhang, D. L., Pillow, T. H., Ma, Y., dela Cruz-Chuh, J., Kozak, K. R., Sadowsky, J. D., Philips, G. D. L., Guo, J., Darwish, M., Fan, P., Chen, J. T., He, C. R., Wang, T., Yao, H., Xu, Z. J., Chen, J. H., Wai, J., Pei, Z. H., Hop, C. E. C. A., Khojasteh, S. C. and Dragovich, P. S., Linker Immolation Determines Cell Killing Activity of Disulfide-

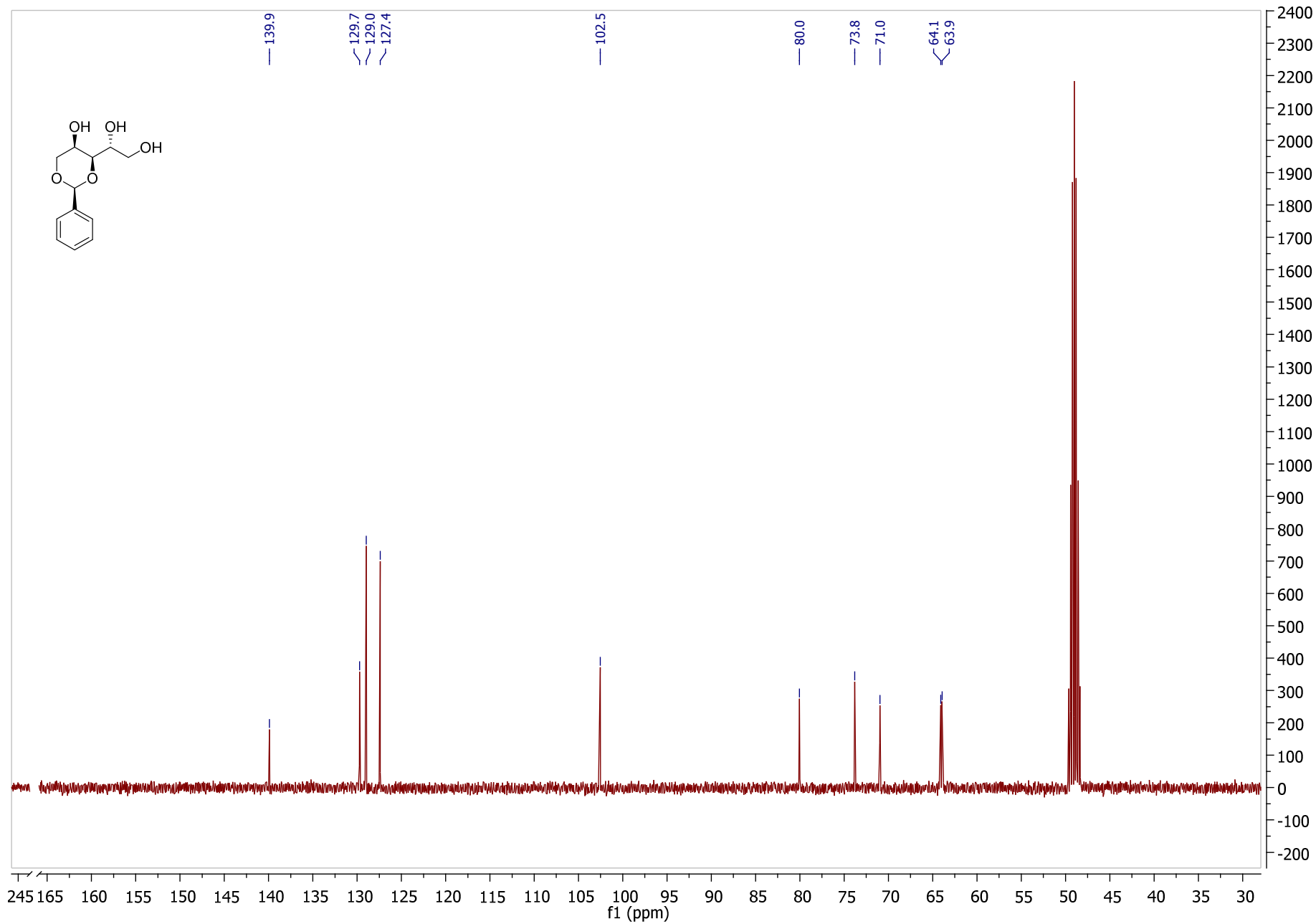
- Linked Pyrrolobenzodiazepine Antibody-Drug Conjugates. *ACS Med. Chem. Lett.*, **2016**, 7, (11), 988-993.
282. Kern, J. C., Cancilla, M., Dooney, D., Kwasnjuk, K., Zhang, R., Beaumont, M., Figueroa, I., Hsieh, S., Liang, L. D., Tomazela, D., Zhang, J., Brandish, P. E., Palmieri, A., Stivers, P., Cheng, M. G., Feng, G., Geda, P., Shah, S., Beck, A., Bresson, D., Firdos, J., Gately, D., Knudsen, N., Manibusan, A., Schultz, P. G., Sun, Y. and Garbaccio, R. M., Discovery of Pyrophosphate Diesters as Tunable, Soluble, and Bioorthogonal Linkers for Site-Specific Antibody-Drug Conjugates. *J. Am. Chem. Soc.*, **2016**, 138, (4), 1430-1445.
283. McCombs, J. R. and Owen, S. C., Antibody Drug Conjugates: Design and Selection of Linker, Payload and Conjugation Chemistry. *Aaps Journal*, **2015**, 17, (2), 339-351.
284. Cal, P. M. S. D., Bernardes, G. J. L. and Gois, P. M. P., Cysteine-Selective Reactions for Antibody Conjugation. *Angew. Chem. Int. Ed.*, **2014**, 53, (40), 10585-10587.
285. de Graaf, A. J., Kooijman, M., Hennink, W. E. and Mastrobattista, E., Nonnatural Amino Acids for Site-Specific Protein Conjugation. *Bioconjugate Chem.*, **2009**, 20, (7), 1281-1295.
286. Koniev, O., Leriche, G., Nothisen, M., Remy, J. S., Strub, J. M., Schaeffer-Reiss, C., Van Dorsselaer, A., Baati, R. and Wagner, A., Selective Irreversible Chemical Tagging of Cysteine with 3-Arylpropionitriles. *Bioconjugate Chem.*, **2014**, 25, (2), 202-206.
287. Zhou, K., Zou, R., Stephanopoulos, G. and Too, H.-P., Metabolite Profiling Identified Methylerythritol Cyclodiphosphate Efflux as a Limiting Step in Microbial Isoprenoid Production. *PLoS ONE*, **2012**, 7, (11), e47513.
288. Rivasseau, C., Seemann, M., Boisson, A.-M., Streb, P., Gout, E., Douce, R., Rohmer, M. and Bligny, R., Accumulation of 2-C-methyl-d-erythritol 2,4-cyclodiphosphate in illuminated plant leaves at supraoptimal temperatures reveals a bottleneck of the prokaryotic methylerythritol 4-phosphate pathway of isoprenoid biosynthesis. *Plant Cell Environ.*, **2009**, 32, (1), 82-92.
289. MongÉlard, G., Seemann, M., Boisson, A.-M., Rohmer, M., Bligny, R. and Rivasseau, C., Measurement of carbon flux through the MEP pathway for isoprenoid synthesis by <sup>31</sup>P-NMR spectroscopy after specific inhibition of 2-C-methyl-d-erythritol 2,4-

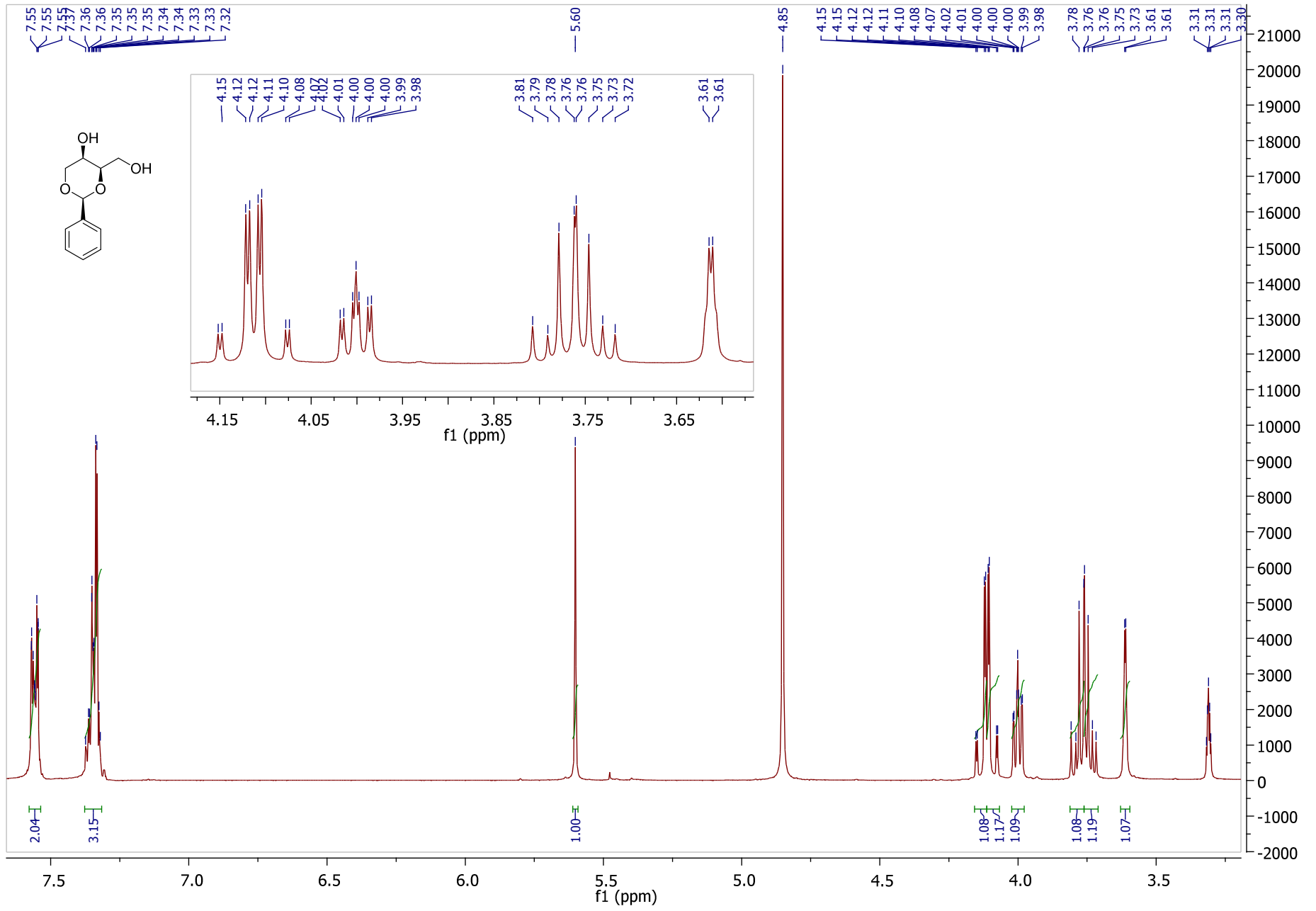
- cyclodiphosphate reductase. Effect of light and temperature. *Plant Cell Environ.*, **2011**, *34*, (8), 1241-1247.
290. Urbansky, M., Davis, C. E., Surjan, J. D. and Coates, R. M., Synthesis of Enantiopure 2-C-Methyl-d-erythritol 4-Phosphate and 2,4-Cyclodiphosphate from d-Arabitol. *Org. Lett.*, **2003**, *6*, (1), 135-138.
291. Swarbrick, J. M. and Gaffney, P. R. J., Synthesis of 4-C-Alkyl Inositol 1,4,5-Trisphosphates and 1,3,4,5-Tetrakisphosphates. *J. Org. Chem.*, **2010**, *75*, (13), 4376-4386.
292. Chelliah, M. V., Eagen, K., Guo, Z., Chackalamannil, S., Xia, Y., Tsai, H., Greenlee, W. J., Ahn, H.-S., Kurowski, S., Boykow, G., Hsieh, Y. and Chintala, M., Himbacine-Derived Thrombin Receptor Antagonists: C7-Spirocyclic Analogues of Vorapaxar. *ACS Medicinal Chemistry Letters*, **2014**, *5*, (5), 561-565.
293. Cao, Z., Zhang, L. and Jiang, S., Superhydrophilic Zwitterionic Polymers Stabilize Liposomes. *Langmuir*, **2012**, *28*, (31), 11625-11632.
294. Dunbar, K. R. and Haefner, S. C., Synthesis and properties of tris(2,4,6-trimethoxyphenyl)phosphine and tris(2,4,6-trimethoxyphenyl)phosphine oxide. *Polyhedron*, **1994**, *13*, (5), 727-736.
295. Isaacman, M. J., Corigliano, E. M. and Theogarajan, L. S., Stealth Polymeric Vesicles via Metal-Free Click Coupling. *Biomacromolecules*, **2013**, *14*, (9), 2996-3000.
296. Sa, M. M., Ramos, M. D. and Fernandes, L., Fast and efficient preparation of Baylis-Hillman-derived (E)-allylic azides and related compounds in aqueous medium. *Tetrahedron*, **2006**, *62*, (50), 11652-11656.
297. de Almeida, G., Sletten, E. M., Nakamura, H., Palaniappan, K. K. and Bertozzi, C. R., Thiacycloalkynes for Copper-Free Click Chemistry. *Angew. Chem. Int. Ed.*, **2012**, *51*, (10), 2443-2447.

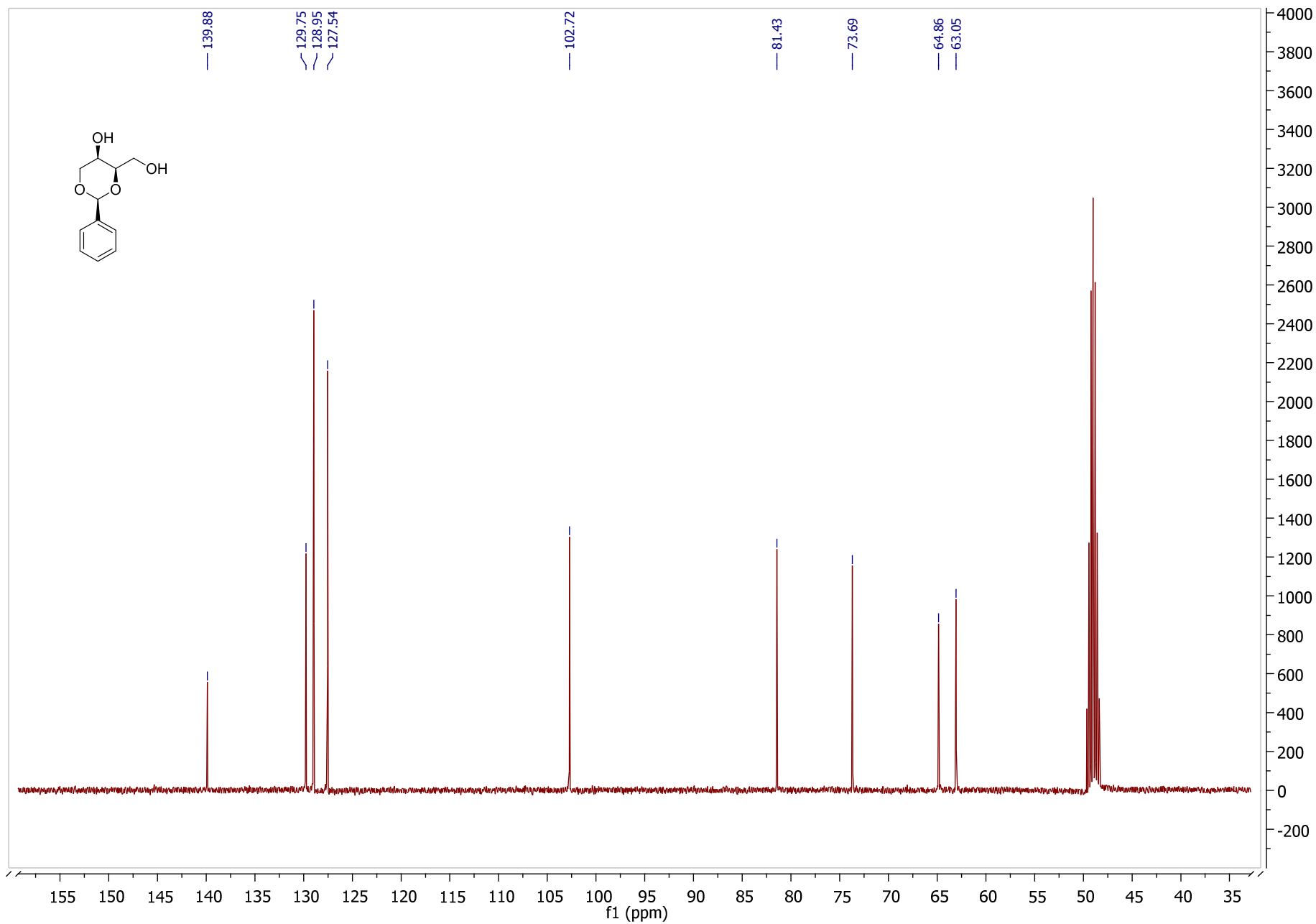
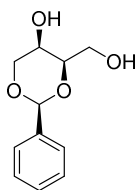
# Appendix

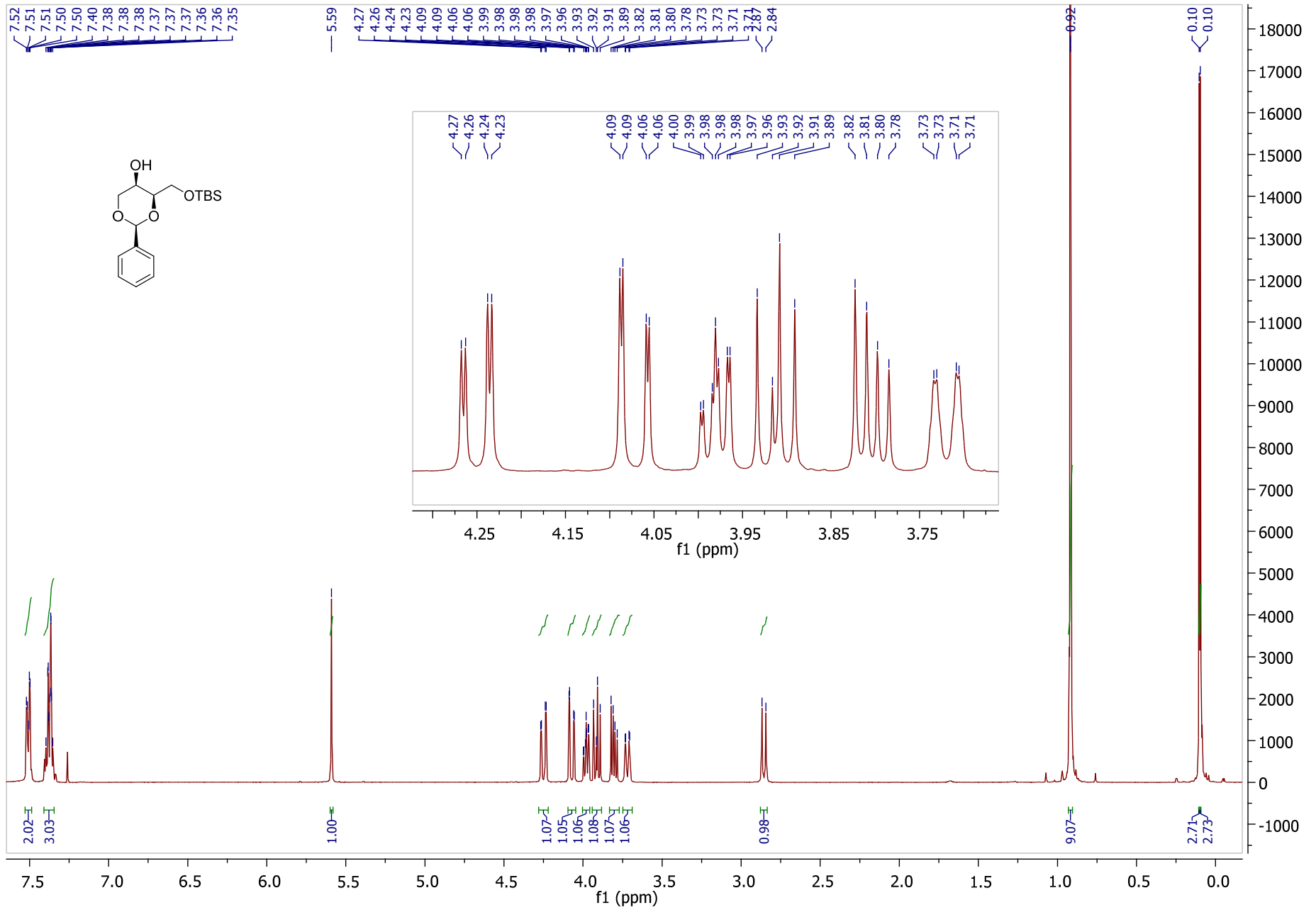
$^1\text{H}$ ,  $^{13}\text{C}$ ,  $^{31}\text{P}$  Spectras

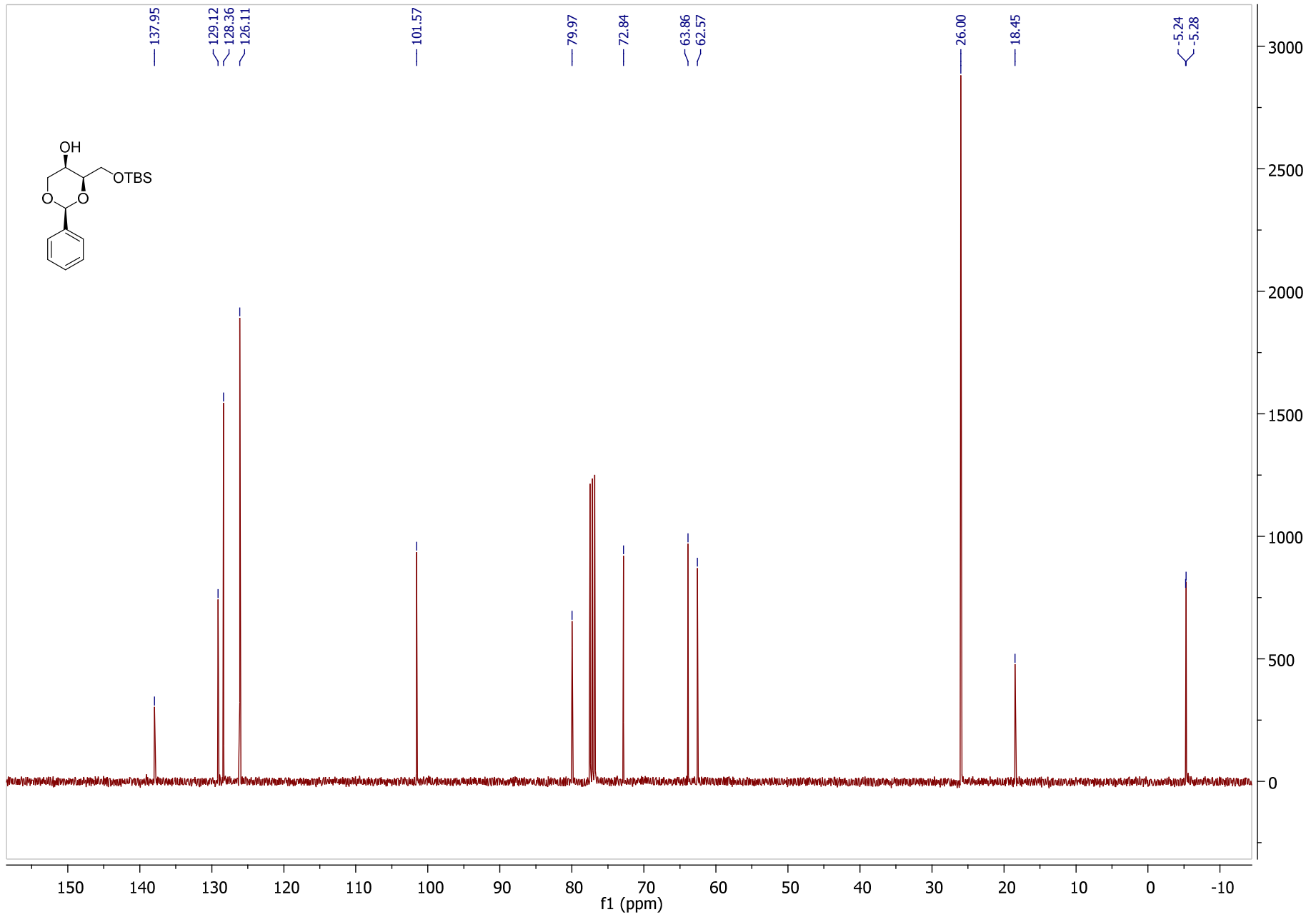
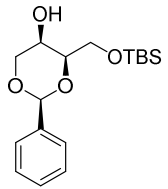


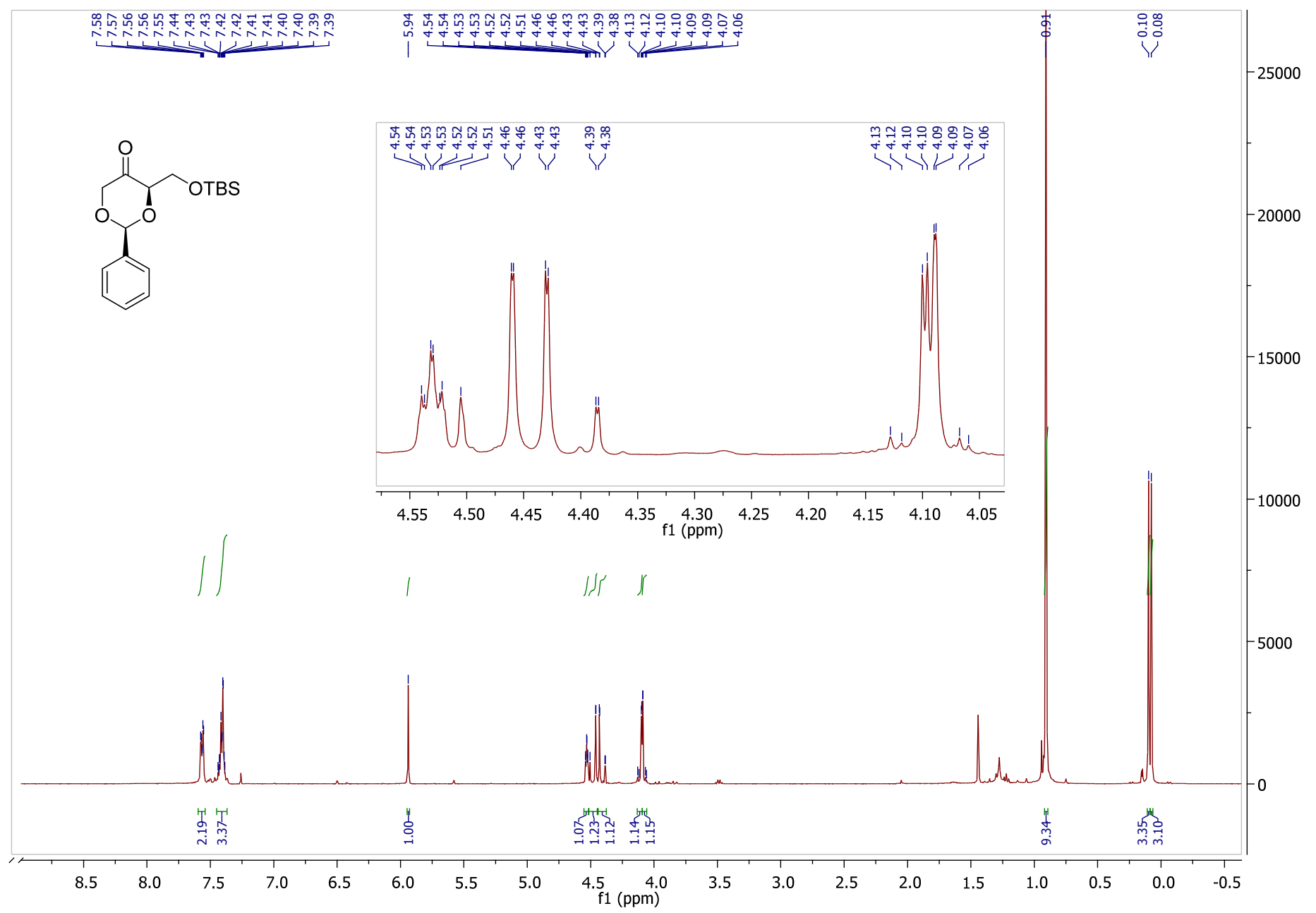
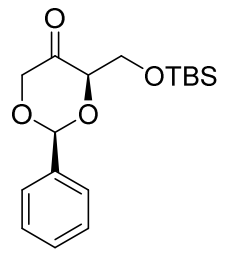


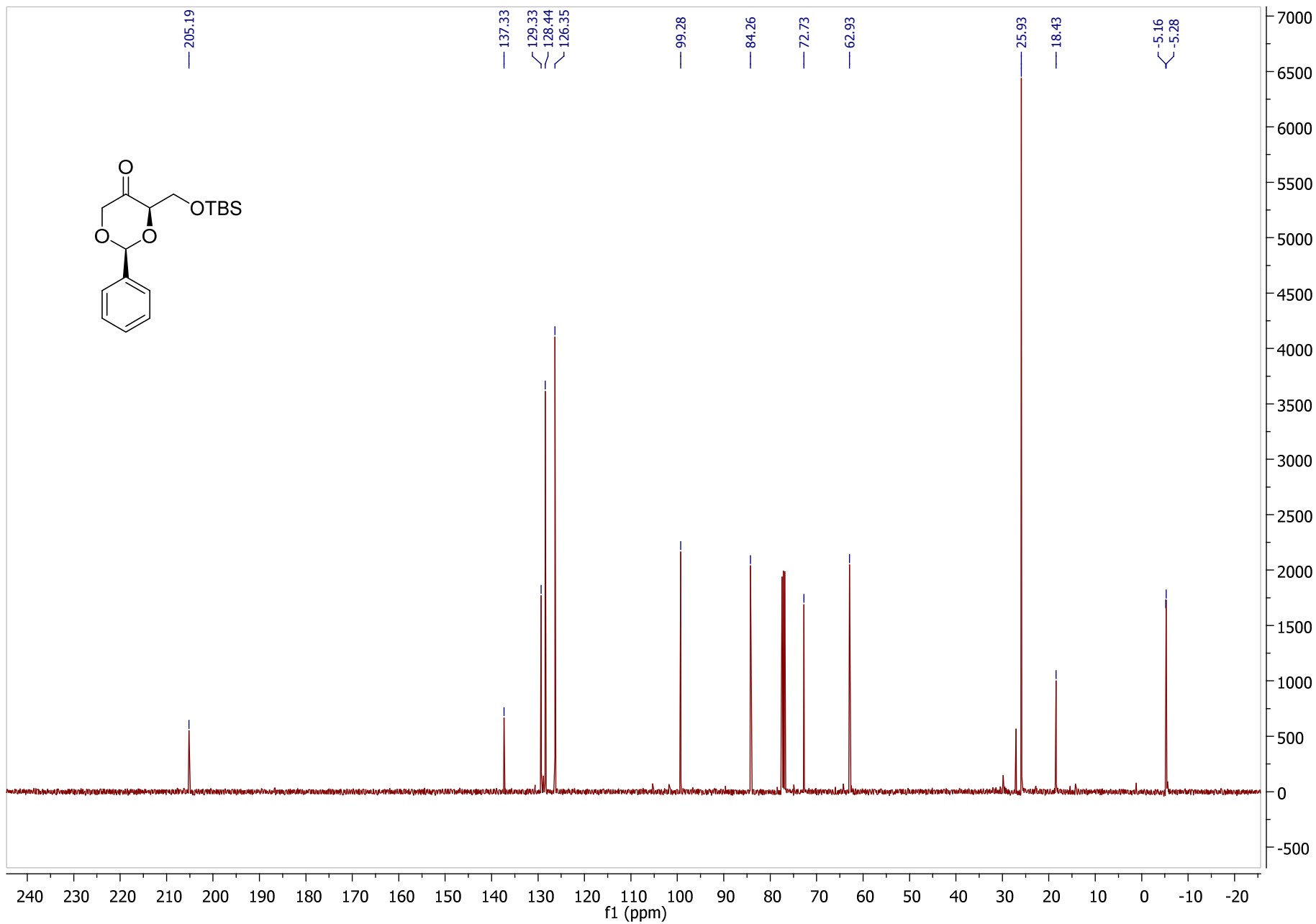
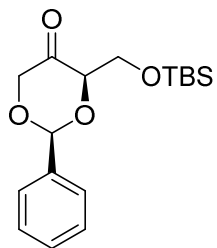


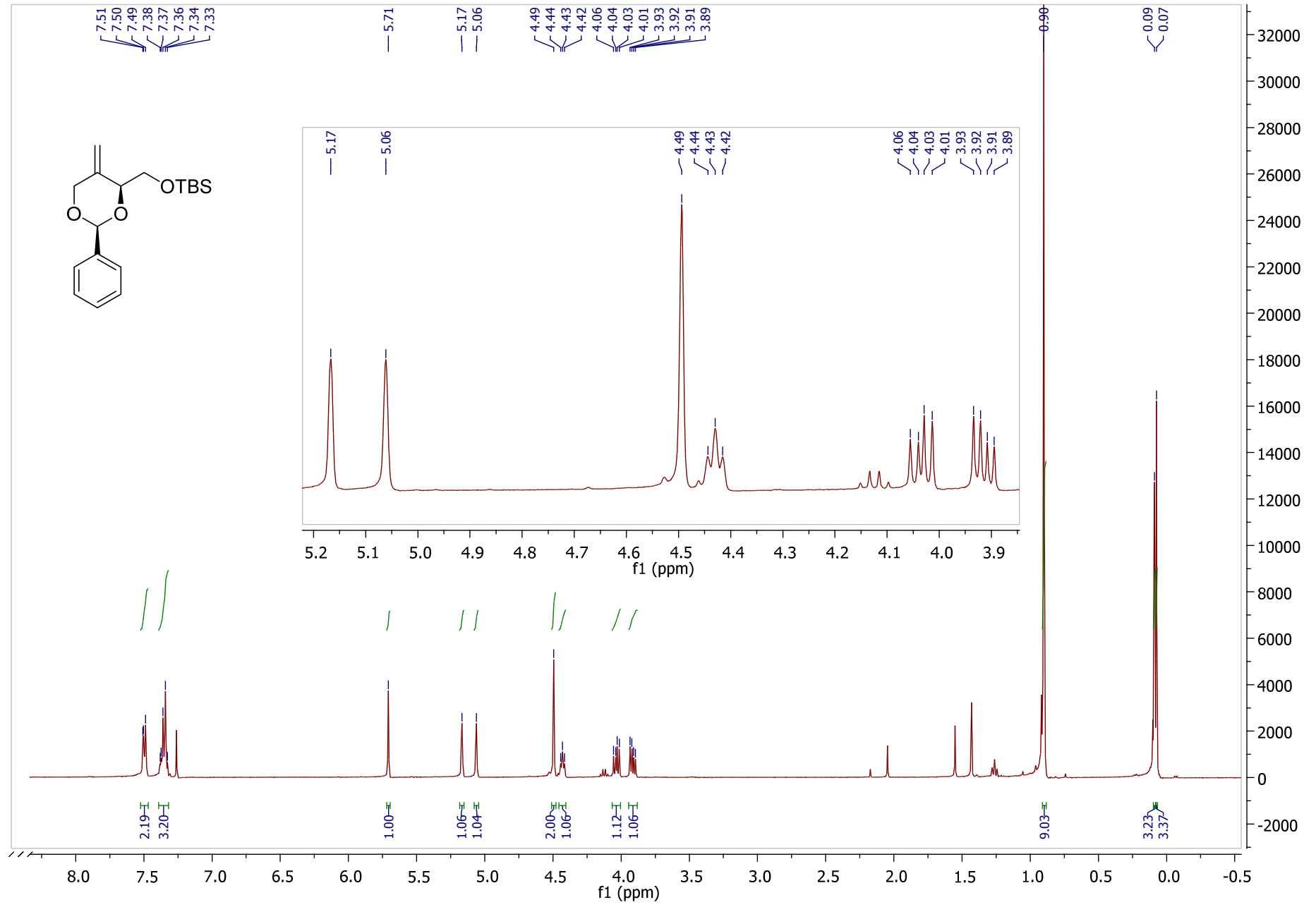
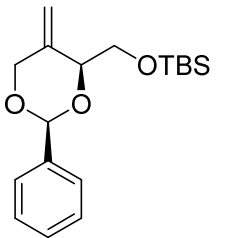


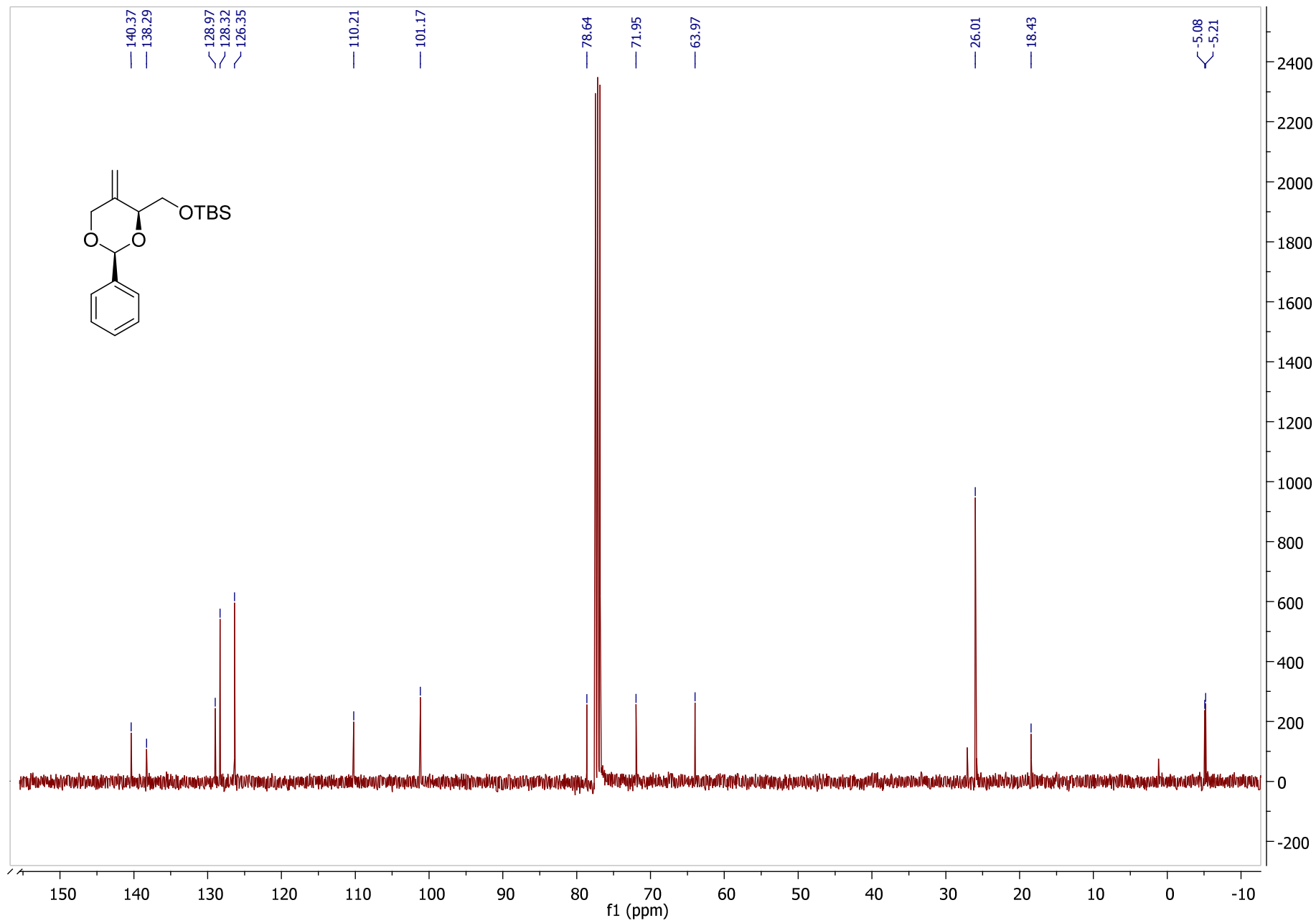


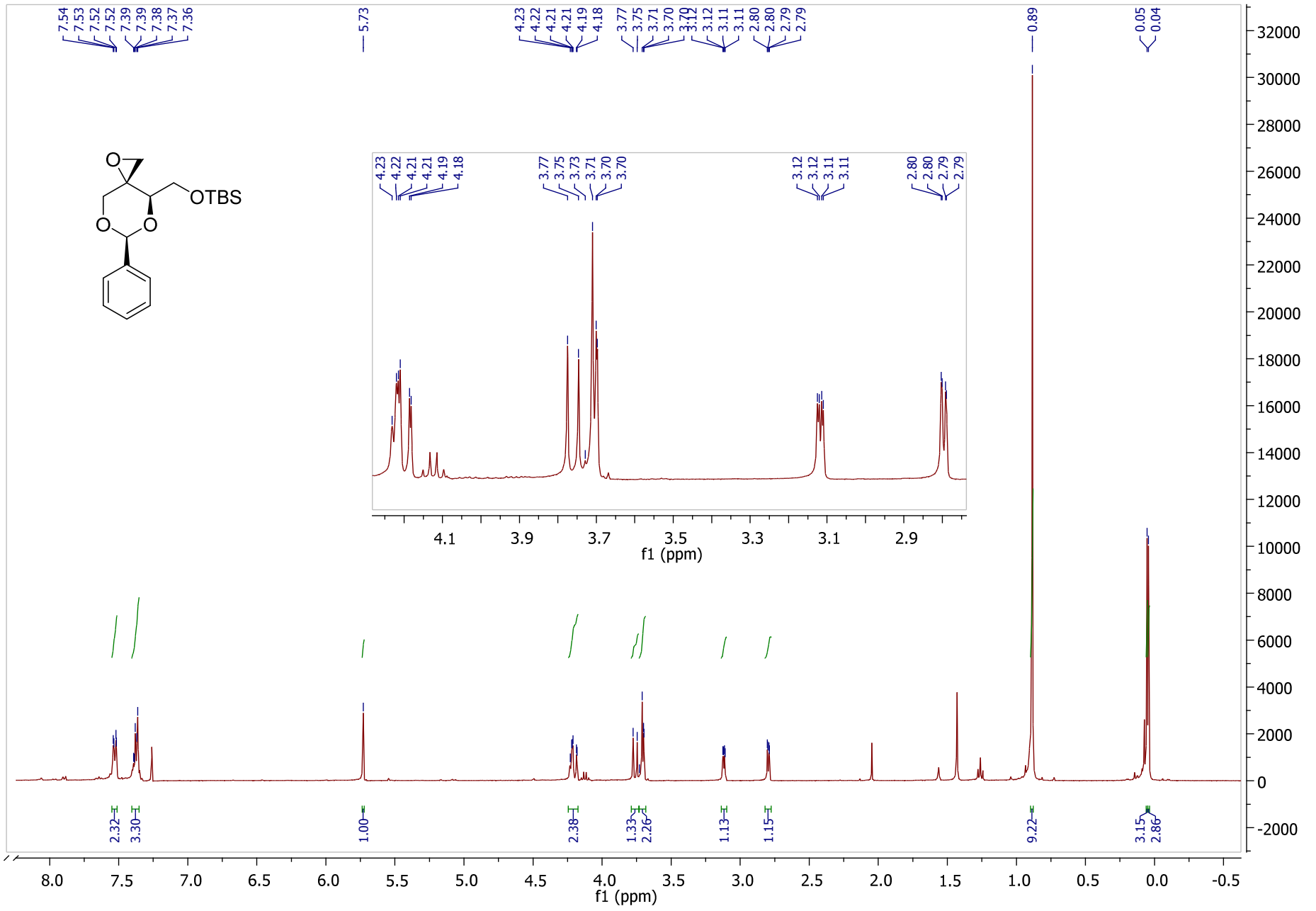


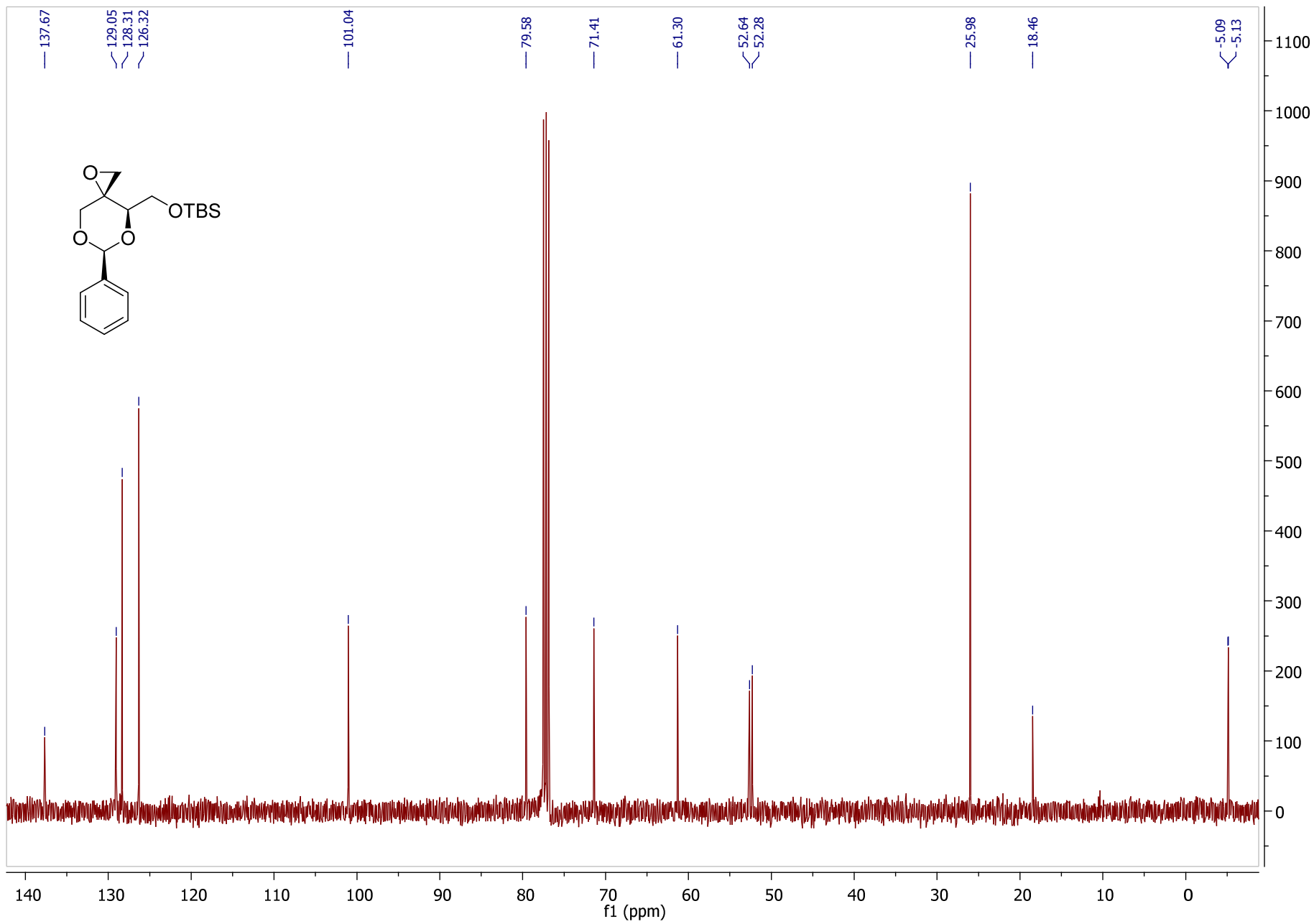


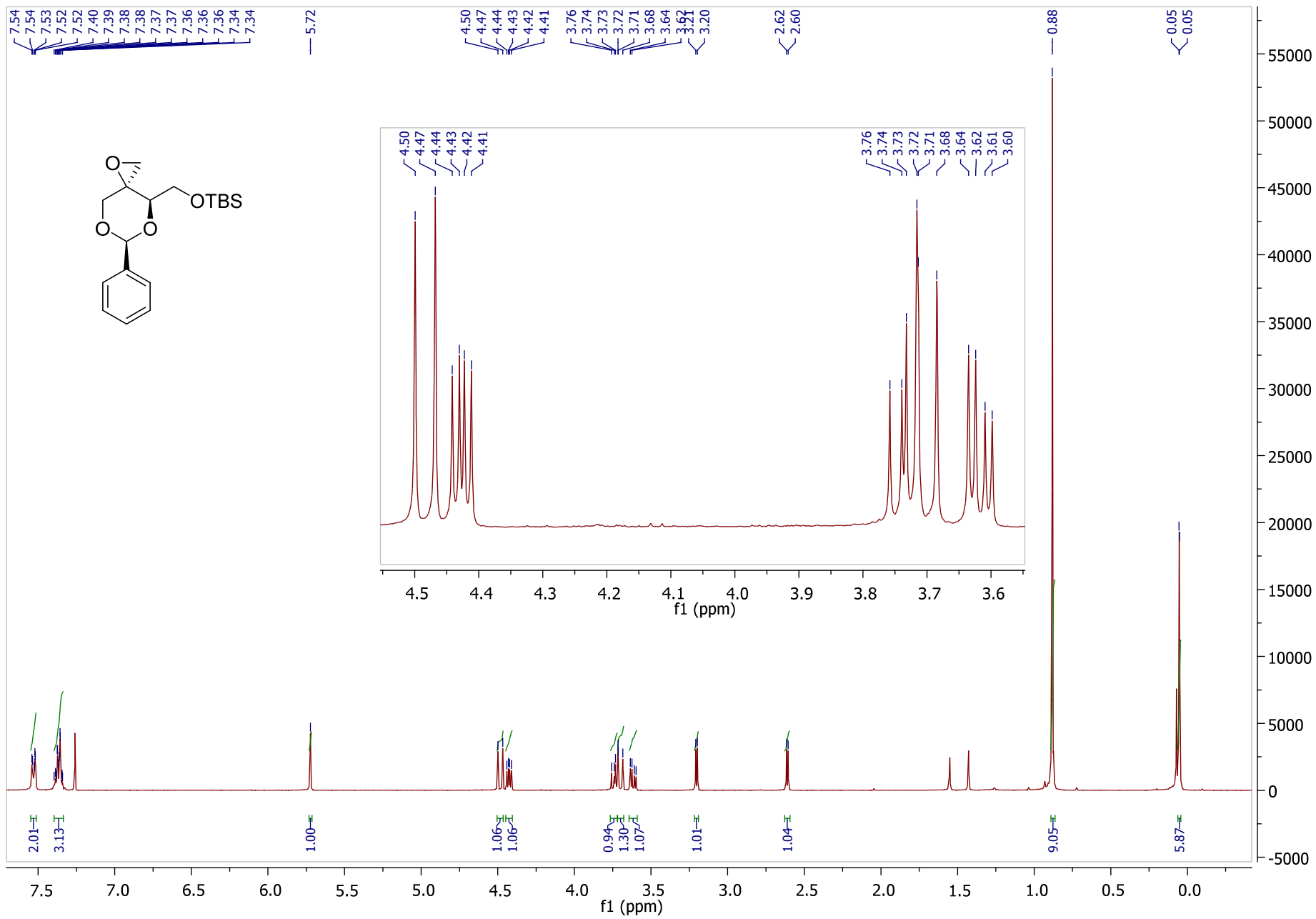


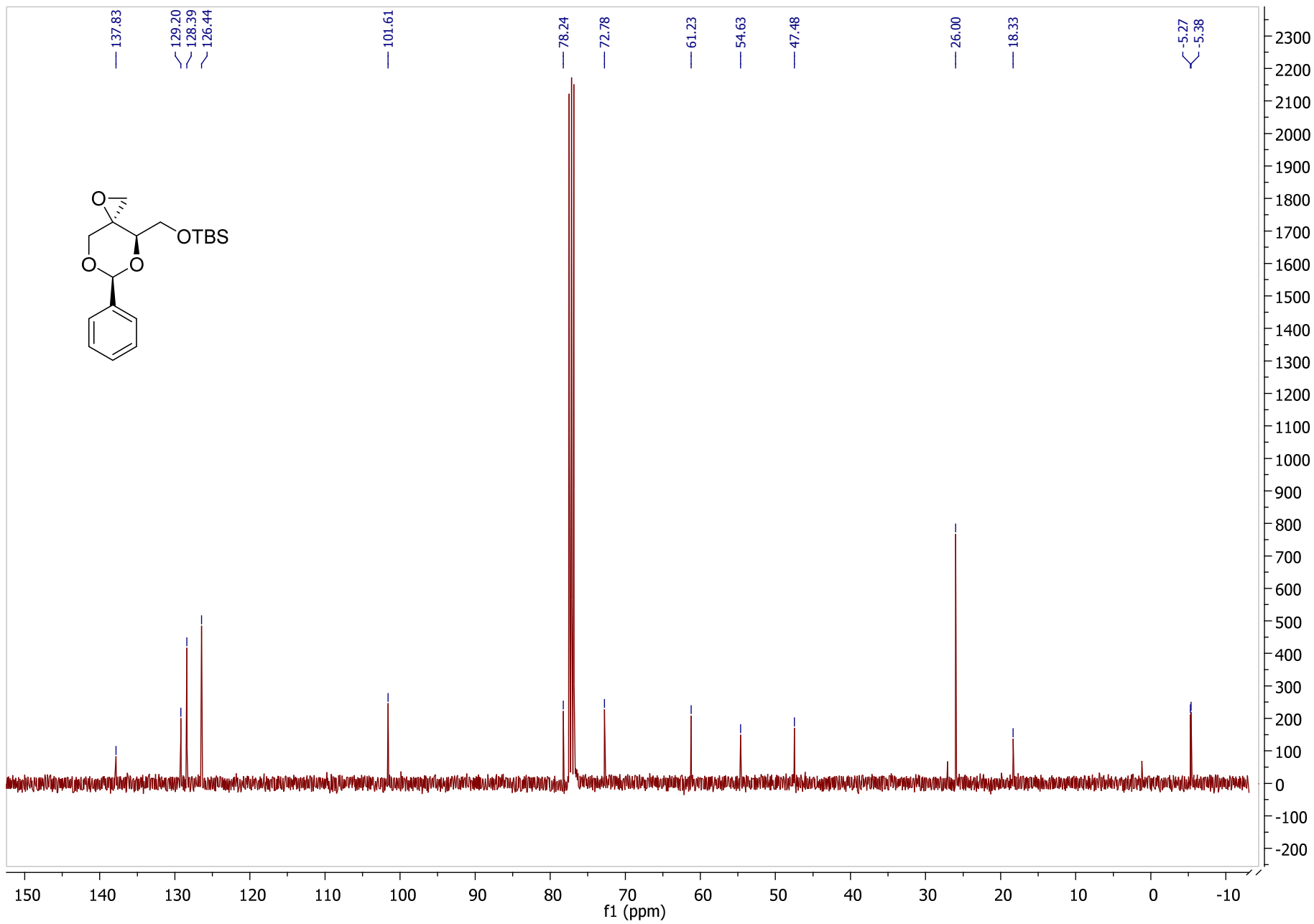


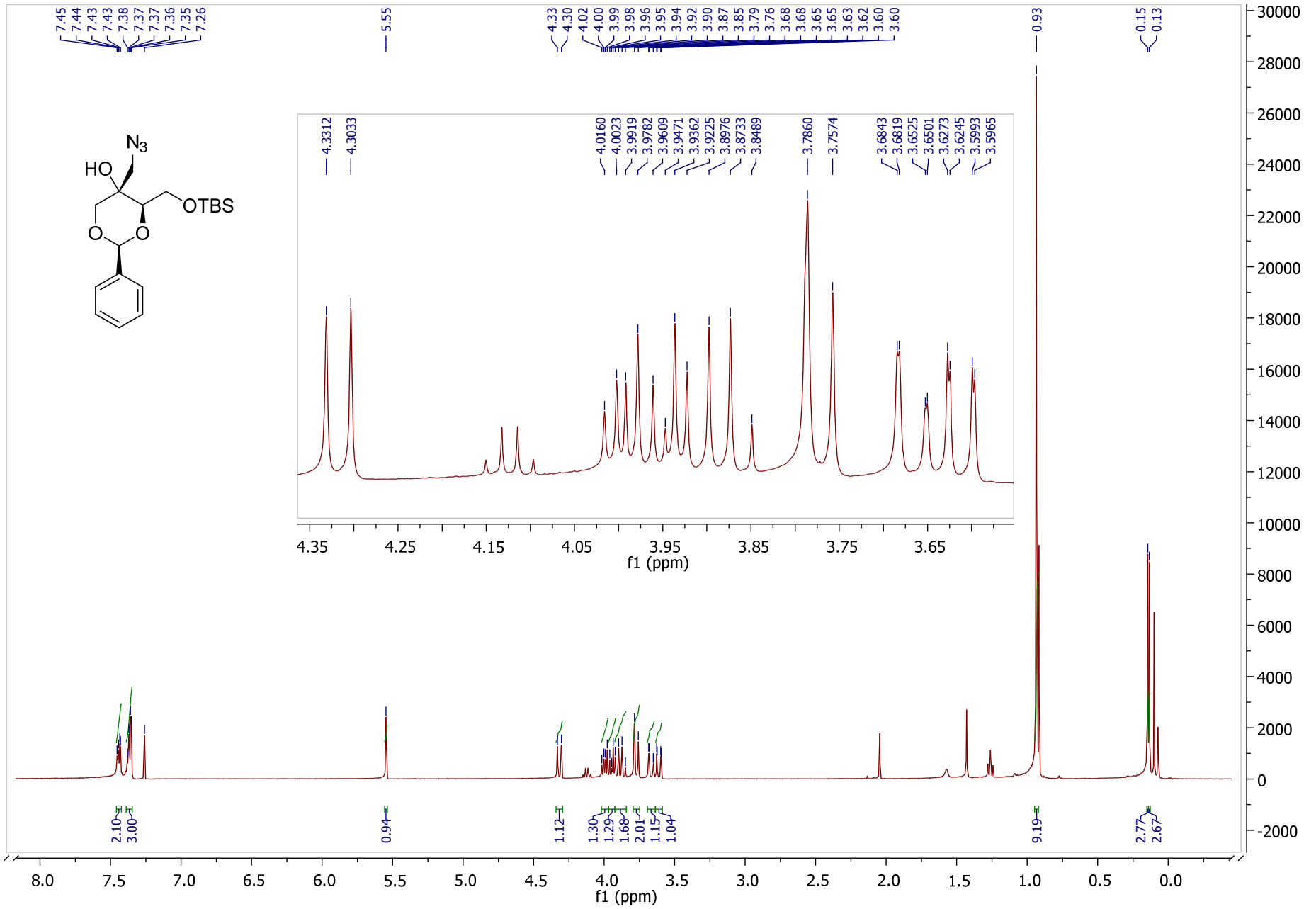


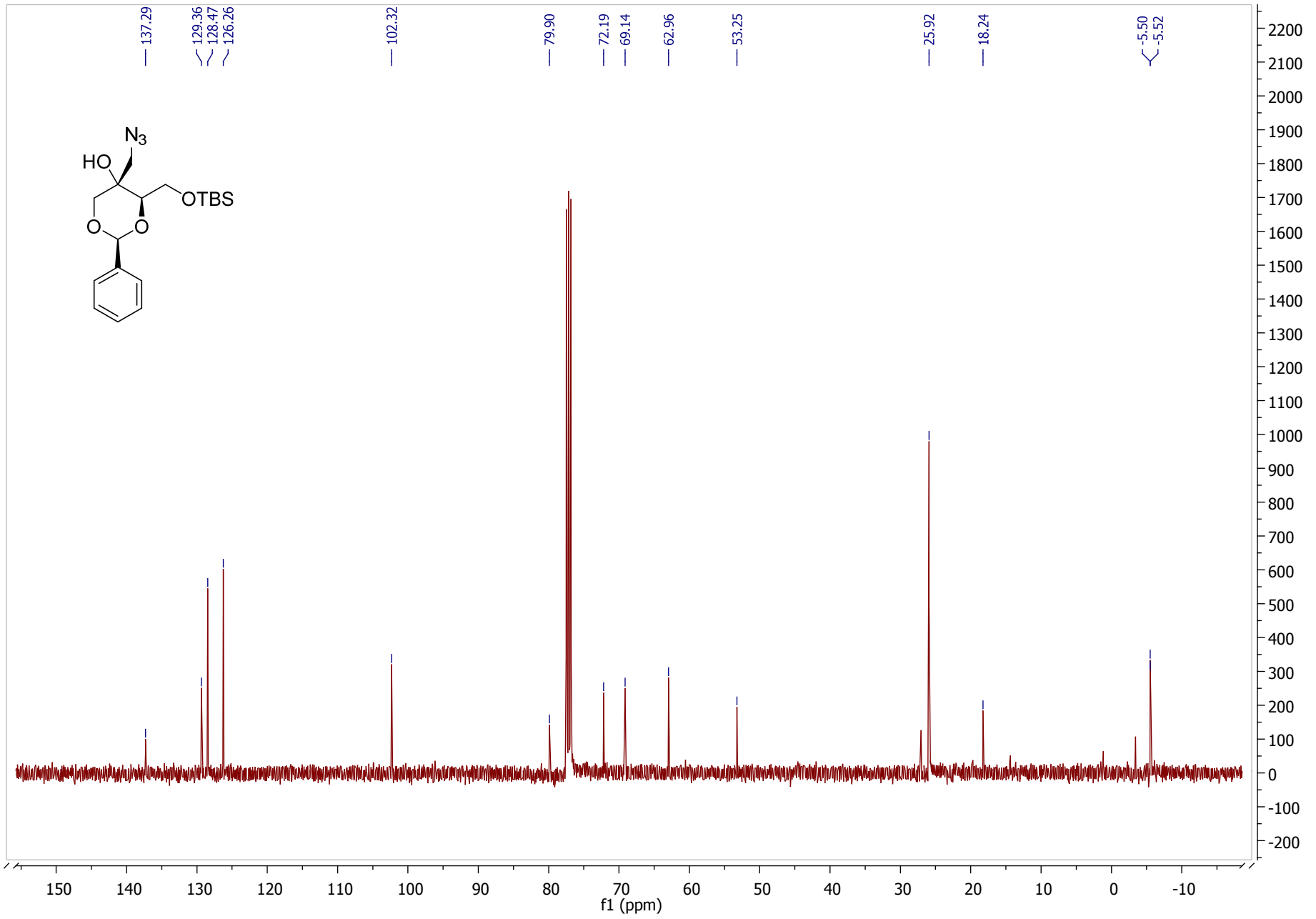


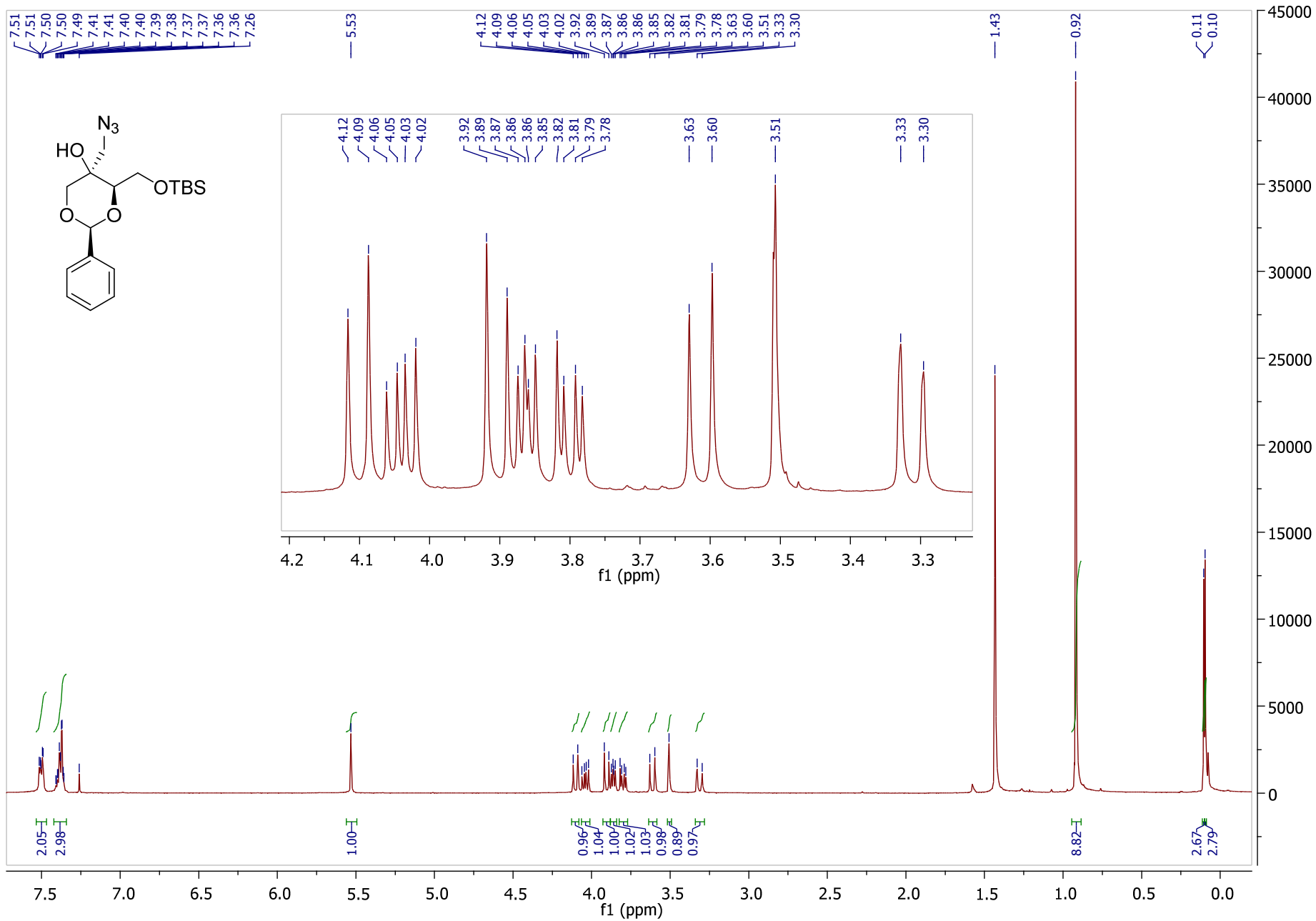


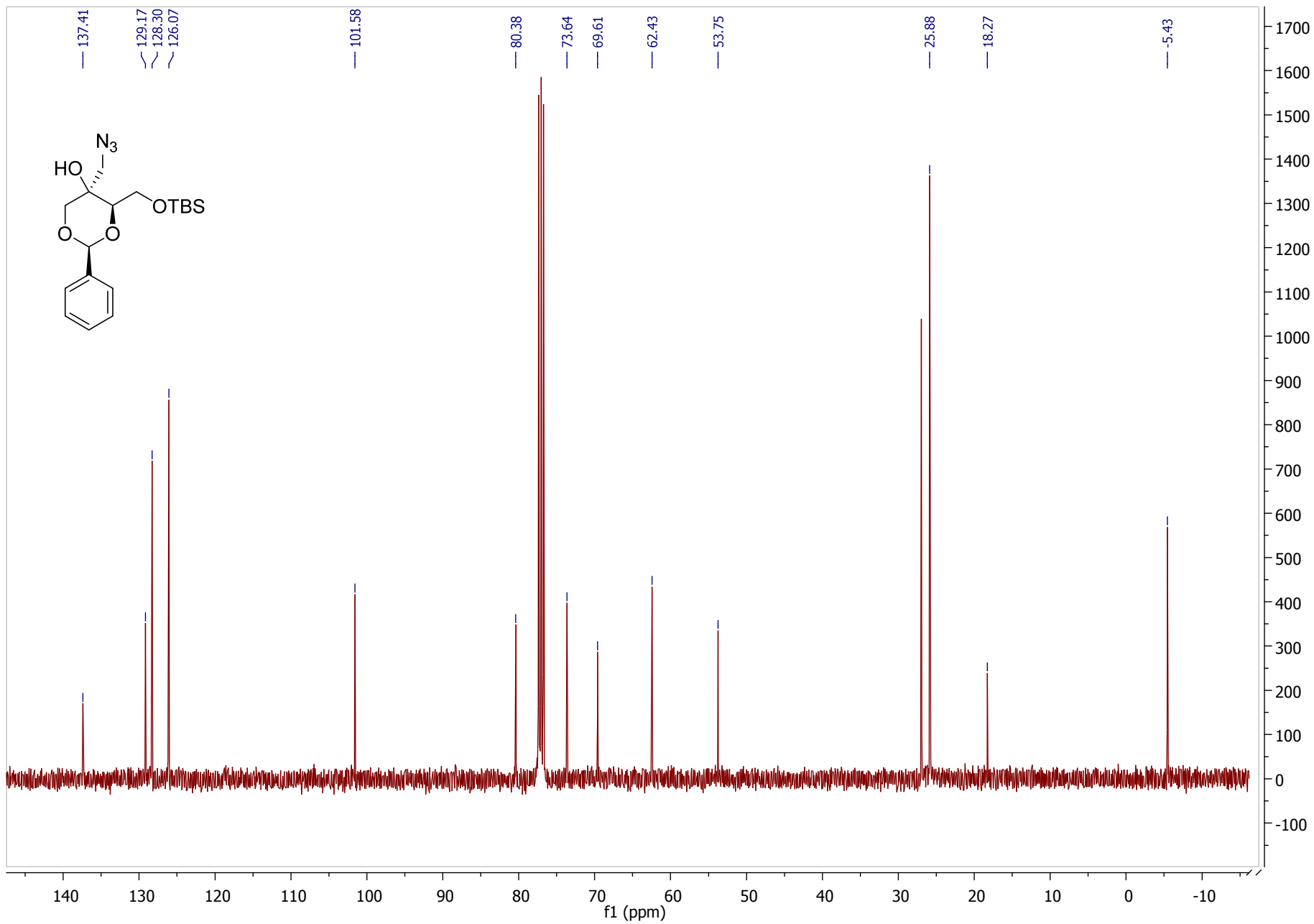


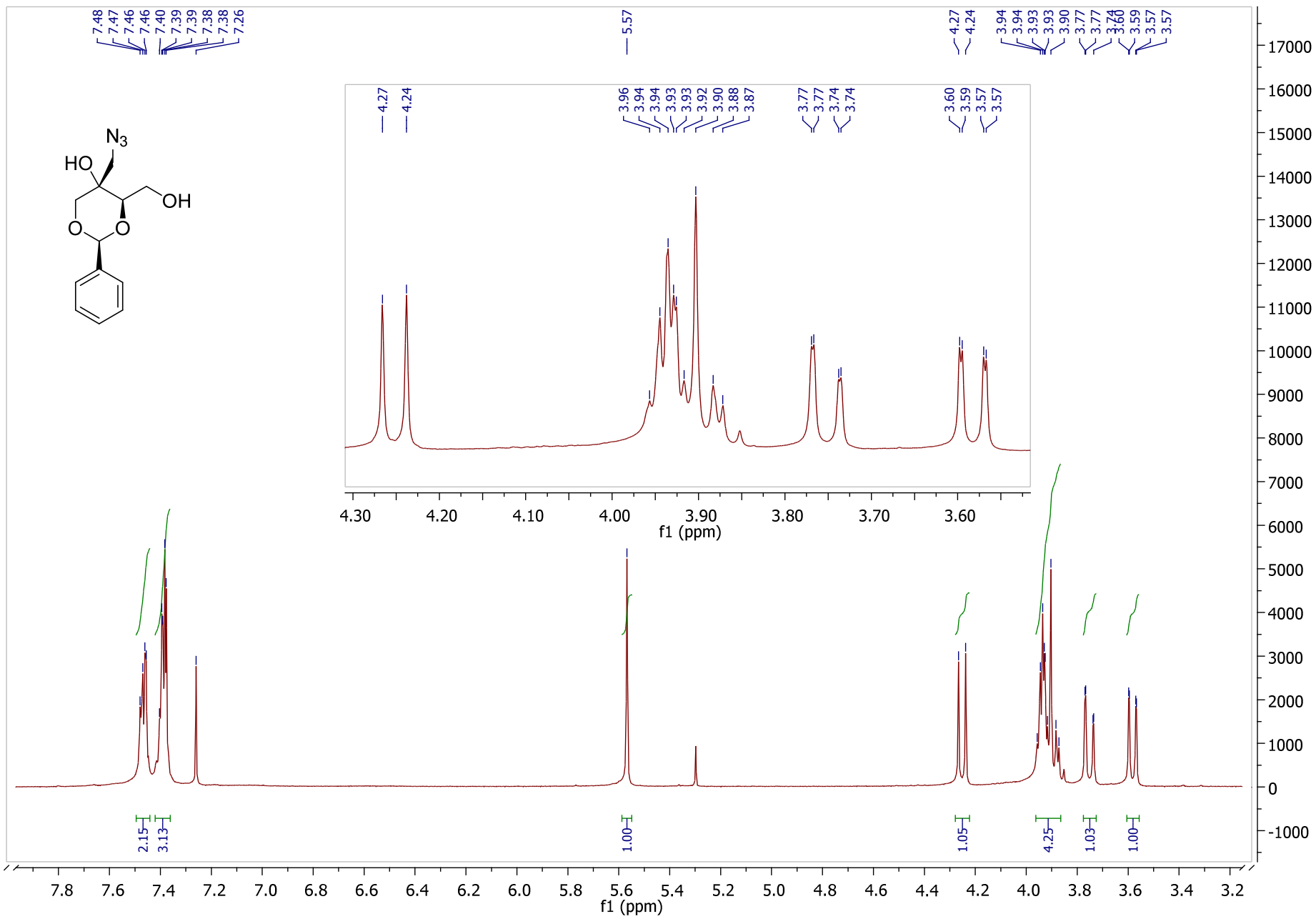
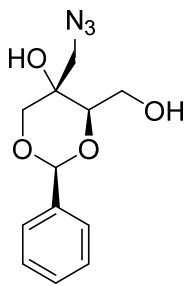


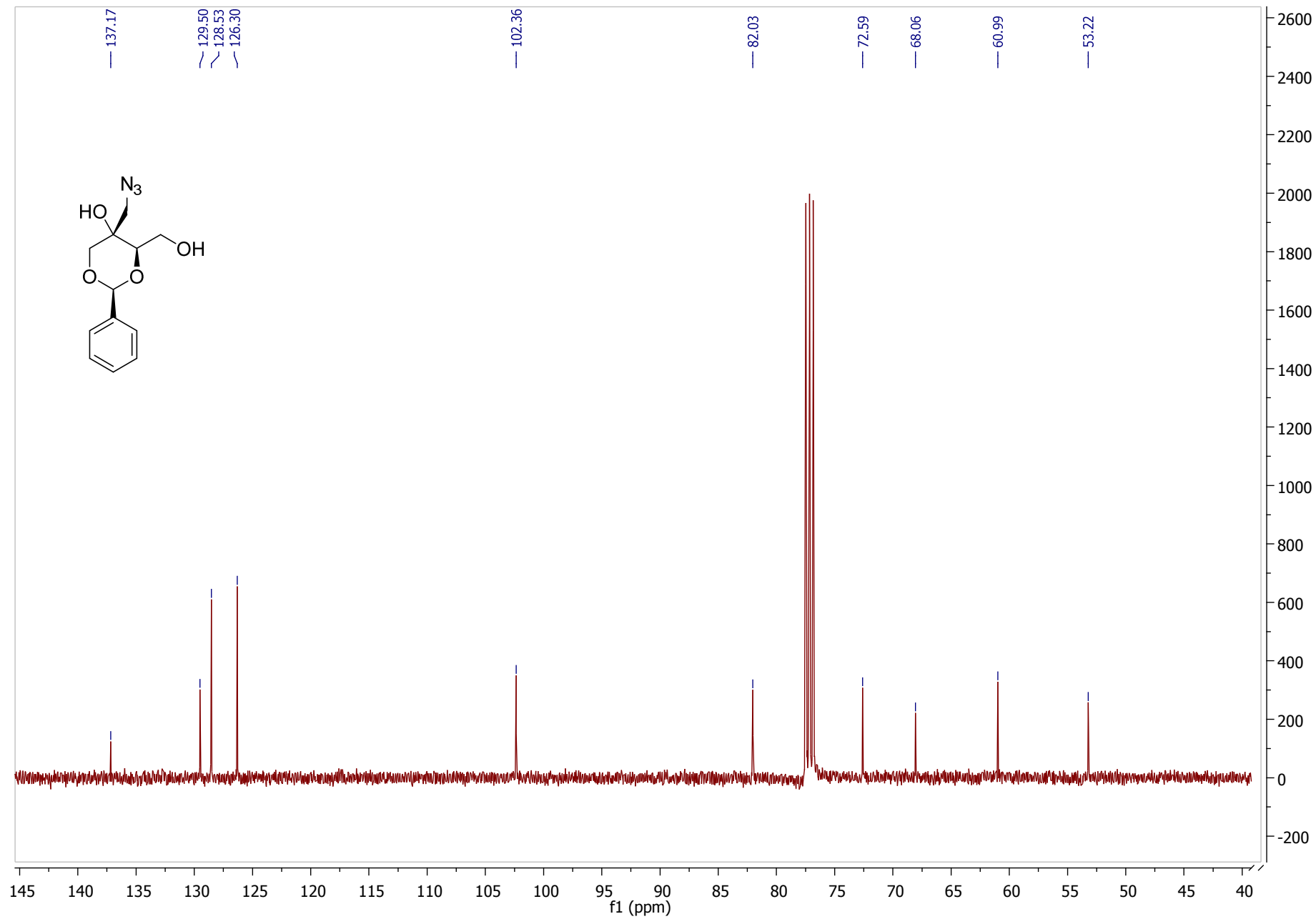


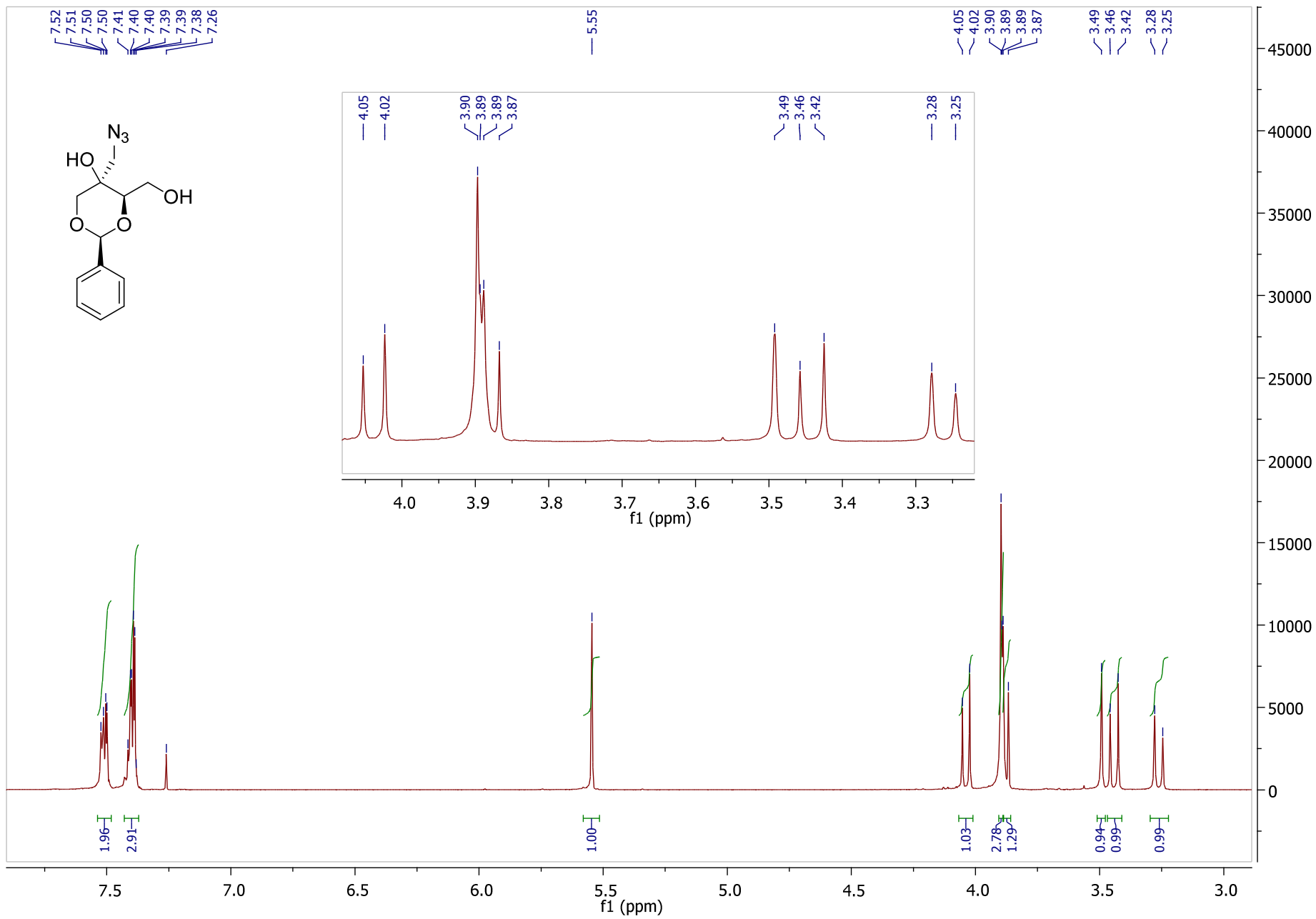


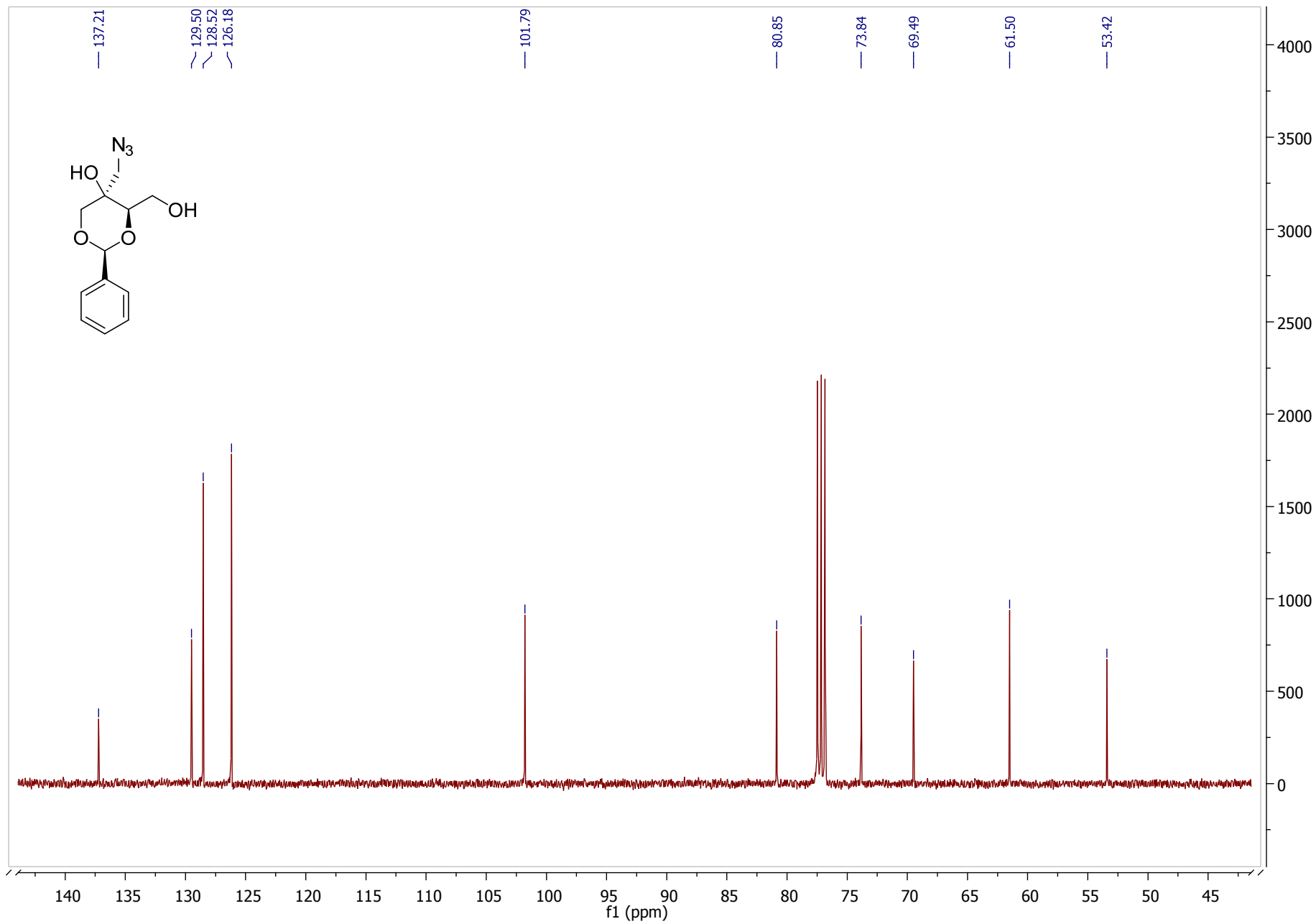
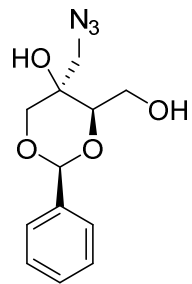


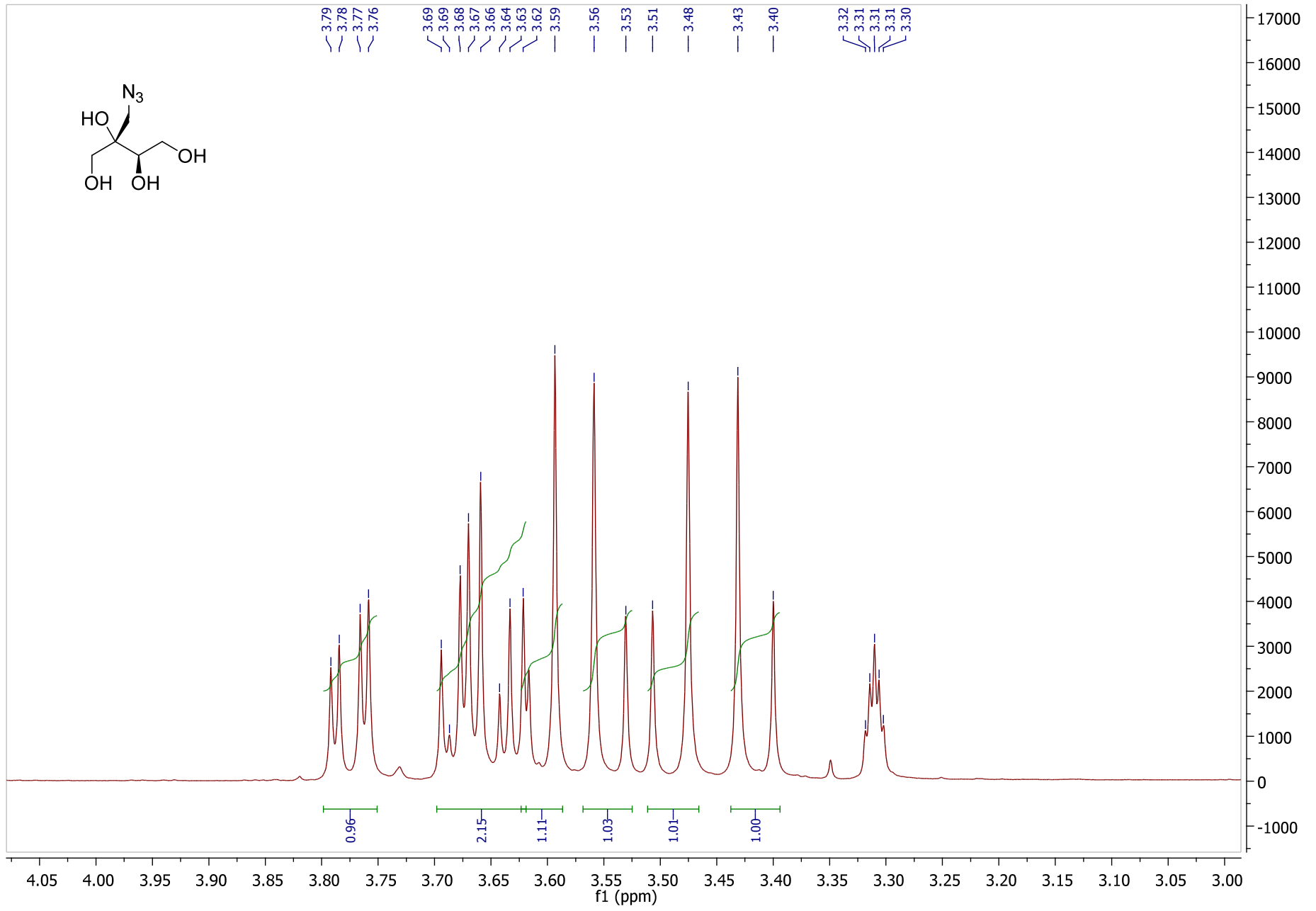
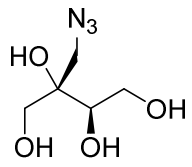


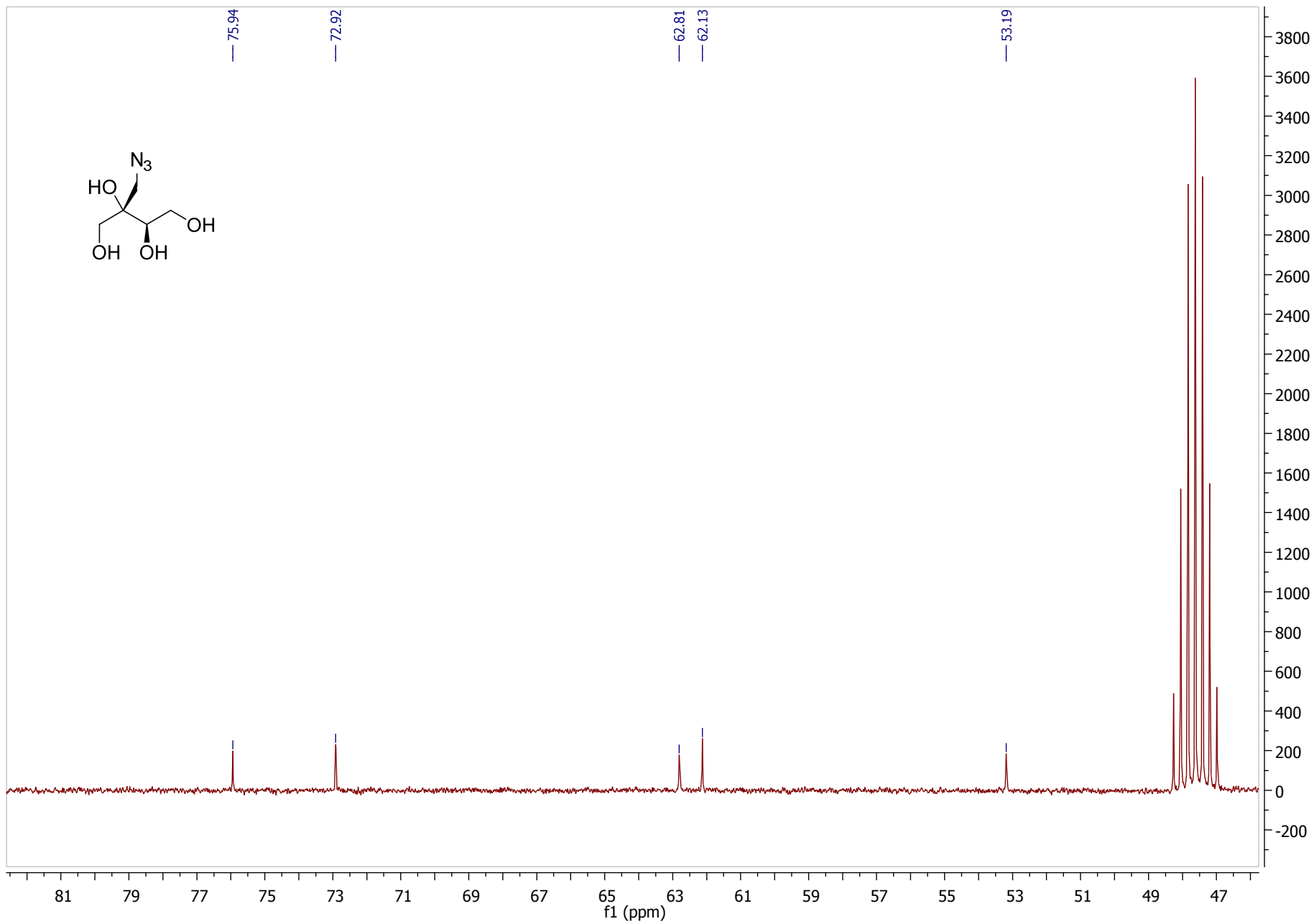
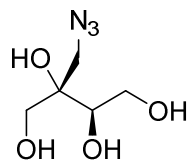


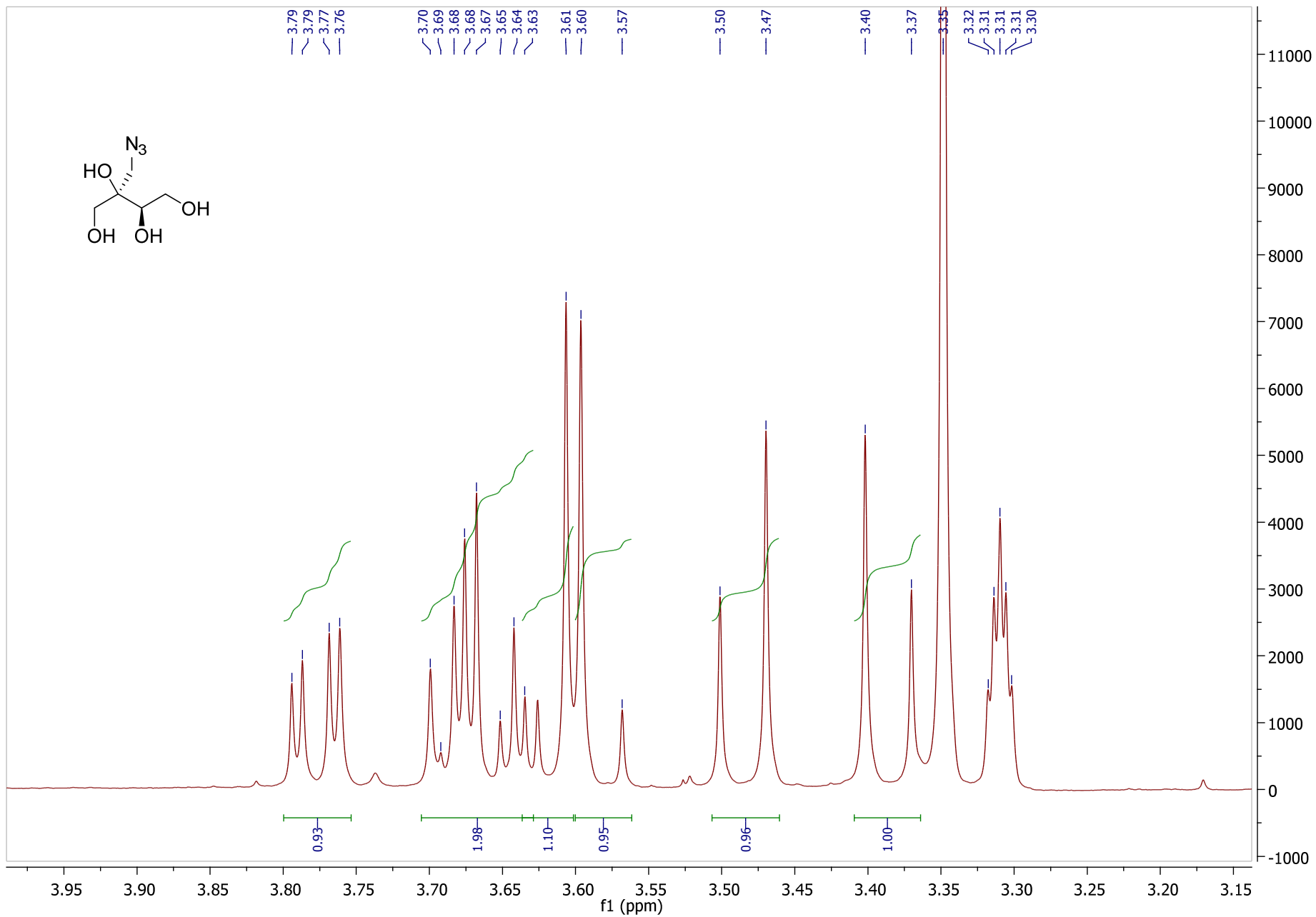
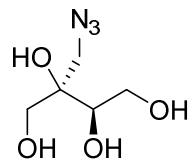


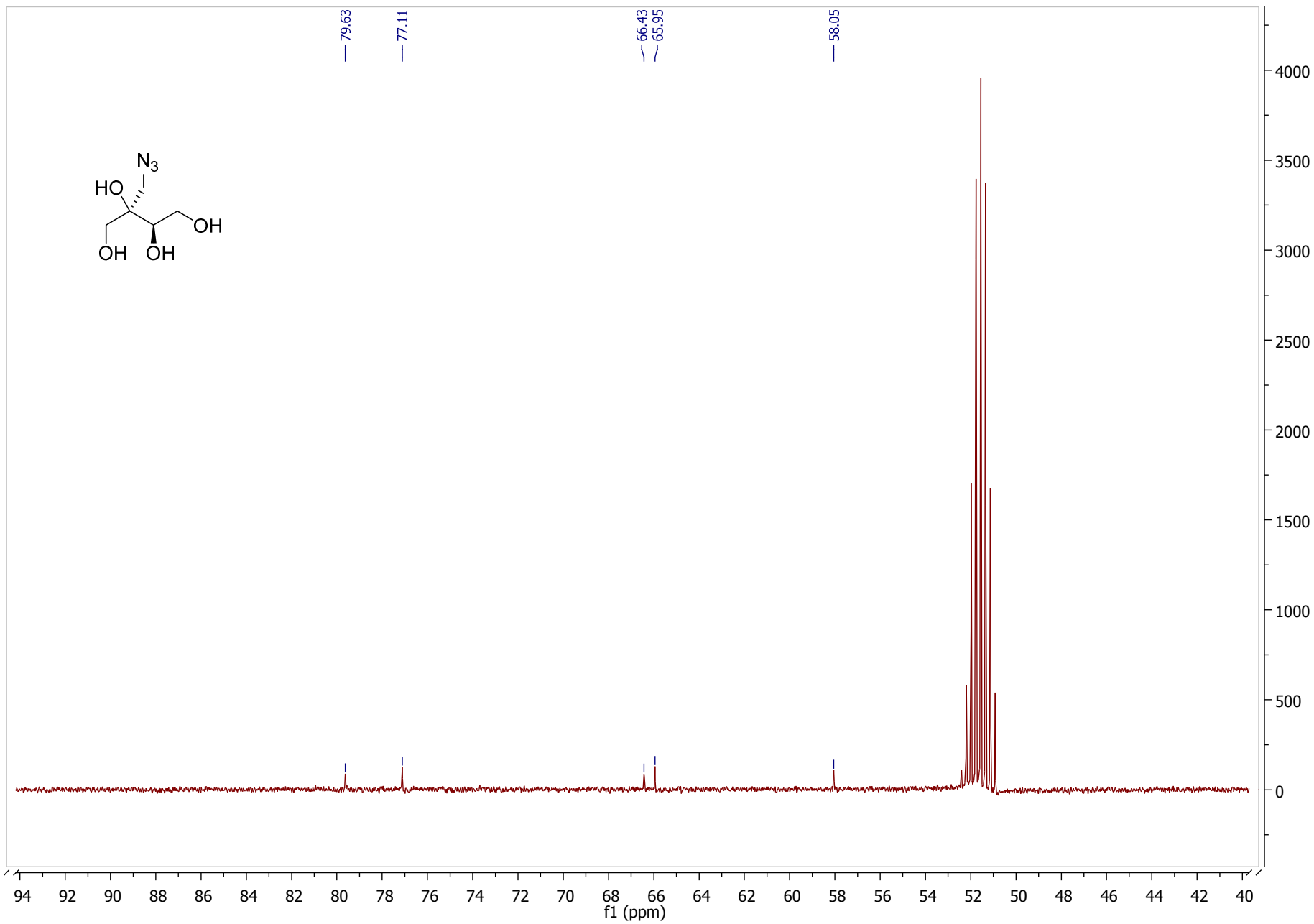
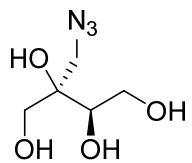


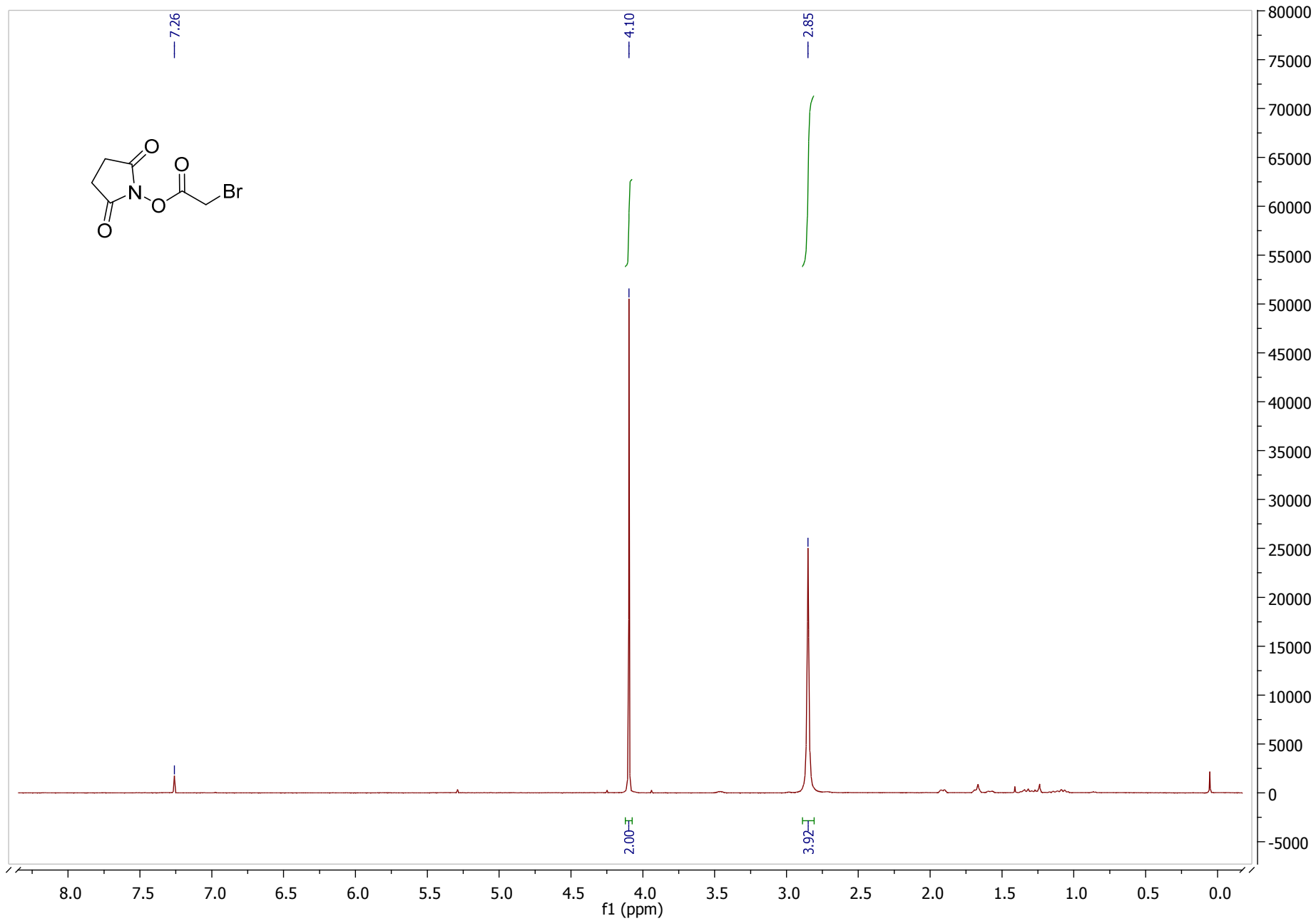
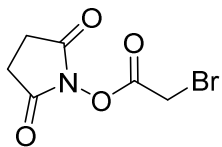


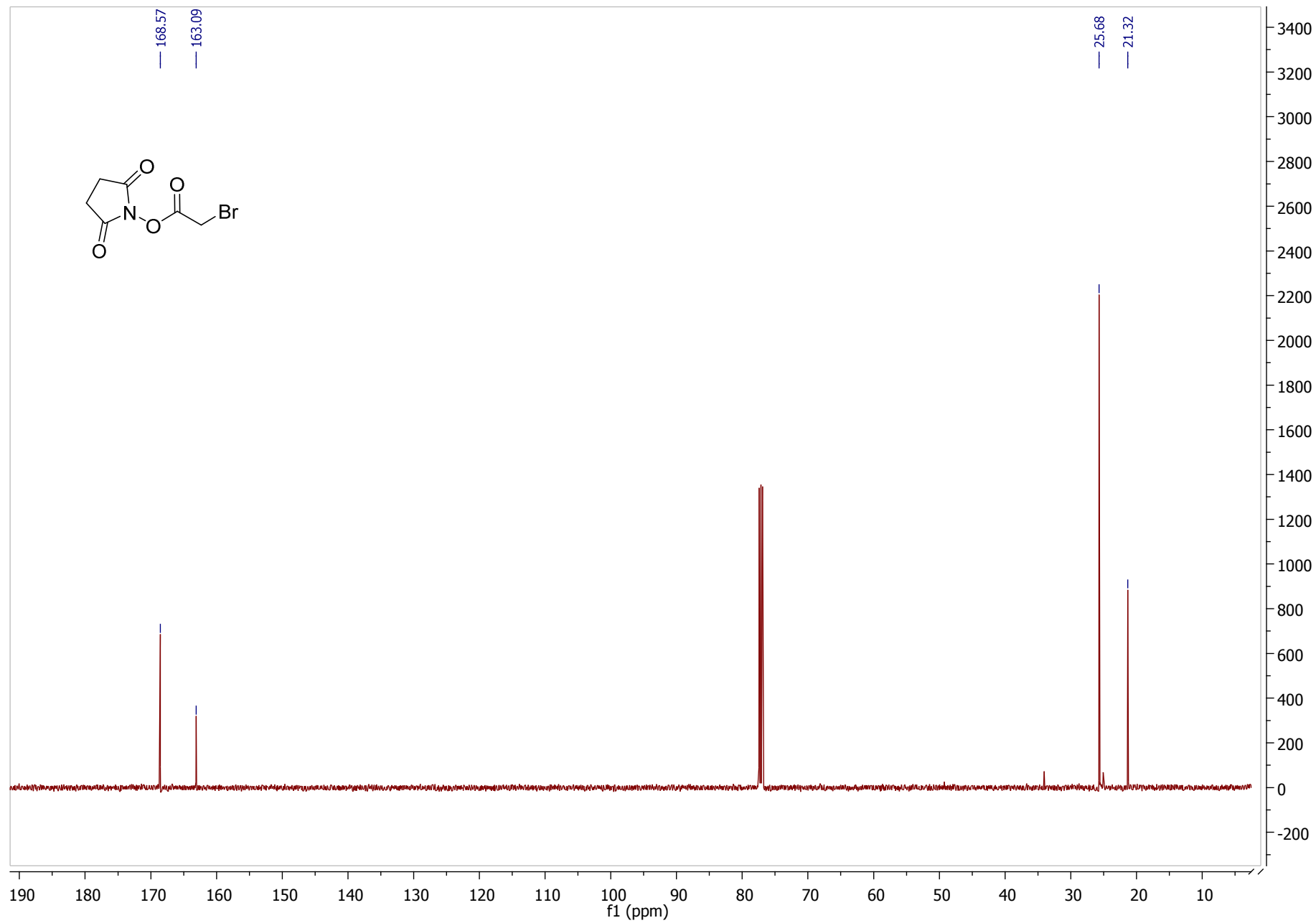


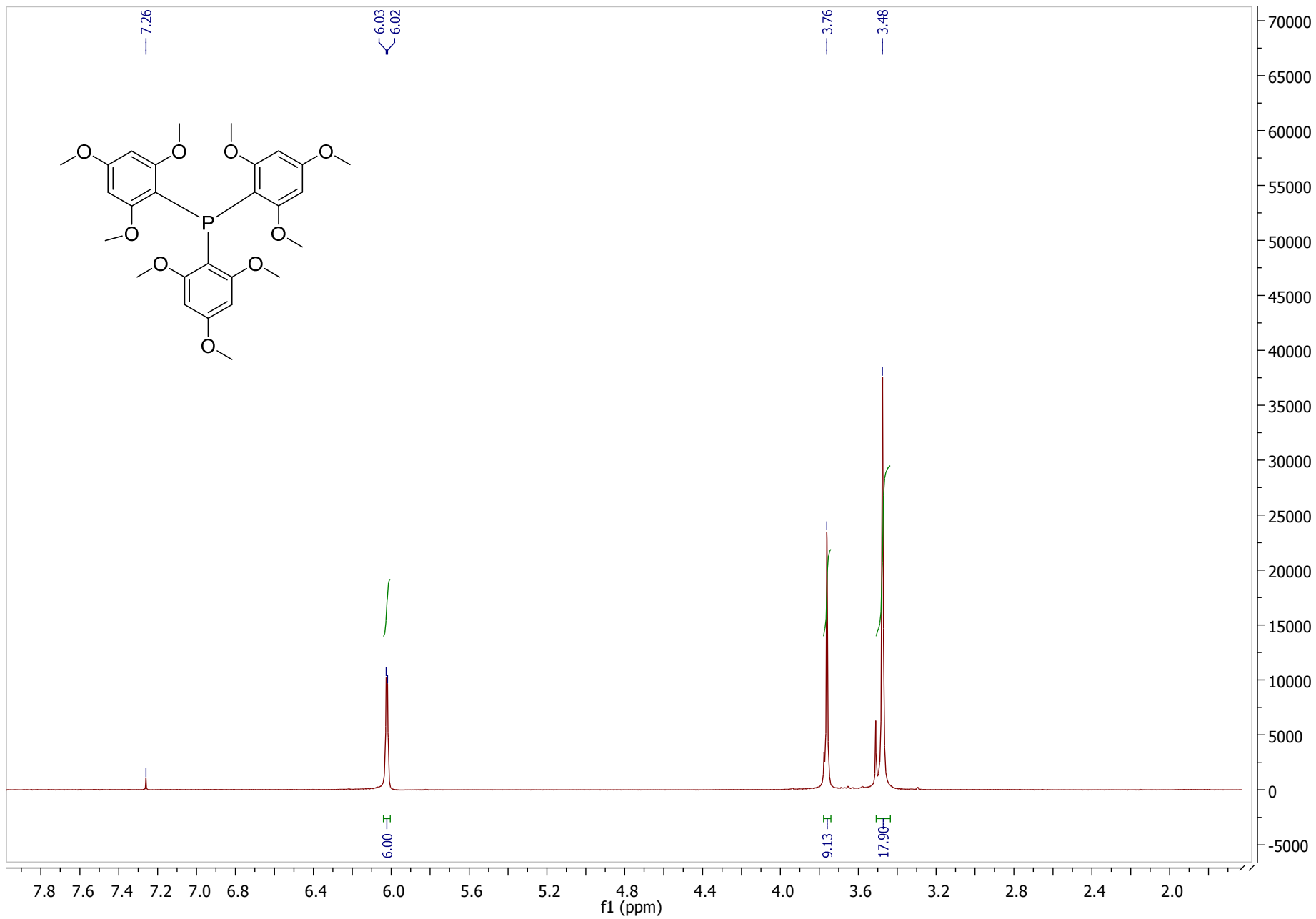


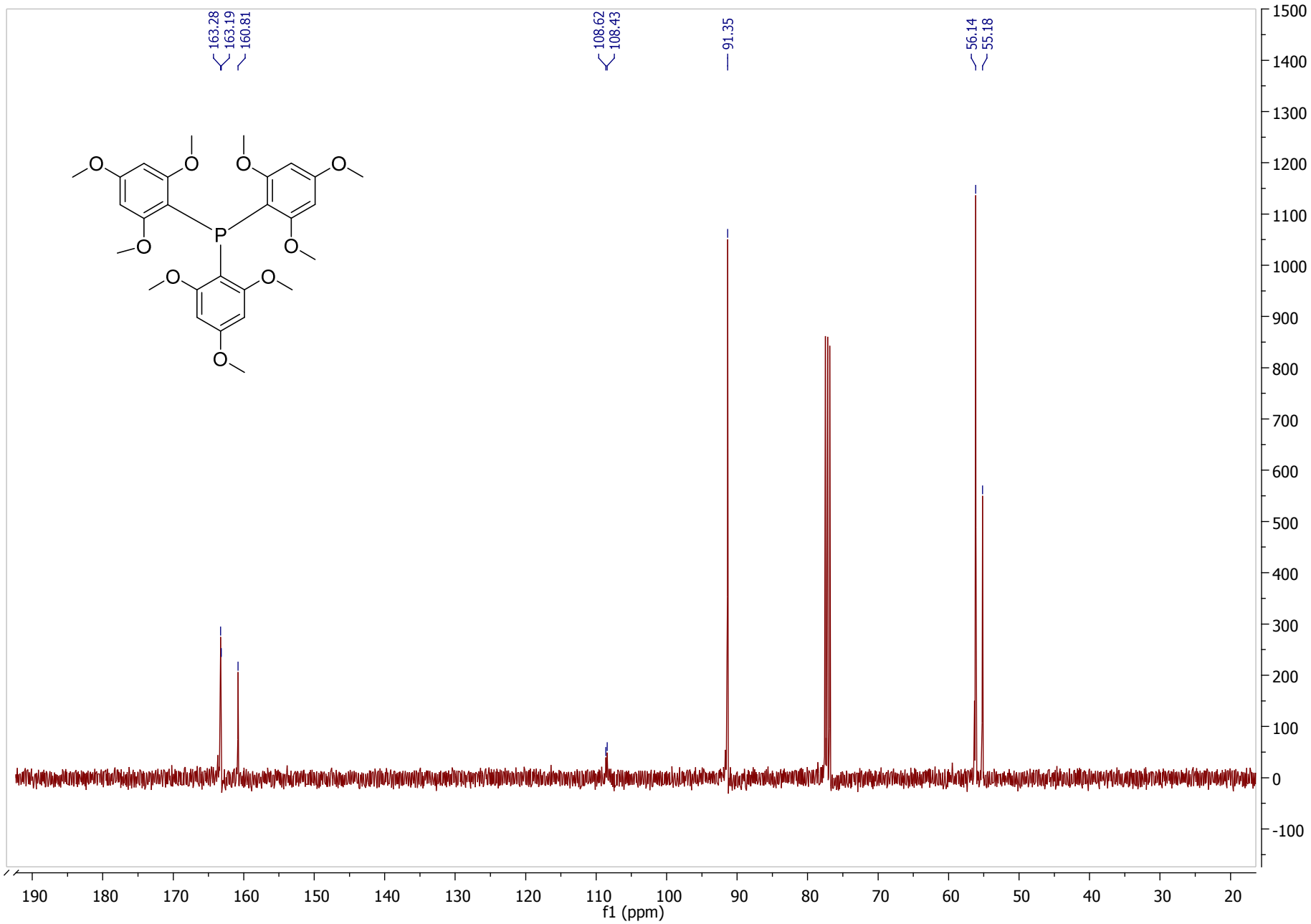


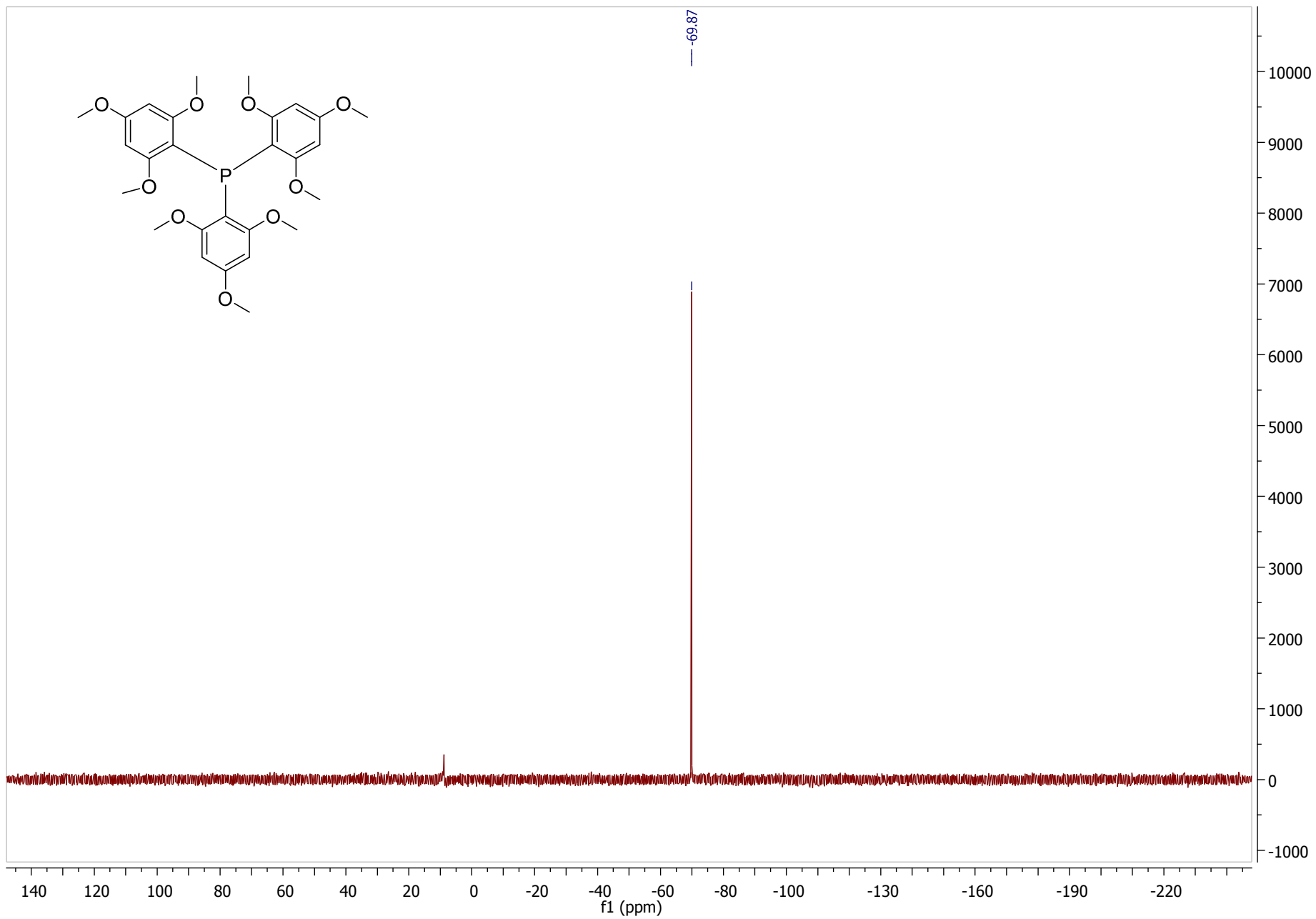
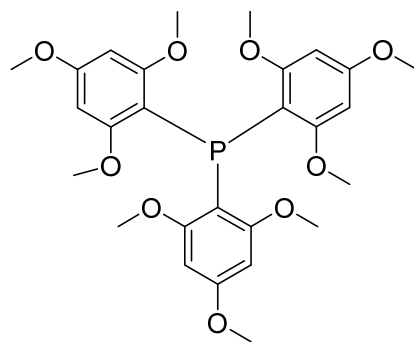


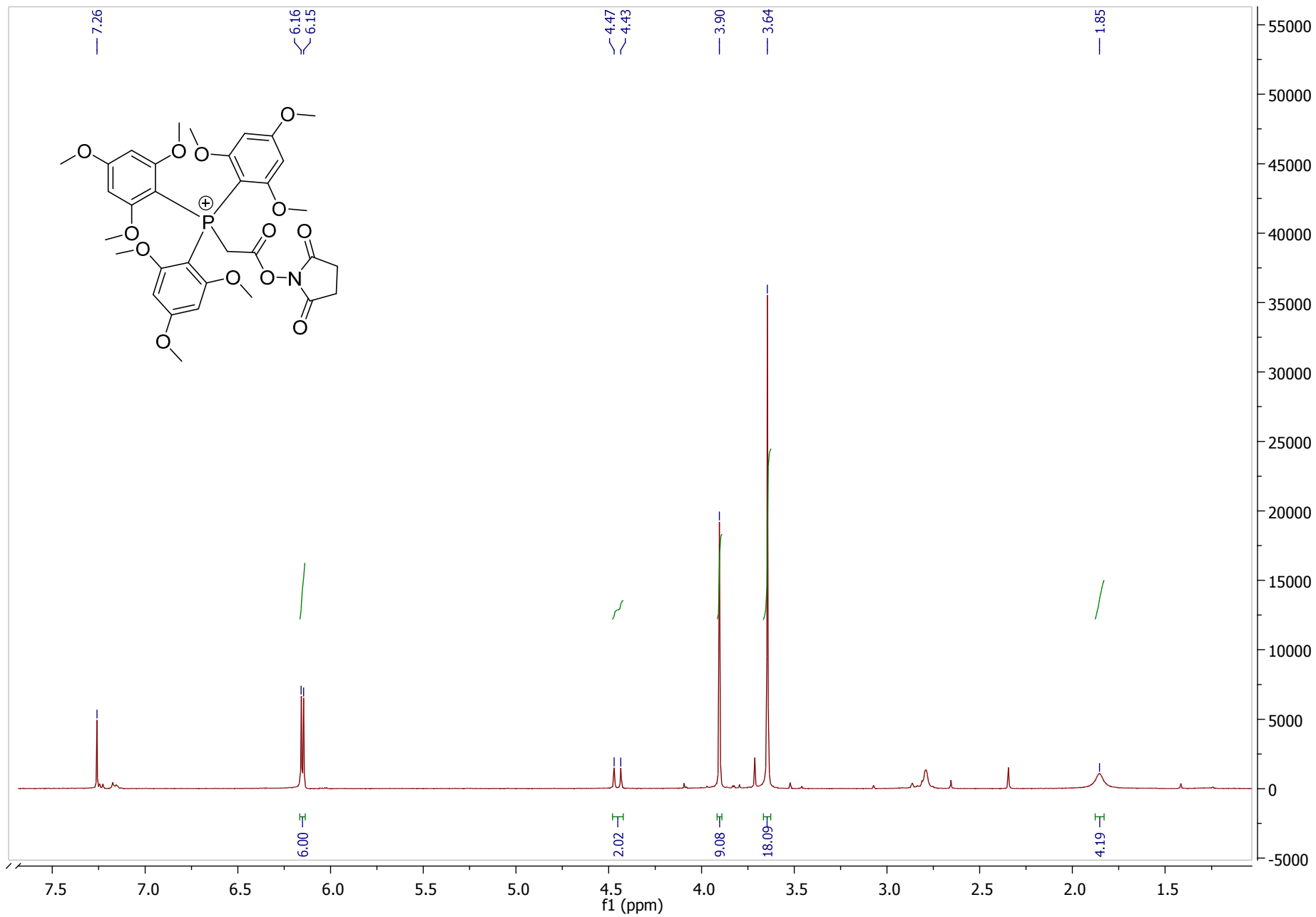


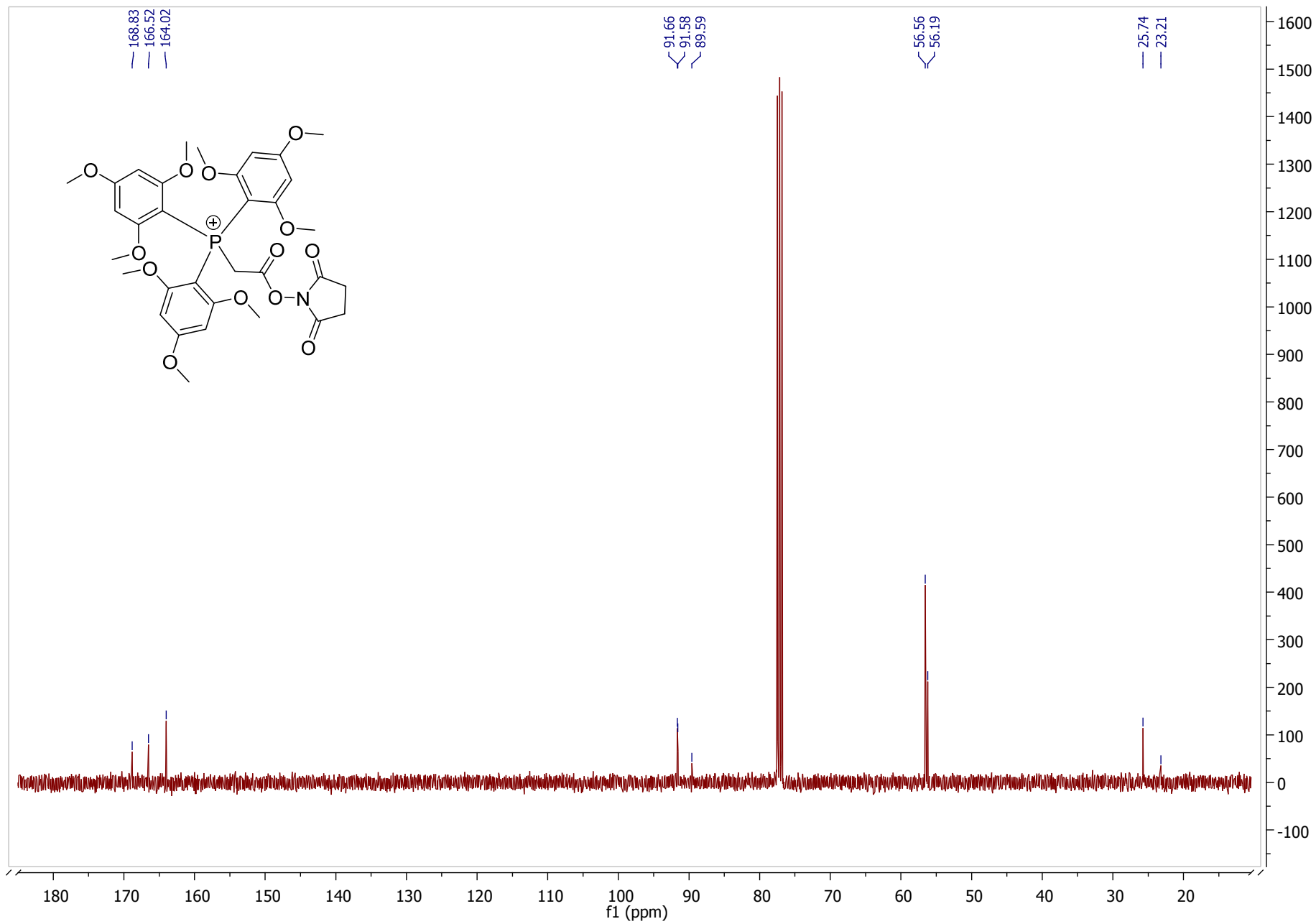


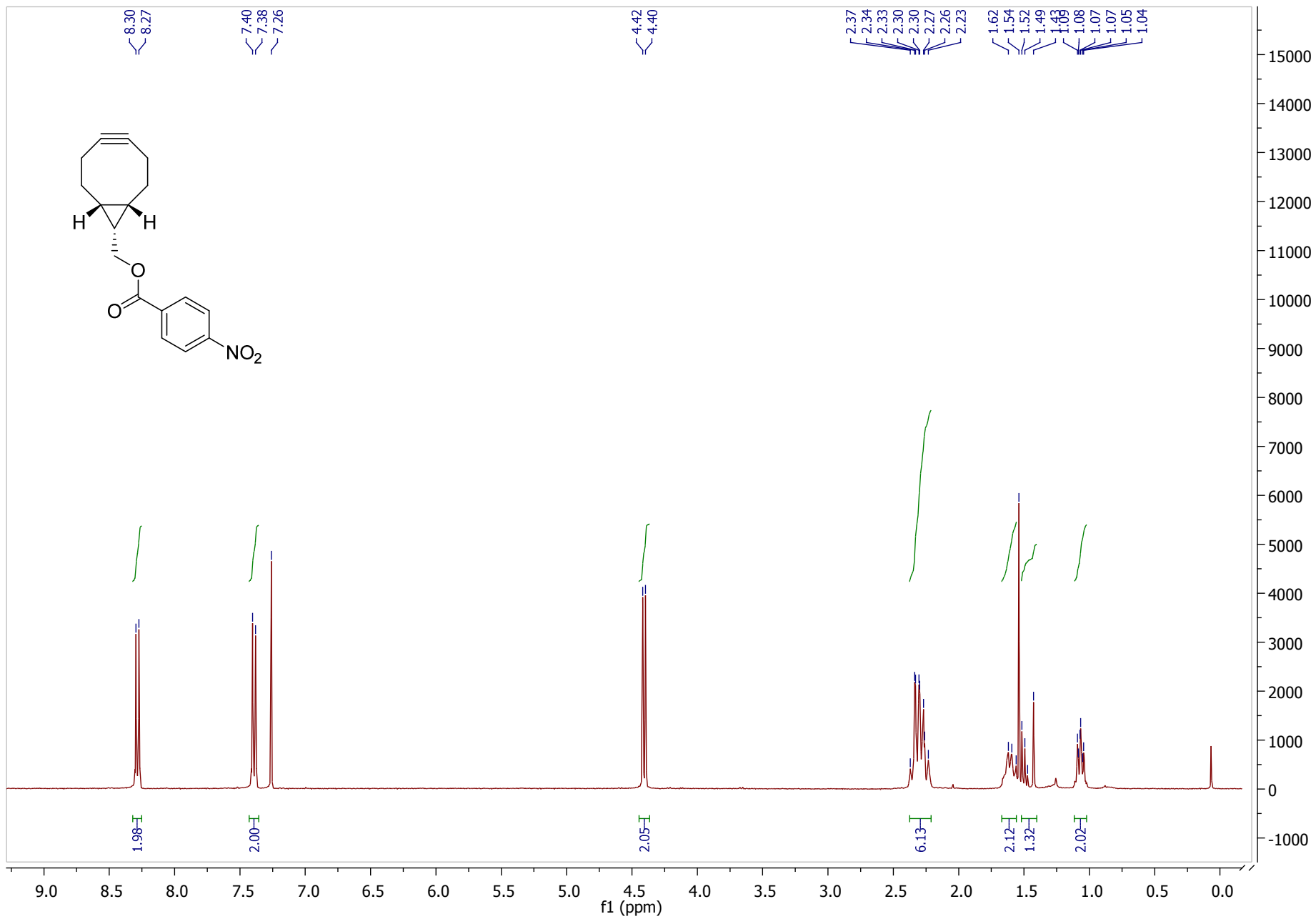


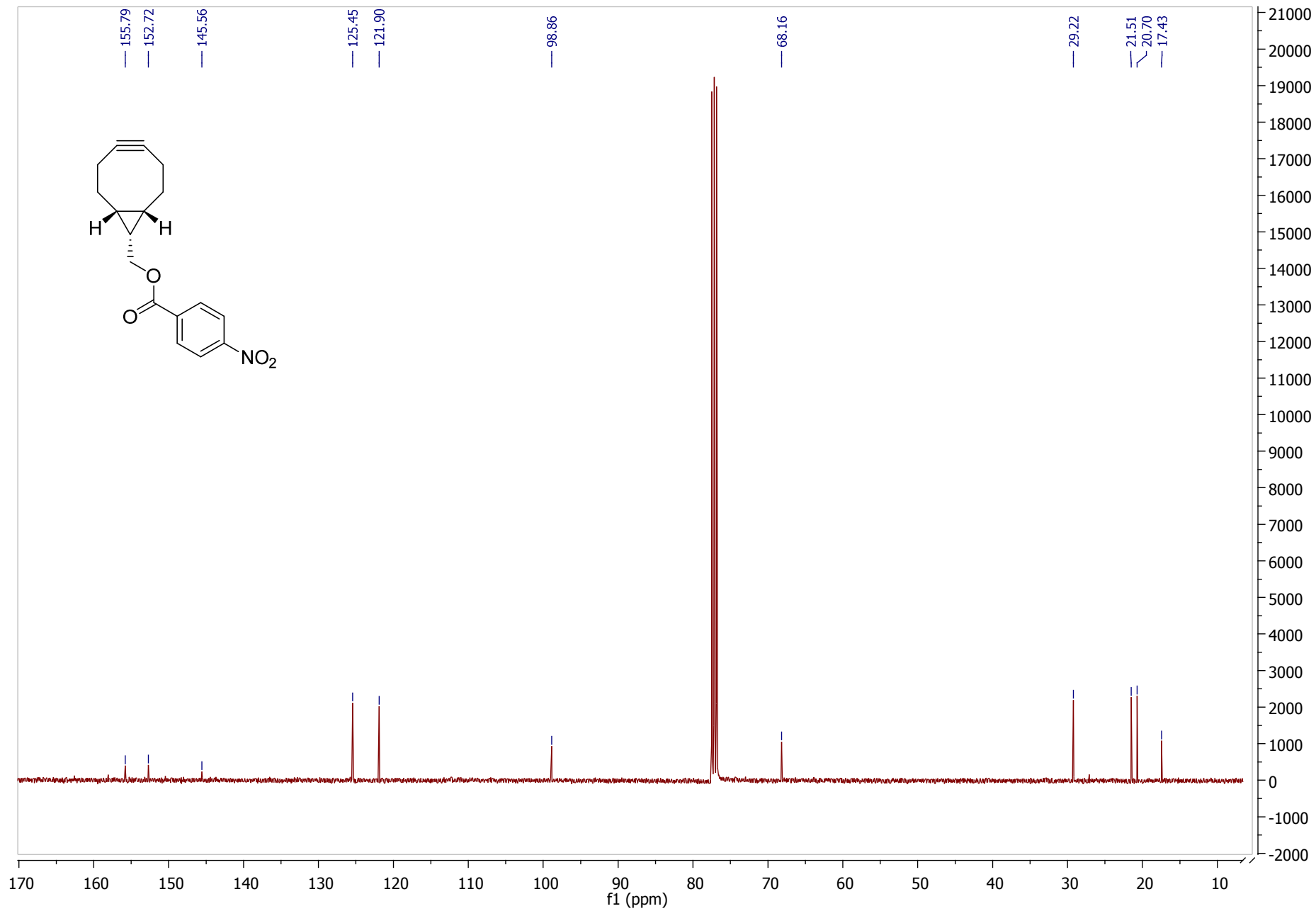


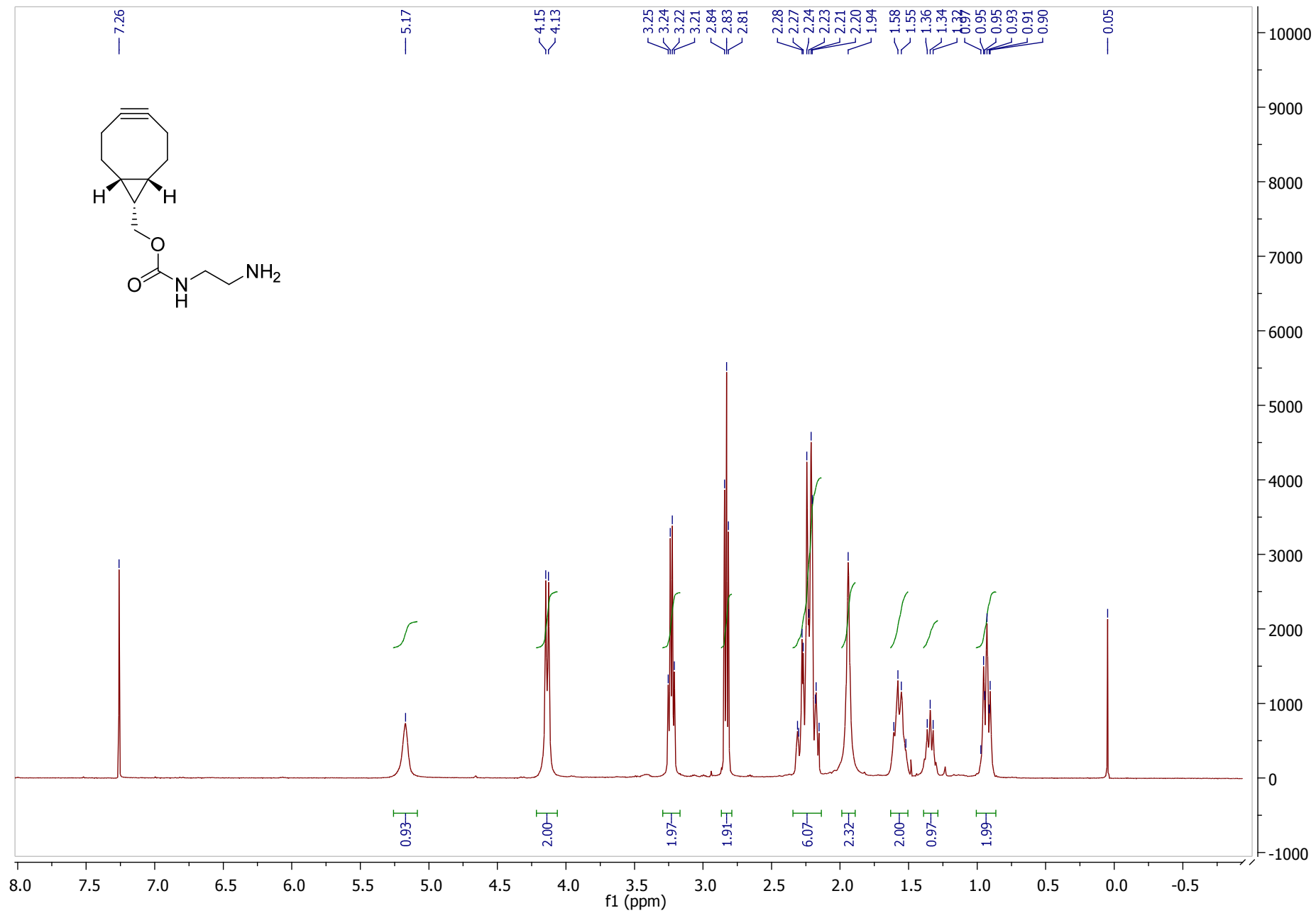


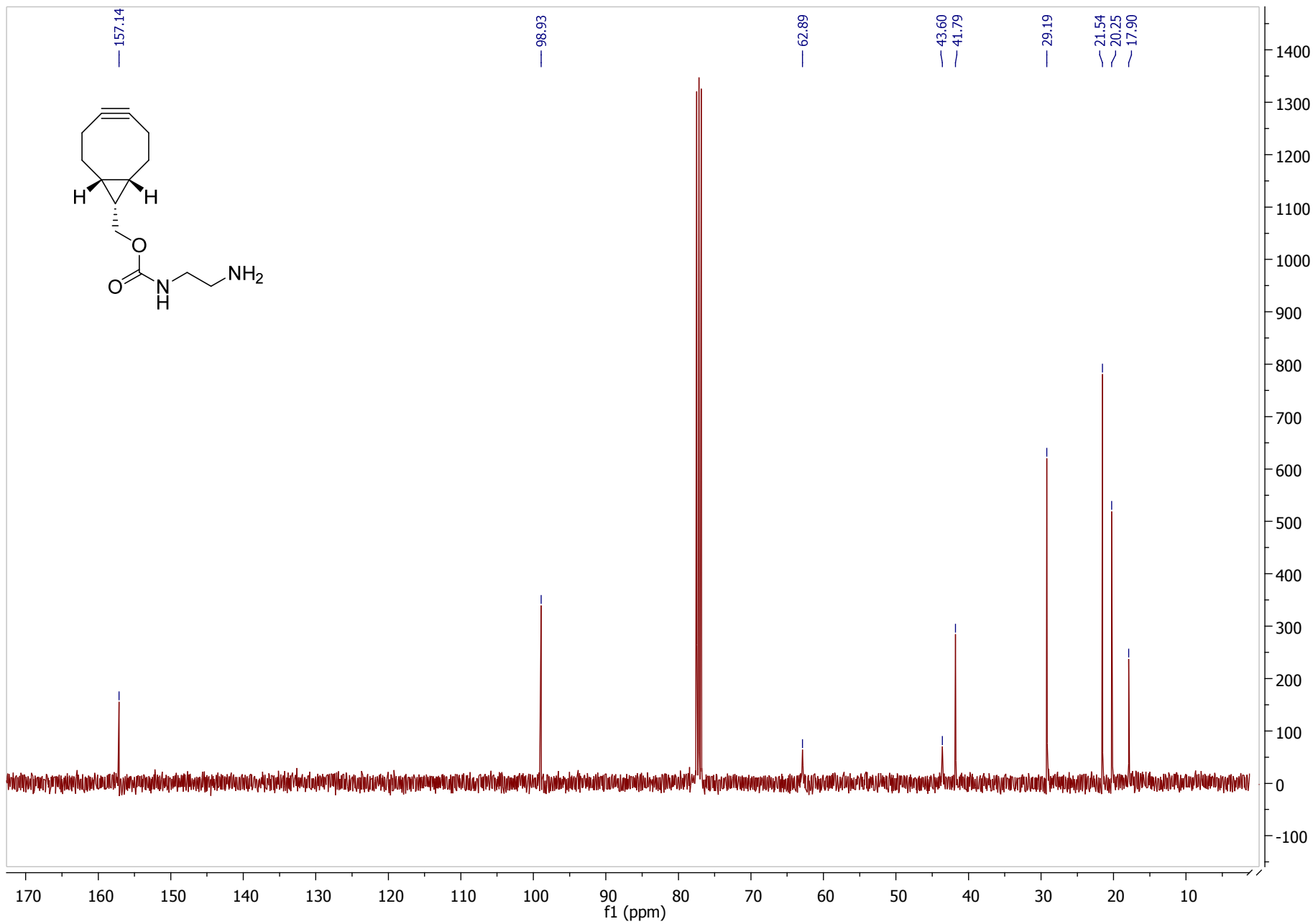


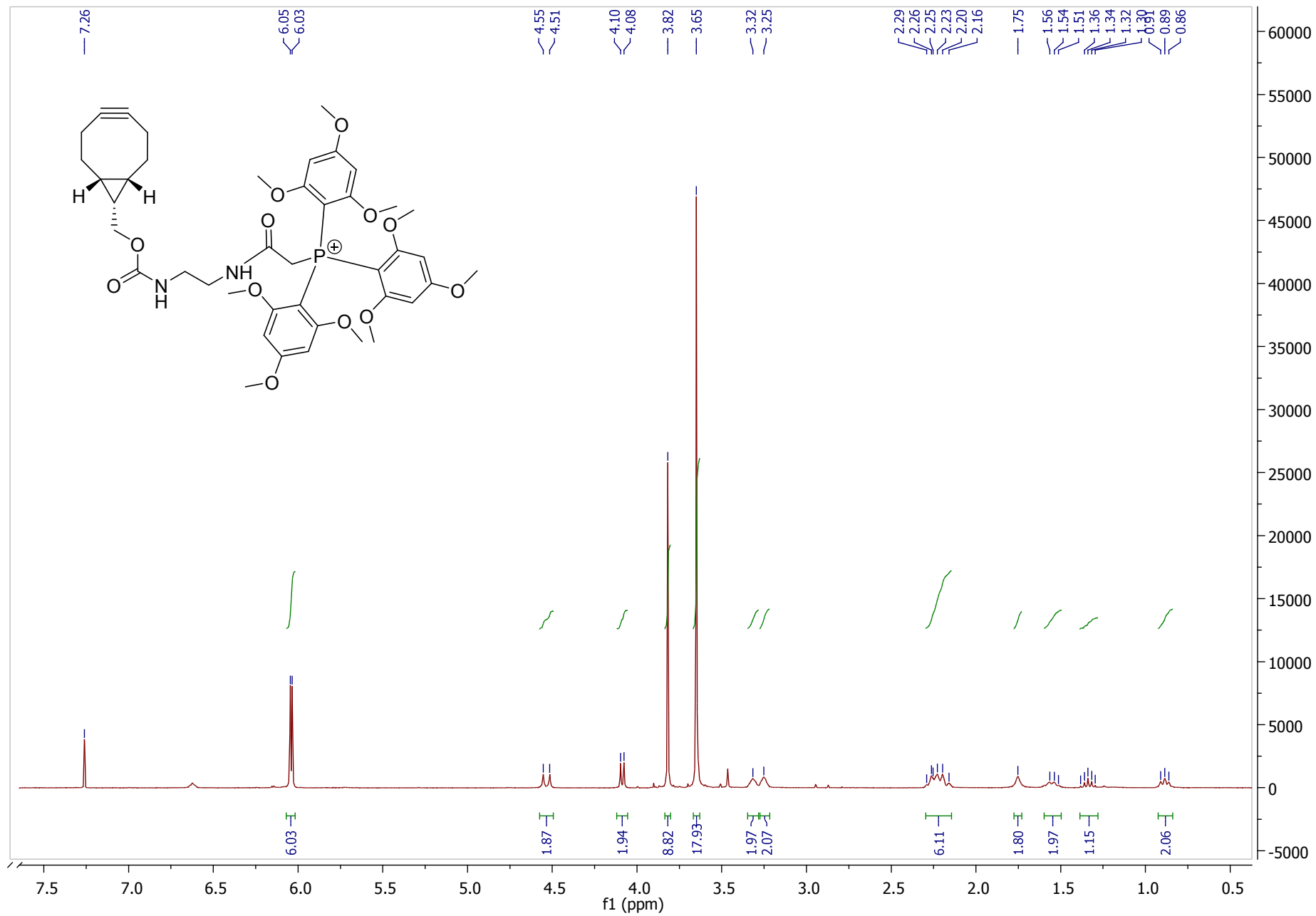


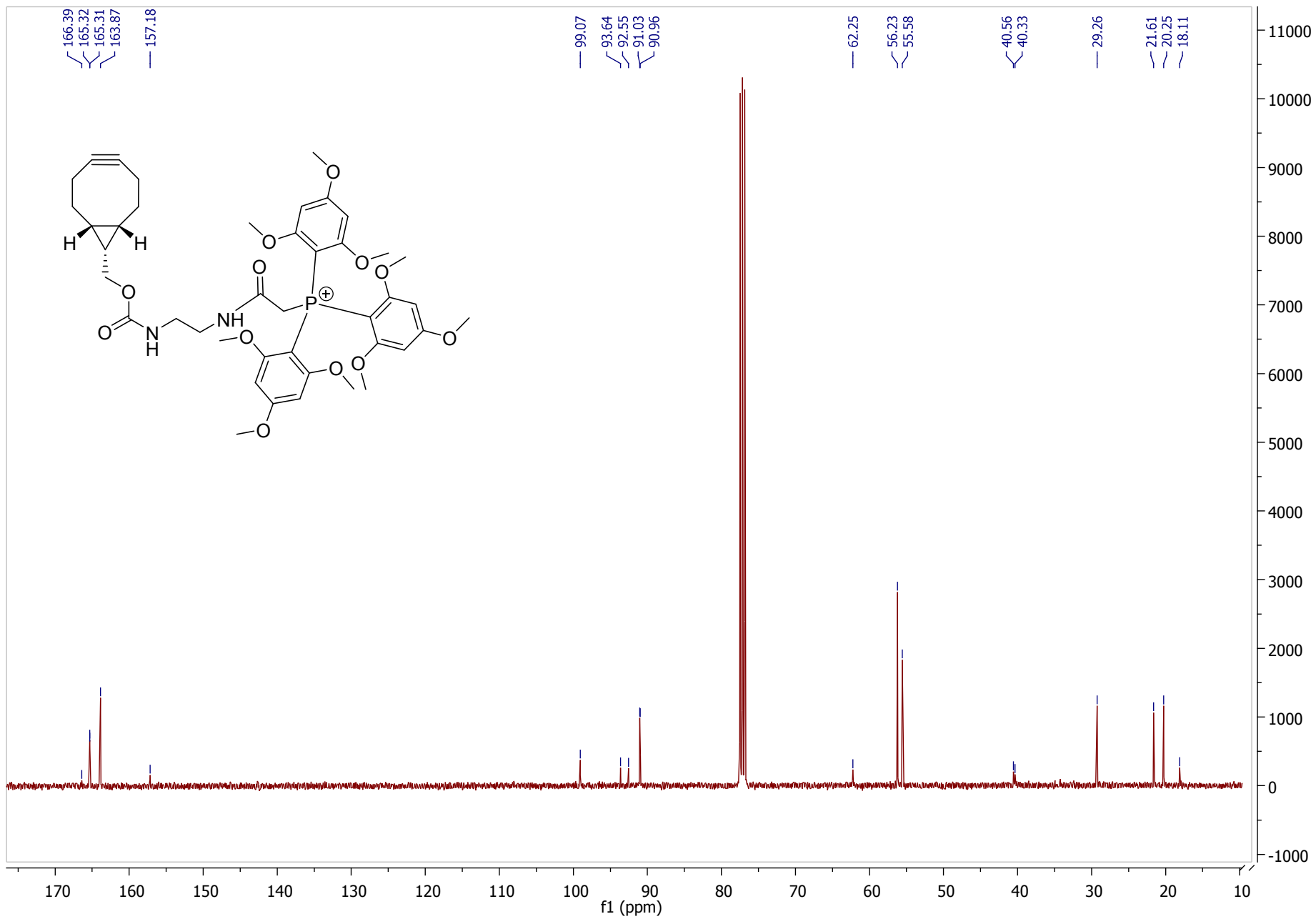


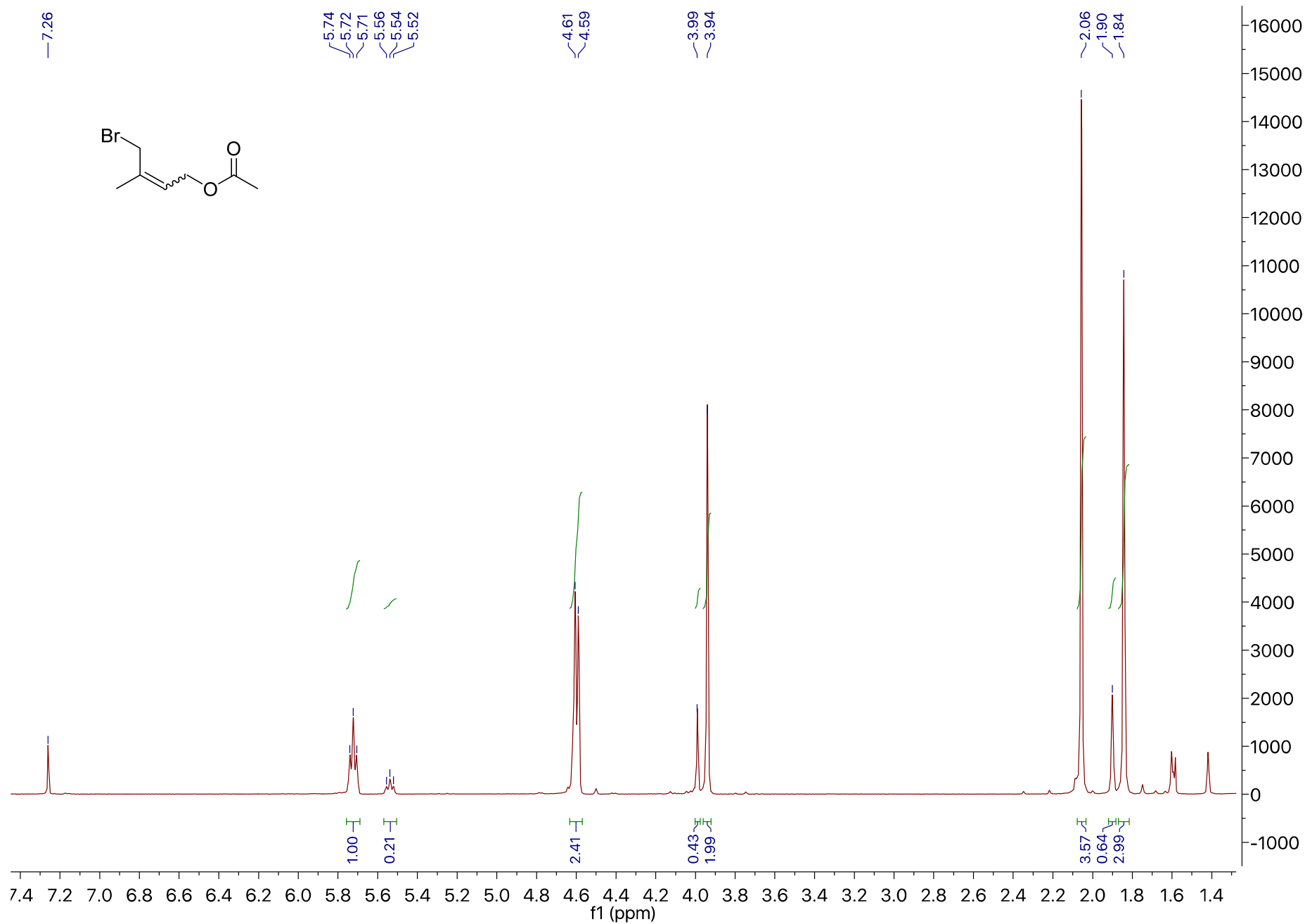
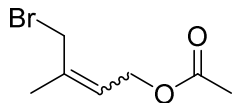


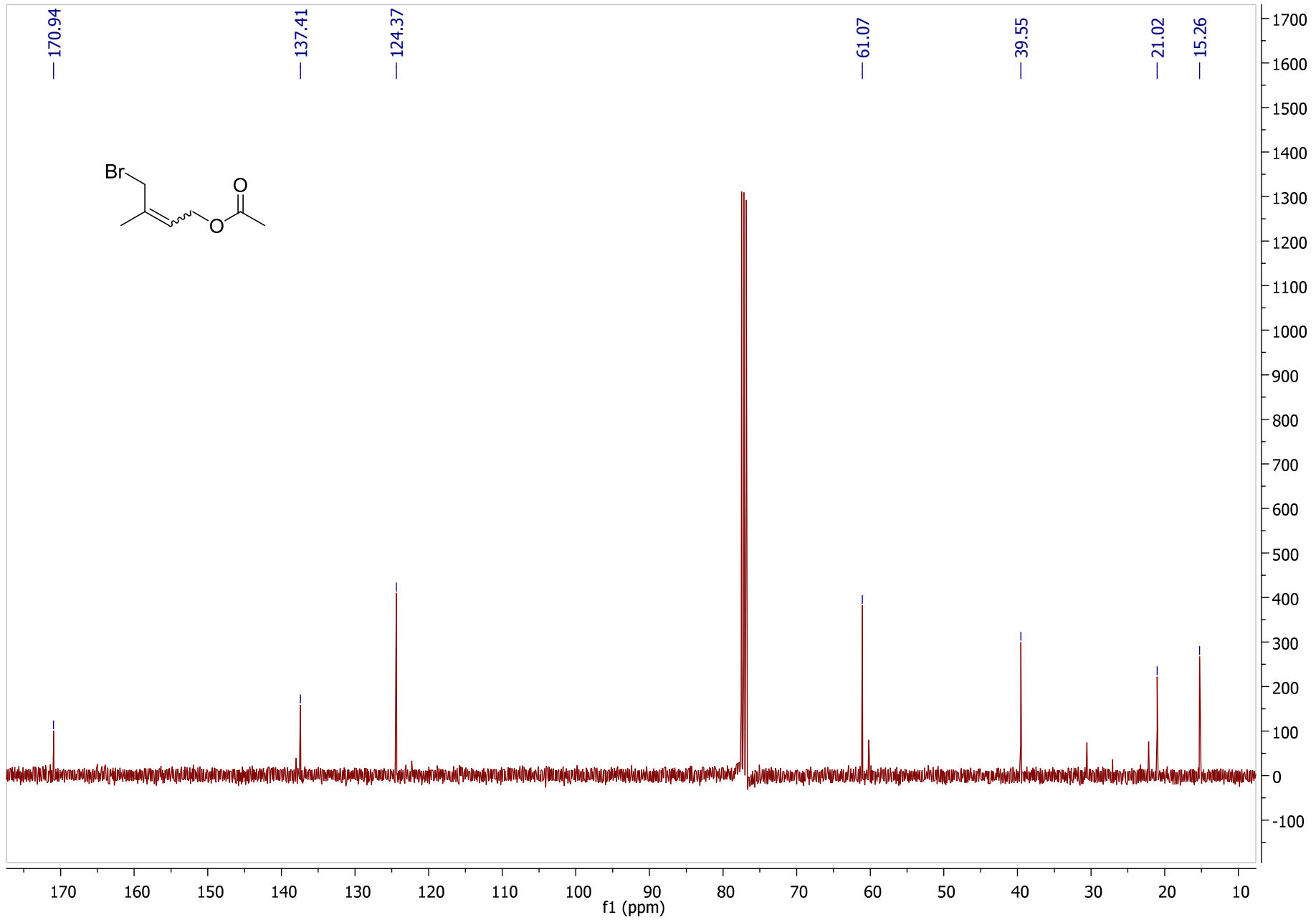


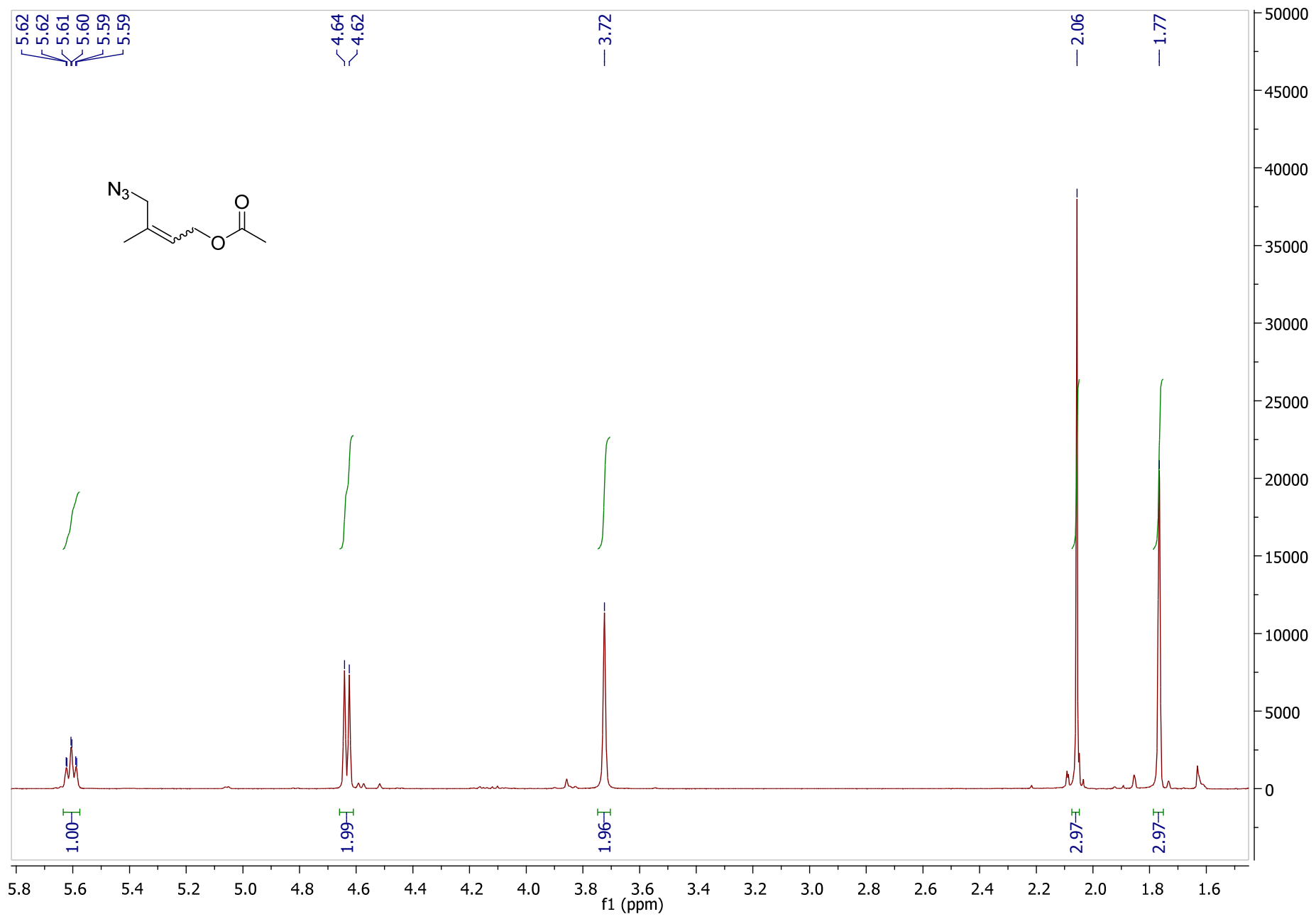


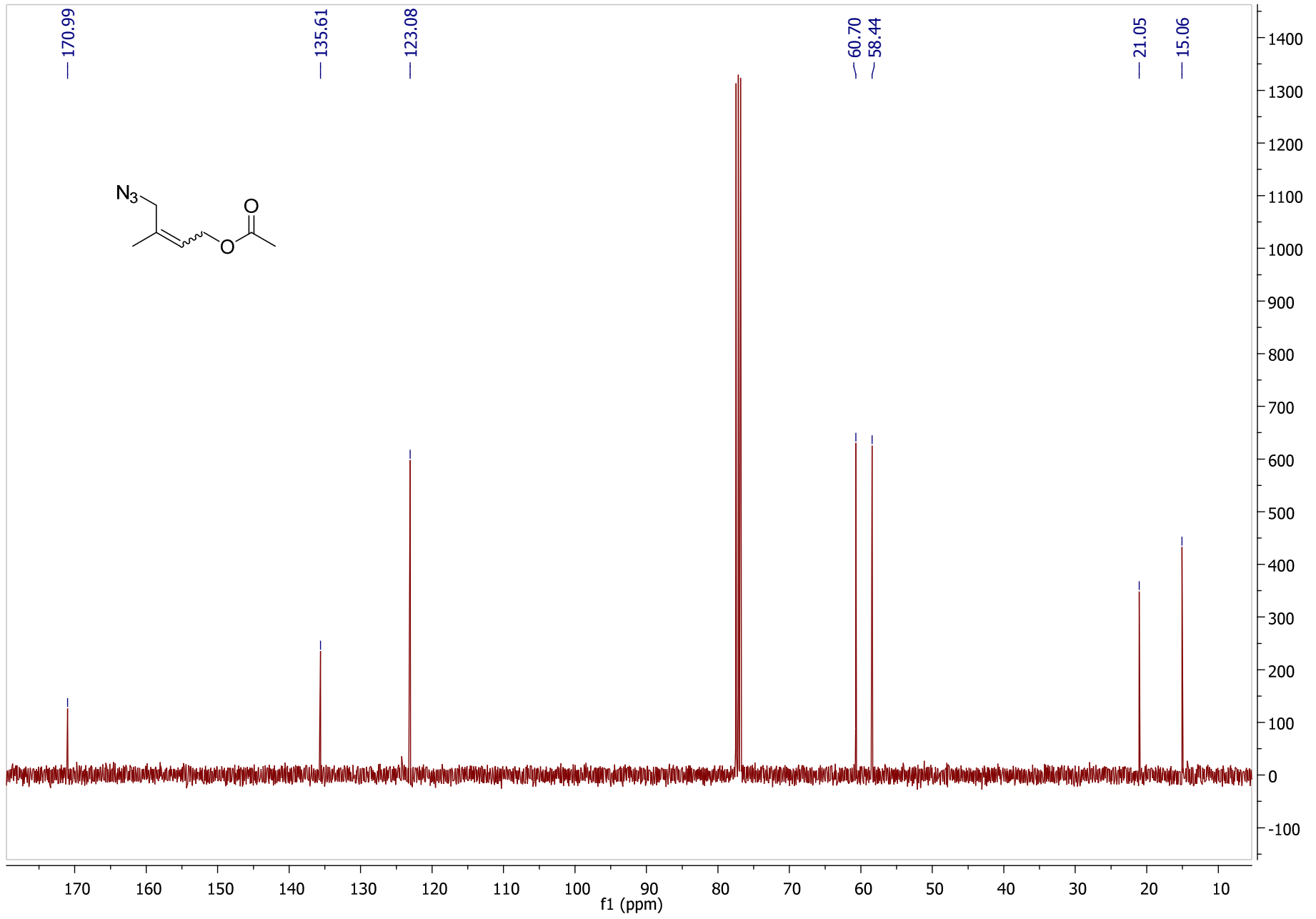


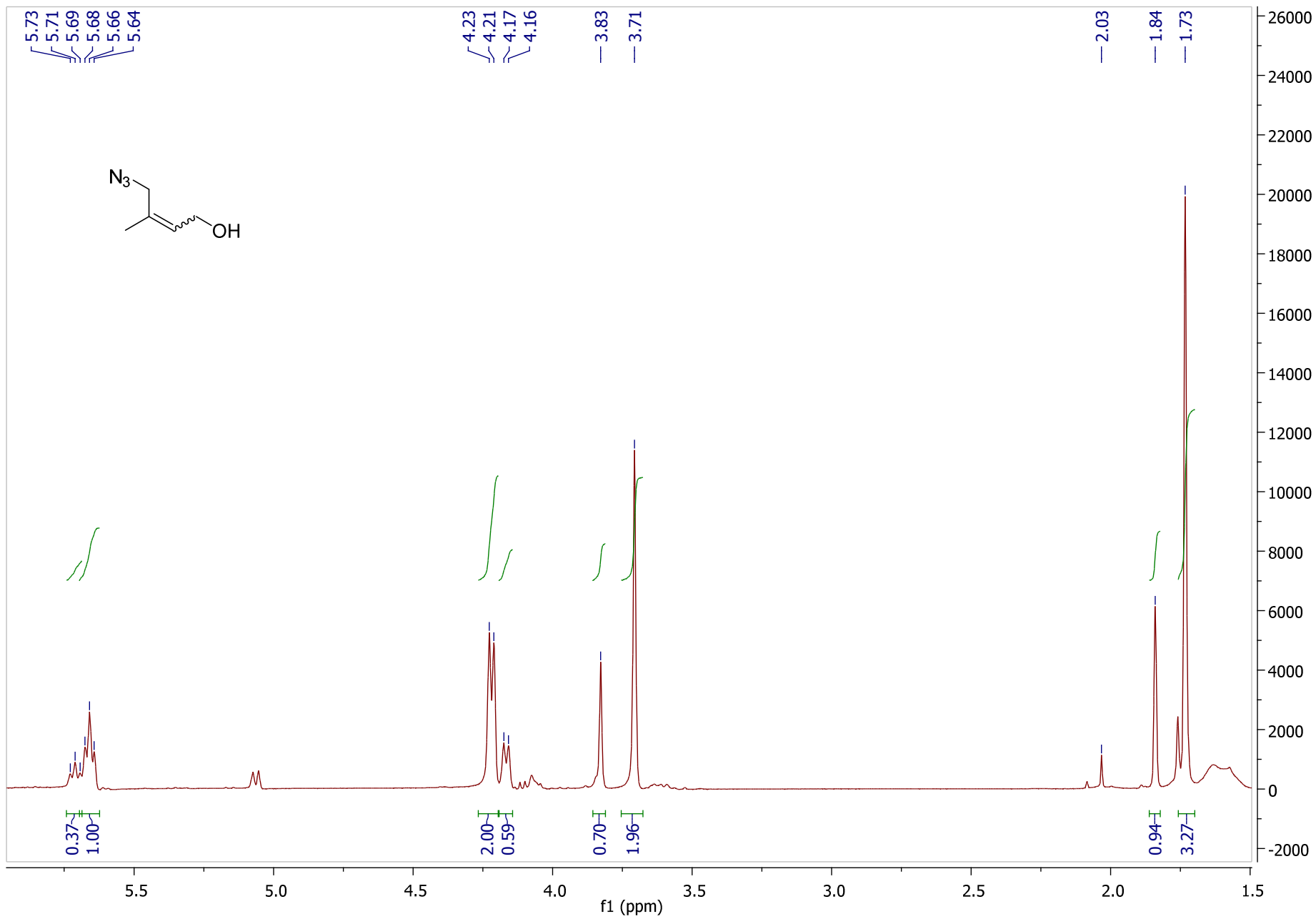


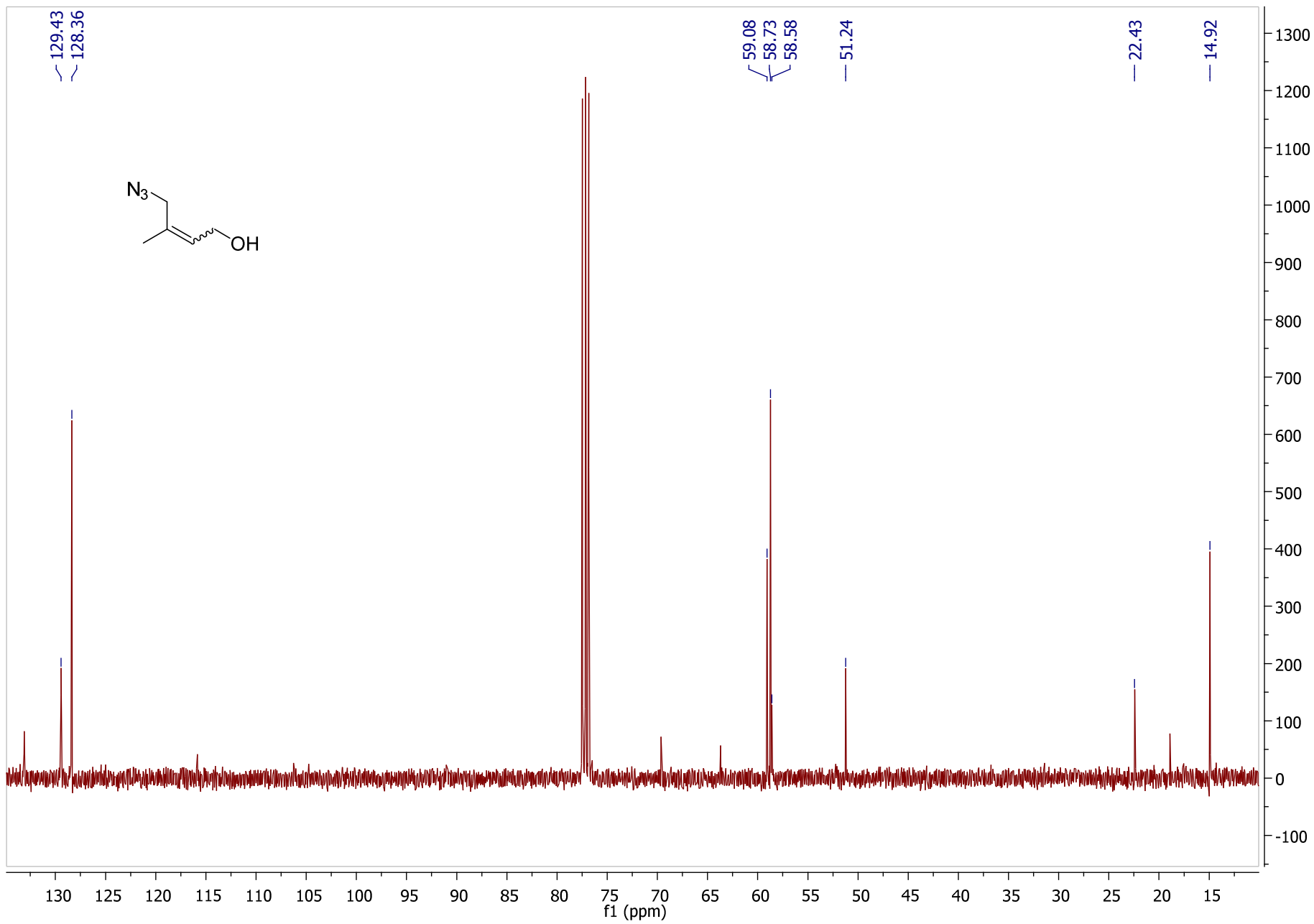


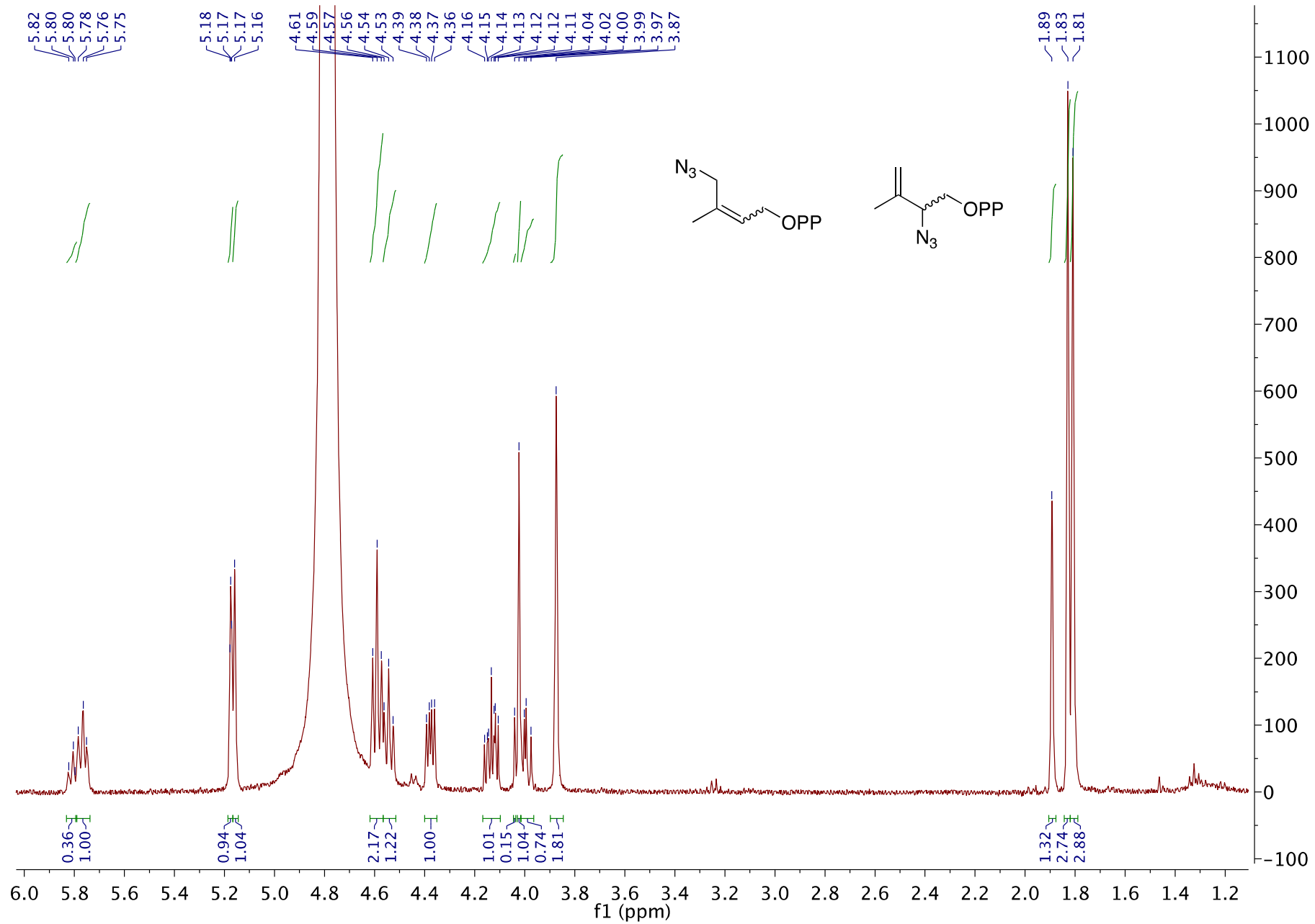


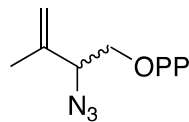
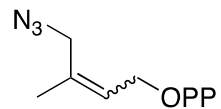




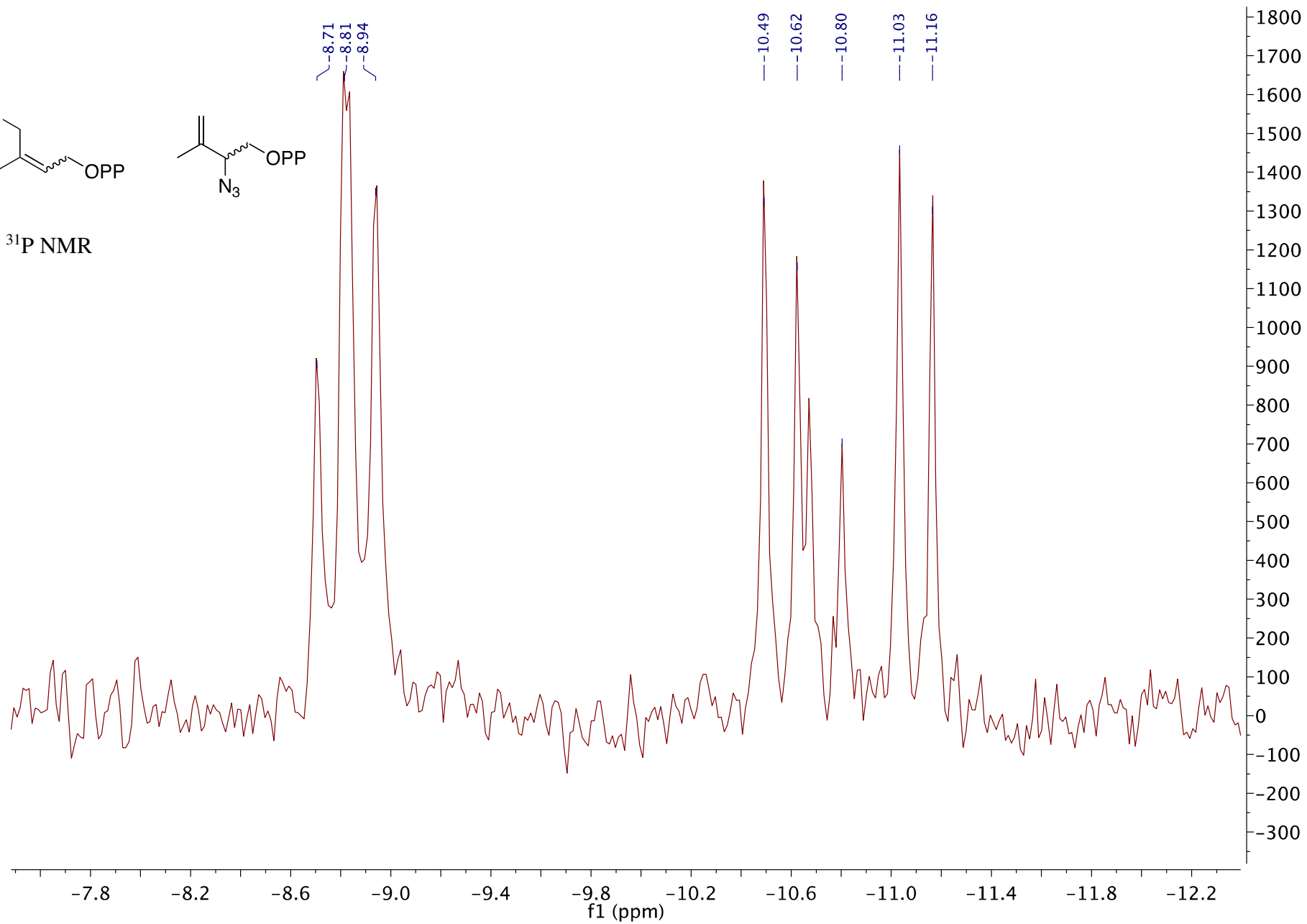


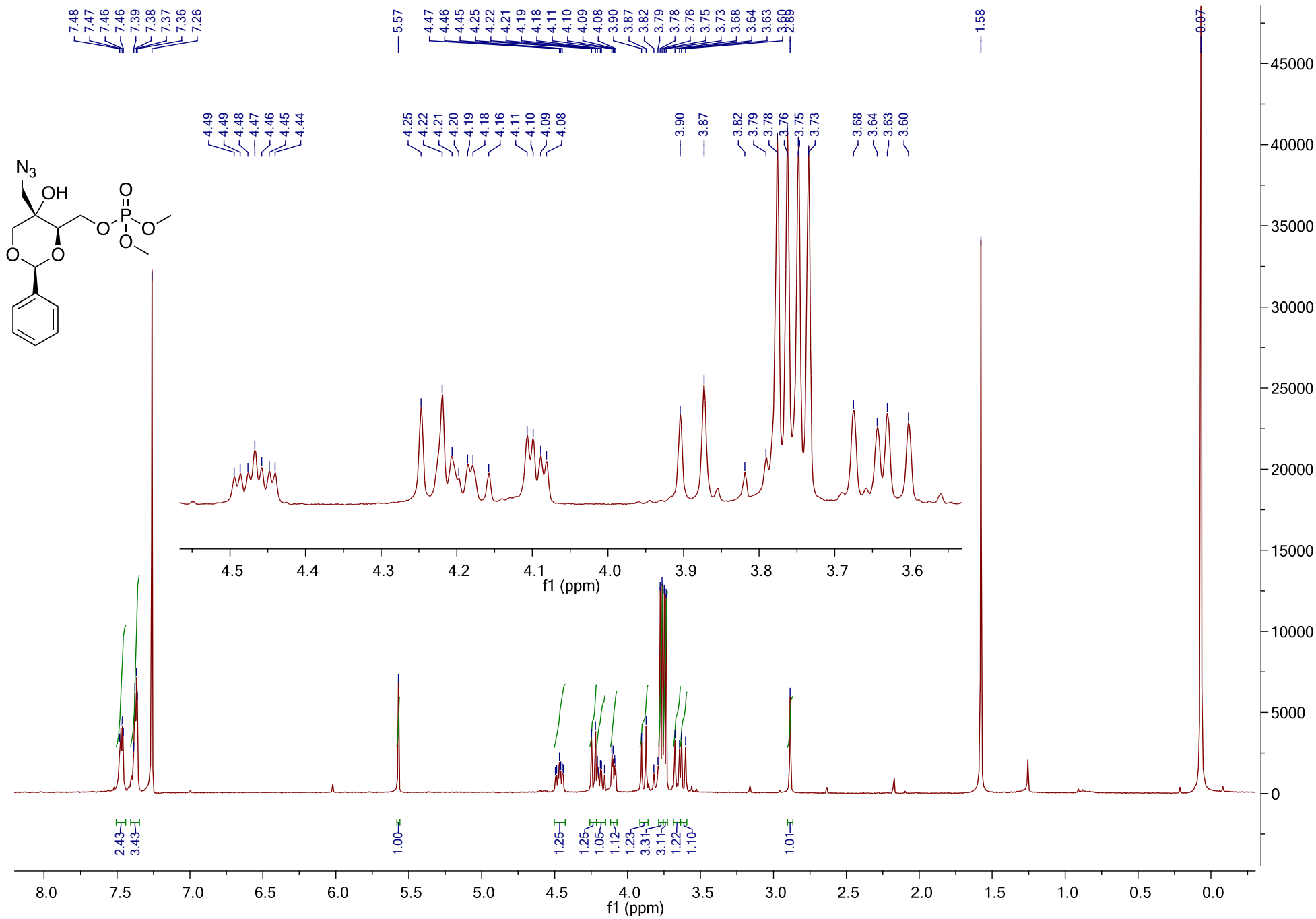


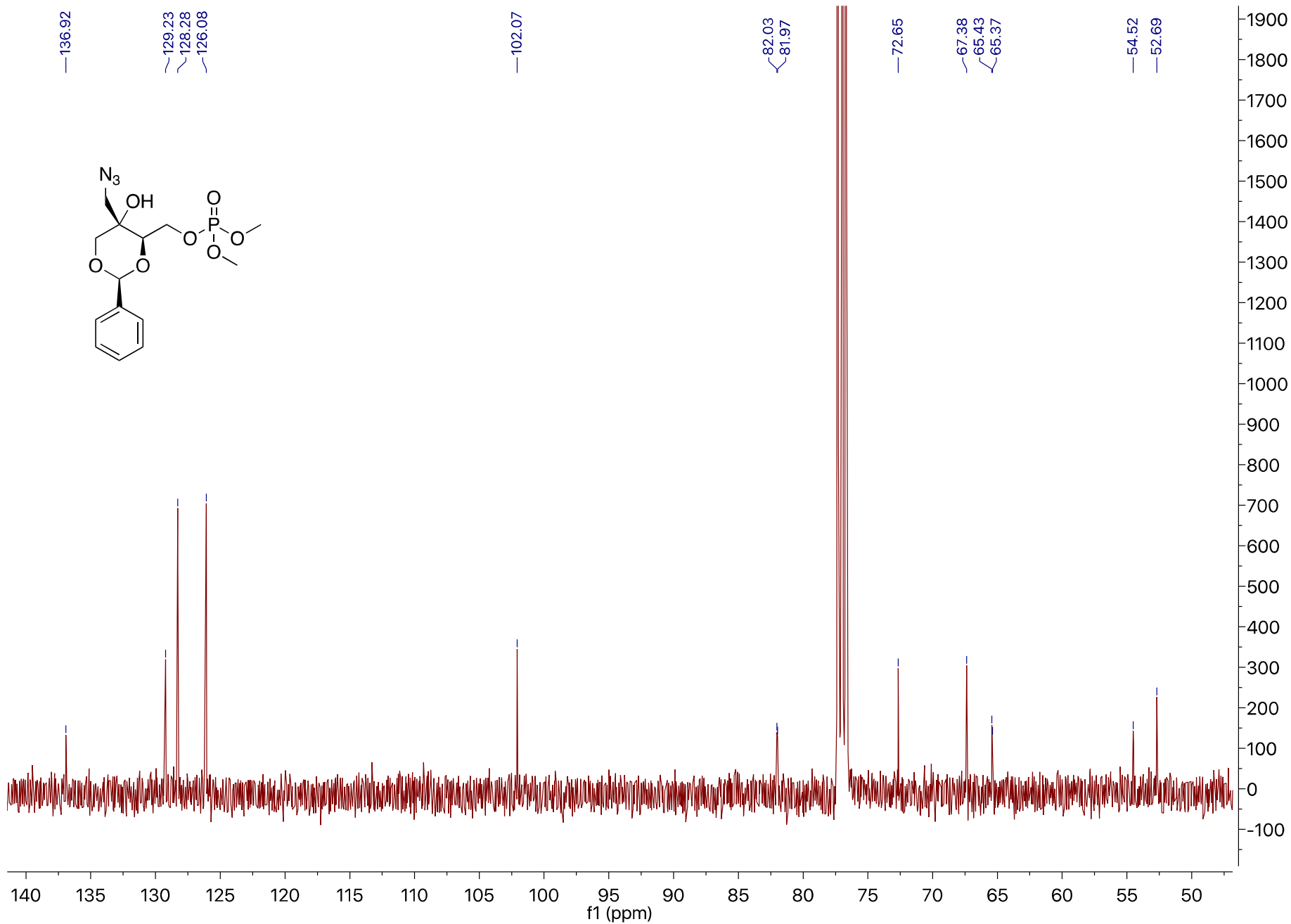
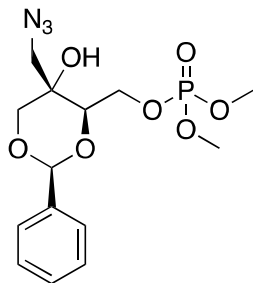


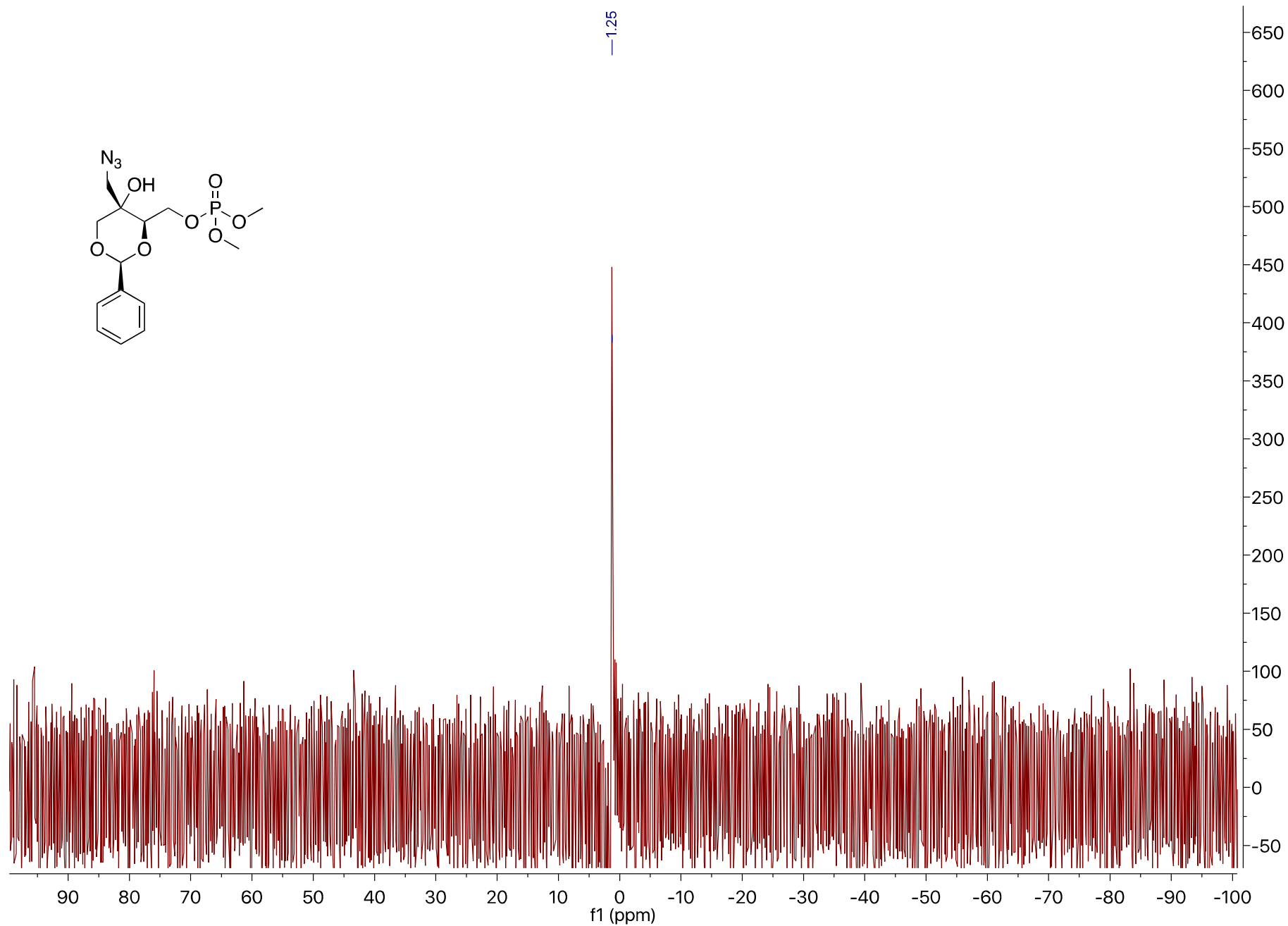
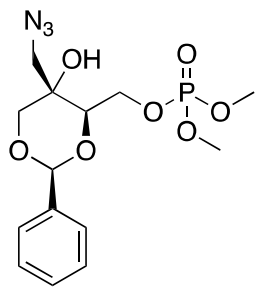


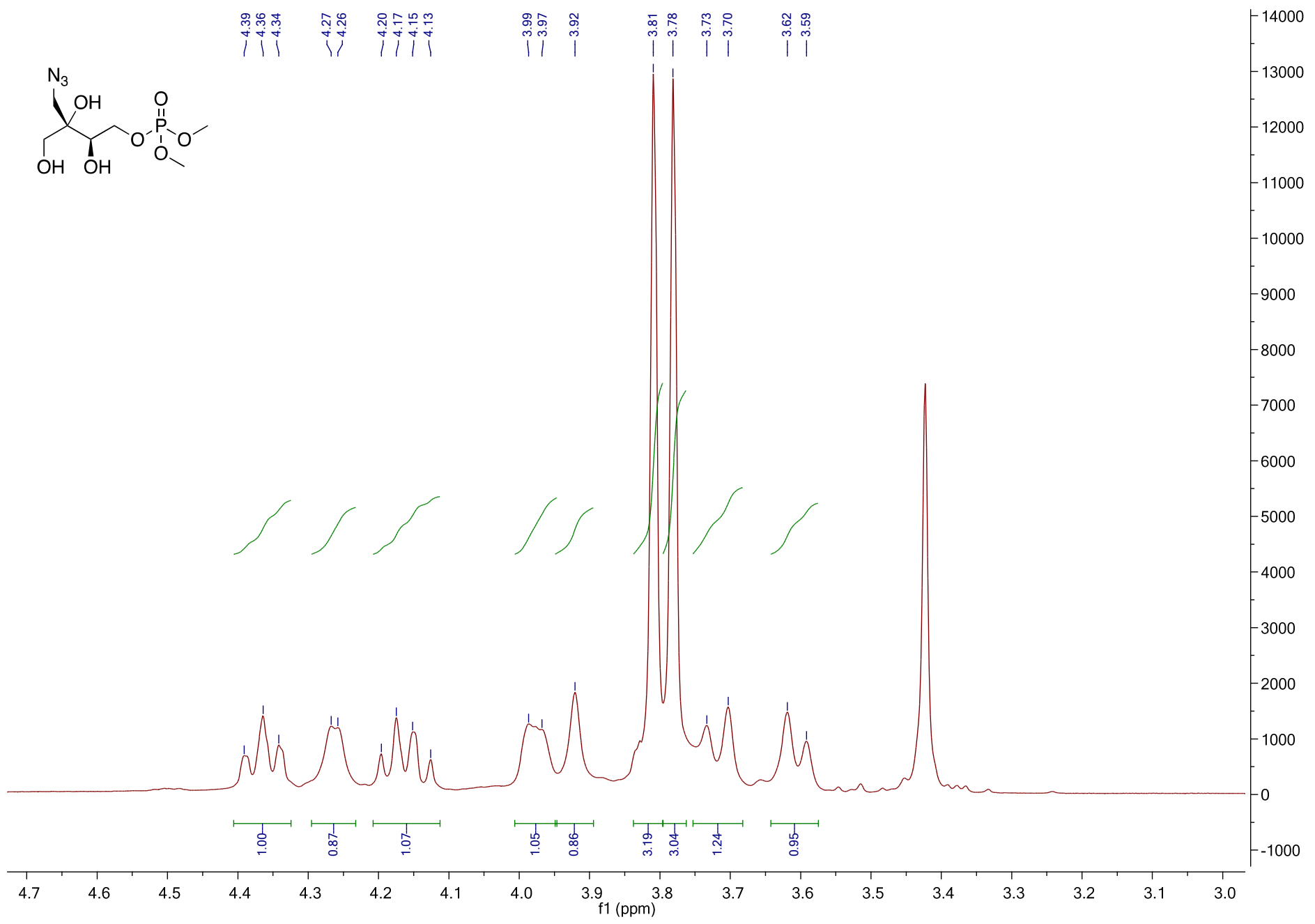
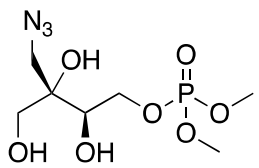
$^{31}\text{P}$  NMR

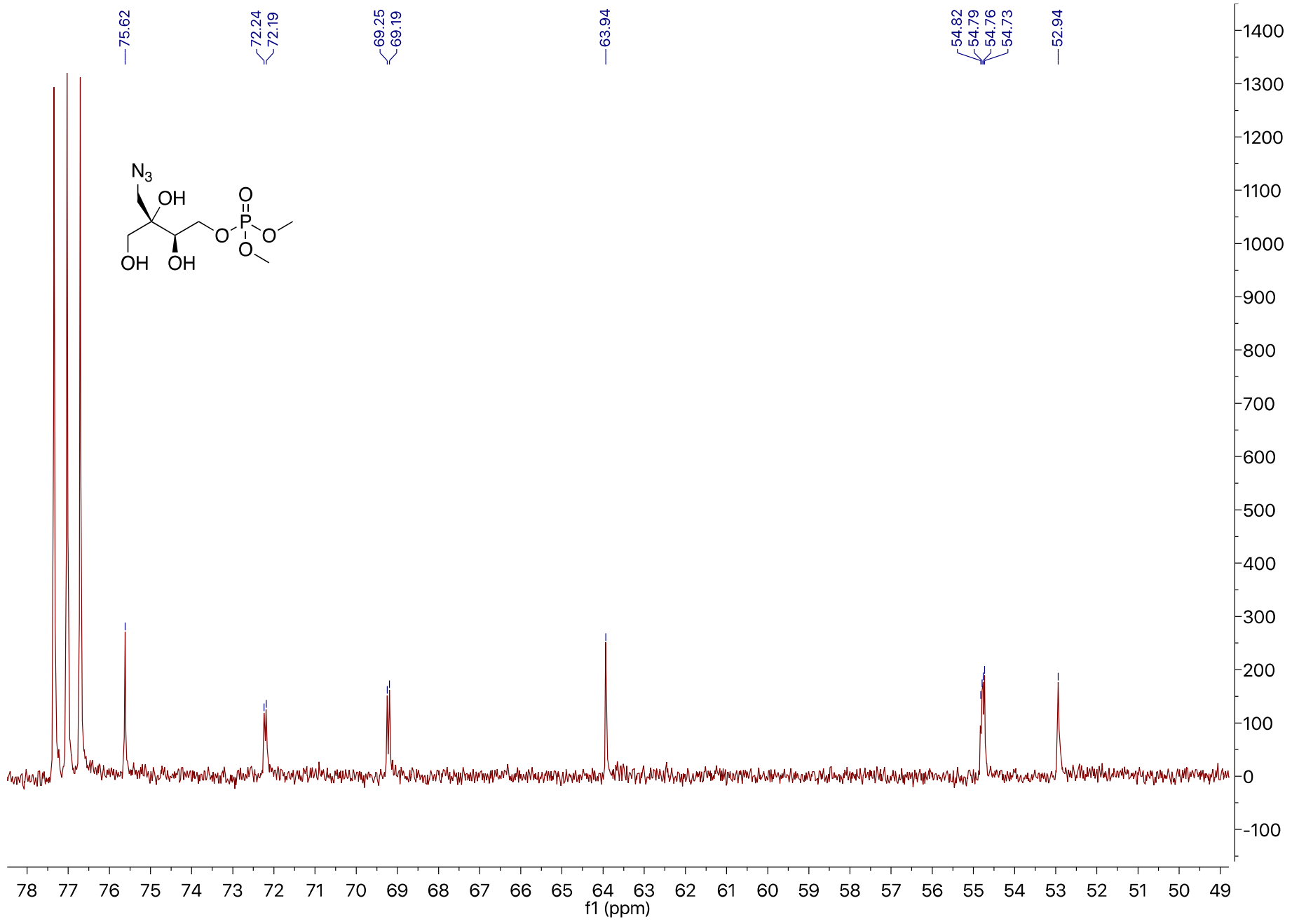


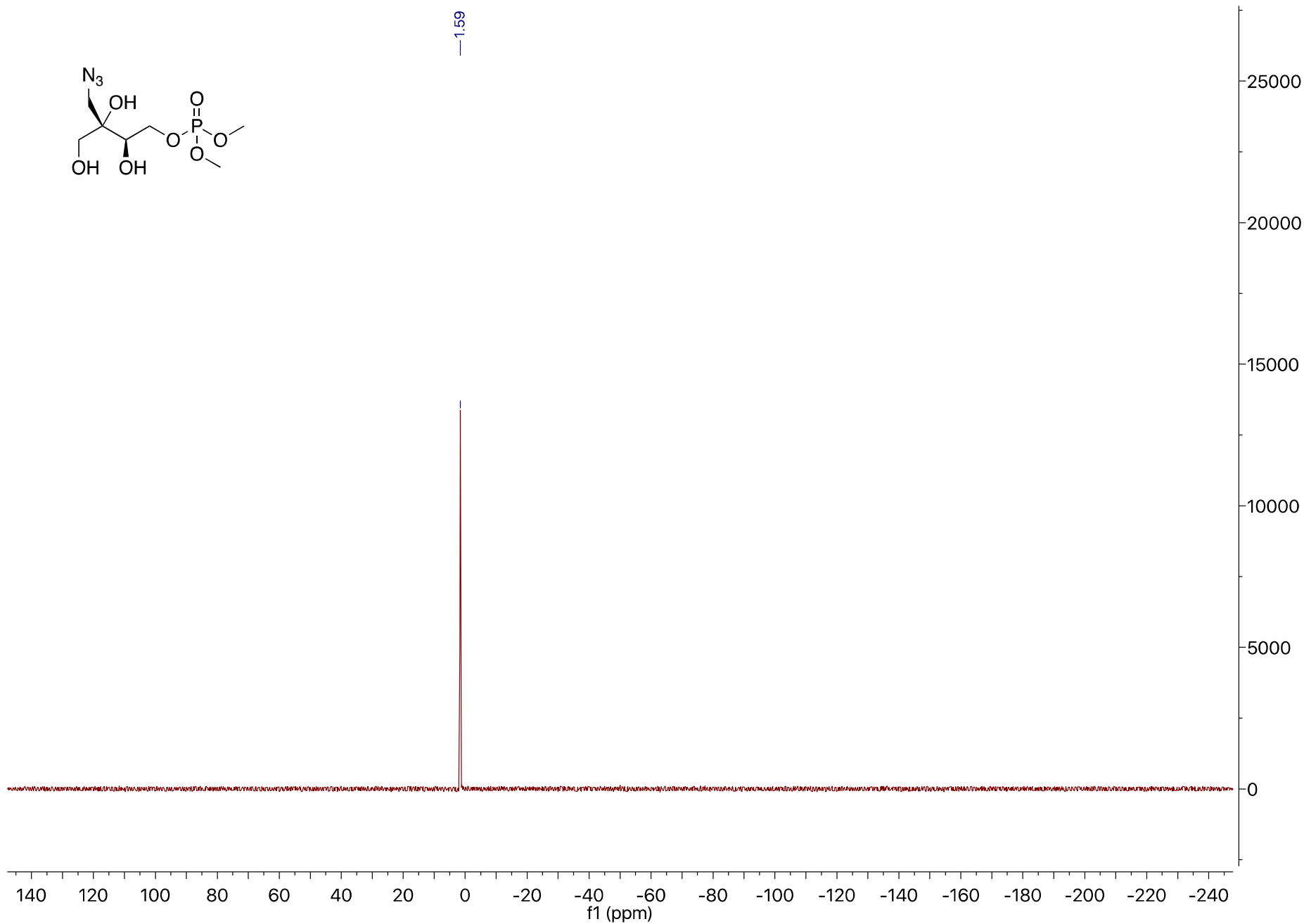
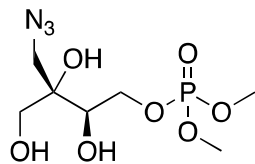


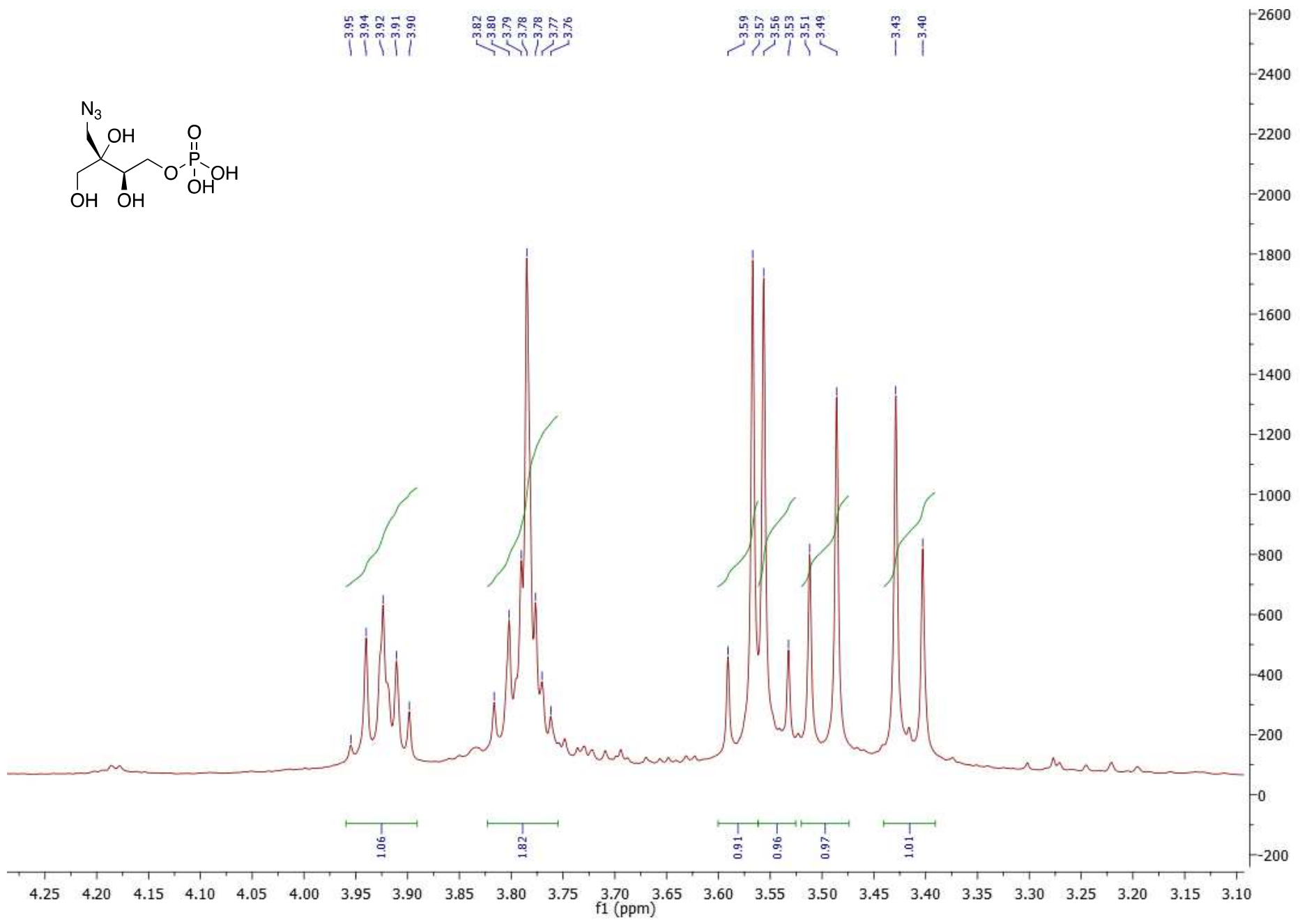
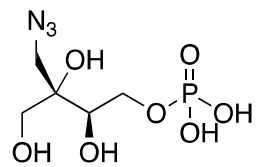


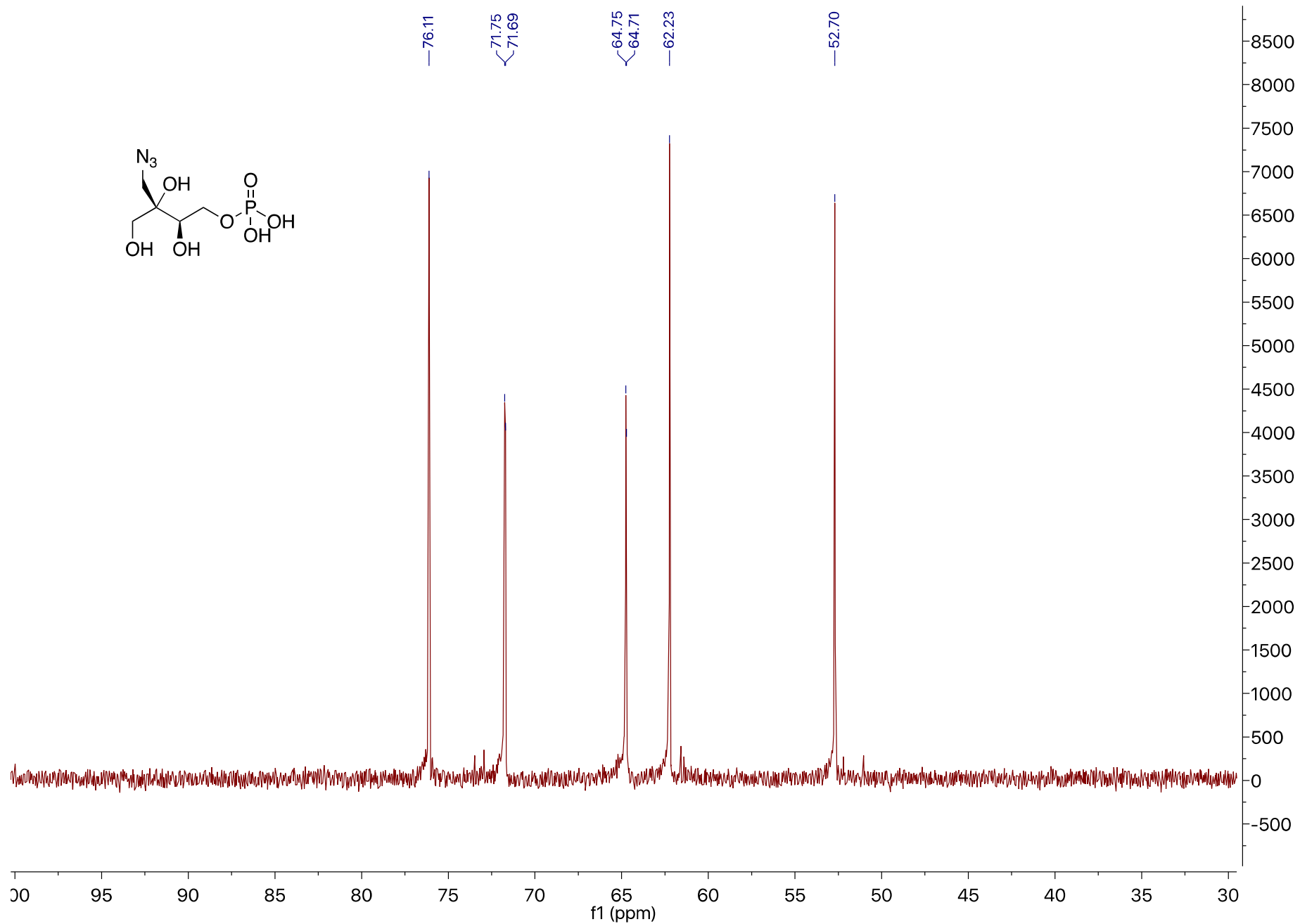
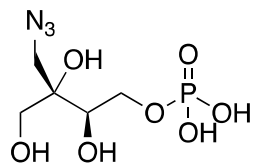


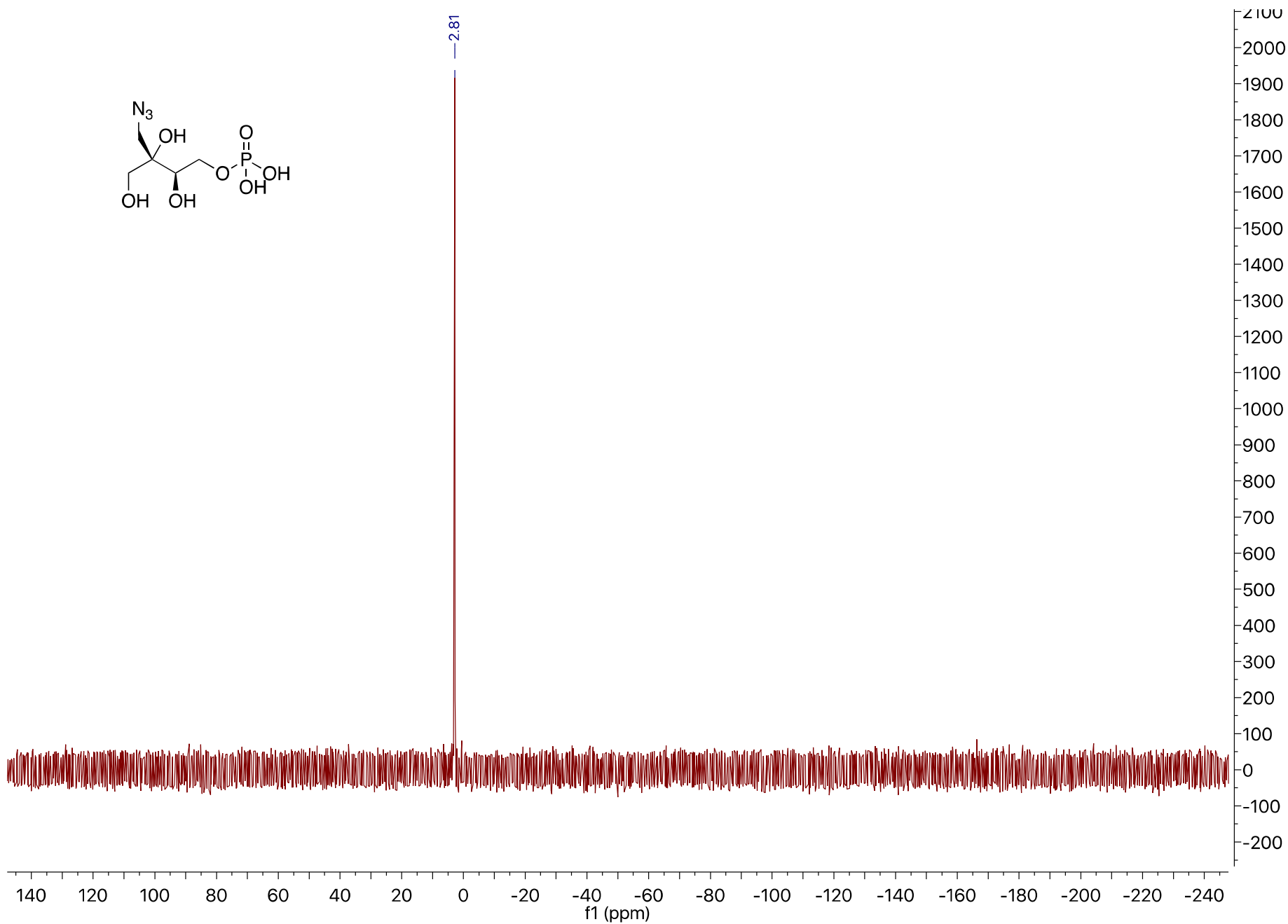
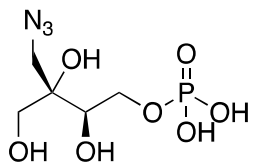














## Summary

Isoprenoids, present in all living organisms, are synthesised according to two routes: the Mevalonate and the Methylerythritol phosphate (MEP) pathways. The MEP pathway, absent in humans, is extensively investigated as it is a target for the development of new antimicrobials. ME-N<sub>3</sub> an azide tagged analogue of methylerythritol was synthesised and utilised for metabolic labelling studies of the MEP pathway using bioorthogonal ligation followed by LC-MS analysis. Interestingly, we found that MEP-N<sub>3</sub>, an analogue of MEP, inhibits *E.coli* IspD (3<sup>rd</sup> enzyme of the MEP pathway). Further inhibition kinetic studies revealed that MEP-N<sub>3</sub> possesses the highest inhibitory activity on *E.coli* IspD when compared to known inhibitors. In addition, the mechanism of inhibition of *E.coli* IspD by MEP-N<sub>3</sub> was found to be best described using a mixed type model. Moreover, determination of the IspD reaction mechanism has been carried out for the first time, by virtue of a bisubstrate steady state kinetic analysis.

Keywords: Isoprenoid, methylerythritol phosphate pathway, IspD, metabolic labelling, enzyme inhibition, enzyme kinetics.

## Résumé

Les isoprénoïdes, présents dans tous les organismes vivants, sont synthétisés selon deux processus: la voie du Mevalonate et la voie Méthylérythritol phosphate (MEP). Cette dernière, absente chez l'humain, est très étudiée car elle représente une cible pour le développement de nouveaux antimicrobiens. Le ME-N<sub>3</sub>, un analogue du méthylérythritol portant un azoture, a été synthétisé et exploité dans des expériences de marquage métabolique de la voie MEP en utilisant un couplage bioorthogonale suivi d'une analyse par LC/MS. De façon intéressante, nous avons découvert que le MEP-N<sub>3</sub>, un analogue du MEP, inhibe l'enzyme IspD d'*E. coli* (3<sup>ème</sup> enzyme de la voie MEP). Les études cinétiques ont révélé que le MEP-N<sub>3</sub> possède la meilleure activité inhibitrice sur IspD d'*E.coli* en comparaison avec les inhibiteurs connus, et que le mécanisme d'inhibition est de type mixte. Une étude détaillée du mécanisme de la réaction catalysée par IspD a été réalisée pour la première fois, en utilisant une analyse cinétique à deux substrats.

Mots-clés: Isoprénoïde, voie du méthylérythritol phosphate, IspD, marquage métabolique, inhibition enzymatique, cinétique enzymatique.